

**THE ROLE OF TROPOMYOSIN DURING HEART DEVELOPMENT  
(PART I)**

and

**NEUROANATOMICAL AND CARDIORESPIRATORY CHANGES  
ASSOCIATED WITH METAMORPHOSIS  
(PART II)**

**IN THE AXOLOTL, *AMBYSTOMA MEXICANUM***

by

**ARUNA NARSHI**

A thesis submitted to the  
College of Life and Environmental Sciences  
of the University of Birmingham  
for the degree of  
**DOCTOR OF PHILOSOPHY**

School of Biosciences  
College of Life and  
Environmental Sciences  
University of Birmingham  
September 2010

UNIVERSITY OF  
BIRMINGHAM

**University of Birmingham Research Archive**

**e-theses repository**

This unpublished thesis/dissertation is copyright of the author and/or third parties. The intellectual property rights of the author or third parties in respect of this work are as defined by The Copyright Designs and Patents Act 1988 or as modified by any successor legislation.

Any use made of information contained in this thesis/dissertation must be in accordance with that legislation and must be properly acknowledged. Further distribution or reproduction in any format is prohibited without the permission of the copyright holder.

## ABSTRACT

The first part of the thesis was a study of the role of tropomyosin in cardiac myofibrillogenesis. The model used was the Mexican axolotl, *Ambystoma mexicanum*. This animal model is very useful for the study of heart development as it has a naturally occurring mutant, the *cardiac (c/c)* lethal, in which the embryos lack organised myofibrils and have low levels of tropomyosin. Antisense oligonucleotides specific to axolotl tropomyosin disrupted myofibril formation in normal heart, whereas sense oligonucleotides encouraged myofibrillogenesis in the mutant hearts, demonstrating the importance of tropomyosin in cardiac muscle development and the effectiveness of cationic liposome transfection system.

A novel isoform of the human tropomyosin-encoding gene *TPM1* gene, designated TPM1 $\kappa$  was discovered and found to be cardiac specific in humans. Interestingly, ectopic expression of GFP.TPM1 $\kappa$  fusion protein promoted myofibrillogenesis in the *cardiac* mutant axolotl heart. The TPM1 $\kappa$  isoform was then found to be expressed in amphibians too and transfection of antisense oligonucleotide blocked TPM1 $\kappa$  expression in whole embryonic hearts of the wild type axolotl.

Previous investigations found that extending the N- or C-terminus of the tropomyosin molecule does not affect cardiac myofibrillogenesis. In this study both ends of tropomyosin were extended simultaneously using the expression construct pEGFP.TPM4 $\alpha$ .E-L-FLAG and transfected into the *cardiac* mutant. The modified tropomyosin formed organised myofibrils in the embryonic axolotl heart.

The second part of this thesis involved the neuroanatomical and cardiorespiratory study of neotenuous, metamorphosing and metamorphosed axolotls. Using the retrograde neural tracer Fluorogold, vagal preganglionic neurones (VPN) were found in the dorsal vagal nucleus (DVN) area in all three developmental stages (neotenuous, metamorphosing and metamorphosed). However, the neotenuous VPN cells were small and appeared spherical, perhaps due to apparent lack of differentiation. The metamorphosing hind brain had more mature looking cells and some appeared to be migratory. The metamorphosed axolotl had

cells that looked like stereotypical nerve cells and some that were migratory too. The VPN were found in two distinct areas, the DVN and in a ventral-lateral position from the DVN. Of all the VPN found in the metamorphosed 18% were located ventro-laterally. This change is hypothesised to be related to the change from predominantly gill ventilation to committed lung ventilation. This was investigated physiologically.

Cardiac and ventilatory behaviour of neotenus and metamorphosed axolotls was examined using electrocardiograms (ECG). The heart rate and ventilation rate of the metamorphosed was higher than that of the neotenus. Atropine raised the heart rate in both, indicating the presence of parasympathetic vagal control, and propranolol lowered the heart rate in both, indicative of sympathetic control via adrenaline.

Neotenus ventilation rate generally followed heart rate but was varied in the metamorphosed axolotl. Preliminary power spectral analysis indicated a cyclic variability in heart rate with respiration in the metamorphosed axolotl, but not in the neotenus.

Heart rate variability in the metamorphosed axolotl is hypothesised to be associated with becoming a committed lung breather, and that it may be the functional role of the VPN relocation. The ventral lateral area in humans is called the nucleus ambiguus and it is involved in cardiorespiratory control. Hence, the VPN in the ventrolateral location in the axolotl may be a primordial nucleus ambiguus.

*To Mum, Dad, Kits, Dee,*

*Tommy and Little Joy*

*It is not the strongest of  
the species that survives,  
nor the most intelligent that  
survives.*

*It is the one that is  
the most adaptable  
to change.*

*Charles Darwin*

## **ACKNOWLEDGEMENTS**

I would like to sincerely thank my supervisor, Professor E. W. Taylor for his wisdom, advice, criticism, encouragement, patience, and unfailing interest throughout this project.

I would like to especially thank him for his unreserved support and understanding throughout my challenging personal circumstances.

I would also like to thank Hugh Wallace for his advice on all things amphibian, Noni for use of her microscope, Tobias Wang for his guidance and support, and Steve Publicover for always being ready to help out.

Thanks to Norman, Pete, and Alan for their continual support, friendship, laughter and time for all the little important things!

I give special thanks to Professor D. K. Dube and Dr S. Dube for providing the opportunity of carrying out part of my project at Upstate Medical University (Syracuse, NY) and for their generous hospitality throughout my time there. I would also like to thank the Upstate team for their time and friendliness, particularly, Rob, Chris, Matt, Masako, Raisa, Nancy, Gloria and Craig.

I would like to thank my family and friends for their love, support, understanding, and for just being there and seeing me through the difficult times.

## DECLARATION

The work in this thesis was carried out by the author under the supervision of Professor E.W. Taylor, School of Biosciences, University of Birmingham, UK.

This thesis is in two parts. The first part was carried out in collaboration with the research team of Professor D.K. Dube, Department of Medicine, SUNY Upstate Medical University, NY. The author was first trained in, and then directly contributed to, the following areas –

***Molecular work:*** dissection of relevant tissues for RNA extraction, RNA extraction, RT-PCR, PCR amplification, gel electrophoresis, cloning and sequencing, Southern blot hybridisation, and *in situ* hybridisation.

***Histological work:*** dissection, whole heart organ culture, liposome mediated transfection of sense, anti-sense oligonucleotides or DNA, preparation of tissue for whole mount immunostaining, confocal and electron microscopy.

***General work:*** data analysis, drafting and preparation of manuscripts, animal care and breeding, the staging and collection of appropriate developmental stages of embryos.

This contribution of the author's work is reflected in articles published in peer reviewed journals.

The second part of the thesis was carried out at the University of Birmingham under the guidance of Professor Ted Taylor.



750 East Adams Street  
Syracuse, NY 13210

Department of Medicine



UniversityHospital

[www.upstate.edu](http://www.upstate.edu)

State University of New York  
**Upstate Medical University**

June 27, 2011

Declaration of Dipak K. Dube, Ph.D., D.Sc.

I, Prof Dipak K Dube, declare that Aruna Narshi (previous surname Choudhury) worked in collaboration with our research team in my laboratory, Department of Medicine, SUNY Upstate Medical University, Syracuse, New York. She was studying the role of tropomyosin in cardiac myofibrillogenesis in vertebrates. We were well aware of the fact that her work would be included in her doctoral dissertation.

Aruna was involved in the laboratory work, data analysis, image capturing and processing, and preparation of manuscripts. She is an author on all publications in which she contributed and I give full permission for these publications to be used to form part of her PhD thesis.

Dipak K Dube, Ph.D., D.Sc.  
Professor  
Department of Medicine  
SUNY Upstate Medical University  
750 East Adams Street  
Syracuse, NY 13210

---

Colleges of: Medicine • Graduate Studies • Health Professions • Nursing • University Hospital

*Improving the health of the communities we serve through education, biomedical research, and health care*

## LIST OF PUBLICATIONS

Please note that I have older publications under Aruna Choudhury and newer ones under Aruna Narshi.

- i. Zajdel, R.W., **Choudhury, A.**, Dube, S., Mehta, S. and Dube, D.K. (2000). Transfection of anti-sense oligonucleotide into whole hearts using cationic liposomes. *Focus (Gibco BRL)*. **22**:28-30.
- ii. Spinner, B.J., Zajdel, R. W., McLean, M. D., Denz, C. R., Dube, S., Mehta, S., **Choudhury, A.**, Nakatsugawa, M., Dobbins, N., Lemanski, L. F. and Dube, D. K. (2002) Characterization of a TM-4 Type Tropomyosin That Is Essential for Myofibrillogenesis and Contractile Activity in Embryonic Hearts of the Mexican Axolotl. *J. of Cell. Biochem.* **85**: 747-761.
- iii. Denz, C. R., **Narshi, A.**, Zajdel, R. W. and Dube, D. K. (2004) Expression of a novel cardiac-specific tropomyosin isoform in humans. *Biochem. Biophys. Res. Comm.* **320**: 1291-1297.
- iv. Zajdel, R. W., Denz, C. R., **Narshi, A.**, Dube, S. and Dube, D. K. (2005) Antisense mediated inhibition of expression of the novel striated tropomyosin isoform TPM1 disrupts myofibril organisation in embryonic axolotl hearts. *J. Cell. Biochem.* **95**: 840-848.
- v. **Narshi, A.**, Denz, C.R., Nakatsugawa, M., Zajdel, R.W., Dube, S., Poiesz, B.J. and Dube D.K. (2005) Cardiac myofibril formation is not affected by modification of both N- and C-termini of sarcomeric tropomyosin. *Cardiovasc Toxicol.* **5**: 1-8.

# CONTENTS

<b>Chapter 1 General introduction .....</b>	<b>1</b>
<b>1.0 Setting the scene.....</b>	<b>1</b>
<b>1.1 Heart development .....</b>	<b>2</b>
1.1a Heart morphogenesis .....	2
<b>1.2 Neuroanatomical overview of the vagus nerve .....</b>	<b>6</b>
1.2a The hindbrain .....	7
1.2b The tenth cranial nerve.....	9
<b>1.3 Overview of the vertebrate nervous system .....</b>	<b>11</b>
1.3a Central nervous system .....	11
1.3b Peripheral nervous system .....	12
1.3c Autonomic nervous system .....	13
1.3d Development of cardiac neural control .....	15
<b>1.4 Nervous control of the heart .....</b>	<b>22</b>
1.4a Innervation of vertebrate hearts .....	27
1.4a.i Cyclostomes .....	27
1.4a.ii Elasmobranches .....	28
1.4a.iii Teleosts .....	29
1.4a.iv Amphibians.....	30
1.4a.v Reptiles.....	30
1.4a.vi Birds.....	30
1.4a.vii Mammals.....	31
<b>1.5 Overview of vertebrate respiratory systems .....</b>	<b>32</b>
1.5a Cutaneous exchange .....	32
1.5b Gills.....	33
1.5c Lungs .....	34
1.5c.i Lung ventilation .....	35
1.5c.ii Positive pressure breathing.....	35
1.5c.iii Negative pressure breathing .....	35
1.5c.iv Ventilation in birds.....	36
<b>1.6 Autonomic control of breathing .....</b>	<b>37</b>
1.6a Alternating inspiration / expiration rhythm .....	38
1.6b Magnitude of ventilation .....	41
1.6c Modification of respiratory activity .....	41
<b>1.7 Heart rate variability and respiratory sinus arrhythmia.....</b>	<b>42</b>
<b>1.8 The Mexican axolotl, <i>Ambystoma mexicanum</i> .....</b>	<b>44</b>
1.8a The cardiac lethal mutant .....	47
1.8b Tropomyosin and the cardiac lethal mutation .....	53

1.8c The model .....	56
<b>1.9 Aims, hypotheses and objectives .....</b>	<b>56</b>

## **Part I – The Role of Tropomyosin in Cardiac Myofibrillogenesis..58**

<b>Chapter 2 Targeted gene disruption in whole hearts by cationic liposome transfection of antisense oligonucleotides ....</b>	<b>59</b>
<b>2.0 Abstract .....</b>	<b>59</b>
<b>2.1 Introduction.....</b>	<b>60</b>
<b>2.2 Methods .....</b>	<b>63</b>
2.2a Whole heart bioassay .....	63
2.2b Transfection .....	64
2.2c Confocal microscopy .....	65
2.2d Total RNA extraction.....	66
2.2e RT-PCR analysis .....	67
<b>2.3 Results.....</b>	<b>69</b>
2.3a Delivery of tropomyosin oligonucleotides.....	69
2.3b Effect of oligonucleotides on heart function.....	70
2.3c RT-PCR of transfected hearts .....	70
<b>2.4 Discussion .....</b>	<b>71</b>
<b>Chapter 3 Expression of a novel cardiac-specific tropomyosin isoform in humans.....</b>	<b>77</b>
<b>3.0 Abstract .....</b>	<b>77</b>
<b>3.1 Introduction.....</b>	<b>78</b>
<b>3.2 Materials and methods .....</b>	<b>79</b>
3.2a Total human RNA.....	79
3.2b RT-PCR.....	79
3.2c DNA sequencing .....	81
3.2d Preparation of expression constructs.....	81
3.2e Transfection of hearts.....	82
3.2f Confocal microscopy .....	82
<b>3.3 Results.....</b>	<b>83</b>
<b>3.4 Discussion .....</b>	<b>85</b>

<b>Chapter 4 Anti-sense-mediated inhibition of expression of the novel striated tropomyosin isoform, TPM1<math>\kappa</math>, disrupts myofibril organisation in embryonic axolotl hearts.....</b>	<b>99</b>
4.0 Abstract .....	99
4.1 Introduction.....	100
4.2 Materials and methods .....	102
4.2a Embryo care .....	102
4.2b Preparation of exon-specific oligonucleotides .....	102
4.2c Transfection of hearts .....	103
4.2d RT-PCR and Southern blot hybridisation .....	104
4.2e Confocal microscopy.....	105
4.2f Specificity for sense- and anti-sense oligonucleotides .	105
4.3 Results.....	106
4.3a Specificity of TPM1 $\kappa$ anti-sense oligonucleotide in vitro..	106
4.3b Anti-sense TPM1 $\kappa$ and TPM1 $\alpha$ specificity in vitro .....	106
4.3c Sense and anti-sense TPM1 $\kappa$ oligonucleotide in vivo...	107
4.3d Confocal microscopy of treated whole hearts .....	107
4.3e Contractions in TPM1 $\kappa$ anti-sense treated hearts.....	107
4.4 Discussion .....	108
<b>Chapter 5 Cardiac myofibril formation is not affected by modification of both N- &amp; C-termini of sarcomeric tropomyosin .....</b>	<b>122</b>
5.0 Abstract .....	122
5.1 Introduction.....	123
5.2 Materials and methods .....	125
5.2a pEGFP.TPM4 $\alpha$ .E-L-FLAG expression construct .....	125
5.2b Embryo care and whole heart organ culture .....	126
5.2c Transfection procedure.....	127
5.2d Confocal microscopy.....	128
5.2e Electron microscopy .....	128
5.3 Results.....	129
5.4 Discussion .....	130

## **Part II – Neuroanatomy and Physiology of Cardiorespiratory**

<b><u>Control</u>.....</b>	<b>139</b>
----------------------------	------------

<b>Chapter 6 Introduction and general methodology.....</b>	<b>140</b>
6.0 Abstract .....	140



## LIST OF ABBREVIATIONS

<b>ACh</b>	Acetylcholine
<b>ANS</b>	Autonomic nervous system
<b>AV</b>	Atrio-ventricular
<b>bpm</b>	Beats per minute
<b>BSA</b>	Bovine serum albumen
<b>c/c</b>	Genotype of the cardiac lethal axolotl mutant
<b>CNS</b>	Central nervous system
<b>CRI</b>	Cardiorespiratory interactions
<b>CV</b>	Cardiovascular
<b>DCM</b>	Dilated cardiomyopathy
<b>DMSO</b>	Dimethylsulfoxide
<b>DTSP</b>	Dithiobis (succinimidyl) propionate
<b>DRG</b>	Dorsal respiratory group
<b>DVN</b>	Dorsal vagal motonucleus
<b>ECG</b>	Electrocardiogram
<b>FG</b>	Fluoro-Gold
<b>FHC</b>	Familial Hypertrophic Cardiomyopathies in humans
<b>FHC</b>	Familial hypertrophic cardiomyopathy
<b>GFP</b>	Green fluorescent protein
<b>HCM</b>	Hypertrophic Cardiomyopathy
<b>HR</b>	Heart rate
<b>HRV</b>	Heart rate variability
<b>LPM</b>	Lateral plate mesoderm
<b>MS-222</b>	Tricaine methanesulfonate
<b>nA</b>	Nucleus ambiguus
<b>PNS</b>	Peripheral nervous system
<b>RSA</b>	Respiratory sinus arrhythmia
<b>RT-PCR</b>	Reverse transcriptase polymerase chain reaction
<b>SA</b>	Sino-atrial
<b>SV</b>	Sinus venosus
<b>TM</b>	Tropomyosin
<b>Tn</b>	Troponin
<b>VPN</b>	Vagal preganglionic (motor) neurons
<b>VRG</b>	Ventral respiratory group

Figure 1-1. Anatomical events of cardiac morphogenesis .....	5
Figure 1-2. The dorsal surface of the adult axolotl brain. ....	7
Figure 1-3. A schematic diagram of a traverse section through the medulla oblongata.....	10
Figure 1-4. Functional hierarchy of the peripheral nervous system.. ....	13
Figure 1-5. Diagram mapping the origin of the various components of the cardiac innervation.. .....	17
Figure 1-6. Ventral view of a young larval axolotl heart .....	21
Figure 1-7. General cardiovascular reflexes in amphibia .....	26
Figure 1-8. External gills of the neotenic axolotl .....	34
Figure 1-9. Respiratory control centres in the brain stem .....	37
Figure 1-10. Diagram of the medulla oblongata showing the topographical proximity of the main nuclei involved in cardiorespiratory interactions .....	38
Figure 1-11. Dorsal view of medulla oblongata and spinal cord indicating regions involved in control of breathing.....	40
Figure 1-12. Abbreviated developmental stage series for the Mexican axolotl highlighting important stages utilized in Part I .....	48
Figure 1-13. Late stage axolotl embryos .....	49
Figure 1-14. Creating chimeric mutant axolotls .....	52
Figure 1-15. Myofibrillogenesis .....	54
Figure 2-1. Confocal micrographs of normal, sense and antisense transfected hearts.....	73-74
Figure 2-2. Localisation of transfected oligonucleotides. ....	75
Figure 2-3. Effect of antisense ATmC-3 on heart beat .....	76
Figure 3-1. Strategy for PCR amplification of TPM1 $\alpha$ and TPM1 $\kappa$ and the splicing pattern for each.....	89
Figure 3-2. Nucleotide and amino acid sequence of human TPM1 $\kappa$ .....	90



Figure 3-3. Amino acid sequence alignment of TPM1 $\kappa$ and TPM1 $\alpha$ from a variety of vertebrates.....	91
Figure 3-4. Identification of a cardiac specific novel isoform of TPM1.....	92
Figure 3-5. TPM1 $\kappa$ is found only in cardiac tissues by PCR amplification with exon 2a specific primer. ....	93
Figure 3-6. TPM1 $\alpha$ is found in both cardiac and skeletal muscle tissues using PCR amplification with exon 2b specific primer .....	94
Figure 3-7. Expression of both TPM1 $\alpha$ and TPM1 $\kappa$ is consistent across four adult heart segments analysed.....	95
Figure 3-8. Confocal microscopy of pEGFP.TPM1 $\alpha$ and pEGFP.TPM1 $\kappa$ transfected hearts from both normal and cardiac mutant Mexican axotl. ....	96-98
Figure 4-1. Strategy for amplification of TPM1 $\alpha$ and TPM1 $\kappa$ by RT-PCR using the same primer-pair and the location of isoform specific detector oligonucleotides for Southern hybridization.. ....	113
Figure 4-2. Scheme for testing the in vitro specificity of sense and anti-sense oligonucleotides.....	114
Figure 4-3. RT-PCR showing specificity of TPM1 $\kappa$ anti-sense oligonucleotide in vitro .....	115
Figure 4-4. Anti-sense TPM1 $\kappa$ and anti-sense TPM1 $\alpha$ specificity in vitro .....	116
Figure 4-5. Effect of TPM1 $\kappa$ sense and anti-sense oligonucleotides on transcript levels in vivo.....	117
Figure 4-6 - Myofibril organization and entry of FITC-tagged oligonucleotide into cells of whole hearts .....	118-119
Figure 5-1. The strategy for making pEGFP.TPM4 $\alpha$ .E-L-FLAG expression construct.. ....	134
Figure 5-2. Confocal micrographs of embryonic stage 39 hearts.....	135
Figure 5-3. Confocal micrograph of stage 39 normal transfected hearts stained with anti-GFP and anti-FLAG antibodies .....	136
Figure 5-4. Confocal micrograph of stage 39 mutant transfected hearts with pEGFP.TPM4 $\alpha$ .E-L-FLAG constructs and stained with anti-GFP and anti-FLAG antibodies .....	137
Figure 5-5. Transmission electron micrograph of portions of normal, mutant, and pEGFP.TMP4 $\alpha$ .E-L-FLAG transfected mutant hearts of embryonic stage 39 .	138

Figure 6-1. Axolotl habitat setup during metamorphic induction.....	153
Figure 6-2. Shedding sheets of skin in the tank during metamorphosis. ....	153
Figure 6-3. Transition from aquatic to aerial habit.....	154
Figure 6-4. Rebound effect .....	155
Figure 6-5. Aerial metamorphic changes.....	156
Figure 7-0. (A) Mid-metamorphic stage axolotl being anaesthetised in MS222.....	165
Figure 7-0. (B) Cannulation of the truncus arteriosus. ....	165
Figure 7-0. (C) Arrangement of the perfusion system.....	166
Figure 7-0.1 (A) Dorsal surface of the axolotl brain.....	167
Figure 7-0.1 (B) Section of brain embedded for neuroanatomical studies.....	168
Figure 7-1. The distribution of cell bodies of vagal preganglionic neurones in the hind brain of the axolotl.....	175-176
Figure 7-2. (A) Diagram of the neotenus axolotl medulla oblongata.....	177
Figure 7-2. (B) Diagram of the metamorphosing axolotl medulla oblongata .....	178
Figure 7-2. (C) Diagram of the metamorphosed axolotl medulla oblongata. ....	179
Figure 7-3.0 Neotenus axolotl medulla oblongata (micrograph references).....	180
Figures 7-3.1 to 7-3.6 Micrographs of transverse 20 $\mu$ m sections of neotenus axolotl medulla oblongata labelled with fluorescent tracer Fluorogold.....	181-186
Figure 7-4.0 Mid-metamorphosed axolotl medulla oblongata (micrograph references) .	187
Figures 7-4.1 to 7-4.7 Photomicrographs of transverse 20 $\mu$ m sections of mid- metamorphosed axolotl medulla oblongata showing vagal preganglionic motoneurones labelled with fluorescent tracer Fluorogold.....	188-194
Figure 7-5.0 Metamorphosed axolotl medulla oblongata (micrograph references). ....	195
Figures 7-5.1 to 7-5.8 Micrographs of transverse 20 $\mu$ m section of metamorphosed axolotl medulla oblongata showing vagal preganglionic motoneurones labelled with the fluorescent tracer, Fluorogold. ....	196-203

Figure 8-0 Electrode placement.....	210
Figure 8-1. An example of the underwater buccal movements of a neotenuous axolotl as picked up by ECG electrodes.....	224
Figure 8-2. The heart rate appears to be occurring around ventilation bouts .....	225
Figure 8-3. Heart rate around an air gulp did not change, indicating there was no heart rate variability present in the neotenuous axolotls.....	226-227
Figure 8-4. Changes in heart rate and gill ventilation rate post atropine injection in the neotenuous axolotl. ....	228-230
Figure 8-5. Effect of propranolol upon heart rate and gill ventilation rate.....	231-232
Figure 8-6. Ventilation rate in the metamorphosed axolotls was around 2 minute intervals .....	233-235
Figure 8-7. Bradycardia and tachycardia in the metamorphosed axolotl.....	236-238
Figure 8-8. The effect of atropine on the heart rate and ventilation rate of a metamorphosed axolotl.....	239-244
Figure 8-9. The effect of propranolol on the heart and ventilation rate of a metamorphosed axolotl.....	245-250
Figure 8-10. Heart rate variability in the metamorphosed axolotl .....	251
Figure 8-11. The effect of atropine and propranolol on the heart rate of the neotenuous and the metamorphosed axolotl .....	252
Figure 8-12. Tachograms of the neotenuous and metamorphosed axolotl.....	253-255
Figure 8-13. Power spectrum analysis of a neotenuous axolotl.....	256
Figure 8-14. Haematoxylin and eosin staining of neotenuous and metamorphosed axolotl hearts.....	257

## LIST OF TABLES

Table 1-1. Functions of the cranial nerves of humans .....	8
Table 1-2. Distinguishing features of the sympathetic and parasympathetic nervous systems.....	15
Table 1-3. Effects of the autonomic system on the heart and structures that influence the heart.....	22
Table 1-4. Amino acid comparisons of ribosomal protein S-3 and gene HoxA5 of axolotls with other vertebrates.....	45
Table 4-1. Nomenclature of various isoforms of TPM1 referred to in his study.....	120
Table 4-2. Five day comparison of synchronous contractions in control, sense, and anti-sense treated whole hearts.....	121

# CHAPTER ONE

## GENERAL INTRODUCTION

### 1.0 SETTING THE SCENE

The central theme of this thesis was looking at cardiac function from different perspectives, using the Mexican axolotl, *Ambystoma mexicanum*. The first part of the thesis looked at the role of tropomyosin in myofibrillogenesis, especially since axolotls have a naturally occurring cardiac mutant strain in which there is cardiac dysfunction thought to be caused by aberrant myofibrillogenesis. The second part of the thesis was the study of the autonomic control of the heart in the gill breathing, neotenuous axolotl and the committed lung breathing, metamorphosed form. The work in the thesis was, therefore split into two parts for clarity. Part I was the study of tropomyosin in cardiac myofibrillogenesis and Part II was the study of autonomic changes associated with the change from essentially a gill breather to an obligate lung breather.

Vertebrate heart development is a complex and highly ordered process that is both spatially and temporally regulated. It involves the migration and differentiation of several embryonic cell types and requires precise interactions between them. For instance, neural crest cells not only form parts of the heart itself, but are also involved in development of the parasympathetic nervous system that innervates the heart. Congenital heart defects, which are the most frequent congenital defects in humans, result when there is a failure in the formation of the various structures of the heart, or when formation occurs at the wrong time. The embryonic heart is fully formed before it becomes innervated. The density of

innervation is high in the sino-atrial (SA) and atrio-ventricular (AV) nodes (Navaratnam, 1987), which are situated within the right atrium.

## **1.1 HEART DEVELOPMENT**

### **1.1a Heart morphogenesis**

The heart is a hollow muscular organ, which by rhythmic contractions, pumps blood around the body. Without it the body would be deprived of nutrients, oxygen, hormones, etc., and poisoned by accumulation of waste products. Accordingly, it is among the first organs to develop a functional role.

The heart and great vessels derive from two distinct populations of cells. The four chambers of the heart originate from anterior lateral plate mesoderm (LPM), whereas parts of the outflow tract and great arteries are derived from the so-called 'cardiac' neural crest cells (located in the caudal hind-brain between rhombomeres 6, 7 & 8; somites 1-3 in chicks). In amphibians, the embryological events associated with heart development have been extensively characterised. In *Xenopus* (Drysdale *et al.*, 1994) and *Ambystoma* (Lemanski, 1973a) the mesodermal tissue lies in a deep equatorial ring prior to gastrulation. Fate maps of this ring have shown that heart is derived from two patches of the most anterior lateral plate mesoderm which lie on either side of the prechordal plate. These patches of precardiac mesoderm involute at the lateral edges of the dorsal blastopore lip during gastrulation, penetrating between the ectoderm and endoderm, and eventually become positioned on either side of the head.

In *Ambystoma mexicanum* the mid-ventral anterior/pharyngeal endoderm is a potent inductor of heart-forming mesoderm differentiation (Smith & Armstrong, 1991). This initial inductive interaction generates the heart field, which is the region of the embryo that has the potential to form heart. However, the heart field is larger than the actual heart primordium, and thus there must be a mechanism which separates the specified region into heart-forming and non-heart-forming areas (Easton, Armstrong & Smith, 1994). As development proceeds, however, the actual size of the heart field decreases.

In all vertebrates, the bilateral precardiac regions of the LPM migrate toward the embryonic midline. Here the primordia fuse to form the heart tube. The heart begins sporadic contractions before the formation of the tubular heart is complete, and simultaneous with the completion of the heart tube are rhythmic pulsations (Lemanski, 1973a), although the onset of nervous control occurs much later. Spontaneous depolarisation is initially seen in the caudal region of the straight heart tube; a region that later forms the SA node, the pacemaker of the heart (Olson & Srivastava, 1996). Initially, the heart is a straight tube and does not exhibit chambered subdivisions. During development the tube flexes into an S-shaped structure by rightward looping, and becomes intermittently constricted and dilated. These movements result in relocations of the heart regions and the formation of four main subdivisions:- (i) sinus venosus; (ii) atrium; (iii) ventricle; and (iv) bulbus cordis. Figure 1-1 depicts the main anatomical events of cardiac looping morphogenesis and chamber formation. Cardiac looping is a complex morphogenetic event in all vertebrates that brings the cardiac chambers into the correct alignment and allows the morphogenesis of valves and septa.

The hearts of bony fish have four chambers: the sinus venosus, atrium, ventricle, and conus arteriosus which are arranged in series so there is no separation of respiratory and systemic circulation. The deoxygenated blood flows from the sinus venosus towards the conus arteriosus direction, then to the gills to be oxygenated. Amphibians possess a single ventricle which pumps blood to both the lungs and the rest of the body. Oxygenation of the blood is also achieved cutaneously. The atrium of the axolotl is divided into two by a septum, although it was found to be incompletely divided in the axolotl at hatching (body length 1.5 cm) (Melinek & Mirolli, 1988) and also in early tadpole stage in *Xenopus laevis* (Mohun *et al.*, 2000).

Cardiac neural crest cells migrate through the circumpharyngeal region to populate the pharyngeal and aortic arches as well as the cardiac outflow tract and proximal great vessels. They form a sheath around the persisting aortic arch arteries and comprise the aorticopulmonary septation complex. Neural crest cells are also involved in the formation of the truncal cushion and membranous portion of the interventricular septum, and development of the semi-lunar valves. In human and mouse embryos the cardiac neural crest cells also appear give rise to the parasympathetic (vagal) postganglionic neurons of the heart (the cardiac ganglia) (Larsen, 1997; Waldo, Lo, & Kirby, 1999).



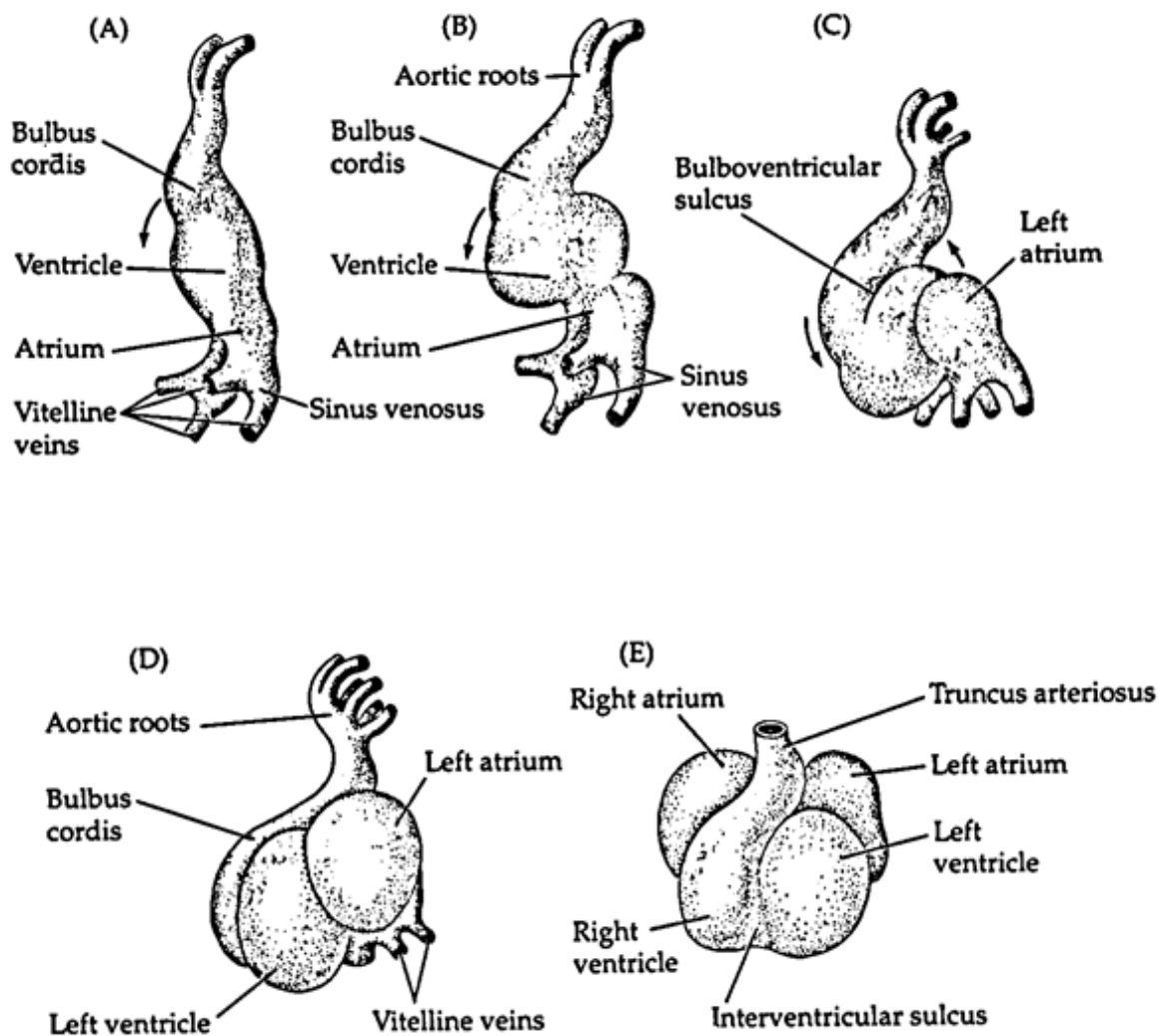


**Figure 1-1. Anatomical events of cardiac morphogenesis.**

The tubular heart (A) initiates rhythmic contractions at about day 23 in human and then undergoes rightward looping (B), which is the first indication of left-right asymmetry in the embryo. The S-shaped structure (C) flexes to bring the left atrium above and behind the left ventricle (D), forming the four-chambered heart (E). The arrows outside the heart depict the direction of twisting of the embryonic heart during development. Note, the diagram is of human heart formation, having a left and right ventricle; amphibians only have one ventricle. (Although, mammalian ontogeny also show one ventricle before they become two).

*Modified from Gilbert (1994)*

The role of the cardiac neural crest in heart development has been demonstrated by studies with chick embryos. Cardiac neural crest ablation in these embryos produces a variety of cardiac defects, mostly of the conotruncus and aortic arch, including persistent truncus arteriosus (Nishibatake, Kirby, & Van Mierop, 1987) and interrupted aortic arch (Kirby & Waldo, 1995). These abnormalities resemble those seen in DiGeorge syndrome, a human congenital syndrome believed to arise from neural crest defects.

## **1.2 NEUROANATOMICAL OVERVIEW OF THE VAGUS NERVE**

The way in which the embryonic brain develops is remarkably constant throughout the vertebrates. This constancy is most evident in the parts of the brain which develops first that could be regarded as most primitive or unspecialised. The summary recapitulation of evolution which occurs during ontogeny has proved invaluable in understanding brain morphology.

In vertebrate embryos the nervous system is one of the earliest groups of tissues to develop. A neural tube is formed by the closure of the neural groove in the dorsal mid-line of the early embryo. The anterior thickening of this tube which occurs, to form the brain, is indicative of the cephalisation of both sense organs and integrative centres which has occurred in vertebrates. Outgrowths of this early nervous system and connections with nervous tissue outside the neural tube form the spinal and cranial nerves. These are the routes by which the animal receives information from its own tissues and the environment, and relays commands to muscles, glands and sense organs through which a response is mediated.

The anterior thickening of the neural tube develops into three distinguishable components: the forebrain, midbrain and hindbrain (Figure 1-2).

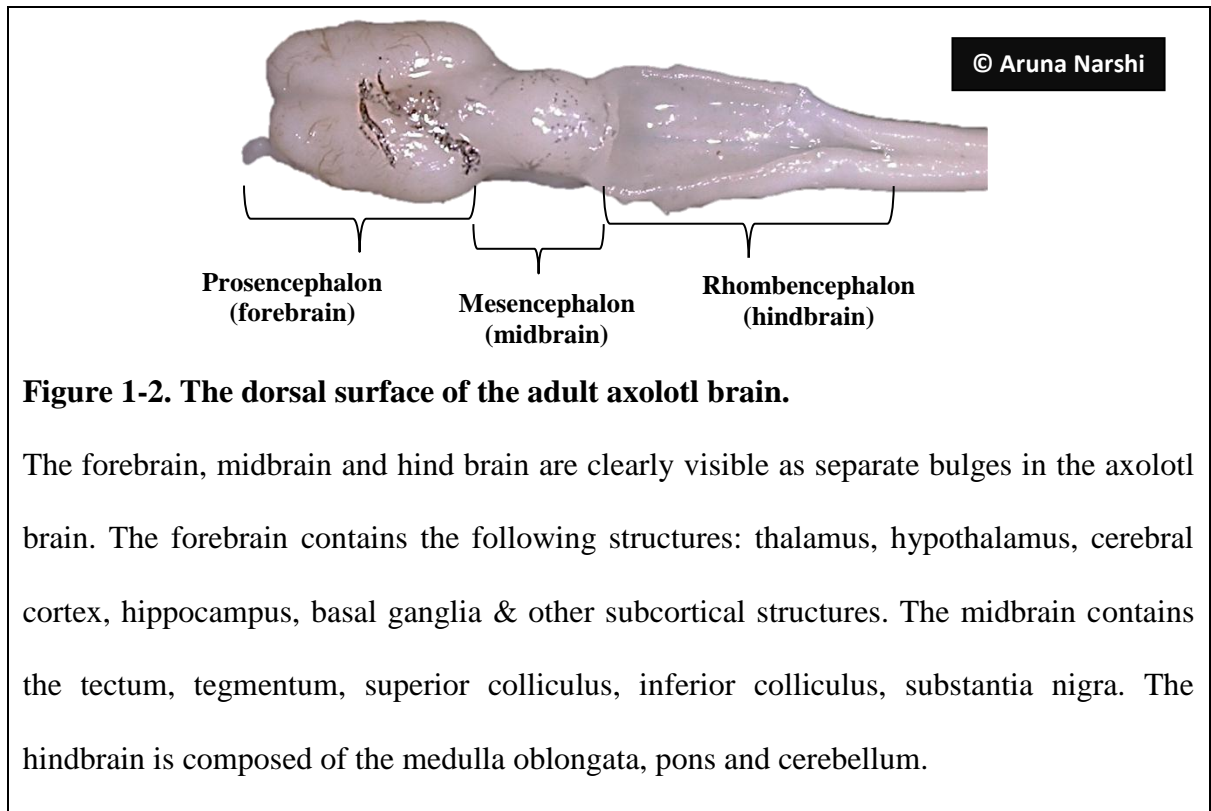


**Figure 1-2. The dorsal surface of the adult axolotl brain.**

The forebrain, midbrain and hind brain are clearly visible as separate bulges in the axolotl brain. The forebrain contains the following structures: thalamus, hypothalamus, cerebral cortex, hippocampus, basal ganglia & other subcortical structures. The midbrain contains the tectum, tegmentum, superior colliculus, inferior colliculus, substantia nigra. The hindbrain is composed of the medulla oblongata, pons and cerebellum.

### **1.2a The hindbrain**

The hindbrain is the most posterior part of the brain and consists of the medulla, the pons and the cerebellum. The medulla oblongata is the enlargement where the spinal cord enters the brain and is located in the skull. Through the cranial nerves emanating from the reflex centres, the medulla controls a number of vital reflexes, such as breathing, heart rate, vomiting, salivation, coughing and sneezing. The cranial nerves include both sensory and motor components, although some include just one or the other (see Table 1-1). The branches of cranial nerve X, the vagus nerve, supply organs in the thoracic and abdominal

cavities. The vagus nerve is the major nerve of the parasympathetic nervous system. Each cranial nerve originates in a nucleus or ‘centre’ (a cluster of neurons within the central nervous system) that integrates the sensory information and regulates the motor output. The cranial nerve nuclei for nerves V through XII are located in the medulla and pons of the hindbrain. Those for cranial nerves I through IV are located in the midbrain and forebrain.

**Table 1-1. Functions of the cranial nerves of humans.**

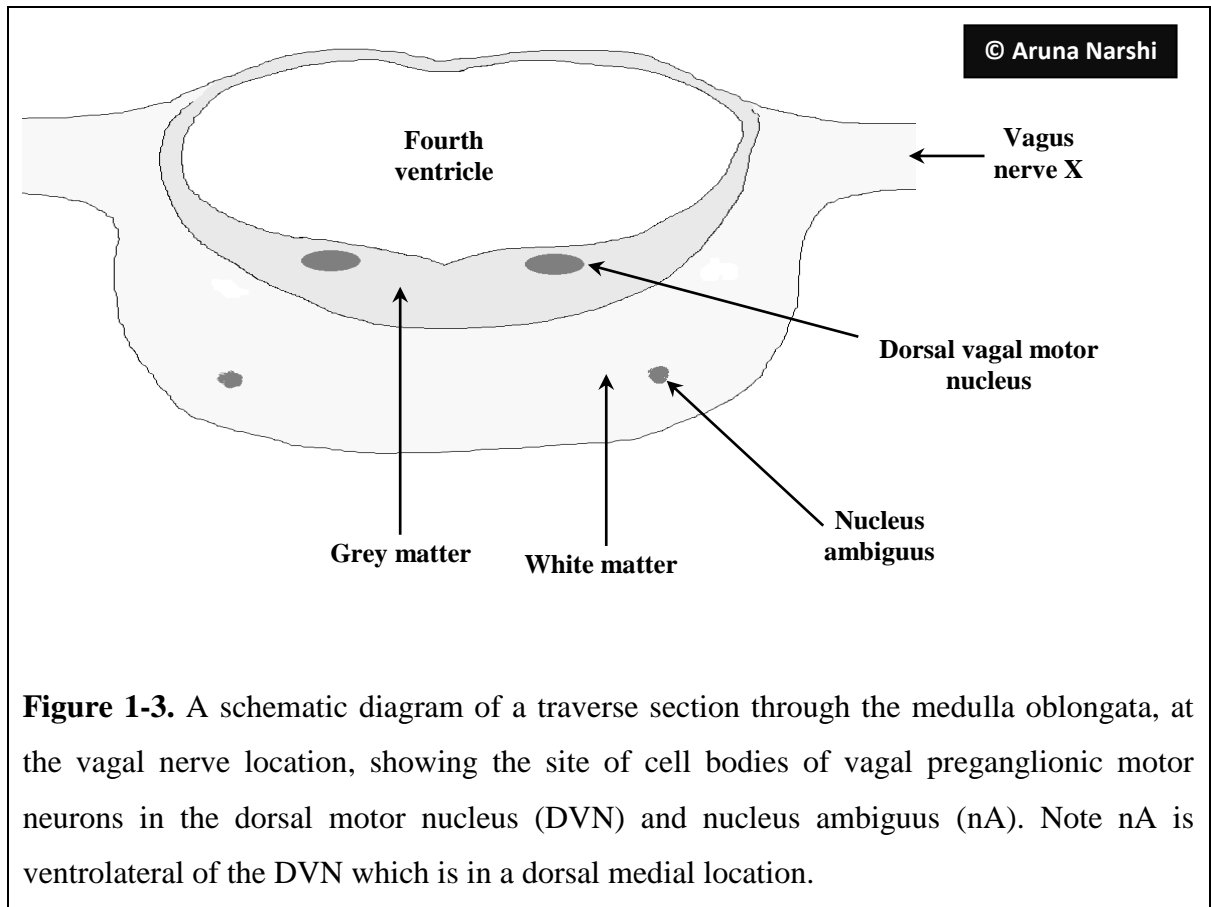
<i>Number and Name</i>	<i>Function of sensory Component</i>	<i>Function of Motor Component</i>
<b><i>I Olfactory</i></b>	Smell	(no motor nerve)
<b><i>II Optic</i></b>	Vision	(no motor nerve)
<b><i>III Oculomotor</i></b>	Sensations from eye muscles	Eye movements, pupil constriction
<b><i>IV Trochlear</i></b>	Sensations from eye muscles	Eye movements
<b><i>V Trigeminal</i></b>	Sensations from skin of face, nose, and mouth	Chewing, swallowing
<b><i>VI Abducens</i></b>	Sensations from eye muscles	Eye movements
<b><i>VII Facial</i></b>	Taste from the anterior two-thirds of the tongue, visceral sensations from the head	Facial expressions, crying, salivation, and dilation of blood vessels in the head
<b><i>VIII Statoacoustic</i></b>	Hearing, equilibrium	(no motor nerve)
<b><i>IX Glossopharyngeal</i></b>	Taste and other sensations from throat and posterior third of tongue	Swallowing, salivation, dilation of blood vessels
<b><i>X Vagus</i></b>	Taste and sensations from neck, thorax, and abdomen	Swallowing, control of larynx, parasympathetic nerves to heart and viscera
<b><i>XI Accessory</i></b>	(no sensory nerve)	Movement of shoulders and head; parasympathetic to viscera
<b><i>XII Hypoglossal</i></b>	Sensation from tongue muscles	Movement of tongue

The pons lies anterior to the medulla; like the medulla, it contains the nuclei for several cranial nerves. The term ‘pons’ is Latin for ‘bridge’; the name reflects the fact that many axons in the pons cross from the left side of the brain to the right, or from the right to the left. The medulla and pons also contain the reticular formation and the raphe system. These systems send axons diffusely through the forebrain, controlling the overall state of nervous arousal.

The cerebellum is an outgrowth of the medulla oblongata. It is best known for its contributions to the control of motor activity associated with limb movement, maintaining posture, and spatial orientation. The relative size of the cerebellum can vary among the vertebrata. Birds and mammals have a large cerebellum which is a reflection of complex locomotor patterns and a common evolutionary history of limb development of phylogeny as terrestrial vertebrates (Yopak *et al.*, 2010). Amphibians often have a rudimentary cerebellum, reflecting their relatively simple locomotor patterns (Taylor *et al.*, 1995).

### **1.2b The tenth cranial nerve**

The cranial nerve nuclei form in the periventricular zone within the medial (motor) and lateral (sensory) regions in the developing brain of vertebrates. Autonomic preganglionic parasympathetic neurons develop in the periventricular grey. This region is the future dorsal vagal motor nucleus (DVN) and in some cases, they migrate out to a ventrolateral position to form the future nucleus ambiguus (nA) (Macchi *et al.*, 2002; Friedland *et al.*, 1995; Brown, 1990). Branchiomic (muscles derived from gill arches) motor nuclei initially develop in the periventricular grey too and then they migrate to occupy the ventrolateral position, nA, in the adult. In adults the nA consists of a thin column of motor neurons in the medulla oblongata. (see Figure 1-3 for relative location of DVN and nA). Detailed images of these areas in the axolotl brain are recorded in Chapter 7).



In humans, and in most other vertebrates, the vagus nerve has sensory axons leading to the brain as well as motor axons leading to the heart and smooth muscles of the visceral organs in the thorax and abdomen. The word ‘vagus’ arises from the word ‘vagrant’ which means wandering from place to place. Its wandering course commences from the brain stem and through organs in the neck, thorax and abdomen. The nerve exits the brain stem through rootlets in the medulla oblongata. As stated earlier the branchial-motor component of the vagus nerve originates in the medulla in the nA and the visceromotor (parasympathetic component) of the vagus nerve originates from the DVN in the dorsal medulla. These cells give rise to axons that travel in the vagus nerve. The visceromotor part of the vagus innervates ganglionic neurons which are located in or adjacent to each target organ.

The target organs for the axons originating from the nA are in the head-neck and include glands of the pharynx and larynx (via the pharyngeal and internal branches). The nA is thought to be important in the regulation of airways (Dergacheva *et al.*, 2010; Kohn *et al.*, 2009; Chen *et al.*, 2007). The DVN acts, through branches entering the thorax, on the lungs for bronchoconstriction, the oesophagus for peristalsis, and the heart for slowing of heart rate. In the abdomen branches enter the stomach, pancreas, small intestine, large intestine and colon for secretion and constriction of smooth muscle. The viscerosensory components of the vagus are derived from nerves that have receptors in the abdominal viscera, oesophagus, heart and aortic arch, lungs, bronchia and trachea. The chemo- and baroreceptor inputs reach the nucleus solitarius (an area lateral to DVN) bringing and processing sensory visceral inputs to cranial nerve nuclei of X and IX (e.g. from the carotid body and sinus) via the solitary tract. So it can be seen that the vagus nerve is composed of both motor and sensory fibres.

### **1.3 OVERVIEW OF THE VERTEBRATE NERVOUS SYSTEM**

#### **1.3a Central nervous system**

All vertebrate nervous systems have some fundamental similarities in central and peripheral elements and a high degree of cephalisation. The brain and the spinal cord make up the central nervous system (CNS). The brain is important in integrating information transmitted from the surrounding environment through an array of sensitive receptors and is housed and protected within the skull. The spinal cord is protected in the vertebral column and it too is involved in relaying messages to and from the brain to the rest of the body. The spinal cord can also by-pass the brain completely and elicit spinal reflexes that

serve important survival value. An example of this is the withdrawal reflex when we are subjected to a sudden painful stimulus.

Axons within the CNS are located in well-defined tracts. They have myelin sheaths which give them a whitish appearance, hence the name white matter in the brain. The grey matter of the CNS is where nerve cell bodies, dendrites, and un-myelinated axons can be found. The narrow central canal of the spinal cord is continuous with cerebrospinal fluid-filled spaces, called the ventricles, in the brain (see Figure 1-3).

### **1.3b Peripheral nervous system**

The cranial nerves discussed earlier, along with spinal nerves, form the peripheral nervous system (PNS). These nerves and associated ganglia innervate the whole body. See Table 1-1 for the functions of the cranial nerves of humans. Mammals have 12 pairs of cranial nerves and 31 pairs of spinal nerves; hence the complexity of the PNS is subdivided into a hierarchy of components based on function (Figure 1-4).



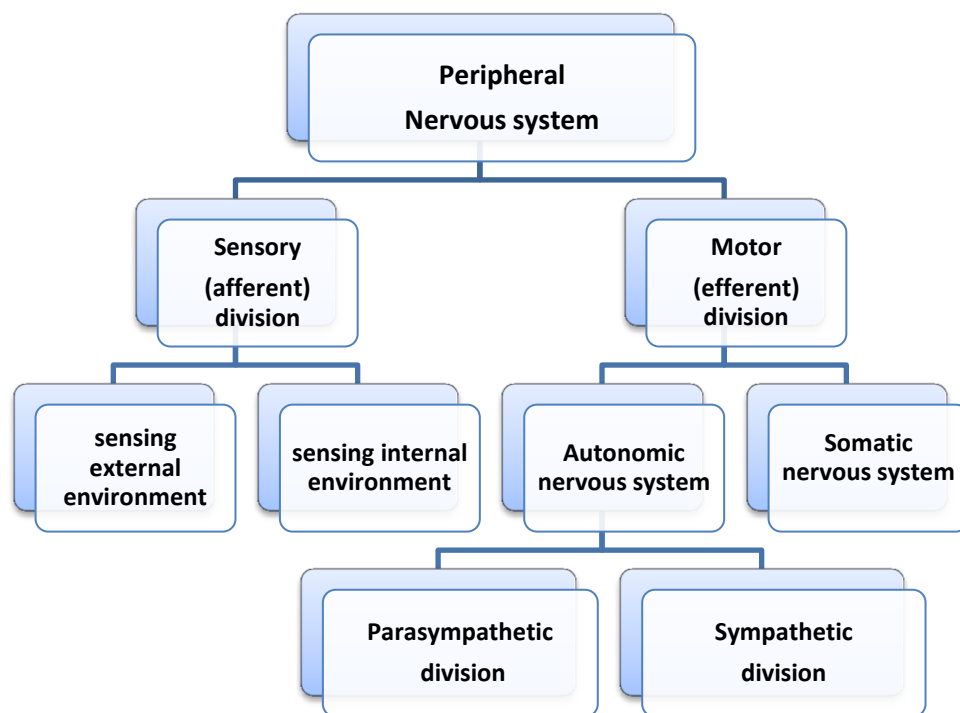


**Figure 1-4. Functional hierarchy of the peripheral nervous system.**

The nerves and ganglia of the vertebrate PNS convey information throughout the body. Sensory and motor divisions of the PNS are organised into a functional hierarchy.

### 1.3c Autonomic nervous system

The autonomic nervous system (ANS) is a set of neurones that receives information from and sends commands to the heart, intestines, and other organs. It is composed of two parts: the sympathetic and parasympathetic divisions. The sympathetic nervous system consists of two paired chains of ganglia lying just to the left and right of the spinal cord in its central regions (the thoracic and lumbar regions) and connected by axons to those spinal cord regions. Postganglionic axons extend from the sympathetic ganglia to the body's organs. The sympathetic nervous system prepares the body for 'fight or flight' activities by increasing heart and breathing rates and decreasing digestive activity.

The parasympathetic nervous system has functions that are related to, and generally opposite to, those of the sympathetic nervous system. The sympathetic and parasympathetic systems are usually active at the same time to varying degrees. However, at times parts of one system may be highly active along with parts of the other system. Table 1-2 illustrates the main differentiating characteristics of the sympathetic and parasympathetic divisions.

Sympathetic and parasympathetic preganglionic fibres release the same neurotransmitter, acetylcholine (ACh), but the postganglionic endings of these two systems release different neurotransmitters (the neurotransmitters that influence the effector organs). Parasympathetic postganglionic fibres release ACh and thus are called cholinergic fibres, along with all autonomic preganglionic fibres. Most sympathetic postganglionic fibres, in contrast, release noradrenaline and are called adrenergic fibres.

Postganglionic autonomic fibres do not end in a single terminal swelling like a synaptic knob. Instead, the terminal branches of autonomic fibres contain numerous swellings, or varicosities, that simultaneously release neurotransmitter over a large area of the innervated organ rather than on single cells. Thus whole organs instead of discrete cells are influenced by the autonomic activity, especially since the diffuse release of neurotransmitter is coupled with the fact that any resulting change in electrical activity is spread throughout a smooth- or cardiac-muscle mass via gap junctions.

**Table 1-2. Distinguishing features of the sympathetic and parasympathetic nervous systems**

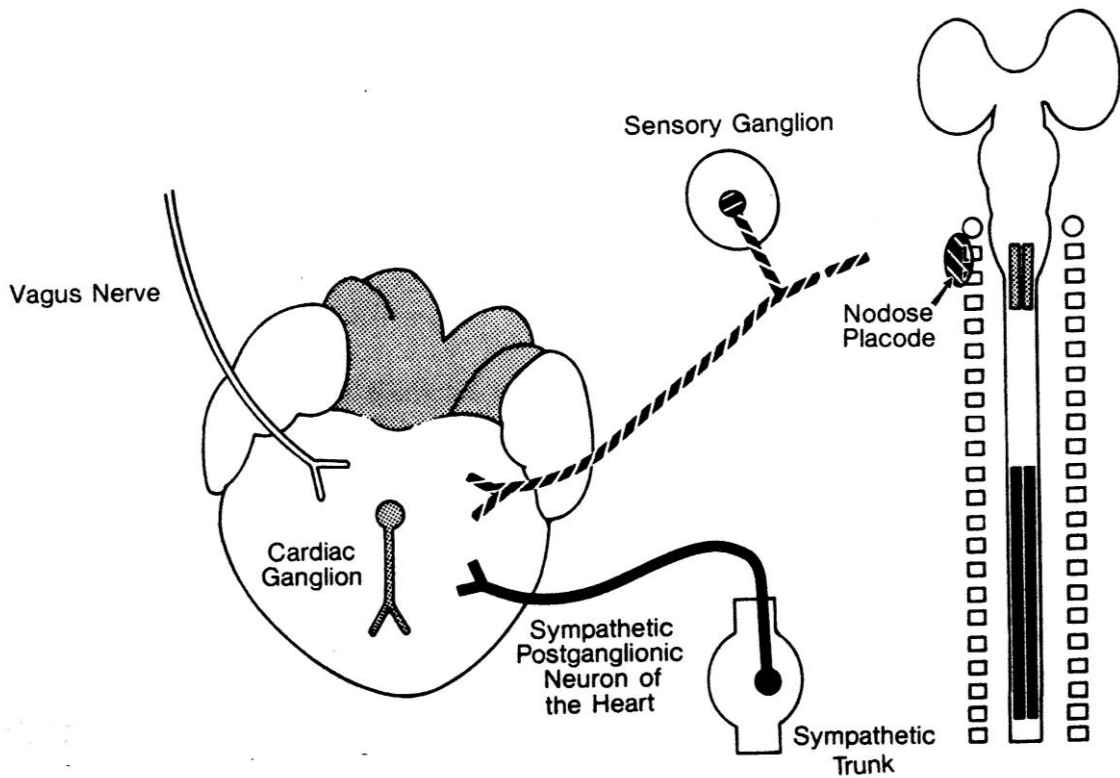
<i>Feature</i>	<i>Sympathetic system</i>	<i>Parasympathetic system</i>
<b>Origin of preganglionic fibre</b>	Thoracic and lumbar regions of spinal cord	Brain and sacral region of spinal cord
<b>Origin of postganglionic fibre (location of ganglion)</b>	Sympathetic ganglion chain (near spinal cord) or collateral ganglia (about halfway between spinal cord and effector organs)	Terminal ganglia (in or near effector organs)
<b>Length and type of fibre</b>	Short cholinergic preganglionic fibres Long adrenergic postganglionic fibres (most) Long cholinergic postganglionic fibres (few)	Long cholinergic preganglionic fibres Short cholinergic postganglionic fibres
<b>Effector organs innervated</b>	Cardiac muscle, almost all smooth muscle, most exocrine glands, and some endocrine glands	Cardiac muscle, most smooth muscle, most exocrine glands, and some endocrine glands
<b>Types of receptors for neurotransmitters</b>	$\alpha$ , $\beta_1$ , $\beta_2$	Nicotinic, muscarinic
<b>Postganglionic neurotransmitter</b>	Mostly noradrenaline Few acetylcholine	Acetylcholine
<b>Dominance</b>	Dominates in emergency 'fight or flight' situations; prepares body for strenuous physical activity	Dominates in quiet, relaxed situations; promotes 'general housekeeping' activities such as digestion
<b>Types of discharge</b>	Frequently mass discharge of whole system; may involve only discrete organs	Normally involves discrete organs rather than mass discharge

### 1.3d Development of cardiac neural control

The heart cannot be described as a fully functional unit until it has been innervated (with the exception of hagfish whose hearts are generally thought to be aneural (Augustinsson *et al.*, 1956; Carlson, 1904; Green, 1902; Jensen, 1965) although Hirsch *et al.* (1964) showed contradictory findings). Innervation of the heart permits regulation of cardiac cycle in tune with the rest of the body. The heart is innervated by the autonomic division of the peripheral nervous system, which develops from neural crest cells. All of the postganglionic neurons of the autonomic nervous system are derived from neural crest cells which migrate extensively during development and give rise to many different cell populations. The heart derives innervation from three sources (see Figure 1-5):

- The postganglionic parasympathetic innervation to the developing chick heart is via the cardiac ganglia. These can be identified around the fifth day of incubation in the bulbar region of the heart. In chicks, cardiac ganglia originate from cranial region (somites 1-2) of the vagal neural crest (somites 1-7) (Kirby, & Stewart, 1983).
- Sympathetic innervation is via the first to fourth thoracic sympathetic ganglia, which, again is derived entirely from neural crest.
- Sensory innervation of the heart is from the nodose ganglion (also called the inferior vagal ganglion), which is the distal cranial ganglion of the vagus nerve. It is derived from cells of the nodose placode (cellular thickening of the ectoderm) and is located laterally and slightly anteriorly to the cardiac neural crest.

**Figure 1-5. Diagram mapping the origin of the various components of the cardiac innervation.**



The parasympathetic postganglionic cholinergic neurons (cardiac ganglia) arise from cardiac neural crest; sympathetic postganglionic adrenergic neurons arise from trunk neural crest (somites 10-20); sensory innervation arises from the nodose placode.

*Taken from Kirby (1988)*

There are a number of factors that have been implicated in the development of the peripheral autonomic nervous system. These include glial-derived neurotrophic factor (Moore *et al.*, 1996); transcription factor Mash1 (Hirsch *et al.*, 1998), and the homeobox containing transcription factor Phox2b (Pattyn *et al.*, 1999) which are necessary for the differentiation and survival of subsets of autonomic neurons.

The ontogenetic development of autonomic innervation of the heart has been studied in most detail in the developing chick embryo (Pappano, 1977; Kirby, McKenzie & Weidman, 1980). They have shown that the heart is responsive to adrenaline and acetylcholine several stages before functional innervation (in Fritsche, 1997). It appears that the adrenergic- and acetylcholine-sensitive receptors differentiate long before effective innervation. It may be that the receptors guide the developing nerve fibres to form postganglionic autonomic varicosities. Observing the development of innervation when the receptors are blocked or activated could test this hypothesis. Interesting experiments to this effect have been carried out by Wang and Halvorsen (1998) who suggest that ciliary neurotrophic factor and its receptor may be involved in the formation of parasympathetic synapses in chick atria.

The chronological sequence of the development of parasympathetic innervation of the chick embryo heart begins with the appearance of receptors for acetylcholine and the activating enzyme acetyl-cholinesterase on day two. On day six the cholinergic neurons grow within the sino-atrial node and the release of acetylcholine is first detected on day ten. It is on day 12 that functional vagal transmission and the appearance of the acetylcholine synthesising enzyme, choline acetyltransferase, is observed. On day 21 the chick hatches (Pappano, 1977). The development of the sympathetic cardiac innervation follows the same sequence as the parasympathetic innervation, except that effective neurotransmission occurs later when compared with the parasympathetic system (Kirby, McKenzie & Weidman, 1980; Verberne *et al.*, 1999). This would mean that the heart rate was only controlled by parasympathetic discharge in the early embryonic stages, or by circulating catecholamines, rather than neurogenic. However, it was found that, in

embryonic chicks, the vagus played no role in CV control and so it appears that CV development occurs in the absence of tonic vagal input (Crossley & Altimiras, 2000). Furthermore, blockade of  $\beta$ -adrenergic receptors resulted in bradycardia in the absence of functional sympathetic efferents to the heart, supporting the idea of there being circulating catecholamines that results in embryonic chicks developing under  $\beta$ -adrenergic tone (Crossley & Altimiras, 2000).

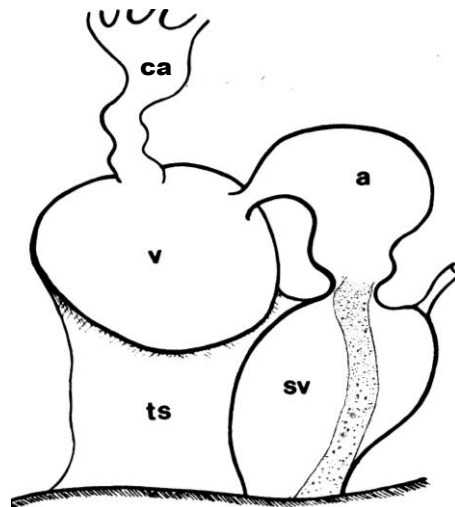
In humans and other animals a similar chronological sequence of autonomic development occurs. The embryonic period in humans lasts eight weeks. During the fourth week neural crest cells begin to migrate away from the neural tube. Although innervation of the heart occurs from about 6-7 weeks gestation (Larsen, 1997), a functional cardiac nerve supply is not present at this time. Effective neurotransmission of the heart occurs from around 4 months gestation (Navaratnam, 1965) and, as in the chick and other animal species, parasympathetic neurotransmission occurs prior to the sympathetic.

The development of cardiac innervation in *Ambystoma mexicanum* has been studied by Melinek & Mirolli (1988) (see Figure 1-6 for heart morphology). They looked at axolotls from hatchling to 12-months of age and noted that there were marked changes in the pattern of innervation with age. Both cholinergic (parasympathetic) and catecholaminergic (sympathetic) staining were absent before hatching. A few days after hatching cholinergic fibres and neurons stained, which was considerably earlier than for catecholaminergic fibre staining. However, both the cholinergic and catecholaminergic innervation of the heart are poorly developed at hatching and only reach their mature state after a few months. The catecholamine found was norepinephrine (approximately 0.5  $\mu\text{g/g}$  in the atria; 0.6  $\mu\text{g/g}$  in

the sinus venosus; 0.2 µg/g in the ventricle), and was confirmed by the presence of its precursor dopamine at the expected concentrations. No neurons containing 5-hydroxytryptamine was found. The number and arborisations of both sets of preganglionic fibres increase during the first 3 months post-hatching. The number of postganglionic parasympathetic neurons also increased considerably during this period. It is unclear if the increase in fibres and neurons is due to a continuous migration of neuroblasts into the heart or whether all or some of the neuroblasts present in the earliest developmental stages continue to divide after hatching. Indeed, both factors may be operating as described in *Xenopus* (Heathcote & Sargent, 1984). Thus, it appears that the development of the innervation of the axolotl heart follows the same pattern as that known for other vertebrates, including mammals (Pappano, 1977).



**Figure 1-6. Ventral view of a young larval axolotl heart.**



The heart consists of four chambers in series: sinus venosus (sv), atrium (a), ventricle (v) and continuous with this, the conus arteriosus (ca). A thin sheet of connective tissue (ts) is found between the sinus venosus and the ventricle and the posterior wall of the pericardium. The cardiac ganglion is found in the tissue sheet and in the dorsal wall of the sinus venosus. The ventral side of the sinus venosus is mainly composed of muscular tissue and contains the pacemaker region. The shaded area indicates the position of the large hepatic vein which opens directly into the atrium. The authors found that the atrium was incompletely divided into two chambers by a thin muscular septum in the young axolotl (body length 1.5 cm).

*Modified from Melinek & Mirolli (1988)*

Intriguingly, the changes in cardiac innervation associated with amphibian metamorphosis appear not to have been studied. Yet, metamorphosis is a very important developmental process. Knowledge of the control of the cardio-respiratory system in larval and adult amphibians could help in understanding the major evolutionary conversions that occur in the control of ventilation between fish with gills and mammals with lungs. In the unmetamorphosed axolotl, the animal relies on its gills for gas exchange. Post metamorphosis, the axolotl is no longer aquatic and uses mainly its lungs for ventilation. Thus, there may indeed be differences in heart innervation, especially since changes in the

cardio-respiratory centres of the brainstem, before and after metamorphosis, have already been noted; The cell bodies of preganglionic neurons of the vagus have shown to relocate ventro-laterally after metamorphosis (Taylor *et al.*, 2001), topologically similar to some lung breathers, thereby suggesting that this relocation may be associated with the predominantly lung ventilation.

#### **1.4 NERVOUS CONTROL OF HEART**

The following section predominantly relates to the mammalian heart, but is also true for most vertebrates. There are some relevant differences and these are highlighted and / or detailed in ‘The nervous control of the heart of vertebrates’ section.

Before the heart is innervated, it has a tendency to beat at an intrinsic rate, known as myogenic rhythmicity. This relates to heart muscle contractions which originate in the sino-atrial (SA) node, which is the pacemaker and driving force of the heart. The electrical signal travels across both atria causing them to contract almost simultaneously. Conduction then reaches the atrio-ventricular node (AV-node), down the Purkinje fibres of the bundle of His and along the right and left branches, down the ventricular septum to enter the Purkinje network that ramifies throughout the ventricles. Because of the extensive branching of the Purkinje network in the ventricles, excitation reaches all parts of both ventricles rapidly causing them to contract simultaneously.

The cardiovascular (CV) centres in the brain alter the intrinsic discharge rate of the SA-node by the dual innervation by antagonistic limbs of the autonomic nervous system

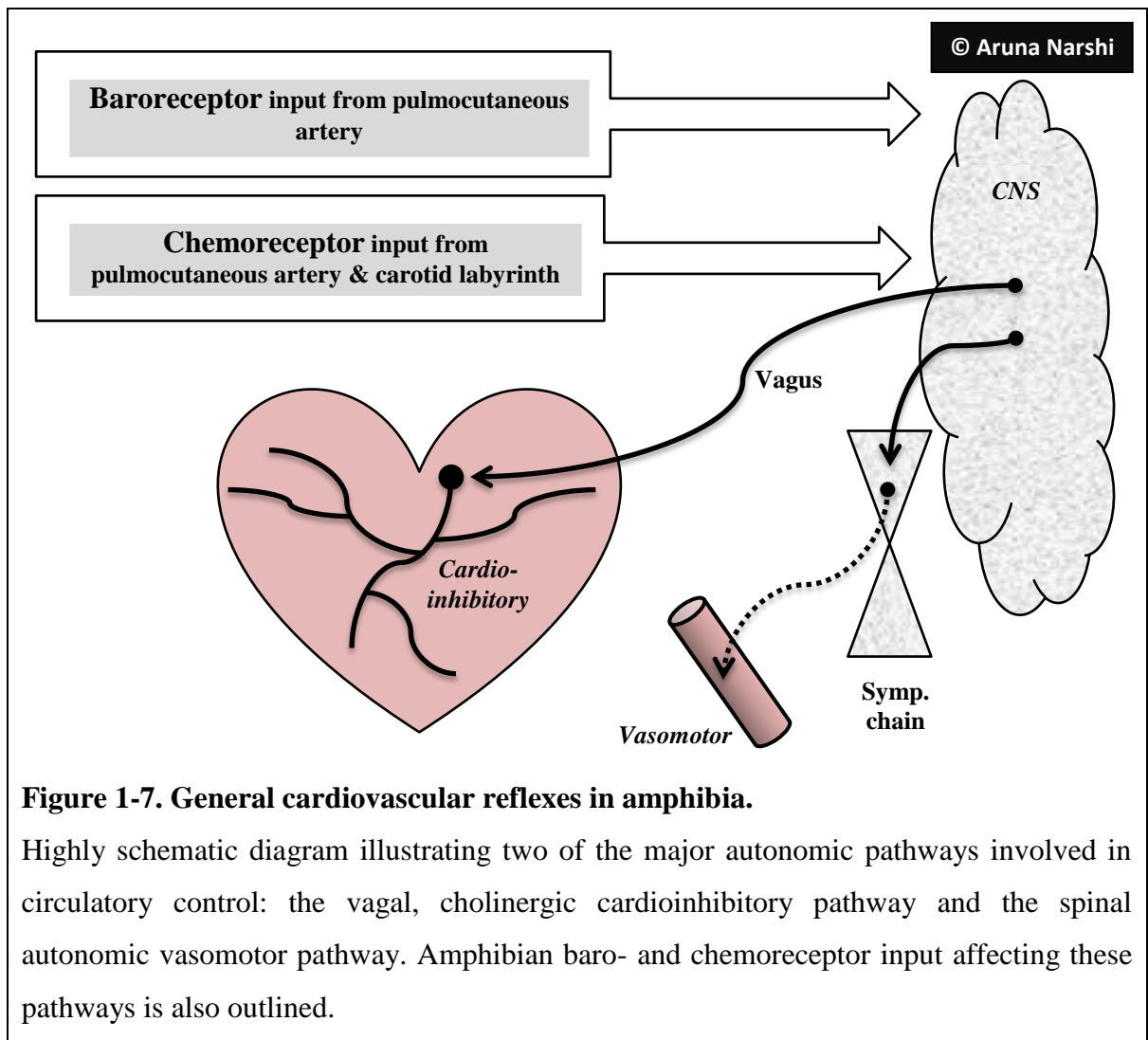
(Samaan, 1935; Glick & Braunwald, 1965). Both the sympathetic and parasympathetic limbs of the autonomic nervous system innervate the SA-node. The postganglionic sympathetic fibres release the neurotransmitter noradrenaline, and adrenaline is released from the adrenal medulla in response to increased sympathetic activity. These bind to  $\beta_1$ -adrenoceptors on plasma membranes of cardiac cells in the SA-node. Sympathetic stimulation results in an increase in heart rate and a rise in the force of cardiac contraction. Acetylcholine, the transmitter released by the parasympathetic fibres, acts on  $M_2$ -muscarinic cholinceptors in the SA-node and causes a decrease in heart rate and a fall in cardiac contractility. Other parts of the heart also receive sympathetic and parasympathetic fibres. For instance, the Purkinje fibres and ventricular muscle receive mainly sympathetic innervation. See Table 1-3 for a summary of the autonomic control of the heart rate.

**Table 1-3. Effects of the autonomic system on the heart and structures that influence the heart.**

<i>Area affected</i>	<i>Effect of parasympathetic stimulation</i>	<i>Effect of sympathetic stimulation</i>
<b>SA node</b>	Decreases rate of depolarisation to threshold; decreases heart rate	Increases rate of depolarisation to threshold; increases heart rate
<b>AV node</b>	Decreases excitability; increases AV nodal delay	Increases excitability; decreases AV nodal delay
<b>Ventricular conduction pathway</b>	No effect	Increases excitability; hastens conduction through bundle of His and Purkinje cells
<b>Atrial muscle</b>	Decreases contractility; weakens contraction	Increases contractility; strengthen contraction
<b>Ventricular muscle</b>	No effect	Increases contractility; strengthen contraction
<b>Adrenal medulla</b>	No effect	Promotes adrenomedullary secretion of adrenaline, which augments the sympathetic nervous system's actions on the heart
<b>Veins</b>	No effect	Increases venous return, which increases strength of cardiac contraction through the Frank-Starling mechanism

The parasympathetic nerve fibres project to the heart in the vagus nerve, and thus their normal activity is often referred to as vagal tone. Bradycardia, for example during sleep, can be due to an increase in parasympathetic discharge and a decrease in, or absence of, sympathetic discharge. In mammals, vagal dominance often predominates and varies under the influence of central and peripheral inputs so that the heart beats at a rate generally slower and more variable than the intrinsic pacemaker rate. The opposite changes in autonomic activity lead to tachycardia, which may occur during stress. Alterations in heart rate are referred to as chronotropy, and a positive chronotrope, such as atropine, increase the heart rate by acting on the SA-node, whereas as propranolol is an example of a negative chronotrope. Propranolol is also a negative inotrope as it blocks  $\beta$ -adrenergic receptors. Inotropes alter the force of muscle contraction and so beta blockers weaken the force of muscular contractions of the heart.

The changes in activity and the associated demands of the tissues are reflected in the relatively large variation in heart rate and cardiac output. The medullary control of the autonomic nervous system has various cardiovascular reflexes that alter heart rate accordingly. For instance, the baroreceptor reflex acts as a buffer which protects the body from excessive swings in systemic arterial pressure. These baroreceptors are located in the carotid sinus and aorta. When there is a rise in pressure the baroreceptors elicit an inhibitory effect on the cardiovascular system which promotes a fall in blood pressure. In amphibians, baroreceptors that trigger a cardioinhibitory reflex reside in the carotid labyrinth and in the pulmocutaneous artery (Figure 1-7) from which sensory fibres run in the laryngeal nerve (Jones & Milsom, 1982). In humans there are also chemoreceptors located in the carotid and aortic bodies which detect changes in oxygen, carbon dioxide and pH in the circulation. Chemoreceptors in amphibians have been unequivocally demonstrated within the complex vasculature of the carotid labyrinth (Smith *et al.*, 1981). The effect of chemoreceptors is primarily on the respiratory system, which will be discussed later. While baroreceptor reflexes directly affect the generation of blood pressure in the vertebrates, the chemoreceptor reflexes are to a major extent, involved in ventilatory control mechanisms. Both central and peripheral receptor sites have been demonstrated in a number of vertebrate groups, but our knowledge of their relationship with the efferent (autonomic) pathways is rudimentary in the non-mammalian groups.



The heart itself has receptors that reflexively alter its rate. At the junction of the vena cava and right atrium are atrial mechano- (stretch) receptors that detect atrial distension. When stimulated they cause tachycardia via vagal afferent and sympathetic efferent pathways, a phenomenon known as the Bainbridge reflex (Bainbridge, 1915). These receptors, when activated lead to reflex diuresis which regulates blood volume. Bainbridge found that baroreceptor stimulation, upon a fall in blood pressure, resulted in a decrease in heart rate in dogs. The Bainbridge reflex is also known to be involved in respiratory sinus arrhythmia (RSA) where the heart rate rises due to an increase in intrathoracic pressure upon

inspiration. Furthermore, the heart has an intrinsic ability to increase the force of contraction when the cardiac muscle is stretched. For instance, when there is an increased volume of blood entering the ventricle, the cardiac muscle contracts more forcefully. This is known as the Frank-Starling law. Of course, heart rate changes occur during integrated processes too, such as during physical exercise, emotion, digestion, and hormonal influences. These changes are mediated by more complex mechanisms with interactions between higher brain centres, centres in the mid-brain, and control centres in the medulla, which is detailed later. Thus, variation in heart rate may be considered a good indicator of the functioning of the physiological system.

#### **1.4a Innervation of vertebrate hearts**

In all vertebrates, with the exception of the myxinooids (hagfish), the heart is innervated by branches from the vagus nerve. However, the way in which the vagus nerve controls the heart differs considerably between the vertebrate groups. It is useful to start with the heart of cyclostomes when studying the evolution of sympathetic and parasympathetic cardiac innervation.

##### **1.4a.i Cyclostomes**

Cyclostomes are lampreys (lampetrooids) and hagfish (myxinooids). The myxinooids have neither a sympathetic nor a parasympathetic supply (Green, 1902; Carlson, 1904; Augustinsson *et al.*, 1956; Jensen, 1965) and are insensitive to drugs which exert marked cardiac effects in other vertebrates. Although the Pacific hagfish (*Eptatretus stoutii*) may be an exception as nerves in the heart and adjacent to it have been reported (Hirsch *et al.*,

1964). The lampetroid heart is innervated by a branch of the vagus nerve (Ransom and Thompson, 1886; Augustinsson *et al.*, 1956) like all other fish hearts.

Unusually amongst vertebrates, vagal stimulation and its subsequent release of acetylcholine, results in an *acceleration* of the heart with an accompanying decrease in the force of contraction (Falck *et al.*, 1966) in lampetroids. The same effect results from nicotinic cholinceptor agonists, such as nicotine (Augustinsson *et al.*, 1956; Falck *et al.*, 1966). Nicotinic cholinceptor antagonists such as tubocurarine and hexamethonium can be used to block the excitatory effect of vagal stimulation or nicotinic agonists (Augustinsson *et al.*, 1956; Falck *et al.*, 1966; Lukomskayo & Michelson, 1972). Drugs adrenaline, noradrenaline, isoprenaline and tyramine also stimulate the lampetroid heart, although the effects are less pronounced than that of acetylcholine. Since the effect of the adrenergic agonists is blocked by propranolol in lampetroids, this suggests that the effect must be through  $\beta$ -adrenoceptors as in the higher vertebrates (Augustinsson *et al.*, 1956; Nayler & Howells, 1965; Falck *et al.*, 1966).

#### **1.4a.ii Elasmobranchs**

Elasmobranchs (cartilaginous fishes, e.g., sharks, dogfishes, skates and rays) are the earliest group of vertebrates in which there is an inhibitory vagal innervation of the heart. There are two pairs of cardiac nerves that supply the heart; one from the fourth branchial branch of the vagus and the other one arises close to the origin of the visceral branch of the vagus. The two cardiac vagi run closely together into the ductus Cuvieri and then break up into an interwoven plexus on the sinus venosus, terminating at the junction with the atrium



(Young, 1933). In elasmobranchs the site of the pacemaker appears to be at the sino-atrial node (Rybak & Cortok, 1956; Satchell, 1971).

There is no sympathetic innervation on the heart. However, it is thought that an adrenergic influence may be exerted by specialised catecholamine-storing endothelial cells in the sinus venosus and atrium. These cells are innervated by cholinergic vagal fibres (Saetersdal *et al.*, 1975; Pettersson and Nilsson, 1979). The stimulation of the vagus nerve has an inhibitory effect on the heart rate. The effect appears to be mediated by muscarinic cholinergic receptors as in higher vertebrates. The effects of adrenaline and noradrenaline in the elasmobranch heart are variable.

#### **1.4a.iii Teleosts**

Teleosts may be considered as the earliest group of vertebrates in which there is both sympathetic and parasympathetic control of the heart. As in the elasmobranchs the cardiac branches of the vagi follow the ductus Cuvieri to the sinus venosus and atrium. The vagal fibres do not reach the ventricle. As in all vertebrates, with the exception of cyclostomes, the vagus is cardio-inhibitory and releases acetylcholine onto muscarinic cholinergic receptors. Studies have found that the level of resting vagal tone decreases with increasing temperature, with adrenergic mechanisms taking over the cardio-acceleratory function at higher temperatures (Priede, 1974; Wood *et al.*, 1979). The positive chronotropic effects of adrenergic agonists and adrenergic nerves are mediated via  $\beta$ -adrenoceptor mechanisms (Randall & Stevens, 1967).

#### **1.4a.iv Amphibians**

The amphibian heart is innervated by vagal fibres and by fibres from the sympathetic chain ganglia that join near the cranium to form 'vagosympathetic trunks'. On each side of the animal the cardiac nerve leaves the visceral branch of the vagus nerve and reaches the atrial septum. The cholinergic vagal fibres have a negative chronotropic and inotropic effect in urodeles and anurans (Bidder, 1868; Gaskell, 1884; Kirby & Burnstock, 1969; Campbell *et al.*, 1982). Vagal tone on the heart seems to be seasonally regulated (Butler & Jones, 1982; Nilsson, 1983), with the toad having vagal inhibition during winter (Iriuchijima, 1959). The spinal autonomic fibres that enter the 'vagosympathetic trunk' of the amphibians are adrenergic and produce positive chronotropic and inotropic effects on the heart (Gaskell, 1884; Elliot, 1905; Loewi, 1921).

#### **1.4a.v Reptiles**

Reptilian hearts have inhibitory cholinergic vagal innervation, thus upon stimulation, negative chronotropic and inotropic effects are observed. These effects are mimicked by acetylcholine and blocked by muscarinic cholinergic antagonists such as atropine (Gaskell, 1884; Berger & Burnstock, 1979). Positive chronotropic and inotropic effects are mediated by adrenergic fibres of spinal autonomic origin that innervate the heart also.

#### **1.4a.vi Birds**

The avian heart has vagal and sympathetic innervation (Bolton, 1971; Bennett, 1974). The vagal fibres are cholinergic and, as in most vertebrates, they mediate negative chronotropic and inotropic effects on the heart. The adrenergic fibres work through the  $\beta$ -adrenoceptor mechanism and mediate positive chronotropic and inotropic effects on the heart (Johansen

& Reite, 1964; Bolton & Raper, 1966; Yamauchi, 1969; Bennett, 1974). Schwaber & Cohen (1978) have found that there are a greater proportion of myelinated fibres in avian cardiac nerves compared mammalian cardiac nerves. Also, when comparing birds with other vertebrates of similar size, the avian heart rate is very high.

#### **1.4a.vii Mammals**

Vagal nerves regulate cardiac rate and rhythm. There is variation in the anatomy of the peripheral cardiac nerves between different mammalian species (Randall & Armour, 1977). The mammalian heart has inhibitory cholinergic vagal innervation that have negative chronotropic and inotropic effects. These cholinergic fibres occur in the pacemaker region (SA-node) and in the atria, and are very scarce or absent in the ventricles, depending on species (Bolton & Raper, 1966). The level of vagal tone on the heart varies between different species. For instance, the cat has a relatively low level of vagal tone (Spyer, 1982).

Adrenergic fibres innervate the SA- and AV-nodes, atria and ventricles. In some species, as in the cat, the ventricle is richly innervated. In other species, particularly in hibernating mammals, the ventricular innervation is sparse (Nielsen & Owman, 1968). These fibres enter the heart mainly along the cardiac nerves from the sympathetic chains. However, there is also a substantial contribution by fibres entering the vagi from the superior cervical ganglia (Nielsen *et al.*, 1969; Campbell 1970; Prioloa *et al.*, 1981). The adrenergic fibres mediate positive chronotropic and inotropic responses on the mammalian heart via  $\beta_1$  and  $\beta_2$  adrenoceptors (Hedburg *et al.*, 1980).

## **1.5 OVERVIEW OF VERTEBRATE RESPIRATORY SYSTEMS**

Aquatic vertebrates can rely on, or use a combination of, cutaneous body surface, external filamentous gills, or internal lamellar gills for gas exchange. Some salamanders (and other vertebrates, such as crabs etc.) use bimodal breathing, which is the ability to exchange gases simultaneously with both air and water. They can use gills for water breathing and lungs for air breathing.

In those animals that made the evolutionary transition between aquatic and terrestrial habitats, bimodal breathing was an important respiratory adaptation. The transition from water- to air-breathing was accompanied by fundamental changes in the structure and function of the respiratory organs. Air-breathing terrestrial vertebrates have lungs instead of gills.

### **1.5a Cutaneous exchange**

Cutaneous gas exchange is carried out to supplement gill or lung ventilation by some aquatic vertebrates (such as aquatic turtles, salamanders with lungs, snakes, fish and mammals).

Most amphibians (e.g., frogs, toads, lungless salamander, and newts) have highly developed cutaneous exchange. In frogs, a uniform capillary network lies in a plane directly beneath the epidermis (Feder & Burggren, 1985; Moalli *et al*, 1980). This vascular arrangement facilitates gas exchange between the capillary bed and the environment by both diffusion and convection.

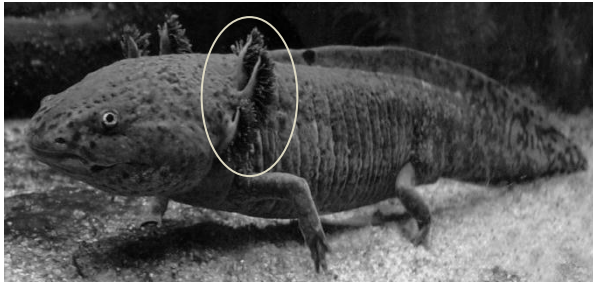
To facilitate this exchange, amphibian skin is kept moist and is protected from injury, thus potential infection, by a slimy, mucous layer (Parakkal & Matoltsy, 1964; Ramsey *et al.*, 2010).

### **1.5b Gills**

A gill is a respiratory organ of many aquatic animals (e.g. crustaceans, fishes, amphibians), a plate like or filamentous outgrowth well supplied with blood vessels at which gas exchange between water and blood occurs. Larval forms of a few fishes and amphibians have external gills projecting from their body (Figure 1-8), whereas adult fishes have internal gills.

Gas exchange in internal gills occurs as blood and water move in opposite direction. Behind the protective operculum are feathery internal gills. Each gill arch consists of many filaments. These filaments have capillaries within lamellae. The countercurrent flow allows the maximal amount of oxygen to be extracted from the water.

**Figure 1-8. External gills of the neotenic axolotl.** The enlarged section shows the fern-like fimbriae (gill filaments) on the 3 rami (stalks). The elaborate external gills have a large surface area for gas exchange.



[http://upload.wikimedia.org/wikipedia/commons/0/00/Axolotl\\_ganz.jpg](http://upload.wikimedia.org/wikipedia/commons/0/00/Axolotl_ganz.jpg)

### 1.5c Lungs

A lung is an internal organ that is specialised for the respiratory uptake of oxygen directly from the air. In vertebrates, lungs are present in air-breathing fishes (the lungfishes, Dipnoi), and tetrapods. In mammals the lungs are a paired mass of spongy tissue made up of finely divided airways lined with moist epithelium extending from the bronchi and ending in small sacs, the alveoli, providing a large surface area for gas exchange between air and bloodstream.

The evolution of the structurally complex lung has paralleled the evolution of the large body sizes and high metabolic rates found in endothermic vertebrates (birds and mammals), which necessitated an increase in lung surface area for gas exchange, compared

to the smaller body size and lower metabolic rates found in the ectothermic vertebrates. However it must be noted that the lungs of birds and mammals are quite different in form and function as detailed below and described by Torday *et al.* (2007) and West *et al.* (2007).

#### **1.5c.i Lung ventilation**

Vertebrates breathe to ventilate their lungs, the purpose of which is to maintain maximum oxygen concentration and minimum carbon dioxide concentration within the alveoli. There are two phases of pulmonary ventilation: inhalation and exhalation.

#### **1.5c.ii Positive pressure breathing**

Frogs have muscles that lower the floor of the buccal cavity, causing it to enlarge, and to draw air in through the nares. The nares and mouth close and the floor of the buccal cavity rises thereby forcing air down the trachea. Hence frogs ventilate their lungs by actually pushing air down the windpipe and this is called positive pressure breathing (Brainerd & Owekowicz, 2006). During exhalation the air is forced back out by elastic recoil of the lungs and compression by the muscles of the body wall.

#### **1.5c.iii Negative pressure breathing**

Mammals ventilate by pulling air, instead of pushing it, down into the lungs. This is known as negative pressure breathing. The result is changes in the volume of the lungs (as opposed to the buccal cavity seen in frogs). During inspiration, external intercostal muscle contraction lifts the ribs up and out and the diaphragm, the major inspiratory muscle, contracts and flattens (Milsom *et al.*, 2004; Klein and Owekowicz, 2006). The diaphragm

is a sheet of skeletal muscle that is innervated by the phrenic nerve and the intercostal muscles are innervated by intercostal nerves. In the relaxed state the diaphragm is dome shaped protruding upwards. These movements increase the size of the thoracic cavity and decrease the pressure to below that of the atmosphere (barometric) around the lungs. This negative pressure causes air to rush into the lungs and they inflate. Expiration follows relaxation of the rib cage and diaphragm muscles, as the increased pressure in the thoracic cavity forces the air out of the lungs. This is achieved by the elastic lungs contracting and compressing the air in the alveoli. With this compression, the alveolar pressure becomes greater than atmospheric pressure causing air to be expelled from the lungs. So lung the air moves down a pressure gradient.

#### **1.5c.iv Ventilation in birds**

Birds have lungs and eight or nine air sacs, some of which are posterior to the small pair of lungs (abdominal air sacs), and others that are anterior to the lungs (thoracic). The air sacs act as bellows that keep air flowing through the lungs. The lungs and air sacs are ventilated when the bird inhales and exhales. The main bronchus that runs through each lung is connected to air sacs, as well as to the lung. During inhalation and exhalation, the air flows through the interconnected system in a circuit that passes through the lungs in one direction only. For instance, during inhalation the posterior air sac fills, causing the air that was in there to move to the lung, and the air that was in the lung moves into the anterior air sac that is empty (after the previous exhalation). During exhalation the air that was in the anterior air sac is expelled into the air and the cycle begins again. Therefore, two full breathing cycles are needed to move the volume of gas taken in during a single inhalation through the entire system out of the body.



## 1.6 AUTONOMIC CONTROL OF BREATHING

Hearts have intrinsic pacemaker cells that enable it to generate its own rhythm. The brain serves only to modify the rate and strength of contraction. In contrast, the pacemaker activity that establishes the rhythmicity of breathing resides in the respiratory control centres in the brain and not in the lung or respiratory muscle themselves. Therefore, nerve supply to the respiratory system is essential in maintaining breathing cycles which are achieved by a central rhythm generator within the respiratory centres (Figure 1-9).

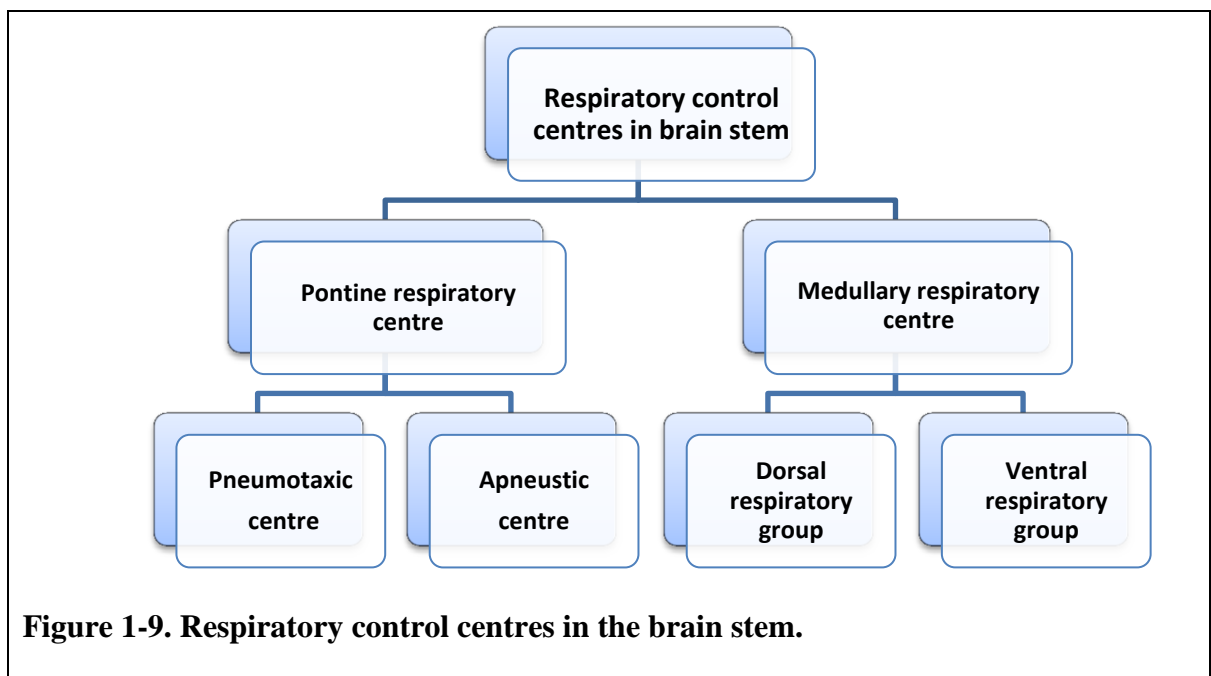


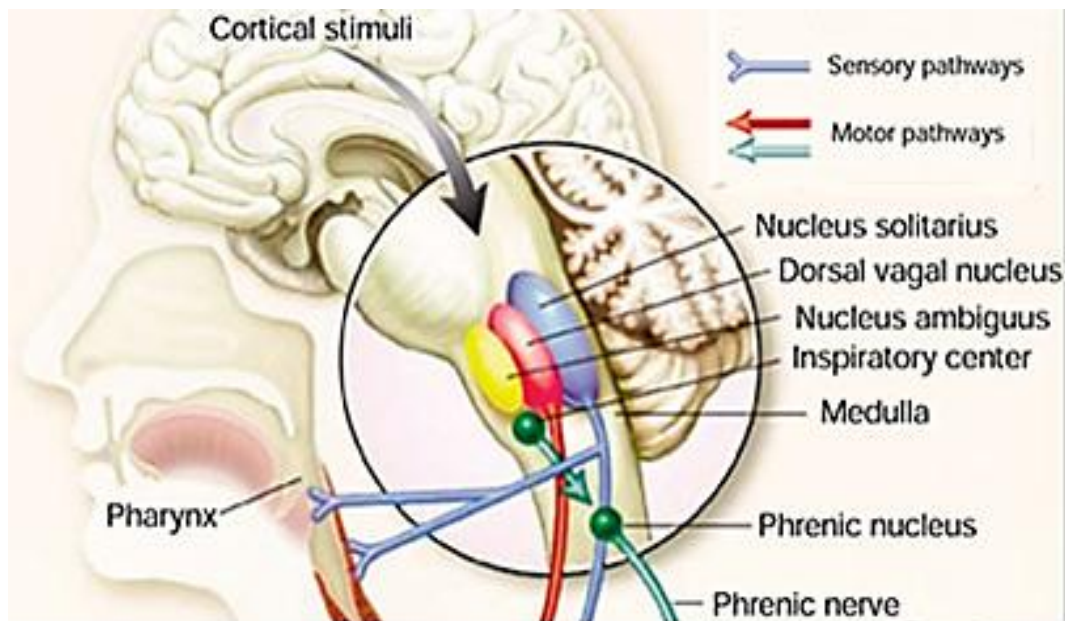
**Figure 1-9. Respiratory control centres in the brain stem.**

The diaphragm and the muscles between the ribs are activated by the phrenic nerve and spinal motoneurons respectively. They receive inputs from groups of neurons that constitute the medullary respiratory centres. There are three distinct components to the neural control of respiration:

### 1.6a (1) Alternating inspiration / expiration rhythm.

In the pons there are two other respiratory centres, the apneustic and pneumotaxic (Figure 1-10). These pontine centres have an influence on the output from the medullary respiratory centre.

**Figure 1-10.** Diagram of the medulla oblongata showing the topographical proximity of the main nuclei that are involved in cardiorespiratory interactions. The pneumotaxic and apneustic centres are located in the pons (around where the large black arrowhead is pictured).



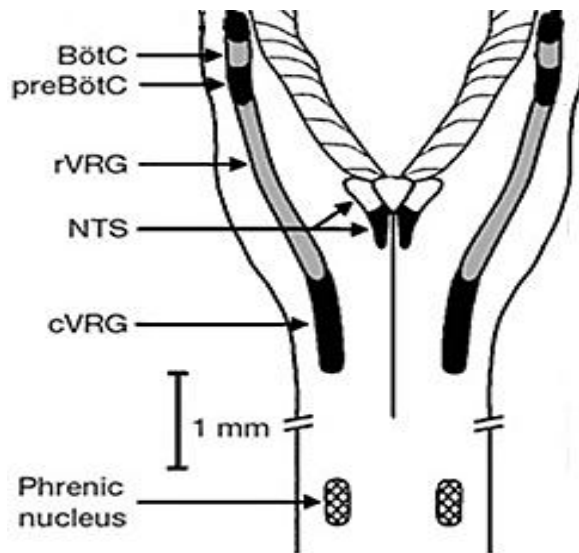
*(Modified from Mittal & Balaban, 1997)*

The dorsal respiratory group (DRG) in the medullary respiratory system consist of mostly inspiration neurons that have fibres to the inspiratory muscles. These neurons have a pacemaker activity that undergoes self-induced action potentials similar to that of the SA node of the heart. The firing of DRG causes inspiration, and when firing ceases, expiration

occurs. Thus the DRG is responsible for the basic rhythm of ventilation. However, the rate of inspiratory nerve firing is influenced by various inputs from other areas of the brain and the rest of the body.

The DRG is interconnected with the ventral respiratory group (VRG) which are composed of inspiratory and expiratory neurons. However, these neurons are inactive during normal quiet breathing, and come into action when there is an increased demand for ventilation. When this is the case the DRG sends impulses to the expiration neurons in the VRG which fire and stimulate the motor neurons supplying the abdominal and internal intercostal muscles. This occurs only when there is active expiration. Likewise, the DRG stimulates the inspiration neurons in the VRG to increase the rate and force of inspiratory activity when ventilation demands are high, for example, during exercise. In mammals DRG and VRG have projections to the pre-Bötzinger complex, an area found to contain the pacemaker neurons and so thought to be the central respiratory-rhythm generator (Smith *et al.*, 1991; Feldman and DelNegro, 2006). It is thought that respiratory rhythm may be generated by interconnected or group-pacemaker cells (Rekling & Feldman, 1998; Feldman *et al.*, 2003). Anatomically, the pre-Bötzinger complex is found rostral to the VRG (Figure 1-11).

**Figure 1-11.** Dorsal view of medulla oblongata and spinal cord indicating regions involved in control of breathing.



*BötC, Bötzinger Complex; preBotC, preBötzinger Complex; rVRG, rostral ventral respiratory group; cVRG, caudal ventral respiratory group.*

*(Modified from Rekling & Feldman, 1998)*

Rhythm activity is maintained by neurons in the pneumotaxic centre. These neurons send impulses to the DRG which inhibit the inspiratory neurons, thus limiting inspiration duration. The apneustic centre acts in the opposite direction and prevents inspiration neuron inhibition. Since the pneumotaxic centre is dominant over the apneustic centre inspiration is halted which allows expiration to occur.

In addition to the 'protective' effect of the pneumotaxic effect, there is also the Hering-Breuer reflex, which is triggered when tidal volume is large. The reflex prevents over-inflation of the lungs. Activated pulmonary stretch receptors, located within the smooth

muscles of the airways, send action potentials through the vagal afferent fibres to the medullary centre and inhibit inspiratory neurons, thus prevent the lungs from becoming over-inflated.

### **1.6b (2) Magnitude of ventilation**

Changes in  $O_2$ ,  $CO_2$ , and pH can affect the rate and depth of breathing (as can sleep, emotions, etc.). Carotid and aortic bodies in mammals, carotid body in birds, and carotid labyrinth in amphibians (Figure 1-7) monitor changes in  $O_2$  and  $CO_2$  in arterial blood. In response, the medulla's breathing control centre alters the rate and depth of breathing, increasing both to dispose the excess  $CO_2$  or decreasing both if  $CO_2$  levels are depressed. The peripheral chemoreceptors in the aorta and carotid arteries also detect changes in  $O_2$  levels in the blood and signal the medulla to increase the breathing rate when levels become very low. These then send nerve impulses, through the branches of either the ninth or tenth (vagus) cranial nerves, to the medulla. In air-breathing vertebrates  $CO_2$  levels dominate over  $O_2$  levels in the control of breathing. Elevations in  $P_{CO_2}$  cause the pH of cerebrospinal fluid to fall which is detected by central chemoreceptors in the medulla. The respiratory centre acts by increasing ventilation in an attempt to 'blow-off' excess  $CO_2$  to homeostatic levels, thereby increasing the pH.

### **1.6c (3) Modification of respiratory activity**

Modification of respiratory activity occurs to serve other purposes, such as voluntary control during speech, singing, whistling, or involuntary control involved in a cough or sneeze to expel irritant materials.

## 1.7 HEART RATE VARIABILITY AND RESPIRATORY SINUS ARRHYTHMIA

Heart rate is not fixed, but shows beat-by-beat fluctuations that reflect rapidly reacting control systems. These control systems respond to interactive central and peripheral inputs that attempt to maintain circulatory homeostasis. The effectors that contribute to *heart rate variability* (HRV) include the already mentioned mechanoreceptors and chemoreceptors which detect cardiovascular and respiratory variables. The information is then coordinated in the central nervous system and the efferent pathways then regulate the cardiovascular system by changing heart rate, blood pressure and blood flow. In the elasmobranch, *Scyllium canicula*, Lutz (1930) pointed out that the cardiac vagus maintains the coordination of heartbeat with ventilation. Therefore, HRV is indicative of cardiac function, representing fluctuations in vagal tone on the heart (McDonald (1980) in Taylor, 1994).

In humans the main contributor of HRV is *respiratory sinus arrhythmia* (RSA) (Hyndman *et al.*, 1971). RSA consists of an increase in heart rate during inspiration and a corresponding decrease during expiration. The vagus nerve, emanating from the cardiac vagal preganglionic neurons in the brainstem and having an efferent pathway to the SA-node, is considered to be predominantly responsible for generating RSA. In vagotomised animals (Samaan, 1935; Anrep *et al.*, 1936b) and when using cholinergic antagonists (Hamlin *et al.*, 1966; Coker *et al.*, 1984) the rhythm is abolished. HRV and RSA are reduced or even abolished in conditions that disrupt autonomic nervous system function, such as autonomic neuropathy associated with diabetes (Wheeler & Watkins, 1973; Divon *et al.*, 1983). For these reasons, RSA may be used as an indicator of autonomic function and the integrity of the brainstem. Previously RSA was used as a reliable measure of parasympathetic control (Katona & Felix, 1975; Hayano *et al.*, 1991), however more

recently, there is evidence that cardiac vagal tone is affected by sympathetic control which can alter the magnitude of RSA; and that RSA can dissociate with RSA under certain conditions, such as when heart rate falls to very low levels (Grossman & Taylor, 2005).

When heart rate and breathing movements of premature human neonates were compared with term neonates, it was found that healthy term new-borns showed RSA as a major contributor to heart rate variability (Thompson *et al.* (1992) in Taylor, 1993). However, this was not observed in early premature neonates. Hence, the contribution of RSA to HRV varies with both pre- and post-natal age in healthy premature neonates. This may reflect maturational development of the underlying mechanisms. Therefore, the loss or absence of sinus arrhythmias in neonates is an important indicator of poor fetal condition, and could constitute a reliable indicator of abnormal brain stem development (Taylor, 1993; 1994).

More recent studies have found that a reduction in HRV is linked to unfavourable health prospects, mainly increased risk of cardiovascular disease. Presence of low HRV has been used to predict mortality in diabetic patients (May & Arildsen, 2011). HRV can be reduced under seemingly low stress situations, such as working night shifts (Kunikullaya *et al.*, 2010), or simply with cognitive decline (Shah *et al.*, 2011), with age (except after the age of 80, where HRV apparently increases again (Tak *et al.*, 2010), or in patients with cardiovascular diseases. Ethnicity too can determine the level of HRV (Bathula *et al.*, 2010).

## **1.8 THE MEXICAN AXOLOTL, *AMBYSTOMA MEXICANUM***

Tissue and organ morphogenesis patterns displayed by amphibians are similar to those of higher vertebrates, and so they are important model systems. The greatest advantage of using amphibian embryos over mammalian is that they can be easily studied and surgically manipulated owing to their external habit. The Mexican axolotl, *Ambystoma mexicanum*, is an excellent model organism since it has relatively large eggs (2.0 mm diameter versus 1.2 mm for *Xenopus* egg) which develop relatively slowly so that important developmental stages are not missed by passing too quickly, which could be problematic when investigating (Armstrong & Malacinski, 1989).

However, it is more significant to study the axolotl because in some cases it appears to be genetically closer to humans than the *Xenopus*, and even some mammals. For instance, those few sequences that have been identified in the axolotl include the ribosomal protein S-3 and the homeobox gene *HoxA5* for which comparisons have been made; see Table 1-4. *Hox-A5* is a sequence-specific transcription factor which is part of a developmental regulatory system that provides cells with specific positional identities on the anterior-posterior axis important in anatomical patterning. As seen in the table the axolotl amino acid sequence for the *Hox-A5* is 100% identical to human and mouse sequences, but only 90% with *Xenopus*. Ribosomes are the particles that catalyse mRNA-directed protein synthesis in all organisms and so they too are vital. Ribosomal protein S-3 form the small unit of the ribosome.



**Table 1-4.** Amino acid comparisons of ribosomal protein S-3 and gene *HoxA5* of axolotls with other vertebrates.

Organism	Axolotl amino acid identity / %	
	Coding regions of ribosomal protein S-3	Homeodomain of HoxA5 gene
Human	93.9	100.0
Mouse	94.3	100.0
Rat	92.8	98.0
Xenopus	93.9	90.0
	<i>Data from Bhatia, Dube &amp; Lemanski, 1996</i>	<i>Data from Gaur, Lemanski &amp; Dube, 1995</i>

Furthermore, the axolotl has been used to test the hypothesis that progressive ventro-lateral location of vagal preganglionic neurons relates to the evolution or development of lung breathing (Taylor, 1994). This is possible since the axolotl is neotenus and can be induced to metamorphose into a salamander-like animal by treatment with analogues of the hormone thyroxine (Prahlad & Delanney, 1965; Ingram, 1970). The treatment causes the loss of gills and forces the axolotl to leave the water to become committed lung breathers. In just the one study carried to date, it was found that after metamorphosis there was an increase in the number of vagal preganglionic neurons and about 15% were found in a more lateral location in the white matter of the medulla (Ihmied & Taylor, 1992). The relocation of vagal preganglionic neurons is thought to have functional relevance that may relate to the switch from gill to lung breathing. A very similar pattern is observed during brain development in mammalian embryos, where some neurons in the brainstem migrate from a dorso-medial position to their final ventro-lateral position.

Currently, no data exists on the embryological development of the vagal motor fibres in the axolotl, and it is not yet clear if there is a direct correlation between the onset of HRV and the migration of vagal preganglionic neurons ventro-laterally. However, the neotenus axolotl serves as an excellent model for determination of the timescale and control of the migration of vagal preganglionic neurons during development, since it can be induced to metamorphose. Measurements of heart rate, and in particular HRV, pre- and post-metamorphosis will allow greater understanding of the functional roles of the migration pattern of vagal preganglionic neurons and its relationship with vagal nerve development upon the heart.

It can be appreciated that the axolotl provides an important model for human development and that its relevance has been underestimated in recent years. It is large enough to be studied with relative ease in comparison with small models, such as zebra fish. They can be induced to breed when needed, and then can be induced to become a committed lung breather when needed. This is a unique character that makes the axolotl a better model than current models. The zebrafish is solely aquatic and so it is inappropriate in lung studies and, or cardiorespiratory interactions; the mouse embryo in internal and so more sophisticated surgery procedures are required; and the *Xenopus* will metamorphose when it is at the developmental stage, and not necessarily under the researchers control. A further advantage of using the axolotl to study heart muscle development is the naturally occurring recessive mutant, the cardiac-lethal.

### **1.8a The cardiac lethal mutant**

The cardiac-lethal mutant (*c*) has abnormal cardio-myogenesis and morphological studies have shown that they lack organised sarcomeric myofibrils (Hill & Lemanski, 1979). This prevents the development of a contracting heart, and thus, the mutants eventually die from lack of circulation. However, these mutants can survive up to a fortnight after hatching in well-oxygenated water without a functional heart (Lemanski, 1973a). This allows a window of opportunity for the study of this dysfunction relatively easily in comparison with lethal mutants of mice or chicks. Figure 1-12 shows the relevant developmental stages of axolotl embryos and Figure 1-13 shows the mutant phenotype at developmental stage 42.

A team in Syracuse, New York have been working on this mutant since the 1970s (initially lead by Larry Lemanski, and now by Dipak Dube). They (along with Smith and Armstrong (1991)) found that the anterior endoderm corrected the heart defect in the cardiac mutant (Lemanski, Paulson, & Hill, 1979). More recently, Armstrong's team have suggested that the cardiac mutant may produce too much of an inhibition factor, preventing appropriate myofibril differentiation (Smith, & Armstrong, 1993; Armstrong, 1989). Their results demonstrated the presence of activator- and inhibitor-like factors in pre-cardiac mesoderm, which provides evidence for their hypothesis that heart development is controlled by a reaction-diffusion system.

**Figure 1-12. Abbreviated developmental stage series for the Mexican axolotl highlighting important stages utilized in Part I**

(20) Cardiac determination/induction complete and the start of cardiac specific gene expression. (30) Bilateral mesoderm mantles have fused at the ventral midline marking the beginning of the structural organization of the heart. (35) Initiation of a heart beat. (38) Continuation of cardiac morphogenesis and the presence of a well-established heartbeat. (41) Embryos hatch from their clear jelly coats. (43) Early post-embryonic life and the latest stage, cardiac mutants are capable of surviving. Numbers in parentheses and below each figure represent stages. (Bordzilovskaya *et al.*, 1989).

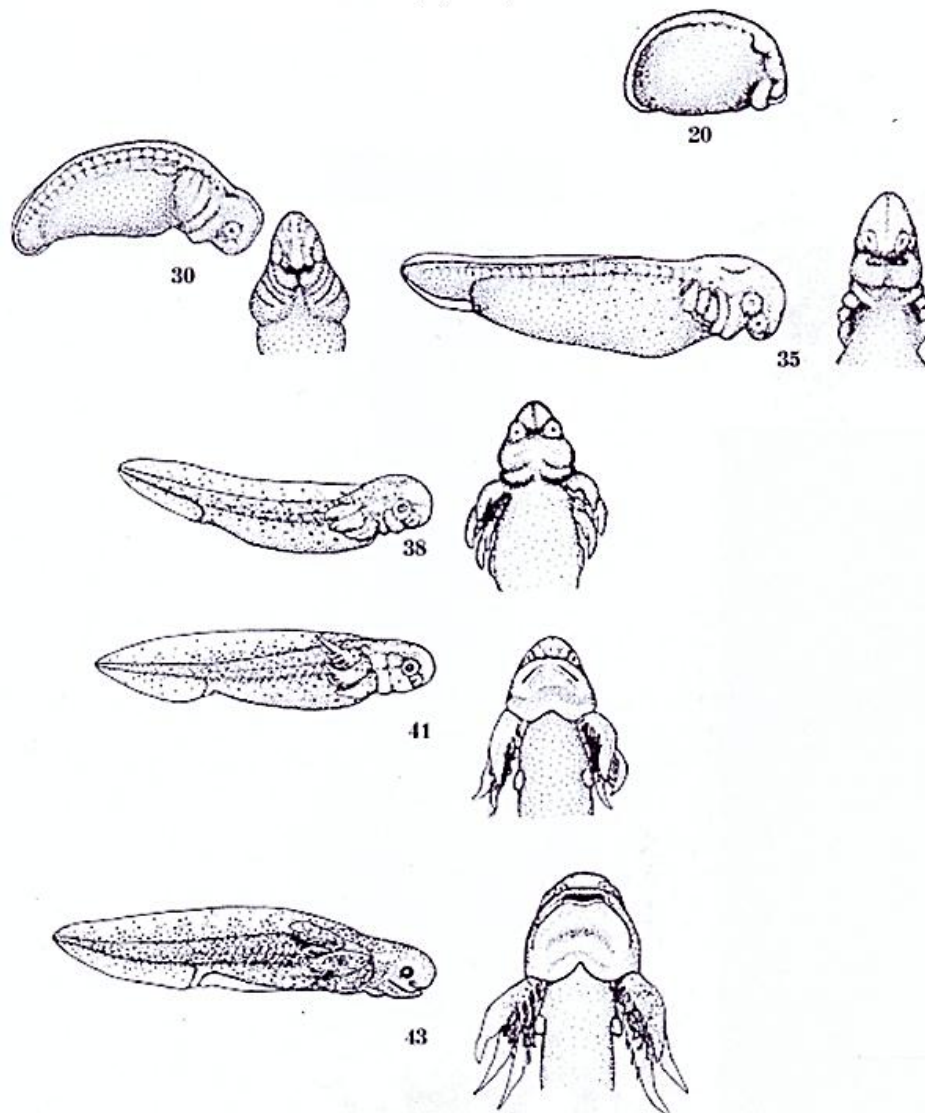
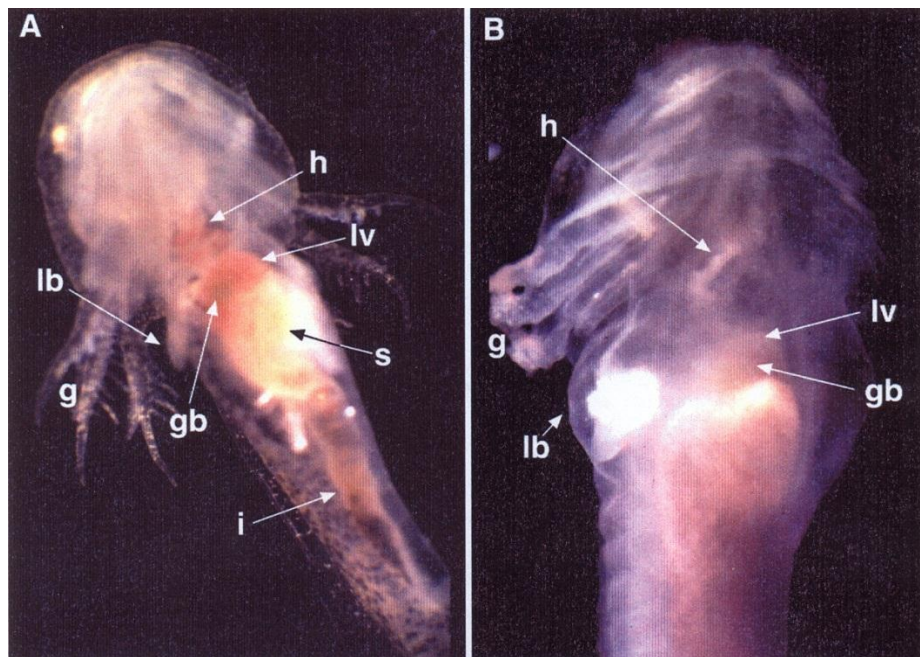


**Figure 1-13. Late stage axolotl embryos.**

Stage 42 normal (A) and cardiac mutant (B) axolotl showing the gross malformation in the cardiac mutant animal resulting from a failure of the heart to beat. Prior to heart beat initiation, normal and mutant animals are indistinguishable from one another. Following heart beat initiation the failure of the mutant ventricles to beat results in blood pooling in the abdomen and accumulation of ascites fluid. The increased fluid leads to a pear shaped body, marked distension of the thorax and abdomen and poor gill formation. At the late developmental stage shown here, the mutant heart (h; Panel B) is only a thin strand like structure. This in comparison to the well-formed, robust heart in normal animal (h; Panel A) Despite the failure of mutant hearts to beat, mutant animals swim normally. (h) heart; (lv) liver; (s) stomach; (lb) limb bud (g) gills; (gb) gall bladder (i) intestine

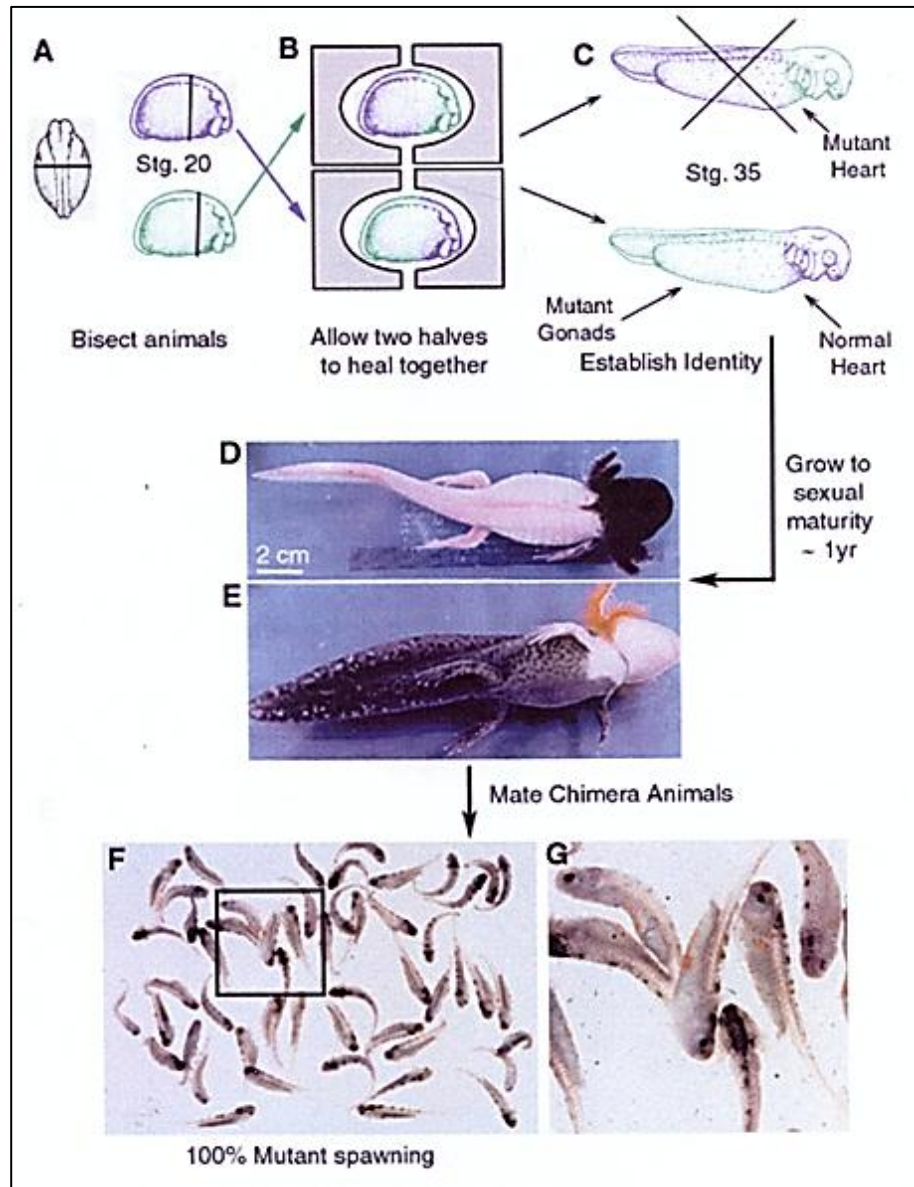


Lemanski's group concentrated on general heart development in the wild-type and mutant axolotl, and examined the relative quantities of muscle specific proteins (e.g., tropomyosin) histochemically (Lemanski, 1973a, b & c; Fransen, & Lemanski, 1988). Since Dube, the group appear to focus on the molecular and genetic characterisations. The expression of myosin heavy chain transcripts have been investigated in both phenotypes (Ward *et al.*, 1996). A C-protein isoform (which is thought to regulate and stabilise thick filaments) has been cloned, sequenced and its expression pattern has been determined in embryonic, juvenile and adult tissues (Ward *et al.*, 1995), as has an isoform of cardiac  $\alpha$ -tropomyosin (Luque, Lemanski, & Dube, 1994; Luque *et al.*, 1997). Alpha-tropomyosin is found in striated muscle and is the predominant isoform in cardiac muscle. Simultaneously, the team have begun a search for *Hox* genes, which are significant in development because they specify pattern formation along the antero-posterior body axis of many organisms. The homologue of murine *HoxA5* has been identified (Gaur, Lemanski, & Dube, 1995), whose expression has been studied in the metamorphosing heart (Gaur *et al.*, 1998). More recently, a novel homeobox gene, *AxNox-1*, has been cloned and sequenced (Gaur, Lemanski, & Dube, 1998). Interestingly, although this gene is expressed predominantly in neural tissue during development, lower levels are seen in heart, lung, liver, gut, and skeletal muscle. The authors make a tentative suggestion that expression may be seen in these organs because they are all innervated, and hence transcripts may be derived from neurons. Whiteley and Armstrong (1991) isolated a partial clone, *Ahox-1*, the homologue of the labial gene of *Drosophila*, which appears to be involved in the development of homologous structures in the axolotl.

While working on axolotls, the Syracuse team have developed technical skills specific for this organism. They have established primary cell culture protocols of cardio-myocytes from mutant and wild axolotl embryos (Zajdel *et al.*, 1995). Organ cultures have been used since Lemanski's work in the '70s. However, the most important contribution of this team is the production of chimeric axolotls which produce embryos that are 100% cardiac mutant phenotype (Lemanski *et al.*, 1998). Conventionally, matings between heterozygous axolotls for the mutant gene (+/*c*) result in only 25% cardiac lethals (*c/c*) in the progeny. Further, the lethals cannot be distinguished from normal siblings until late tailbud stage, when the heart would normally begin beating. As a consequence, it has not been possible to efficiently examine pre-heartbeat stages in the past. The chimeras, composed of wild (+/+) head heart regions grafted onto the bodies of mutant (*c/c*) embryos, which develop mutant (*c/c*) gonads, enable researchers to investigate perturbations at the earliest stages of development (Figure 1-14).

**Figure 1-14. Creating chimeric mutant axolotls.**

Schematic diagram of the process used in making surgical axolotl chimera to create spawnings containing 100% mutant animals. (A) Stage 20 embryos from either the same or different spawnings are bisected near the midline with hair loops, sharpened tungsten needles and watchmaker forceps (B) The anterior half of one bisected animal is aligned with the posterior half of a similarly bisected animal and allowed to heal. The two halves are pushed together while healing and annealing of the two complementary halves takes place



using 10 x 5 x 1mm stainless steel plates with a half circle in one end. (C) The stainless steel plates are removed 3-24 hours after alignment of the two halves and the pairs maintained separately in 60 mm agarose or parafilm lined sterile petri dishes until the phenotype of the animals can be determined. (D and E) Animals are grown until sexual maturity. The two animals here were created using two different spawnings, one white and the other pigmented. (F) Spawnings containing 100% mutant animals were obtained by mating pairs of animals with *c/c* gonads. The genotype of chimera animals was established by first mating animals with presumptive *c/c* gonads with known *+/c* animals. The resultant cross (*c/c* x *+/c*) would be expected to produce embryos where 50% are normal and 50% are mutant. Following this cross, 2 pairs of animals were selected and mated. Embryos were grown until the phenotype could be accurately determined and 100% of these embryos were of the mutant phenotype. (G) Digitally enlarged area outlined in (F) showing the characteristic blood pooling in abdomen and ascites fluid accumulation. (Bordzilovskaya *et al.*, 1989).

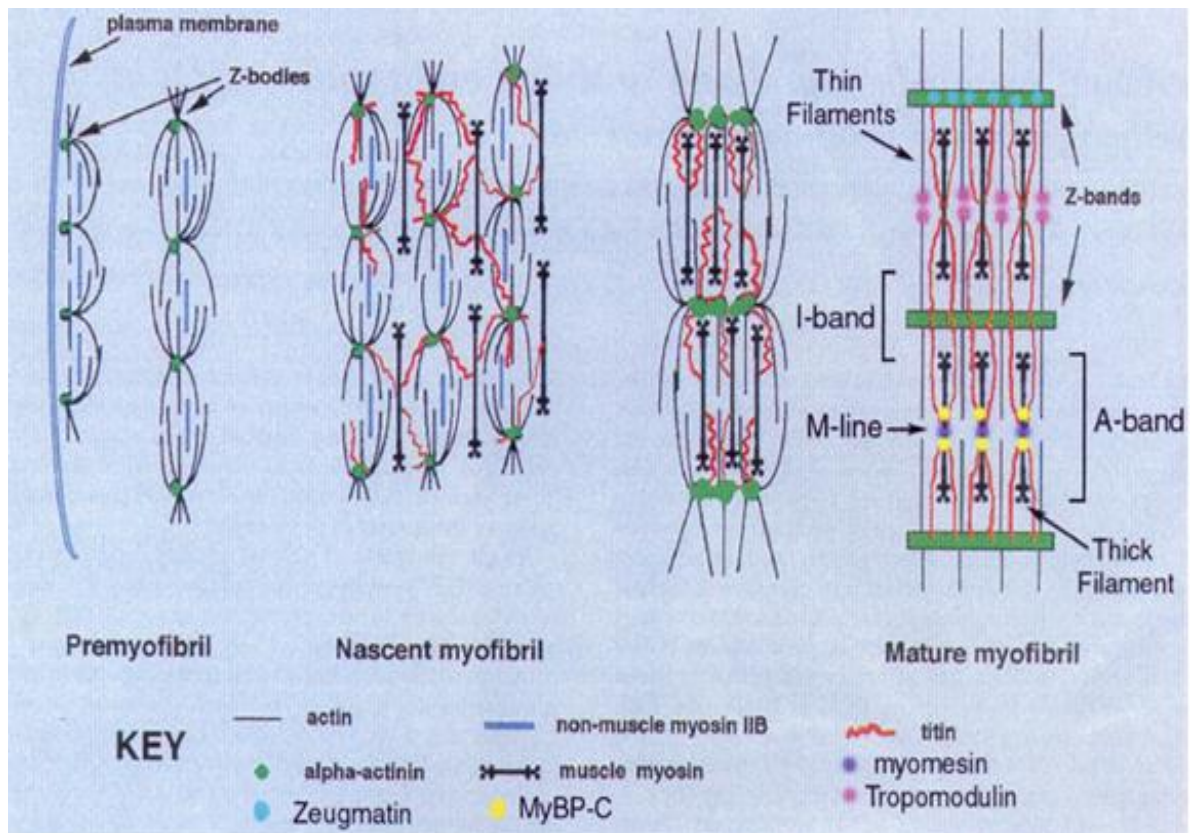


### **1.8b Tropomyosin and the cardiac lethal mutation**

Electron microscopy of the cardiac lethal mutant heart shows a few abnormal characteristics. It shows a lack of mature organised myofibrils in the mutant myocardium, which appears to cause the lack of beating, and large collections of amorphous material (Lemanski, 1973a). The addition of purified tropomyosin protein to these mutant hearts not only reduces the amorphous collections, but also leads to the formation of short 6nm filaments. These findings suggest that the amorphous collections are non-filamentous actin which fail to assemble into filamentous structures due to the lack in significant quantities of tropomyosin. It is now believed that the mutant hearts have reduced tropomyosin protein, or more likely a specific tropomyosin isoform (Lemanski *et al.*, 1980; Lemanski *et al.*, 1976; Moore and Lemanski, 1982). However, Fuldner *et al.* (1984) could not detect any difference. It may be that there is a presence of multiple tropomyosin isoforms (Lees-Miller and Helfman, 1991) in the developing heart and that only one particular form is deficient. See Figure 1-15 for normal myofibrillogenesis.

**Figure 1-15. Myofibrillogenesis.**

In this model of myofibrillogenesis, the pre-myofibril forms at or near the plasma membrane surface. It is characterized by  $\alpha$ -actinin containing Z-bodies and short filaments of non-muscle myosin IIB. Z-bodies initially appear as discrete  $\alpha$ -actinin aggregates along the pre-myofibril but as width of the sarcomere increases the z-bodies appear to become laterally aligned. The laterally aligned z-bodies continue to fuse to form Z-bands. A transition stage exists between pre- and mature myofibrils termed nascent myofibrils. This stage is marked by the addition of titin, gradual growth and fusion of the z-bodies into larger structures and a gradual incorporation of muscle myosin. The nascent myofibril therefore contains both muscle and non-muscle myosin isoforms that appear in a continuous pattern since they have not yet aligned in register. The nascent myofibril matures further with additional fusion of z-bodies to form Z-bands and a loss of non-muscle myosin IIB. Actin thin filaments obtain their mature lengths through a yet undiscovered mechanism. Borrowed and adapted from Dabiri, (1997).



In the developing axolotl heart three tropomyosin isoforms have been described. These are ATmC-1 (Axolotl Tropomyosin Cardiac-1) (Luque *et al.*, 1994), ATmC-2 (Spinner *et al.*, 1997b) and ATmC-3 (Spinner *et al.*, 1997a). Messenger RNA for all three appear to be present in relatively equal quantities between normal and mutant hearts (Spinner *et al.*, 1997a). Of these, ATmC-1 and ATmC-2 appear to be products of the putative  $\alpha$ -tropomyosin gene. Interestingly, ATmC-2 is a novel splice variant of the  $\alpha$ -tropomyosin gene containing the smooth muscle exon 2a instead of the typical striated muscle exon 2b (Spinner *et al.*, 1997b). Furthermore, ATmC-1 is recognised by CH1 (Spinner *et al.*, 1997b), a monoclonal antibody against sarcomeric tropomyosin (Lin *et al.*, 1985) but it does not recognise ATmC-2. ATmC-2 protein is recognised only by anti-C-2, a specific polyclonal antibody that was generated against a synthetic peptide derived from its exon 2 region. ATmC-2 protein was found to be present in both normal and mutant axolotl hearts (Spinner *et al.*, 1997b).

ATmC-3 is likely a separate gene product (Spinner *et al.*, 1997a) and is most homologous (97%) to the *Xenopus* cardiac TM-4 gene (Hardy, 1995). This isoform of tropomyosin is developmentally regulated in the axolotl. Its mRNA is detected around the time of heart beat initiation (stage 35) but is not detected in the adult heart (Spinner *et al.*, 1997a), nor in the skeletal muscle, unlike the other two isoforms, ATmC-1 and ATmC-2 (Luque *et al.*, 1994; 1997). A reduction of tropomyosin mRNA using anti-sense oligonucleotides specific for ATmC-1, -2 and -3 suggests that ATmC-2 and ATmC-3 only are necessary to maintain myofibril structure in developing axolotl ventricle (Zajdel *et al.*, 2000). ATmC-3 is recognised by CH1 antibody and since it is only expressed in the heart (while ATmC-1 and ATmC-2 are present in skeletal muscle and heart tissue) it is tempting to speculate a

requirement for this recently described tropomyosin isoform in cardiac myofibrillogenesis. Experiments suggest that the defect in the mutant axolotl is probably due to a lack of specific tropomyosin and that its reduction appears to inhibit the ability of myofibrils to form. This is supported by the recent report that ectopic expression of heterologous  $\alpha$ -tropomyosin cDNA or the introduction of heterologous tropomyosin protein into mutant hearts resulted in the formation of mature myofibrils (Zajdel *et al.*, 1998). The maturity of these myofibrils can be assessed using an antibody against tropomodulin which is a protein that has been described as a late marker for myofibrillogenesis.

### **1.8c The model**

The capability of axolotls to retain the larval appearance, even when sexually mature, and the sensitivity of their tissues to exogenous thyroid hormones (Lynn & Wachowski, 1951; Etkin, 1964) could further investigations into the developmental cardio-neuro-biology of vertebrates. This will surely lead to a more comprehensive understanding of the relationship between the animal's physiological demands and the development of its nervous system.

## **1.9 AIMS, HYPOTHESES AND OBJECTIVES**

This thesis is divided into two parts. In the first part we looked at non-beating hearts to see what exactly was needed or important for a functional heart that had myogenic rhythmicity. It was known that tropomyosin was lacking in axolotl cardiac lethal mutants and so the aim was to see what tropomyosin introduction would have on these dysfunctional hearts, and if the expression of tropomyosin was disrupted in normal, wild-

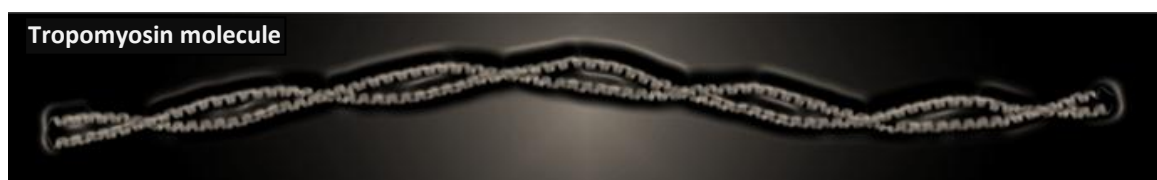
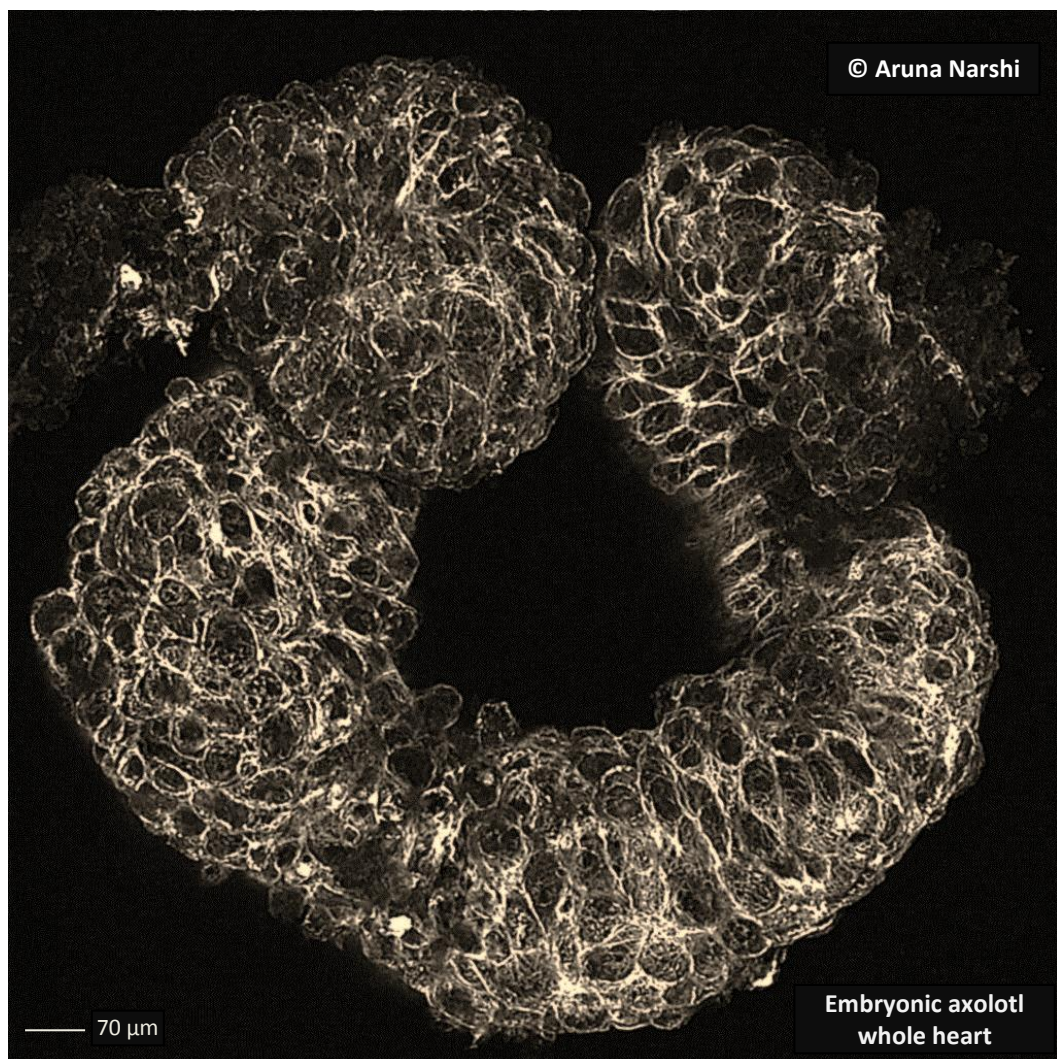
types heart, would it lead to the cardiac mutant phenotype. Firstly, an effective delivery system had to be designed, liposome mediated transfection, to transfect tropomyosin specific oligonucleotides into whole heart organ cultures (Chapter 2). We then used this effective method to see if human specific tropomyosin could rescue the cardiac lethal mutant (Chapter 3). The research team identified a novel tropomyosin isoform that was found to be expressed in other organisms. Therefore the aim of Chapter 4 was to see what effect this isoform had on axolotl embryonic hearts. The final aim of Part I of the thesis was to look at the structural / functional relationship of tropomyosin in organising myofibrils. The tropomyosin molecule was altered at both ends then transfected into whole heart organ cultures, using the transfection method, to see how it would affect myofibrillogenesis.

In the second part we took functional hearts of mature gills breathers and induced them to become committed lung breathers to see if they displayed heart rate variability (HRV). HRV is thought to be associated with the relocation of VPN in a ventrolateral position to the DVN. So the aim was to reassess the possible migration of VPN to this new location post metamorphosis in the axolotl, but this time using the retrograde cholinergic tracer which would not damage the nerves (like the HRP method would as used by the previous researcher). And then to see if there are cardiorespiratory changes associated with this change in VPN location.

Essentially this thesis was the study of hearts that did not beat, hearts that were likely to display little, if any, heart rate variability, and hearts that did show heart rate variability. And the model used was the Mexican axolotl, *Ambystoma mexicanum*.

# Part I

## The Role of Tropomyosin in Cardiac Myofibrillogenesis



Published in 2000 in *Focus (Life Technologies/Invitrogen)* **22** (2-3); 28-30.

Data included in Spinner *et al.*, (2002) *J. of Cell. Biochem.* **85**: 747-761.

## CHAPTER TWO

### TARGETED GENE DISRUPTION IN WHOLE HEARTS BY CATIONIC LIPOSOME TRANSFECTION OF ANTISENSE OLIGONUCLEOTIDES

#### 2.0 ABSTRACT

In this study cationic liposome-mediated delivery was used to introduce sense and antisense oligonucleotides into whole hearts of embryonic axolotls. These embryonic hearts provide a suitable surface area for the action of cationic liposomes owing to the fact that they are only one to two cells thick. The Mexican axolotl provides an uncommon, but particularly useful, model in which to study the role of tropomyosin protein during myofibril formation in the heart. In this animal model there is a naturally occurring mutant, the *cardiac lethal*, in which the embryos lack organized myofibrils and have altered expression of contractile proteins. Oligodeoxynucleotides specific to axolotl tropomyosin isoforms (namely, ATmC-1 and ATmC-3) were successfully introduced into the normal hearts. The antisense oligonucleotide replicated the disruption of myofibril formation seen

## ***I. The Role of Tropomyosin in Cardiac Myofibrillogenesis***

in mutant hearts, while the sense strands did not. Antisense ATmC-3 oligonucleotide also disrupted heart beating. In contrast, ATmC-1 antisense oligonucleotide did not cause a disruption of the myofibrillar organization of the ventricle (but did in the future outflow tract from the ventricle region, known as the conus). Control hearts were transfected with fluorescein-tagged sense oligonucleotides which demonstrated their successful introduction into cells of the whole intact hearts. Thus, this study showed how disruption of tropomyosin expression in normal hearts, by using the anti-sense oligonucleotides, resulted in a lack of organized myofibrillar structures, which appears to lead to loss of a functional heartbeat. It appears that tropomyosin is involved in the organisation of contractile proteins that are essential for contraction of heart muscle. Also, the ability to use whole hearts in this procedure is important for the study of myofibrillogenesis in normal hearts (at the DNA, RNA, and/or protein levels) by the use of cationic liposome transfection.

### **2.1 INTRODUCTION**

Transfection (a term derived from ‘*transformation by infection*’) is a method of introducing nucleic acids into eukaryotic cells which can help elucidate gene function and protein expression. Transfection techniques are especially useful because they allow transfer of nucleic acids across cell membranes which would normally be impossible owing to the fact that DNA and RNA backbones are negatively charged, as are cell membranes. The transfection method addresses the problem of negatively charged nucleic acids by coating the DNA in a positive charge, thereby neutralising the molecule. This can



## ***I. The Role of Tropomyosin in Cardiac Myofibrillogenesis***

be achieved by chemicals like calcium phosphate and diethylaminoethyl-dextran or with cationic lipid-based reagents that positively coat the negative DNA. The DNA/transfection reagent complex can then easily cross the membrane.

A 'liposome' is a colloidal particle that forms lipid bilayers in an aqueous medium (Sessa & Weissmann, 1968). Cationic liposomes have been used to facilitate introduction of DNA (from small oligonucleotides to relatively large yeast artificial chromosomes), RNA, and proteins into cultured cells (Felgner *et al.*, 1987; Lee & Jaenisch, 1996; Malone *et al.*, 1989; Lin *et al.*, 1993; Zajdel *et al.*, 1998; 1999; 2000). The negative phosphates of the DNA or RNA associates with the cationic head group of the lipid compound. The liposome/nucleic acid complexes then enter the cell by either endocytosis or by fusing with the cell membrane (Gao & Huang, 1995), and are then carried in endosomes, and eventually into the nucleus. How the nucleic acids cross the nuclear membrane, however, is still not clear. The cytoplasm is the site of action for RNA, protein or antisense oligonucleotides that are delivered by liposomes, whereas DNA needs to enter the nucleus.

Liposome techniques can be used on cells for both transient expression studies and long term experiments where DNA needs to integrate into the chromosome. Furthermore, this method of nucleic acid transfer can be used *in vivo* in animals and humans (Felgner *et al.*, 1995). Other valuable characteristics of liposome transfection include protecting DNA and RNA from nucleases and the ability to transport active substances to the nucleus of the transfected cell (Zelphati & Szoka, 1996). Perhaps the most intriguing potential use of cationic liposome transfection is the inhibition of gene expression that may be obtained with transfection of isoform-specific antisense oligonucleotides. Antisense

## ***I. The Role of Tropomyosin in Cardiac Myofibrillogenesis***

oligonucleotides would bind to the sense strands of mRNA, thereby preventing translation, and so no protein would be made. This study describes the use of cationic liposomes for transfection of an intact organ that maintains important cell-cell structure. In this way, targeted gene-disruption of specific tropomyosin isoforms was used to examine the effect on structure and function.

Transfection procedures have been performed mainly on isolated cells in culture. However, cell culture procedures create cardiac myocytes that have an initial disruption of myofibrils that eventually reform. Enzymatic treatment and cell culture procedures may also have other unknown effects on the cardiomyocytes. Thus, one could propose that the maintenance of intercellular connections in a whole organ would be optimal. Initially, we developed transfection procedures on cultured cells using calcium phosphate (Xu *et al.*, 1992) and the cationic lipid reagent LIPOFECTIN<sup>®</sup>. However, LIPOFECTIN was more effective on cardiomyocytes and also could be used on whole hearts in contrast to calcium phosphate. Whole hearts have the advantage of maintaining intercellular connections and mechanical load, especially since it is essential that the cardiomyocytes synchronously contract with neighbouring cells in-order to function as the pumping organ.

Tropomyosin is a component of the thin filament in sarcomeric myofibrils. It interacts with actin and the troponin complex in the thin filament, and these proteins are involved with contraction and relaxation of the myofibrils. Three isoforms of tropomyosin have been isolated for this animal model, the Mexican axolotl (*Ambystoma mexicanum*): ATmC-1 (Axolotl Tropomysin Cardiac-1) and ATmC-2 (Luque *et al.*, 1994; 1997); and ATmC-3 (Spinner *et al.*, 1997). Current research in this laboratory is focused on elucidating the role

## ***I. The Role of Tropomyosin in Cardiac Myofibrillogenesis***

of these isoforms in heart. It has been found that ATmC-3 (made by *TM-4* gene) is exclusively expressed in axolotl cardiac tissue. The gene transcript is detected between stages 30 (pre heart beat) and stage 35 (heart beat initiation), but not in the adult heart. Its amino acid sequence is 97% homologous and nucleic acid sequence 82% homologous to the *Xenopus laevis* cardiac TM-4 tropomyosin isoform (Hardy *et al.*, 1995). The transient expression of TM-4 tropomyosin exclusively in cardiac tissues strongly implies that it plays a role in cardiac development in the axolotl. Here, we describe the possible role of ATmC-3 in the ventricle of normal hearts and the effect of treatment with antisense isoform-specific oligonucleotides.

## **2.2 METHODS**

### **2.2a Whole heart bioassay**

Wild type axolotl embryos were obtained from matings between animals from a colony at SUNY Upstate Medical University or the Indiana University axolotl (salamander) colony. Animals were maintained in aquaria in 50% Holfreter's solution (29 mM NaCl, 0.45 mM CaCl<sub>2</sub>, 0.33 mM KCl, 0.1 mM MgSO<sub>4</sub>, and 4.76 mM NaHCO<sub>3</sub>) and fed commercial salmon pellets as recommended by Indiana University.

Embryos from stages 37–39 (staging system of Bordzilovskaya *et al.*, (1989)) were mechanically released from their jelly coats with watchmaker forceps (number 5) and washed 4 times in filter-sterilized Steinberg's buffered salt solution [58 mM NaCl, 0.67 mM KCl, 0.9 mM CaCl<sub>2</sub>, 0.2 mM MgSO<sub>4</sub>, 4.6 mM HEPES (pH 7.4), containing 1% GIBCO BRL<sup>®</sup> Antibiotic/Antimycotic (100 units/ml penicillin G sodium salt, 0.1 g/ml

## ***I. The Role of Tropomyosin in Cardiac Myofibrillogenesis***

streptomycin sulfate, 0.25 µg/ml amphotericin B)]. Embryos were then anesthetized with MS-222 (Tricaine methanesulfonate). Hearts were extirpated with heat-sterilized forceps, sharpened tungsten needles and hair loops, as needed, under a dissecting microscope and placed into 100 µl of Steinberg's solution without antibiotics for transfection. Approximately 50 hearts were collected for each sample.

### **2.2b Transfection**

Sense and antisense oligonucleotides were designed for ATmC-1 and ATmC-3 tropomyosin isoforms. The ATmC-1 antisense chimeric oligonucleotide was

A\*G\*G \*ACT CCG AGT ACT TGT C\*C\*A \*C.

The ATmC-3 exon 2 antisense and sense chimeric oligonucleotides were

5'-T\*A\*C TAG CTC GTC CTC AAG C\*T\*G C-3' and

5'-<sup>f</sup>G\*C\*A GCT TGA GGA CGA GCT A\*G\*T \*A-3' respectively,

where \*N represents a phosphorothioate-blocked nucleotide and <sup>f</sup>G represents a guanine tagged with fluorescein at the 5' end (IDT, Inc.). The sense oligodeoxynucleotide was tagged with fluorescein (FS-ODN) as a positive control and to confirm localization within the myocytes.

## ***I. The Role of Tropomyosin in Cardiac Myofibrillogenesis***

The cationic liposome solution, LIPOFECTIN Reagent (Gibco-BRL) was mixed with Steinberg's solution for 30-45 minutes at 0.28 mg/ml. Then, 10  $\mu$ l of oligonucleotide (final concentration of 0.1  $\mu$ M) was added for 15 minutes. Drops of lipofectin solution (5  $\mu$ l) were placed on Parafilm lined 60 mm Petri dishes that were previously exposed to ultraviolet light. The hearts were transferred with 5  $\mu$ l of Steinberg's solution into the lipofectin drops to make a total volume of 10  $\mu$ l and to give the appropriate concentrations. The hearts were visually monitored for beating on a daily basis using a dissecting microscope. All these procedures were carried out at room temperature. During the culture period the hearts were also examined for introduction of FS-ODN and for myofibril formation with the confocal microscope at 4, 24, 48, 72, 96, and 120 hours. These hearts were examined live or fixed with 2% paraformaldehyde for 1 hour. For double staining to visualise nuclei, 1 mg/ml Hoechst dye was placed on randomly selected hearts for 10 minutes. At the end of the culture period all of the hearts were washed several times in Steinberg's solution and treated for confocal microscopy (see below).

### **2.2c Confocal microscopy**

Normal hearts processed for fluorescent staining were processed by a method adapted from Bell *et al.* (1987) which permits the fixation and permeabilization simultaneously using dithiobis (succinimidyl) propionate (DTSP, Pierce Biochemical, Inc.). Briefly, hearts were placed in 1 mM DTSP (cross-linking fixative reagent) dissolved with 1% dimethylsulfoxide (DMSO) in Steinberg's solution for 15 min. Thereafter, further permeabilization occurred in 0.5% Nonidet<sup>®</sup> P-40 in Steinberg's solution for 15 minutes. The reaction was quenched by two 10-minute washes in 0.1 M glycine. Hearts were then incubated in monoclonal anti-tropomyosin primary antibody (CH1 (Lin *et al.*, 1985))

## ***I. The Role of Tropomyosin in Cardiac Myofibrillogenesis***

diluted to 1:30 in Steinberg's solution for one hour at room temperature. Nonspecific background was blocked with 0.1 mg/ml bovine serum albumen (BSA) or non-fat dry milk by 3 washes of 10 minutes each. Hearts were then transferred to a rabbit anti-mouse lissamine rhodamine secondary antibody (Jackson Immunoresearch, West Grove Pa) at a 1:50 dilution was added for 30 minutes. The hearts were rinsed several times in BSA in Steinberg's solution and post-fixed in 2% paraformaldehyde overnight. The fixation was quenched by 0.1 M glycine for 30 minutes and then placed in Steinberg's solution.

The hearts were mounted on slides in Biorad Fluorogard antifade reagent. Three layers of fingernail polish were used to support the glass coverslips to and to act as spacers to prevent crushing of the whole hearts. Coverslips were sealed using nail polish, and the specimens were viewed on a Biorad MRC-1024ES confocal laser scanning microscope. Black and gain levels were set using normal hearts stained with CH1 and then all samples were examined under identical conditions. A 24-section (0.5- $\mu\text{m}$ /section) Z-series (optical sections) was made for each sample, and the Lasersharpe system software was employed to display the image on the monitor. Digital image processing was performed with Adobe Photoshop<sup>®</sup> 5.0 software and printed with a Kodak<sup>®</sup> 8600 thermal dye printer.

### **2.2d Total RNA extraction**

Total RNA was extracted from the transfected heart tissues using a Qiagen mini-RNA extraction kit. The total RNA was treated with RNase-free DNase (Gibco BRL) for 15 minutes at room temperature, then phenol:chloroform extracted and precipitated with ethanol at -70°C for 1 hour or overnight at -20°C. RNA purity and concentration was estimated on a Pharmacia Biotech GeneQuant II RNA/DNA calculator.

### **2.2e RT-PCR analyses**

Reverse transcriptase polymerase chain reaction was used to evaluate the expression of transcripts ATmC-2 and ATmC-3 in the transfected embryonic heart RNA. Each first strand cDNA synthesis reaction was completed with 1.0  $\mu\text{l}$  total RNA using Gibco BRL SuperScript<sup>TM</sup> II Reverse Transcriptase with Oligo(dT)<sub>12-18</sub> primer. The reaction mix contained 1  $\mu\text{g}$  of total RNA (~50 stage 37-39 embryonic hearts), 1  $\mu\text{g}$  Oligo(dT)<sub>12-18</sub> primer, and dH<sub>2</sub>O to 12  $\mu\text{l}$ , which was incubated at 70°C for 10 minutes then placed on ice. Subsequently, 7  $\mu\text{l}$  of a reaction mix [per reaction: 2  $\mu\text{l}$  10X PCR buffer, 2  $\mu\text{l}$  25 mM MgCl<sub>2</sub>, 1  $\mu\text{l}$  dNTP stock (10  $\mu\text{M}$  each of dATP, dCTP, dGTP, and dTTP), and 2  $\mu\text{l}$  0.1 M DTT] was added to the RNA-primer mixture and incubated at 42°C for 5 minutes. Then 1  $\mu\text{l}$  (200 units) of SuperScript<sup>TM</sup> II Reverse Transcriptase was added to the reaction and incubation for 50 minutes at 42°C. This was followed by a 15 minute incubation at 70°C to terminate the reaction, after which the samples were placed on ice. RNase H was added to each tube and incubated at 37°C before amplification of the target cDNA. 2  $\mu\text{l}$  of the first strand synthesis reaction was subsequently used for amplification in a 100  $\mu\text{l}$  PCR reaction. Primer-pairs used were TMC3(+) (sense strand ATmC-3, exon 5) with TMBS(-)2 (antisense strand ATmC-3, 3' UTR region) and TM+9 with TMend(-) which are specific for full length cloning of ATmC-2. Polymerase chain reaction was performed with a PE 9600 thermocycler using AmpliTaq DNA polymerase (Perkin-Elmer). The program used to amplify the target cDNA was:

## *I. The Role of Tropomyosin in Cardiac Myofibrillogenesis*

- (1) 2 minutes at 50°C,
- (2) 15 minutes at 70°C,
- (3) 2 cycles –
  - a. Denaturing for 1 minute at 94°C
  - b. Annealing for 30 seconds at 53°C
  - c. Extension for 30 seconds at 68°C
- (4) 7 cycles –
  - a. Denaturing for 10 seconds at 95°C
  - b. Annealing for 10 seconds at 55°C
  - c. Extension for 10 seconds at 72°C
- (5) 35 cycles –
  - a. Denaturing for 10 seconds at 90°C
  - b. Annealing for 10 seconds at 60°C
  - c. Extension for 10 seconds at 72°C
- (6) Hold at 72°C

The PCR products were electrophoresed on 1-1.5% agarose gel.



## **2.3 RESULTS**

Normal embryonic axolotl hearts, from stages 37-39, were treated with sense and antisense oligonucleotides for ATmC-1 and ATmC-3 tropomyosin isoforms using cationic liposomes. Normal control hearts had widespread branching myofibrils when stained with tropomyosin specific CH1 antibody (Figure 2-1a) or other contractile protein antibodies. Furthermore, double staining of the nuclei with Hoechst dye at 5 days clearly showed co-localization of the fluorescein and nuclear staining (Figure 2-2). Fluorescein-tagged sense oligonucleotides provided a clear indicator of transfection efficiency. Analysis of the fluorescein and Hoechst staining showed up to 90% efficiency of oligonucleotide delivered to the nucleus.

### **2.3a Liposome-mediated delivery of tropomyosin oligonucleotides**

At 5 days after transfection of sense oligonucleotide, myofibrils were present in the heart and the fluorescein-labelled oligonucleotide was detected in the nuclei (Figure 2-1b). Before 5 days, the fluorescein was detected in the cytoplasm. Transfection of antisense ATmC-1 into whole hearts primarily disrupted the conus region (an area which later becomes the outflow chamber from the ventricle), but not the ventricle. At 3 days, the fluorescein-tagged oligonucleotide was within the heart, but not all localized to the nuclei (Figure 2-1c). Transfection with antisense ATmC-3 revealed a decrease in tropomyosin protein in the ventricle, but not the conus (Figure 2-1d). Tropomyosin was reduced about the same amount in each section. Myofibril organization was significantly disrupted in these antisense-transfected hearts.

### **2.3b Effect of oligonucleotides on heart function of whole heart organ cultures**

Transfection of normal hearts with sense ATmC-3 chimeric oligonucleotide retained their ability to contract at an average of 14 beats per minute. All 8 hearts continued to beat for 5 days after which they were fixed (Figure 2-3). However, beating was disrupted in the hearts transfected with antisense ATmC-3 transcript. Out of these 12 hearts contractions stopped completely in 8, and the average beats per minute of the remaining 4 hearts was half of those transfected with the sense oligonucleotide at 7 beats per minute (see Figure 2-3). Antisense oligonucleotide transfection effectively replicated the phenotype of the cardiac mutant (*c/c*) hearts in this animal model (Starr *et al.*, 1989), with a reduction of tropomyosin expression, a subsequent disruption of organized myofibrils, and a lack of beating.

### **2.3c RT-PCR of transfected hearts**

RT-PCR of whole hearts transfected with antisense ATmC-3 showed decreased ATmC-3 transcript. In contrast, transfection of sense ATmC-3 did not comparatively decrease the ATmC-3 transcript. Also in the antisense ATmC-3-transfected hearts, RT-PCR for the isoform ATmC-2 transcript did not demonstrate a decrease in the ATmC-2 transcript, as might be expected (see Spinner *et al.*, (2002) for further details).

## **2.4 DISCUSSION**

Tropomyosin forms an alpha-helical coiled coil dimer in a head to tail arrangement and is closely associated with actin and troponin subunits (Ebashi, 1980). Hence, the lack of organised myofibrils may be caused by an error in the tropomyosin protein. This was demonstrated by the use of antisense oligonucleotides, where the blockade of tropomyosin transcript caused disordered myofibrillogenesis. It was noted that the antisense ATmC-1 oligonucleotide disrupted the myofibrils of the future outflow tract (conus) and not the ventricle; whereas the opposite was true for antisense ATmC-3 oligonucleotide – only the myofibrils of the ventricles were in disarray. RT-PCR confirmed the decrease of ATmC-3 transcript in those hearts transfected with antisense ATmC-3 oligodeoxynucleotides, hence the efficacy of cationic liposome-mediated transfection.

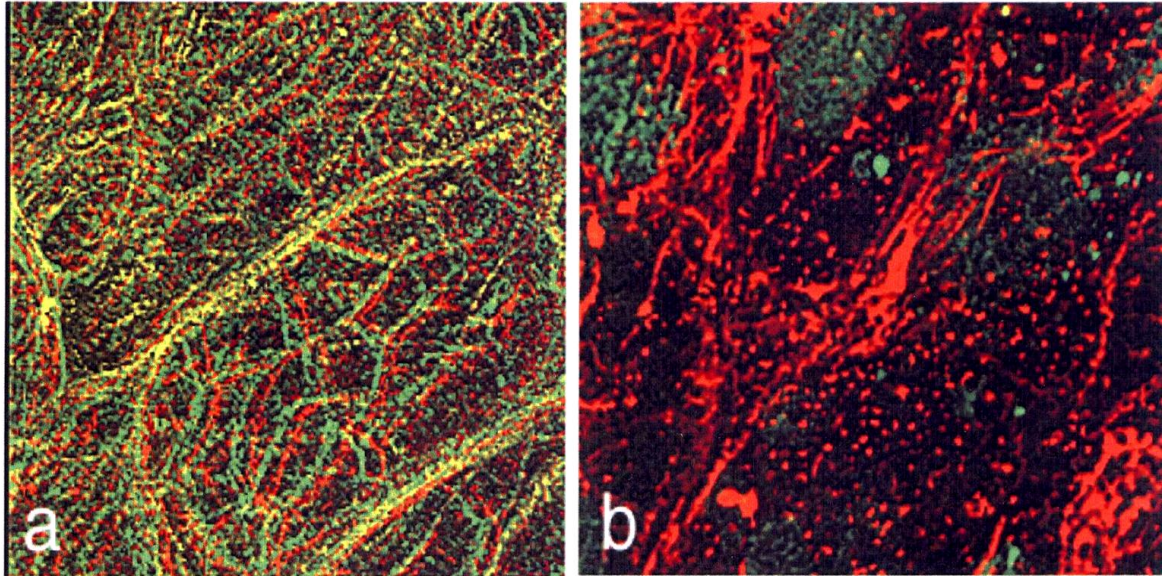
The effect of tropomyosin antisense oligonucleotides is like that seen in the naturally occurring mutation that affects the development and function of the myocardium in the Mexican axolotl. Mutant embryos survive for a short period of time without establishing normal circulation. Their hearts do not beat and have been found to show a disruption of the myofibril organization (Lemanski, 1973). These *cardiac (c/c)* lethal mutants are characterised by a severe reduction in tropomyosin (as confirmed by biochemical studies (Moore & Lemanski, 1982; Starr *et al.*, 1989)) and a lack of organised myofibrils (morphologically observed (LaFrance & Lemanski, 1995)). Although the mutants have near normal levels of actin, they are found in amorphous collections instead of as thin filaments as in the wild types. Liposome mediated introduction of tropomyosin protein in living mutant whole hearts have resulted in the formation of thin filamentous actin as well

## ***I. The Role of Tropomyosin in Cardiac Myofibrillogenesis***

as organised sarcomeric myofibrils (Zajdel *et al.*, 2000). It thus appears that tropomyosin is necessary for the stabilisation of thin actin filaments.

Transfection of oligonucleotides with LIPOFECTIN Reagent provided a method to examine function of a specific protein in an intact organ. Intercellular communications and mechanical load were maintained in these transfected hearts, which was critical because of the complex branching of myofibrils among the myocytes and the complex communications inherent in heart muscle. Staining with fluorescein-tagged sense oligonucleotide and Hoechst staining of the nuclei demonstrated delivery of the oligonucleotide to the nucleus in the majority of the cardiomyocytes. A disruption of structure and function in whole hearts was demonstrated after transfection of antisense oligonucleotides. Cationic transfection used in this manner could provide varied and interesting 'knock-out' models to study the importance of particular proteins as illustrated in this study. It has been found that ATmC-3 is important in myofibril organisation as well as the functional beating of the heart.

**Figure 2-1. Confocal micrographs of normal, sense and antisense transfected hearts.**



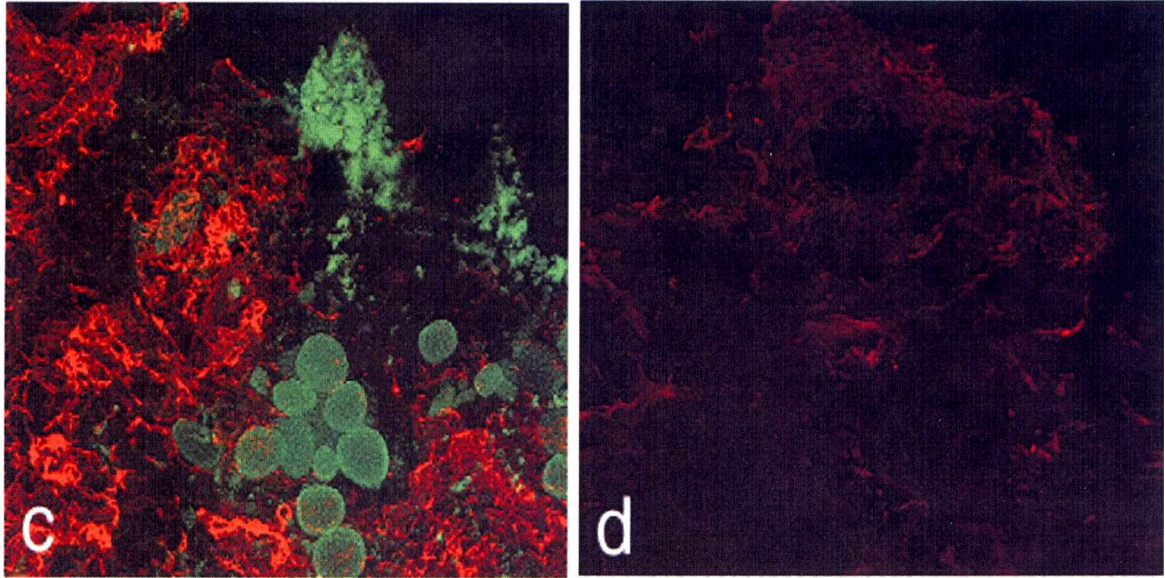
Scale bar = 5µm —

**Figure 2-1a** - Stereo anaglyph of a normal heart (12-µm thickness) stained with tropomyosin antibody. Branching myofibrils can be observed throughout the field.

*Note: Stereo anaglyphs are best viewed with red/green glasses.*

**Figure 2-1b** - Compressed Z series of a heart transfected with fluorescein-tagged ATmC-3 sense oligonucleotide (green) and stained with tropomyosin antibody (red). This micrograph is composed of two optical sections (1-µm total thickness) to best show the nuclei.

**Figure 2-1. Confocal micrographs of normal, sense and antisense transfected hearts.**

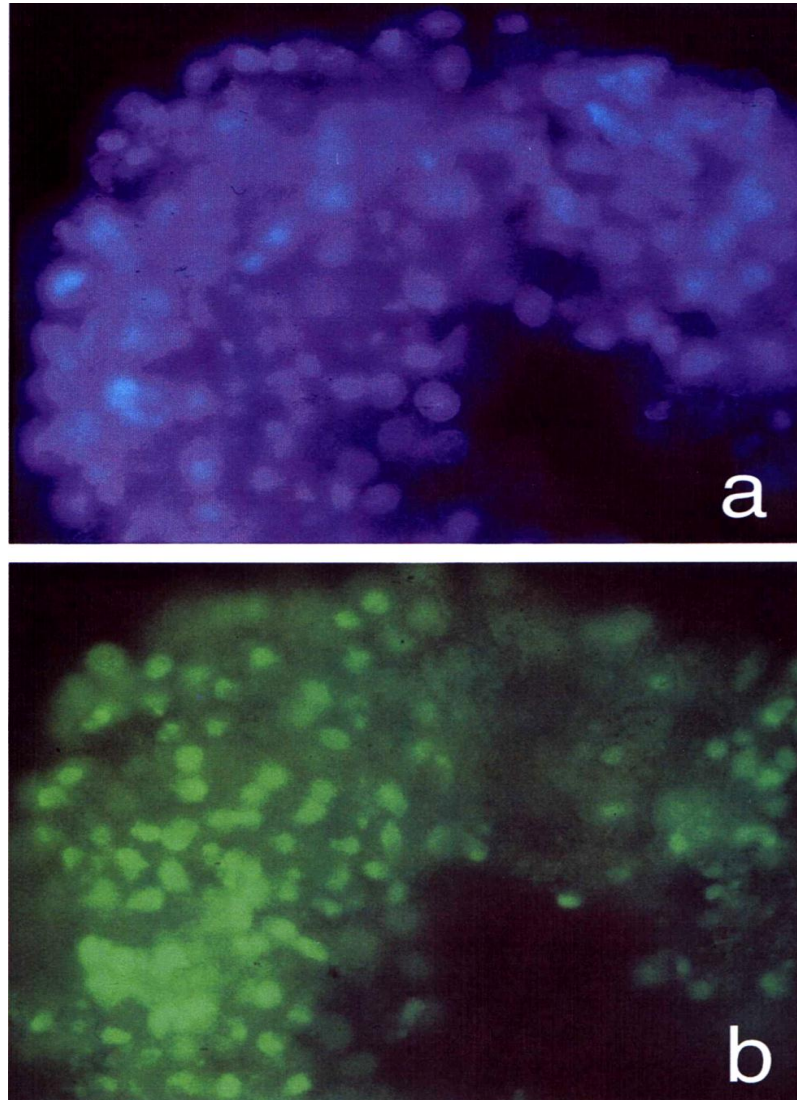


Scale bar = 50µm —

**Figure 2-1c** - Conus (12-µm total thickness) transfected with ATmC-1 fluorescein-tagged antisense oligonucleotide (green) and stained with tropomyosin antibody (red).

**Figure 2-1d** - Heart (12-µm total thickness) transfected with ATmC-3 antisense oligonucleotide and stained with tropomyosin antibody (red).

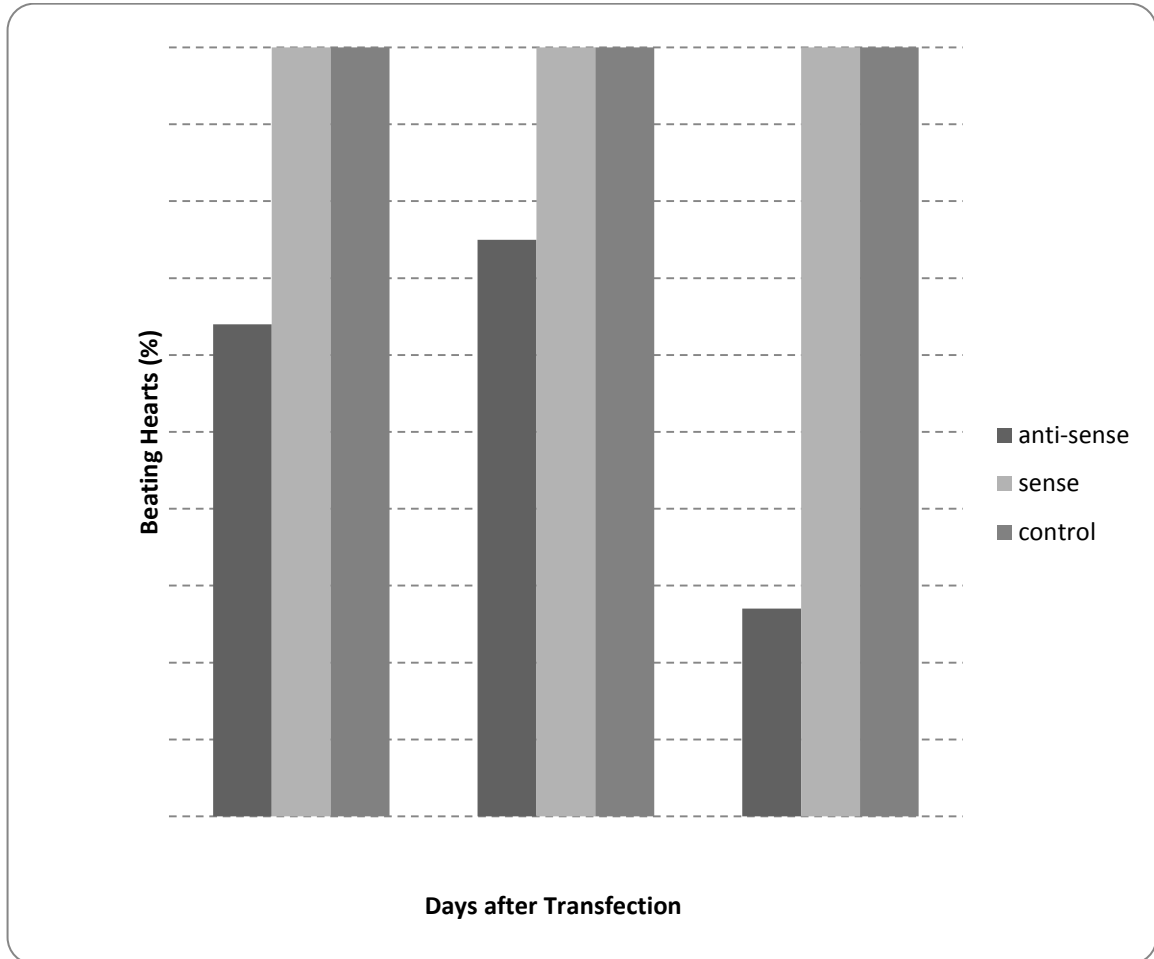
**Figure 2-2. Localisation of transfected oligonucleotides**



Scale bar = 100 $\mu$ m 

Hearts were stained with Hoechst (blue – Figure 2-2a) 5 days after they were transfected with fluorescein-tagged sense ATmC-3 (green – Figure 2-2b).

**Figure 2-3. Effect of antisense ATmC-3 on heart beat**



Heart beats are the average of 11 hearts for control, 8 hearts for sense, and 12 hearts for antisense oligonucleotides.



Published in 2004 in *Biochemical and Biophysical Research Communications* **320**; 1291-1297.

## CHAPTER THREE

### EXPRESSION OF A NOVEL CARDIAC-SPECIFIC TROPOMYOSIN ISOFORM IN HUMANS

#### 3.0 ABSTRACT

Tropomyosins are a family of actin binding proteins encoded by a group of highly conserved genes. Humans have four tropomyosin-encoding genes: *TPM1*, *TPM2*, *TPM3*, and *TPM4*, each of which is known to generate multiple isoforms by alternative splicing, promoters, and 3' end processing. *TPM1* is the most versatile and encodes a variety of tissue specific isoforms. The *TPM1* isoform specific to striated muscle, designated TPM1 $\alpha$ , consists of 10 exons: 1a, 2b, 3, 4, 5, 6b, 7, 8, and 9a/b. In this study, using RT-PCR with adult and fetal human RNAs, we present evidence for the expression of a novel isoform of the *TPM1* gene that is specifically expressed in cardiac tissues. The new isoform is designated TPM1 $\kappa$  and contains exon 2a instead of 2b. Ectopic expression of human GFP.TPM1 $\kappa$  fusion protein can promote myofibrillogenesis in cardiac mutant axolotl hearts that are lacking in tropomyosin.

### **3.1 INTRODUCTION**

Vertebrate tropomyosins (TMs) are a family of actin binding proteins encoded by a group of highly conserved genes that likely evolved as a result of gene duplication over the evolutionary periods. In humans, there are four tropomyosin-encoding genes: *TPM1* (located on chromosome 15q22), *TPM2* (chromosome 9p13), *TPM3* (chromosome 1q21.2), and *TPM4* (chromosome 19p13.1) (Perry, 2001; Martson & Redwood, 2003; Lees-Miller & Helfman, 1991; Wieczorek *et al.*, 1988; Nadal-Ginard, 1990). Each gene is known to generate multiple isoforms via alternative splicing, alternative promoters, and different 3' end processing (Wieczorek *et al.*, 1988; Nadal-Ginard, 1990). Of the four, *TPM1* is the most versatile and encodes a variety of tissue specific isoforms via alternative splicing and/or the use of two promoters; the transcripts encode proteins of either 248 or 284 amino acids in length. Tropomyosins may be divided into three categories: striated muscle TMs, smooth muscle TMs, and cytoplasmic TMs. The striated muscle isoforms are a component of the thin filaments of myofibrils, the contractile apparatus of striated muscle tissues. The *TPM1* isoform specific to striated muscle consists of 10 exons: 1a, 2b, 3, 4, 5, 6b, 7, 8, and 9a/b and is designated TPM1 $\alpha$  (Figure 3-1) (Wieczorek *et al.*, 1988; Nadal-Ginard, 1990). The smooth muscle specific isoform of the *TPM1* gene is designated TPM1 $\beta$  and consists of exons: 1a, 2a, 3, 4, 5, 6b, 7, 8, and 9c/d (Wieczorek *et al.*, 1988; Nadal-Ginard, 1990).

## ***I. The Role of Tropomyosin in Cardiac Myofibrillogenesis***

This study presents evidence for expression of a novel isoform of the *TPM1* gene that is expressed in the cardiac tissue of humans and contains “smooth muscle type” exon 2a. The hearts of cardiac mutant Mexican axolotls are an ideal system for studying myofibrillogenesis in vitro because they are deficient in tropomyosin protein (Zajdel *et al.*, 1998; Zajdel *et al.*, 2002; Zajdel *et al.*, 2003). As a result, these hearts do not have organized myofibrils (the contractile apparatus of cardiac muscle) and therefore do not beat. One can promote myofibrillogenesis by ectopic expression of tropomyosin. For example, when murine TPM1 $\alpha$  is expressed in organ cultured mutant hearts, organized myofibrils are formed. We were interested to know whether TPM1 $\alpha$  and TPM1 $\kappa$  from human have the ability to promote myofibrillogenesis in mutant axolotl hearts.

### **3.2 MATERIALS AND METHODS**

#### **3.2a Total human RNA**

Human total RNA was procured from a number of commercially available RNA banks; adult heart and skeletal RNA (Clontech), fetal heart and skeletal >6 weeks old (Stratagene), fetal heart and skeletal = 6 weeks (Genotech), and adult left ventricle, left atrium, right ventricle, and right atrium (Ambion).

#### **3.2b Reverse transcriptase polymerase chain reaction**

Reverse transcriptase polymerase chain reaction (RT-PCR) with RNA from adult and fetal sources was carried out with gene and isoform specific oligonucleotides (as outlined in

## ***I. The Role of Tropomyosin in Cardiac Myofibrillogenesis***

Figure 3-1) to determine the expression pattern of TPM1 $\kappa$  and TPM1 $\alpha$ , following our standard protocol (Zajdel *et al.*, 2002). Using 2  $\mu$ g of total RNA, first strand synthesis of cDNA was done using Superscript II with oligo(dT) priming following the manufacturer's protocol (Invitrogen). PCR was carried out in an Applied Biosystems 9700 thermal cycler. Subsequent to PCR amplification and gel electrophoresis, Southern blot analysis was performed with isoform specific oligonucleotides as previously described (Zajdel *et al.*, 2002). The oligonucleotides used in this study are as follows:

P1(+): 5'-TCG AAT TCA TGG ACG CCA TCA AGA-3'

and

P2(-): 5'-ATG TCG ACC TTA TAT GGA AGT CAT ATC G-3'

which are common to both TPM1 $\alpha$  and TPM1 $\kappa$ . Primer P1 contains an *Eco*RI restriction site and P2 contains a *Sal*I site to facilitate directed ligation into the pEGFP expression vector.

P3(+): 5'- TGT CAC TGC AAA AGA AAC TC-3'

and detector oligonucleotide

D1(+): 5'-AAG ATG AAC TGG ACA AAT AC-3'

are specific to exon 2b of TPM1 $\alpha$ .

P4(+): 5'-TCG AGG AGG ACA TCG CGG CC-3'

and detector

D2(+): 5'-GAA GTT GCT GCG GGT GTC GG-3'

## ***I. The Role of Tropomyosin in Cardiac Myofibrillogenesis***

are specific to exon 2a of TPM1 $\kappa$ . As a control, RT-PCR was performed for the human glyceraldehyde 3-phosphate dehydrogenase (GAPDH) house-keeping gene with gene specific primer-pair

(+): 5'-GTT TAC ATG TTC CAA TAT GAT TCC AC-3'

and

(-): 5'-TCA TAT TTG GCA GGT TTT TCT AGA C-3'.

### **3.2c DNA sequencing.**

DNA sequencing was performed at Cornell University DNA Sequencing Facility in Ithaca, NY.

**3.2d Preparation of pEGFP.HumTPM1 $\alpha$  and pEGFP.HumTPM1 $\kappa$  expression constructs.** Using our published strategy (Zajdel *et al.*, 2003), we amplified either TPM1 $\alpha$  or TPM1 $\kappa$  T/A cloned cDNA using primer-pair P1(+) and P2(-), which contains the restriction sites *EcoRI* and *SaII*, respectively, for ligation into the pEGFP expression vector (Clontech). Subsequent to restriction enzyme digestion and purification, T4 DNA ligase was used to insert each fragment into pEGFP. The ligation mix was then transformed into INV $\alpha$  F' competent *Escherichia coli* cells (Invitrogen) and grown on LB plates in the presence of kanamycin selection (50  $\mu$ g/ml). Colony hybridization using nitrocellulose membranes was carried out with isoform specific oligonucleotides end-labelled with <sup>32</sup>P. Positive colonies were selected and DNA extracted for confirmation of insertion by sequencing. The GFP expression is driven by a CMV promoter with the tropomyosin isoform linked in frame to carboxy terminal end of the GFP.

### **3.2e Transfection of embryonic axolotl hearts**

Normal and mutant axolotl embryos were obtained from the Indiana University Axolotl Colony. Stage 37–39 embryos were washed in Steinberg's solution (58mM NaCl, 0.67mM KCl, 0.9mM CaCl<sub>2</sub>, 0.2mM MgSO<sub>4</sub>, and 4.6mM Hepes [pH 7.4], containing 1% Invitrogen antibiotic/antimycotic [100 U/ml penicillin G, 0.1 g/ml streptomycin sulfate, and 0.25 µg/ml amphotericin B] and filter sterilized). Hearts were dissected out of MS-222 (tricaine methanesulfonate) anesthetized embryos using fine-tip forceps and placed into Steinberg's solution. Transfection of dissected hearts was facilitated by Lipofectin reagent (Invitrogen). Steinberg's solution and Lipofectin were mixed 1:1 and allowed to incubate at room temperature for 30–45 min. Plasmid DNA at a concentration of 5 µg (either pEGFP.HumTPM1 $\alpha$  or pEGFP.HumTPM1 $\kappa$ ) was then added to the Lipofectin/Steinberg's mix and incubated for another 15 min. The hearts were then transferred into the transfection solution, incubated for 48 h at 19°C, transferred to fresh Steinberg's, and incubated for another 72 h.

### **3.2f Confocal microscopy**

Subsequent to incubation in the transfection media, embryonic axolotl hearts (normal and mutant) were processed for fluorescent staining using a process adapted from Zajdel *et al.* (1998). Hearts were placed in 1 mM DTSP dissolved in 1% DMSO in Steinberg's for 15 min to mildly fix and permeabilize. The hearts were further permeabilized in 0.5% NP-40 in Steinberg's for 10 min, and then quenched in two 10 min washes in 0.1 M glycine. Monoclonal anti-tropomyosin (CH1) at a concentration of 1:30 in Steinberg's or polyclonal anti-GFP at 1:100 was used for immunohistochemical staining of embryonic

## ***I. The Role of Tropomyosin in Cardiac Myofibrillogenesis***

hearts. Hearts were incubated in antibody solution overnight. Non-specific background binding was blocked with 0.1 mg/ml BSA by three 10 min washes. Secondary antibodies, lissamine rhodamine (red) anti-mouse and FITC (green) anti-rabbit at a 1:50 dilution in Steinberg's, were used for secondary staining. The hearts were rinsed in BSA in Steinberg's and fixed in 2% paraformaldehyde for ~2 h. The fixation was quenched using 0.1 M glycine for 30 min and then placed in Steinberg's. Hearts were mounted on slides using Fluorogard antifade reagent (Bio-Rad) and viewed on an MRC-1024ES confocal laser scanning microscope at 20x. A multiple section Z-series was taken for each heart and visualized using Lasersharpe system software.

### **3.3 RESULTS**

Total human heart RNA obtained commercially. TPM1 $\alpha$  and TPM1 $\kappa$  cDNA was amplified using PCR via the strategy depicted in Figure 3-1. The PCR product for each was then cloned into a T/A cloning vector (Invitrogen) and filter hybridization was carried out with isoform specific detector oligonucleotides to identify the positive clones, i.e., D1 for TPM1 $\alpha$  and D2 for TPM1 $\kappa$  (Figure 3-1). DNA was extracted from the positive colonies and nucleotide sequence of each of the clones was determined. Figure 3-2 depicts the nucleotide sequence of the coding region of the TPM1 $\kappa$  isoform.

Using RT-PCR, we determined the expression pattern of TPM1 $\alpha$  and TPM1 $\kappa$  in skeletal muscle and cardiac tissues from humans at various stages of development. The results presented in Figure 3-4A show that the full coding sequence of TPM1 $\alpha$  and TPM1 $\kappa$  (~860 nucleotides long) can be amplified by "generic" primer pair P1(+)/P2(-). Southern

## ***1. The Role of Tropomyosin in Cardiac Myofibrillogenesis***

hybridization with the TPM1 $\alpha$  specific probe D1 shows that TPM1 $\alpha$  is expressed in all tissues (Figure 3-4B). However, TPM1 $\alpha$  expression in adult (lane 2) and fetal skeletal muscles (lanes 4 and 6) is lower relative to its expression in cardiac tissues (adult heart, lane 1; and fetal cardiac tissues (lanes 3 and 5)). The most intriguing observation is that TPM1 $\kappa$  is expressed only in cardiac muscle tissues (adult, lane 1; and fetal, lanes 3 and 5, in Figure 3-4C) and not in skeletal muscles (adult, lane 2; and fetal, lanes 4 and 6). For normalization, we performed RT-PCR of human housekeeping gene, GAPDH (Figure 3-4D).

In order to confirm the cardiac specificity of TPM1 $\kappa$ , we performed RT-PCR using isoform specific primer pair P4(+) and P2(-) (Figure 3-5A). Additionally, we carried out Southern hybridization with isoform specific detector oligonucleotides (D1 for TPM1 $\alpha$  and D2 for TPM1 $\kappa$ ). The results presented in Figure 3-5B show that the primer-pair used does not amplify TPM1 $\alpha$  since none was detected by D1. Figure 3-5C indicates that TPM1 $\kappa$  is expressed only in cardiac tissues (adult, lane 1; and fetal, lanes 3 and 5) but not in skeletal muscles (adult, lane 2; and fetal, lanes 4 and 6) when probed by D2. Ethidium staining of the RT-PCR amplification of human GAPDH is shown in Figure 3-5D. Expression of TPM1 $\alpha$  can be seen in both cardiac and skeletal muscles tissues when amplified using isoform specific primers P3(+) and P2(-) (Figures 3-6A and B). The Southern hybridization in Figure 3-6C shows the specificity of the TPM1 $\alpha$  primer pair since no TPM1 $\kappa$  can be detected by D2.

RNA from an adult individual's left ventricle, left atrium, right ventricle, and right atrium was used for RT-PCR to see if there was any variability in expression of either TPM1 $\kappa$  or  $\alpha$  between heart segments. As can be seen in the Southern hybridization data in Figures 3-7B and C, the expression of both isoforms is present across the four hearts segments analysed.



## ***I. The Role of Tropomyosin in Cardiac Myofibrillogenesis***

Two expression constructs with human TPM1 $\alpha$  and TPM1 $\kappa$ , designated as pEGFP.HumTPM1 $\alpha$  and pEGFP.HumTPM1 $\kappa$  were created to differentiate between the two isoforms of tropomyosin. Confocal microscopy was used to show that both GFP.HumTPM1 $\alpha$  (Figures 3-8C and D) and GFP.HumTPM1 $\kappa$  (Figures 3-8E and F) could be incorporated into organized myofibrils in both normal and mutant axolotl heart. The proteins were observed by staining with both anti-GFP antibody (green) and CH1 anti-tropomyosin antibody (red) that recognizes both TPM1 $\alpha$  and TPM1 $\kappa$ , with yellow indicating areas of co-localization.

### **3.4 DISCUSSION**

This is the first report of a cardiac specific tropomyosin isoform that is an alternative splice product of the *TPM1* gene. The new isoform is designated as TPM1 $\kappa$  (to signify the 10th and newest isoform) and contains exons 1a, 2a (instead of 2b as in TPM1 $\alpha$ ), 3, 4, 5, 6b, 7, 8, and 9a/b (Figure 3-1). From human heart RNA, Denz (of Denz *et al.* (2004)) identified, cloned, and sequenced the cDNA of TPM1 $\kappa$  and using RT-PCR determined the expression pattern of both striated muscle isoforms TPM1 $\alpha$  and TPM1 $\kappa$  in striated muscle tissues of humans during development. Expression patterns of both isoforms have also been determined in different segments of human heart (i.e., left ventricle, left atrium, right ventricle, and right atrium). In addition, ectopic expression of GFP.Hum-TPM1 $\alpha$  or GFP.HumTPM1 $\kappa$  fusion protein can promote myofibrillogenesis in mutant axolotl hearts, which are practically devoid of tropomyosin protein and therefore lack organized myofibrils (Lemanski, 1973; Zajdel *et al.*, 1998). Thus if we can understand the processes

## ***I. The Role of Tropomyosin in Cardiac Myofibrillogenesis***

of myofibrillogenesis in the axolotl then we can easily extrapolate the findings to help elucidate the mechanisms involved in human cardiac diseases.

This study has demonstrated the expression of a novel tropomyosin isoform of the human *TPM1* gene, TPM1 $\kappa$ . An alignment of the nucleotide sequence of both the TPM1 $\alpha$  form and the TPM1 $\kappa$  form shows them to be exactly the same, with the exception of exon 2 (Figure 3-1). TPM1 $\alpha$  contains exons that are specific to striated muscle, including exon 2b, whereas TPM1 $\kappa$  contains exon 2a, an exon normally associated with smooth muscle type isoform (TPM1 $\beta$ ) from the *TPM1* gene. The sequences for TPM1 $\alpha$  and TPM1 $\kappa$  have been submitted to GenBank (Accession Nos. Y640415 and AY640414, respectively). Interestingly, exon 2 sequences of TM isoforms from various vertebrate species illustrates the highly conserved nature of both exon 2a, found in TPM1 $\kappa$ ; and exon 2b, found in TPM1 $\alpha$  (Figure 3-3).

It is known that the striated muscle isoform of the *TPM1* gene is primarily involved in cardiac muscle contractility and that the striated muscle isoform of the *TPM3* gene (a.k.a. TM-30 or  $\alpha$ -slow tropomyosin) is primarily involved in the contractile activity of skeletal muscles in humans. This would account for the reduced amount of *TPM1* expression in skeletal muscle versus cardiac tissues. The use of specific detector oligonucleotides during Southern hybridization, namely D1 and D2 for TPM1 $\alpha$  and TPM1 $\kappa$ , respectively, strongly suggest that the splicing event(s) for generating TPM1 $\kappa$  is specific for cardiac tissues in humans.

Currently, the theory of segmental heart development is gaining popularity. According to this theory, different segments of vertebrate hearts come from different heart fields (Markwald *et al.*, 1996). This theory is supported by the differential gene expression

## ***I. The Role of Tropomyosin in Cardiac Myofibrillogenesis***

(transcription factors in particular) in different heart segments (Lyons, 1996). For example, in mice the *dHAND* gene is expressed in the left ventricle and the *eHAND* gene is expressed in the right (Srivastava, 1997). The splice factor(s) responsible for generating TPM1 $\kappa$  from the *TPM1* gene in humans is/are specific to cardiac tissues. Hence we were interested in finding out whether there was a differential expression pattern of TPM1 $\kappa$  or TPM1 $\alpha$  within the four chambers of the human heart. Expression of both isoforms was found in all four chambers and so there was no evidence of variable gene expression of TPM1 $\alpha$  and TPM1 $\kappa$  in the human heart (Figure 3-7).

Unfortunately, one of the difficulties in the field of tropomyosin research is the unavailability of isoform specific antibodies. CH1 anti-tropomyosin antibody recognizes both TPM1 $\alpha$  and TPM1 $\kappa$ . This problem has been overcome by the creation of GFP fusion proteins for each of the two isoforms from the Mexican axolotl that have the ability to form myofibrils in axolotl hearts (Zajdel *et al.*, 2002).

Confocal microscopy images (Figure 3-8) suggest that the human and axolotl proteins are interchangeable. Striated myofibrils form in the mutant axolotl heart using either axolotl tropomyosin specific constructs GFP.ATmC-1 and GFP.ATmC-2 (Zajdel *et al.*, 2002) or these human tropomyosin constructs GFP.HumTMP1 $\alpha$  and GFP.HumTPM1 $\kappa$ . However, the expression pattern of TPM1 $\kappa$  in humans is quite different from that seen in *Ambystoma mexicanum* (Mexican axolotl) where TPM1 $\kappa$  is expressed both in skeletal muscle and cardiac tissues (Luque *et al.*, 1997) and the relative expression of TPM1 $\kappa$  to TPM1 $\alpha$  is higher in axolotl heart than in human heart (Zajdel *et al.*, 2002). In chickens, both TPM1 $\alpha$  and TPM1 $\kappa$  are expressed in embryonic heart but neither is expressed in adult heart (Zajdel *et al.*, 2003). In addition, TPM1 $\alpha$  but not TPM1 $\kappa$  is expressed in skeletal muscles from both adult and embryonic birds. The cardiac specific nature of TPM1 $\kappa$  in chickens, as well

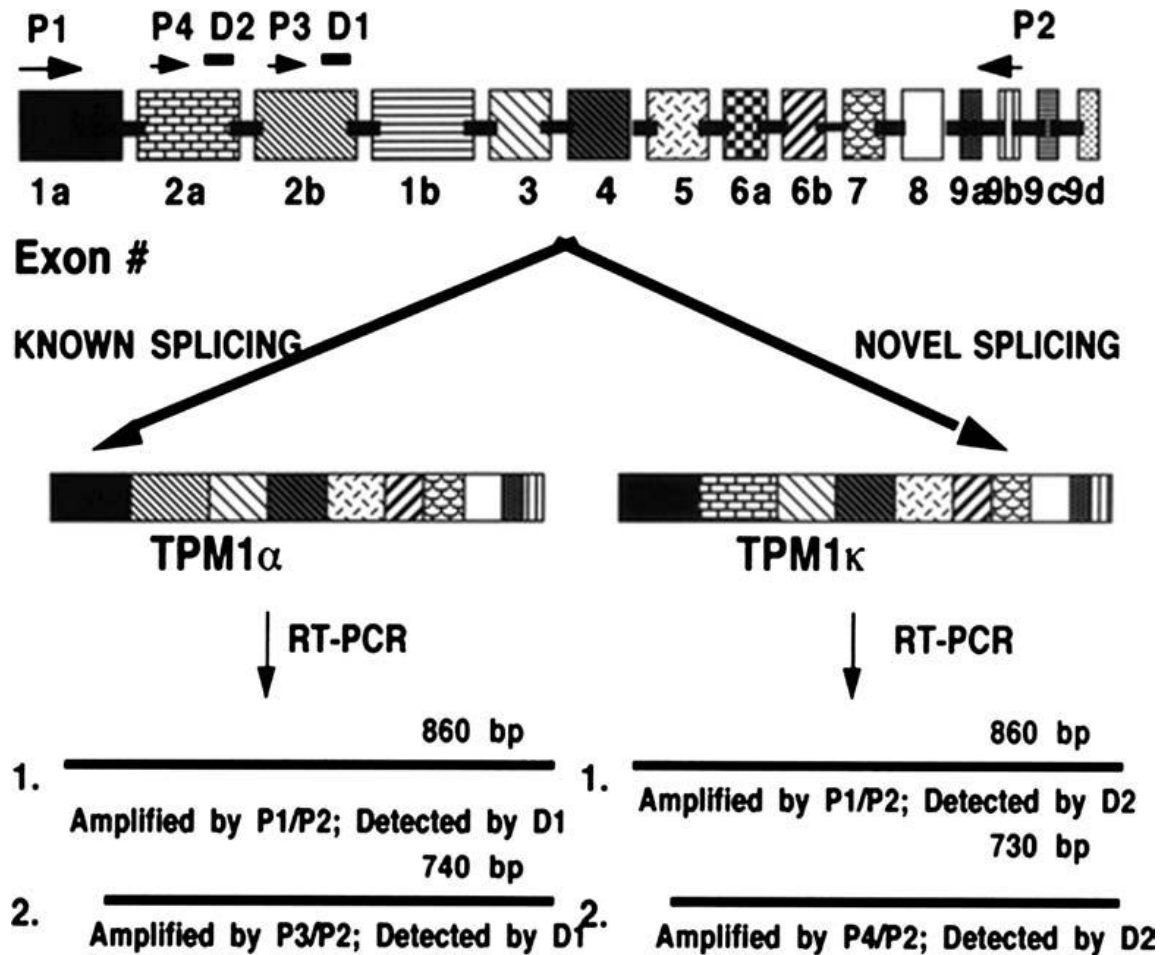
## ***I. The Role of Tropomyosin in Cardiac Myofibrillogenesis***

as the role it may play developmentally, makes this newly found human TPM1 $\kappa$  isoform an interesting focal point when considering how mutations in tropomyosin leading to various heritable cardiomyopathies may function.

Mutant axolotl hearts can be used for studying the structural/functional relationship of human tropomyosin proteins. Several missense mutations in the *TPM1* gene have been implicated in familial hypertrophic cardiomyopathy (FHC) and dilated cardiomyopathy (DCM) (Marston & Redwood, 2003; Muthuchamy *et al.*, 1999; Bottinelli *et al.*, 1997). Two of them have been found in exon 5 (D175N (Asp175Asn) and E180G (Glu180Gly) (Thierfelder *et al.*, 1994; Prabhakar *et al.*, 2001)), the putative troponin-T binding region that have been conserved during evolution. These two mutations appear to cause partial unwinding of the tropomyosin coiled-coil by alteration of surface charge in the troponin T binding regions (Golitsina *et al.*, 1997). When studies have been done on human cardiomyopathies, generally only the striated muscle isoform, TPM1 $\alpha$  is considered. However, the novel isoform TPM1 $\kappa$  also shares the latter two mutations since exon 5 is common to both. If it is found that TPM1 $\kappa$  also plays a role in cardiac myofibril formation in humans, one should consider that this novel isoform might also play an important role in the pathogenesis of human cardiomyopathies as well.

Given the cardiac specific nature of TPM1 $\kappa$  as well as the FHC and DCM missense mutation found to be associated with the *TPM1* gene, it would be logical to consider this novel splice variant as a new research avenue for discovering the mechanisms human cardiac dysfunction.

**Figure 3-1.** Strategy for PCR amplification of TPM1 $\alpha$  and TPM1 $\kappa$  and the splicing pattern for each.



On the left is the known splicing of TPM1 $\alpha$  with exon 2b and on the right is the novel TPM1 $\kappa$  splicing pattern with exon 2a, typically found in smooth muscle type TMs. The location of the specific oligonucleotides used for amplification and detection is shown along with the size of fragment observed after gel electrophoresis (sequences of each oligonucleotide can be found in Materials and methods).

**Figure 3-2. Nucleotide and amino acid sequence of human TPM1κ**

```

1   ATGGACGCCATCAAGAAGAAGATGCAGATGCTGAAGCTCGACAAGGAGAACGCCTTGGAT
   -----+-----+-----+-----+-----+
61  M D A I K K K M Q M L K L D K E N A L D
   CGAGCTGAGCAGGCGGAGGCCGACAAGAAGGCGGCGGAAGACAGGAGCAAGCAGCTCGAG
   -----+-----+-----+-----+
121 R A E Q A E A D K K A A E D R S K Q L E
   GAGGACATCGCGGCCAAGGAGAAGTTGCTGCGGGTGTCTGGAGGACGAGCGGGACCGGGTG
   -----+-----+-----+-----+
181 E D I A A K E K L L R V S E D E R D R V
   CTGGAGGAGCTGCACAAGGCGGAGGACAGCCTCCTGGCCGCCGAAGAGGCCGCCGCCAAG
   -----+-----+-----+-----+
241 L E E L H K A E D S L I A A E E A A A K
   GCTGAAGCCGACGTAGCTTCTCTGAACAGACGCATCCAGCTGGTTGAGGAAGAGTTGGAT
   -----+-----+-----+-----+
301 A E A D V A S L N R R I Q L V E E E L D
   CGTGCCAGGAGCGTCTGGCAACAGCTTTGCAGAAGCTGGAGGAAGCTGAGAAGGCAGCA
   -----+-----+-----+-----+
361 R A Q E R L A T A L Q K L E E A E K A A
   GATGAGAGTGAGAGAGGCATGAAAGTCATTGAGAGTCCGAGCCCAAAAAGATGAAGAAAA
   -----+-----+-----+-----+
421 D E S E R G M K V I E S R A Q K D E E K
   ATGGAAATTCAAGGATCCAAGTAAAGAGGCCAAGCACATTGCTGAAGATGCCGACCCGC
   -----+-----+-----+-----+
481 M E I Q E I Q L K E A K H I A E D A D R
   AAATACGAAGAGGTGGCCCGTAAGCTGGTCATCATTGAGAGCGACCTGGAACGTGCAGAG
   -----+-----+-----+-----+
541 K Y E E V A R K L V I I E S D L E R A E
   GAGCGGGCTGAGCTCTCAGAAGGCAAATGTGCCGAGCTTGAAGAAGAATTGAAAAGTGTG
   -----+-----+-----+-----+
601 E R A E L S E G K C A E L E E E L K T V
   ACCGAACGACTTGAAGTCACTGGAGGCTCAGGCTGAGAAGTACTCGCAGAAGGAAGACAGA
   -----+-----+-----+-----+
661 T N D L K S L E A Q A E K Y S Q K E D R
   TATGAGGAAGAGATCAAGGTCTTTCCGACAAGCTGAAGGAGGCTGAGACTCGGGCTGAG
   -----+-----+-----+-----+
721 Y E E E I K V L S D K L K E A E T R A E
   TTTGCGGAGAGGTGAGTAACTAAATTGGAGAAAAGCATTGATGACTTAGAAGACGAGCTG
   -----+-----+-----+-----+
781 F A E R S V T K L E K S I D D L E D E L
   TACGCTCAGAACTGAAGTACAAAGCCATCAGCGAGGAGCTGGACCACGCTCTCAACGAT
   -----+-----+-----+-----+
841 Y A Q K L K Y K A I S E E L D H A L N D
   ATGACTTCCATATAAGTT
   -----+-----+-----+-----+
858 M T S I * V

```

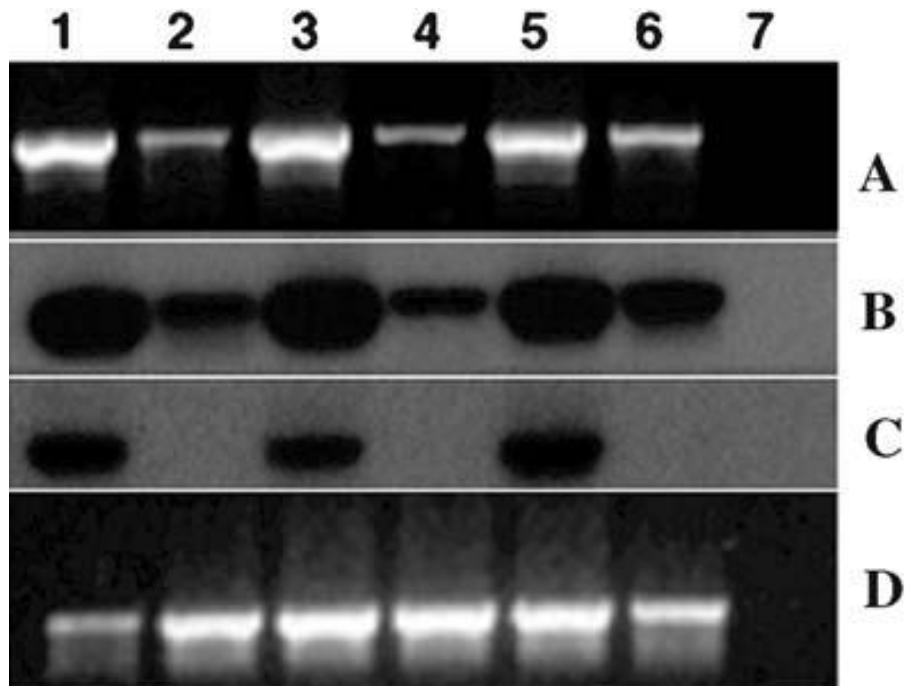
The sequence shares 100% homology with human TPM1α except at exon 2 (base pair 115–248). (Accession No. AY640414).

**Figure 3-3.** Amino acid sequence alignment of TPM1 $\kappa$  and TPM1 $\alpha$  from a variety of vertebrates.

HuTPM1 $\kappa$	LEEDIAAKEKLLRVSEDERDRVLEELHKAEDSLAEEAAK
ChTPM1 $\kappa$	..D..QLE..Q...T..S...Q....S.....S...N...
AxTPM1 $\kappa$	...E.....I.....V..... E...T.D.K...
RaTPM1 $\kappa$	.....S.....A..H.....D.T...
HuTPM1 $\alpha$	..DELVSLQ.K.KGT..EL.KYS.A.KDAQEK.EL..KK.TD
ChTPM1 $\alpha$	..DELVALQ.K.KGT..EL.KYS.S.KDAQEK.EL.DKK.TD
AxTPM1 $\alpha$	..DELVALQ.K.KGT..EL.KYS.S.KDAQEK.EL.DKK.TK
RaTPM1 $\alpha$	..DELVSLQ.K.KGT..EL.KYS.A.KDAQEK.EL..KK.TD

Hu, human; Ch, chicken; Ax, axolotl; and Ra, rat.

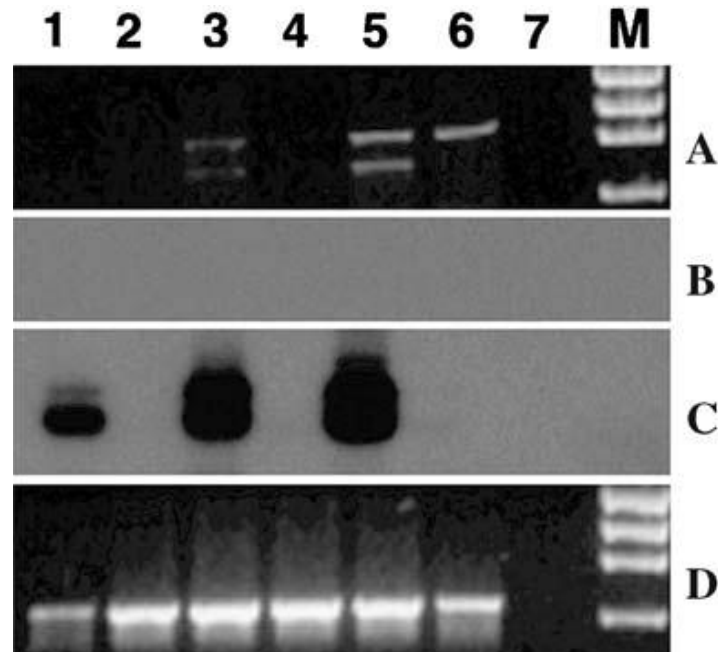
**Figure 3-4. Identification of a cardiac specific novel isoform of *TPM1*.**



PCR amplification of both TPM1 $\alpha$  and TPM1 $\kappa$  using “generic” primer pair P1(+)/P2(-) followed by Southern hybridization with isoform specific detector oligonucleotides. RNA from: lane 1, adult heart; lane 2, adult skeletal muscle; lane 3, fetal heart >6 weeks old; lane 4, fetal skeletal muscle >6 weeks old; lane 5, fetal heart = 6 weeks old; lane 6, fetal skeletal muscle = 6 weeks old; and lane 7, primer control. (A) Ethidium staining of PCR amplification using P1(+) and P2(-) primer pair. (B) Southern hybridization using D1 probe specific to exon 2b of TPM1 $\alpha$  shows this isoform to be present each tissue. (C) Southern hybridization using D2 probe specific to exon 2a of TPM1 $\kappa$ . This novel isoform is expressed only the cardiac tissues: lanes 1, 3, and 5. (D) Ethidium staining of human GAPDH as a loading control.

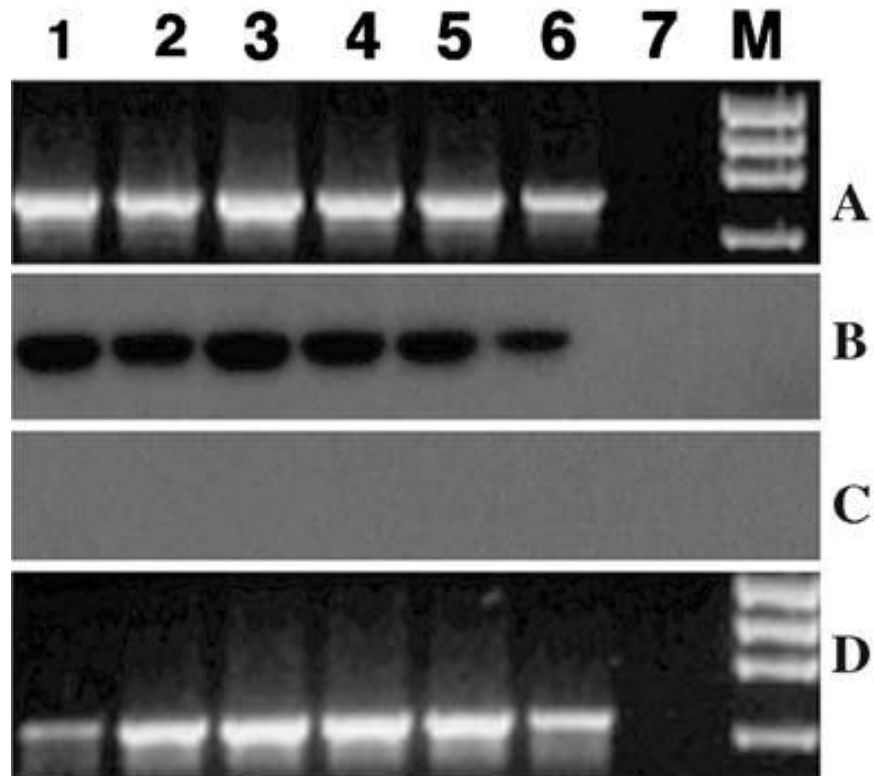


**Figure 3-5.** TPM1 $\kappa$  is found only in cardiac tissues by PCR amplification with exon 2a specific primer.



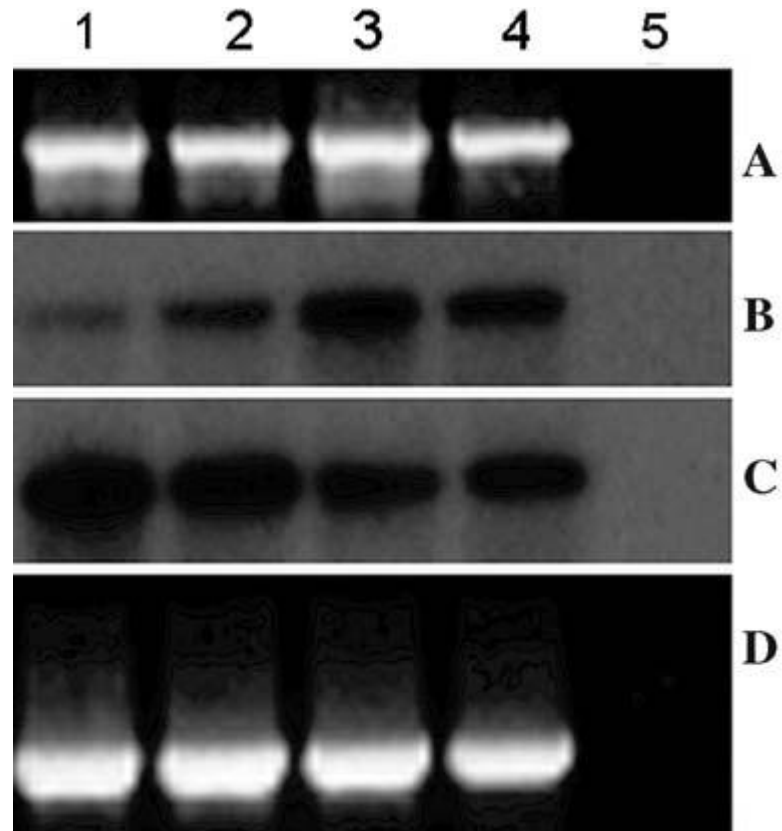
RNA from; lane 1, adult heart; lane 2, adult skeletal muscle; lane 3, fetal heart >6 weeks old; lane 4, fetal skeletal muscle >6 weeks old; lane 5, fetal heart = 6 weeks old; lane 6, fetal skeletal muscle = 6 weeks old; and lane 7, primer control. Marker: top, 1353, 1078, 872, and 603 bp. (A) Ethidium staining of PCR amplification using P4(+) and P2(-) primer pair. Strong staining is seen in both fetal heart lanes with weaker staining in adult heart. Lane 6 skeletal muscle shows staining which appears to be non-specific amplification since no hybridization is seen in B or C. (B) No Southern hybridization is seen using D1 probe specific to TPM1 $\alpha$ . (C) Southern hybridization using D2 specific probe to TPM1 $\kappa$  confirms the presence of this isoform in adult heart, albeit with weaker expression than the fetal heart tissues. This could suggest a possible down-regulation of TPM1 $\kappa$  or isoform switching during development, however further analysis is required. (D) Ethidium staining of human GAPDH.

**Figure 3-6.** TPM1 $\alpha$  is found in both cardiac and skeletal muscle tissues using PCR amplification with exon 2b specific primer.



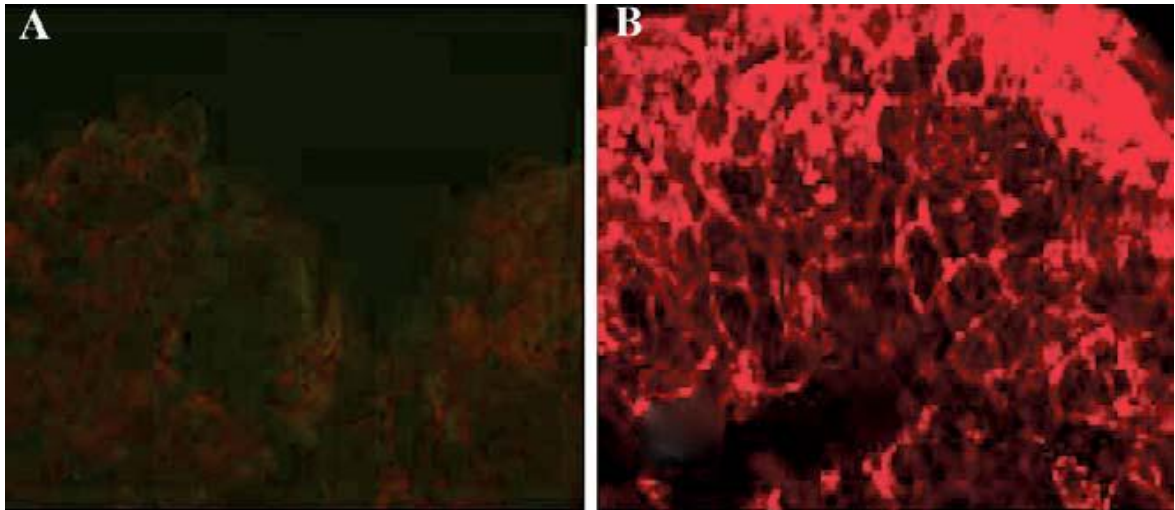
RNA from: lane 1, adult heart; lane 2, adult skeletal muscle; lane 3, fetal heart >6 weeks old; lane 4, fetal skeletal muscle >6 weeks old; lane 5, fetal heart = 6 weeks old; lane 6, fetal skeletal muscle = 6 weeks old; and lane 7, primer control. Marker: top, 1353, 1078, 872, and 603 bp. (A) Ethidium staining of PCR amplified products using P3(+) and P2(-) primer pair. Strong staining is observed across all tissues. (B) Southern hybridization with D1 probe specific to TPM1 $\alpha$  shows expression in all lanes. (C) No hybridization is seen when probed with D2 probe specific to TPM1 $\kappa$ . (D) Ethidium staining of human GAPDH.

**Figure 3-7.** Expression of both TPM1 $\alpha$  and TPM1 $\kappa$  is consistent across four adult heart segments analysed.



RNA from adult: lane 1, left ventricle; lane 2, left atrium; lane 3, right ventricle; lane 4, right atrium; lane 5, primer control. (A) Ethidium staining of PCR amplification using P1(+) and P2(-) primer pair. (B) Southern hybridization with D1 probe specific to TPM1 $\alpha$  and (C) D2 specific to TPM1 $\kappa$ . No difference in expression is seen for either isoform. (D) Ethidium staining human GAPDH.

**Figure 3-8 (A & B). Confocal microscopy of pEGFP.TPM1 $\alpha$  and pEGFP.TPM1 $\kappa$  transfected hearts from both normal and cardiac mutant Mexican axolotl.**



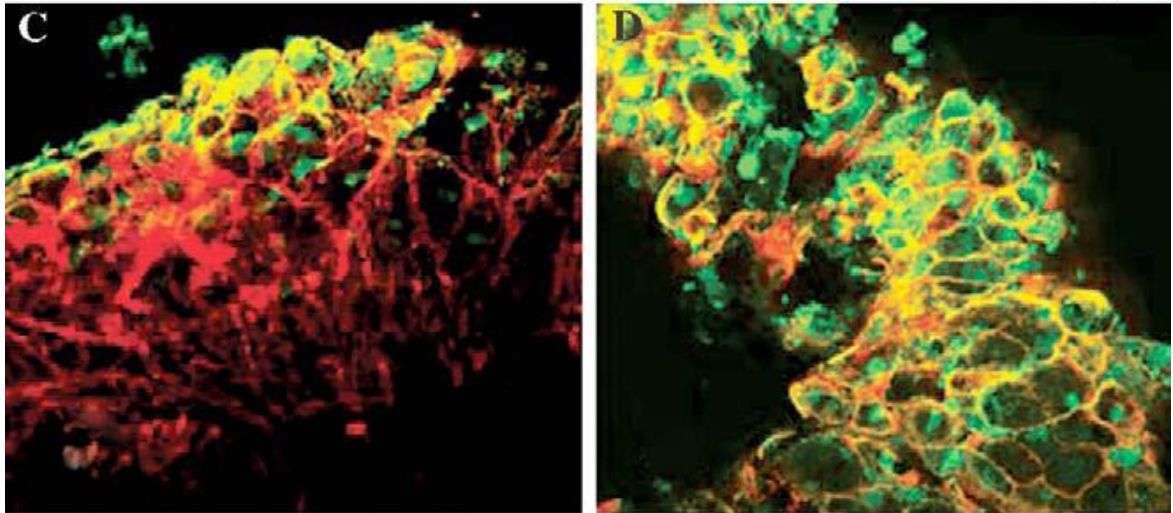
Scale bar = 50 $\mu$ m —

Red: (CH1 anti-tropomyosin) recognizes both endogenous and GFP tagged tropomyosin;  
green: (anti-GFP) binds only to GFP tagged tropomyosin.

**Figure 3-8A** - CH1 staining of a mutant axolotl heart shows lack of tropomyosin. A small amount of background staining is observed. The mutant control serves to establish the levels of detection for the subsequent images.

**Figure 3-8B** - Normal CH1 stained heart shows intact myofibril structure of embryonic axolotl. Myofibrils can be seen as outlines of myocardial cells with some banding beginning to form in the upper region.

**Figure 3-8 (C & D). Confocal microscopy of pEGFP.TPM1 $\alpha$  and pEGFP.TPM1 $\kappa$  transfected hearts from both normal and cardiac mutant Mexican axolotl.**

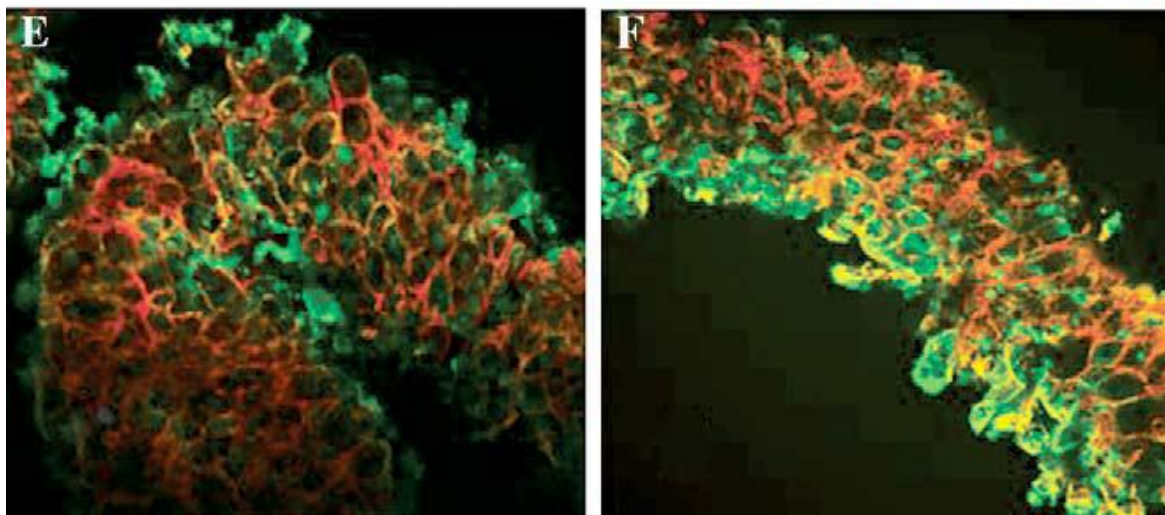


Scale bar = 50 $\mu$ m —

**Figure 3-8C** - Mutant heart transfected with GFP.TPM1 $\alpha$  and double labeled with CH1 and anti-GFP. Myofibril formation indicates GFP.TPM1 $\alpha$  's ability to rescue the mutant heart phenotype. Upper region of heart shows strong expression and co-localization (yellow) of GFP.TPM1 $\alpha$  with CH1 stained tropomyosin. Presence of yellow bands indicates incorporation of GFP.TPM1 $\alpha$  into myofibrils.

**Figure 3-8D** - Normal heart with GFP.TPM1 $\alpha$  transfection. Double label staining shows prominent co-localization demonstrating human TPM1 $\alpha$  's compatibility with endogenous tropomyosin in the formation of myofibrils.

**Figure 3-8 (E & F). Confocal microscopy of pEGFP.TPM1 $\alpha$  and pEGFP.TPM1 $\kappa$  transfected hearts from both normal and cardiac mutant Mexican axolotl.**



Scale bar = 100 $\mu$ m —

**Figure 3-8E** - Mutant heart transfected with novel isoform GFP.TPM1 $\kappa$  which is also capable of rescuing the mutant heart, as seen by myofibril formation and incorporation of fusion protein (orange/yellow bands).

**Figure 3-8F** - Normal heart with GFP.TPM1 $\kappa$ . Double label staining is similar to the pattern seen with TPM1 $\alpha$ . Yellow/orange banding shows incorporation and co-localization GFP.TPM1 $\kappa$  with endogenous tropomyosin that indicates the inter-changeability of the two. Note. Co-localization of CH1 (red) and GFP (green) staining is observed throughout the heart, however, when the images are merged together the red staining can appear more predominant in regions of less GFP.TPM1 expression. Also, the accessibility of antibodies to certain heart regions may be limited, causing the co-localization appearance to range from yellow to red-orange.

Published in 2005 in *Journal of Cellular Biochemistry*. 95: 840-848.

## CHAPTER FOUR

### **ANTI-SENSE-MEDIATED INHIBITION OF EXPRESSION OF THE NOVEL STRIATED TROPOMYOSIN ISOFORM, TPM1 $\kappa$ , DISRUPTS MYOFIBRIL ORGANISATION IN EMBRYONIC AXOLOTL HEARTS.**

#### **4.0 ABSTRACT**

Striated muscle tropomyosin (TM) is described as containing ten exons; 1a, 2b, 3, 4, 5, 6b, 7, 8, and 9a/b. Exon 9a/b has critical troponin binding domains and is found in striated muscle isoforms. This team have recently discovered a smooth (exon 2a)/striated (exons 9a/b) isoform expressed in amphibian, avian, and mammalian hearts, designated as an isoform of the *TPM1* gene (TPM1 $\kappa$ ). TPM1 $\kappa$  expression was blocked in whole embryonic axolotl heart by transfection of exon-specific anti-sense oligonucleotide. Reverse transcriptase polymerase chain reaction (RT-PCR) confirmed lower transcript expression of TPM1 $\kappa$  and in vitro analysis confirmed the specificity of the TPM1 $\kappa$  anti-sense oligonucleotide. Altered expression of the novel TM isoform disrupted myofibril structure and function in embryonic hearts.

#### **4.1 INTRODUCTION**

Tropomyosin (TM) is an actin binding two stranded  $\alpha$ -helical coiled-coil protein found in every living cell. Diverse expression of TM isoforms in muscle and non-muscle cells is achieved through alternative splicing (Nadal-Ginard, 1990; Lees-Miller & Helfman, 1991; Pittenger *et al.*, 1994). This occurs in a tissue specific pattern (for example, brain (Vrhovski *et al.*, 2003); fibroblast and epithelial (Percival *et al.*, 2000); Golgi apparatus (Heimann *et al.*, 1999) and developmentally regulated (Hook *et al.*, 2004; Clayton & Johnson, 1998) . The splicing pattern for each isoform serves to adapt TM to a specific role in a given cell. For instance, skeletal muscle tropomyosin, in association with the troponin complex, regulates the actin-myosin interaction that results in calcium dependent contraction in vertebrate striated muscle. These muscle isoforms have 284 amino acid residues and a highly conserved N-terminal region. Within the cytoskeleton, the non-muscle tropomyosin is involved in stabilising the actin filaments. These tropomyosin isoforms are generally smaller than striated muscle tropomyosin and tend to vary in their N-terminal region. However, the mechanism by which the presence or absence of a certain exon in TM makes it more suited to a specific function is still unclear. By inhibiting the expression of TM isoforms containing a specific exon, it is possible to determine if knockdown of an isoform is of functional significance.

Recent technological advances allowed for the discovery of many unknown isoforms of TM in heart (Cooley and Bergstrom, 2001). Most of these isoforms fall into previous categories for TM. Four TM genes have been characterized in vertebrates:  $\alpha$ -TM (*TPM1*),  $\beta$ -TM (*TPM2*),  $\gamma$ -TM (*TPM3*), and  $\delta$ -TM (*TPM4*) including localization to their human



## ***I. The Role of Tropomyosin in Cardiac Myofibrillogenesis***

chromosomes (Laing *et al.*, 1995; Perry, 2001; Martson and Redwood, 2003). A predominant striated muscle isoform is composed of exons 1a, 2b, 3, 4, 5, 6b, 7, 8, 9a/b from the *TPM1* gene (Nadal-Ginard, 1990; Lees-Miller & Helfman, 1991; Pittenger *et al.*, 1994). Exon 9a/b (amino acids 258-284 at the carboxyl end of the molecule) is particularly important for the function of the striated muscle tropomyosin isoforms (Mak & Smillie, 1981; Luque *et al.*, 1997) as it contains the Troponin-T-binding domain. The smooth muscle specific isoform of the *TPM1* gene is designated *TPM1 $\beta$*  and consists of exons: 1a, 2a, 3, 4, 5, 6b, 7, 8, and 9c/d (see Table 4-I).

An isoform of TM that bridges the two descriptive categories has been described (Zajdel *et al.*, 2000; 2002). This novel TM contains a smooth muscle exon 2a as well as striated muscle type exon 9a/9b is expressed primarily in heart tissues of amphibian, avian, and mammalian species. This TM has been designated as *TPM1 $\kappa$*  to signify the 10th isoform to be discovered as an alternative splice product of the *TPM1* gene. No specific antibody that is distinct for all exons is currently available to examine the protein expression of this isoform but expression of a GFP-TM construct and incorporation into myofibrils is now possible (Zajdel *et al.*, 2002). Since we have found the *TPM1 $\kappa$*  isoform to be present in cardiac tissues of various species and because it is capable of incorporation into myofibrils, we set out to determine its importance by inhibiting its expression *in vivo*.

The use of anti-sense oligonucleotide mediated inhibition of mRNA expression has proven useful in determining what role a particular protein may play in cellular functions. The present study uses an exon 2a-specific antisense oligonucleotide to block expression of the *TPM1 $\kappa$*  isoform in whole embryonic axolotl hearts to see what effect knocked-down

expression of this isoform may have. Whole hearts were preferred for this work because they are amenable to transfection procedures and maintain intercellular connections and signalling pathways.

## **4.2 MATERIALS AND METHODS**

### **4.2a Embryo care**

Axolotl embryos were obtained from the Indiana University axolotl colony and the axolotl colony at SUNY Upstate Medical University. Animals were maintained in aquaria in 50% Holfreter's solution (29 mM NaCl, 0.45 mM CaCl<sub>2</sub>, 0.33 mM KCl, 0.1 mM MgSO<sub>4</sub>, and 4.76 mM NaHCO<sub>3</sub>) and fed commercial salmon pellets. The embryos were staged according to the standard staging system (Bordzilovskaya *et al.*, 1989).

### **4.2b Preparation of exon-specific oligonucleotides**

Sense and anti-sense oligonucleotides were designed for exon 2 of the axolotl TPM1 $\kappa$  TM isoform. Axolotl TPM1 $\alpha$  and TPM4 $\alpha$  isoforms were used as controls to the TPM1 $\kappa$  isoform. The TPM $\alpha$  isoform is the predominant isoform found in axolotl skeletal muscle, while the TPM4 $\alpha$  (ATmC-3) isoform is the predominant TM isoform in embryonic axolotl hearts (Spinner *et al.*, 2002). TPM1 $\alpha$  and TPM1 $\kappa$  nucleotide sequences used for this experiment were the following:

## ***I. The Role of Tropomyosin in Cardiac Myofibrillogenesis***

TPM1 $\alpha$ sense, 5'-AGT ACT CGG AGT CCT TGA-3';

TPM1 $\alpha$  anti-sense, 5'- A\*G\*G\*A CTC CGA GTA CTT GTC \*C\*A\*A-3'.

TPM1 $\kappa$  sense, 5'-fG\*C\*A\*C ACT GCT GAC GAG AAA \*G\*C\*C\*-3',

where \*N represents a phosphorothioate blocked nucleotide and fG represents G tagged with fluorescein (FITC) at the 50-end (IDT, Inc.).

TPM1 $\kappa$  anti-sense, 5'-G\*C\*G\*G CTT TCT CGT CAG CAG TG\*T\*G\*C-3';

### **4.2c Cationic liposome mediated transfection in whole hearts**

Transfection of oligonucleotides and cDNA was performed according to previously published methods (Zajdel *et al.*, 1998). Stage 38 normal embryos were anesthetized and then hearts were dissected free with watchmaker's forceps and placed into Steinberg's solution. Four microliters of sense and anti-sense oligonucleotides (10 mM) were placed into 20 ml of lipofectin and 20 ml of Steinberg's solution. All hearts were beating immediately after dissection. The transfection solution was prepared and applied in a single blind method for the initial experiments examining beating (so that the person counting the heartbeats was not aware of which samples were control or treated). Transfected whole hearts were maintained in culture for 5 days.

#### **4.2d RT-PCR and Southern blot hybridization**

RT-PCR with oligo dT priming was performed to evaluate the expression of TPM1 $\kappa$ , TPM1 $\alpha$ , and TPM4 $\alpha$  isoforms using our previously published protocol (Zajdel *et al.*, 2000). The strategy for RT-PCR amplification of TPM1 $\alpha$  and TPM1 $\kappa$  simultaneously with the same primer-pair and subsequent detection using isoform-specific detector oligonucleotide is presented in Figure 4-1. The sequence of PCR primers used are as follows:

TPM1 $\kappa$  and TPM1 $\alpha$ : (+) 5'-ATG GAC GCC ATC AAG AAG AAG-3'; and

(common to both isoforms): (-) 5'-ACG CTC CTG AGC ACG ATC CA-3';

TPM4 $\alpha$ : (+) 5'-CCG CTC CCT GAC ACC GGT TCC CG-3' and

(-) 5'-GCT CTC CCT CCA GAA TAA CAA GTT-3'.

Southern blot hybridization was carried out using with (<sup>32</sup>P)-labelled isoform specific detector oligonucleotides, the sequence of which are as follows:

TPM1 $\kappa$ : 5'- AGG GTG CTG GAT GAA CTG CAC AA-3';

TPM1 $\alpha$ : 5'-AGT ACT CGG AGT CCT TGA-3'; and

TPM4 $\alpha$ : 5'-TGG CGC GCG GAC GGG GTG TTG CT-3'.

**4.2e Confocal microscopy**

Whole mount immunostaining and confocal microscopy were performed according to the laboratory's published procedures (Zajdel *et al.*, 1998). Monoclonal antibody, CH1 (obtained from Developmental Hybridoma Bank, Johns Hopkins University) was used for the immunodetection of TM (Lin *et al.*, 1985) with Lissamine Rhodamine anti-mouse used as a secondary antibody. FITC tagged oligonucleotides could be visualized without immunodetection. Specimens were viewed on a BioRad MRC 1024ES confocal laser system mounted on a Nikon Eclipse E600 microscope. Control hearts and treated hearts were examined using identical confocal settings. A simultaneous or sequential (double staining) Z-series was made for each.

**4.2f *In vitro* analysis of the isoform specificity for sense- and anti-sense oligonucleotides**

Total RNA (5 µg) from axolotl heart was annealed with 10 pmoles of isoform specific sense or anti-sense oligonucleotide at 65°C for 5 min, after which the annealed mixture was chilled on ice. One microliter of RNase Inhibitor was added to the annealed mixture with 1 µl of RT-buffer, and 1 µl of RNase H (Invitrogen superscript First Strand Synthesis Kit). The mixture was incubated at 37°C for 20 min followed by denaturation at 70°C for 10 min to inactivate the enzyme. The 10-µl reaction was then chilled. RT reaction was performed using 5 µl of the above reaction mix in a total volume of 20 µl following Invitrogen's standard oligo dT protocol. Finally, PCR amplification was carried out with 2 µl of the RT product using isoform specific primer-pairs followed by the Southern blot analysis with (<sup>32</sup>P)-labelled isoform specific detector oligonucleotides.

## **4.3 RESULTS**

### **4.3a Specificity of TPM1 $\kappa$ anti-sense oligonucleotide *in vitro***

The specificity of the TPM1 $\kappa$  anti-sense oligonucleotide was examined *in vitro* (Figure 4-3), using the strategy outlined in Figure 4-2. TPM4 $\alpha$  probe was used as a control. TPM4 $\alpha$  has a striated muscle exon 2b compared to smooth muscle type exon 2a in TPM1 $\kappa$ . Sense and antisense expression was relatively equal for the TPM4 $\alpha$  probe. TPM1 $\kappa$  expression was reduced for TPM1 $\kappa$  antisense oligonucleotide with the TPM1 $\kappa$  probe. The sense oligonucleotide did not reduce expression as seen with the TPM1 $\kappa$  probe.

### **4.3b Anti-sense TPM1 $\kappa$ and anti-sense TPM1 $\alpha$ specificity *in vitro***

Three isoforms of TM have currently been identified in embryonic axolotl heart. TPM1 $\alpha$  and TPM1 $\kappa$  are derived from the same TPM1 ( $\alpha$ -TM) gene (Zajdel *et al.*, 2000) while TPM4 $\alpha$  is from a TM-4 type gene (Luque *et al.*, 1994; Spinner *et al.*, 2002). Figure 4-4 illustrates the expression of these three isoforms in anti-sense TPM1 $\kappa$ - and TPM1 $\alpha$ -treated heart RNA. Lane 1 shows that expression of TPM1 $\alpha$  or TPM4 $\alpha$  was not reduced with the use of the anti-sense TPM1 $\kappa$  oligonucleotide for each probe, respectively. The use of the TPM1 $\kappa$  probe clearly demonstrates reduced expression of this isoform with anti-sense TPM1 $\kappa$  oligonucleotide treatment. Likewise, TPM1 $\alpha$  anti-sense oligonucleotide treatment reduced expression of TPM1 $\alpha$  as indicated by that probe. TPM1 $\alpha$  and TPM4 $\alpha$  expression was not reduced with antisense TPM1 $\kappa$  oligonucleotide.

**4.3c Sense and anti-sense TPM1 $\kappa$  specific oligonucleotide *in vivo***

TPM1 $\kappa$  exon 2 specific oligonucleotides were transfected into whole normal hearts. Whole hearts were used to maintain intercellular pathways and connections. After 5 days, the expression of mRNA was examined by TPM1 $\kappa$  and TPM4 $\alpha$  probes. TPM4 $\alpha$ , a TM-4 type TM is the predominant TM found in these embryonic hearts and this probe was used as a control. Figure 4-5 demonstrates a reduction in TPM1 $\kappa$  expression in TPM1 $\kappa$  exon 2 anti-sense-treated hearts. Expression was not decreased in the sense treated normal whole hearts. TPM4 $\alpha$  expression was unaffected in TPM1 $\kappa$  sense or anti-sense oligonucleotide-treated normal hearts.

**4.3d Confocal laser scanning microscopy of TPM1 $\kappa$  sense- and anti-sense-treated whole hearts**

Confocal laser scanning microscopy was used to examine the thickness of the whole normal hearts. Normal hearts transfected with antisense TPM1 $\kappa$  oligonucleotides (Figure 4-6a) demonstrated a disruption of myofibril organization with few sarcomeric myofibrils compared to normal hearts transfected with FITC-tagged TPM1 $\kappa$  sense oligonucleotides that showed no disruption in myofibrils (red) (Figure 4-6b). The presence of the sense oligonucleotide was confirmed by FITC detection (green) localized to the nucleus of the myocytes.

**4.3e Contractions in TPM1 $\kappa$  anti-sense oligonucleotide treated hearts**

Synchronous contractions of the whole hearts were monitored during the course of the experiments in a single blind method (Table 4-II). The normal control hearts and oligonucleotide treated hearts were not descriptively labelled so that they were examined

blindly. Normal and TPM1 $\kappa$  whole hearts were used as a control and had no reduction in beating with contractions continuing for the full 5 days in 11 of 11 in both categories. Contractions were disrupted in the experimental hearts during the course of the experiments. At 4 and 5 days of treatment, 3 of 11 hearts were not beating, which coincides with the reduction in TPM1 $\kappa$  RNA expression. There appeared to be a partial recovery or compensation of the TPM1 $\kappa$  anti-sense treated hearts at day 2 and 3, but by day 4 and 5, the number of beating hearts was again reduced. The heart rate of the hearts still beating was reduced compared to the normal controls. Even during this period of possible recovery, the heart rate of the beating hearts averaged below the control hearts.

#### **4.4 DISCUSSION**

The predominant TM isoform expressed in striated muscle has been considered to be TPM1 $\alpha$  expressed by the *TPM1* gene (Lees-Miller and Helfman, 1991). TPM1 $\alpha$  consists of exons 1a, 2b, 3, 4, 5, 6b, 7, 8, and 9a/b, typical of striated muscles. This team have cloned and sequenced cDNAs for three striated muscle isoforms of TM from axolotl hearts. These isoforms are designated as TPM1 $\alpha$ , TPM1 $\kappa$ , and TPM4 $\alpha$ . Of these, TPM1 $\kappa$  is the novel isoform, which unlike TPM1 $\alpha$  contains smooth muscle type exon 2a (in place of exon 2b). We believe TPM1 $\alpha$  and TPM1 $\kappa$  are alternatively spliced products of the *TPM1* gene. This novel splicing is not unique to the Mexican axolotl. We have cloned and sequenced the TPM1 isoform, TPM1 $\kappa$ , from avian as well as mammalian species, including human (Luque *et al.*, 1997; Zajdel *et al.*, 2003; Denz *et al.*, 2004).



## ***I. The Role of Tropomyosin in Cardiac Myofibrillogenesis***

The cardiac mutant axolotl heart has specific advantages for determining the structural/functional relationships of TM because mutant hearts are deficient in the sarcomeric TM protein (Lemanski, 1979; Lemanski *et al.*, 1996; Zajdel *et al.*, 1998). Unfortunately, a lack of isoform specific antibodies limits the study of which TM isoform is essential for the formation of myofibrils *in vivo* or, whether various combinations of the three isoforms play a crucial role in forming myofibrils as well as affecting the contractility of cardiac muscle *in vivo*. In addition, gene knock-out technology is not well established in amphibian systems, and even if it was it would not be possible to knockout a single isoform at this present time. Furthermore, it is difficult to utilize a transgenic mouse model, since  $\alpha$ -TM (*TPM1*) knock-out has been found to be embryonic lethal (Rethinasamy *et al.*, 1998). In any case, knockout technology cannot be used to eliminate exon 2a as it is a component of both, the novel isoform, TPM1 $\kappa$ , and TPM1 $\beta$ , a smooth muscle isoform, as shown in Table 4-1. Therefore, since exon 2a is required for another essential TM isoform, TPM1 $\beta$ , simply knocking out this exon will not provide the information as to whether TPM1 $\kappa$  is essential for cardiac contractility and cardiogenesis.

This issue has been addressed by inhibiting the expression of TPM1 $\kappa$  using an exon 2a specific anti-sense oligonucleotide. The specificity of this oligonucleotide was determined *in vitro* (Figures 4-3 and 4-4). Annealing of the antisense oligonucleotide specific for exon 2a to total heart RNA and subsequent RNase H treatment allowed the degradation of TPM1 $\kappa$  mRNA (in the RNA-DNA hybrid) but not TPM1 $\alpha$  or TPM4 $\alpha$  (see Figure 4-2). On the other hand, the exon 2a specific sense oligonucleotide did not have any effect. Additionally, transfection of the exon 2a anti-sense oligonucleotide into normal axolotl hearts in organ culture reduced the concentration of TPM1 $\kappa$  transcripts but not

## ***I. The Role of Tropomyosin in Cardiac Myofibrillogenesis***

TPM4 $\alpha$ , which has already been reported to play an essential role in the cardiac contractility in axolotl (Figure 4-4) (Spinner *et al.*, 2002). On the contrary, anti-sense TPM1 $\alpha$  was previously found to have an insignificant effect on the myofibril formation in axolotl heart in culture (Zajdel *et al.*, 2000).

The TPM1 $\kappa$  specific anti-sense oligonucleotide, but not its sense counterpart, decreased cardiac contractility (Table 4-II). At 24 h post treatment with TPM1 $\kappa$  anti-sense (day 1), the number of hearts beating (3/12) was significantly lower than either the control or TPM1 $\kappa$  sense treated hearts (11/11). By day 2 and 3, the number of anti-sense treated hearts beating increased, but not to the level seen in the controls nor the same rate (25 and 28 beats/min, respectively, compared to 38 beats/min for the controls). At day 4 and 5 post-treatment with TPM1 $\kappa$  anti-sense, the number of beating hearts was again reduced to levels seen at day 1 (3/11 for both) as well and the rate of beating for those 3 hearts (12 and 11 beats/min, respectively). The rate of contraction and number of beating hearts stayed consistent in the control and TPM1 $\kappa$  sense treated hearts. The partial recovery seen in the anti-sense treated hearts could indicate partial compensation for the TPM1 $\kappa$  reduction, possibly through upregulation of another TM isoform, but that was ultimately insufficient to maintain proper contraction. After 5 days, some of the hearts restarted beating possibly suggesting the ability to overcome the anti-sense inhibition.

The anti-sense oligonucleotide specific for TPM1 $\kappa$  caused disorganization of the myofibrils in normal axolotl heart (Figure 4-6a). In contrast, the FITC labelled sense oligonucleotide, although it can be detected within the myocardium of transfected axolotl heart, did not affect the existing myofibrils or cardiac contractility (Figure 4-6b and Table

## ***I. The Role of Tropomyosin in Cardiac Myofibrillogenesis***

4-2). Hence, it is tempting to conclude that TPM1 $\kappa$  plays a critical role in the contractility as well as myofibrillogenesis of axolotl hearts. Our results do not permit us to conclude that the TPM1 $\kappa$  specific anti-sense oligonucleotide that has been used in this study does not affect other important isoforms, such as TPM1 $\beta$ , because exon 2a is also a part of this isoform. However, the smooth muscle isoform is not known to play any significant role in cardiac contractility or cardiac myofibrillogenesis.

Another important question that remains is how does TPM1 $\kappa$  affect the process of myofibril formation in striated muscles, and especially in cardiac muscle? There is evidence of TPM1 $\kappa$  being cardiac specific in human (Denz *et al.*, 2004), chicken (Zajdel *et al.*, 2003), and rat (unpublished results). The mechanism for formation of a mature myofibril in cardiac muscles may follow the three-step process of myofibrillogenesis proposed by Rhee *et al.* (1994). According to this model, the formation of mature myofibrils is mediated by the initial deposition of pre-myofibrils in close association with the cell surface. Pre-myofibrils then give rise to nascent myofibrils that subsequently help to form mature myofibrils. Each of these stages is associated with specific sarcomeric protein markers; for example, non-muscle myosin IIB is present in pre-myofibrils but is replaced by myosin in nascent myofibrils. The costameric proteins, talin and vinculin, first appear in mature myofibrils. The pre-myofibril model of myofibrillogenesis also appears to be applicable to myofibrillogenesis in skeletal muscle cells (Rhee *et al.*, 1994; Rethinasamy *et al.*, 1998).

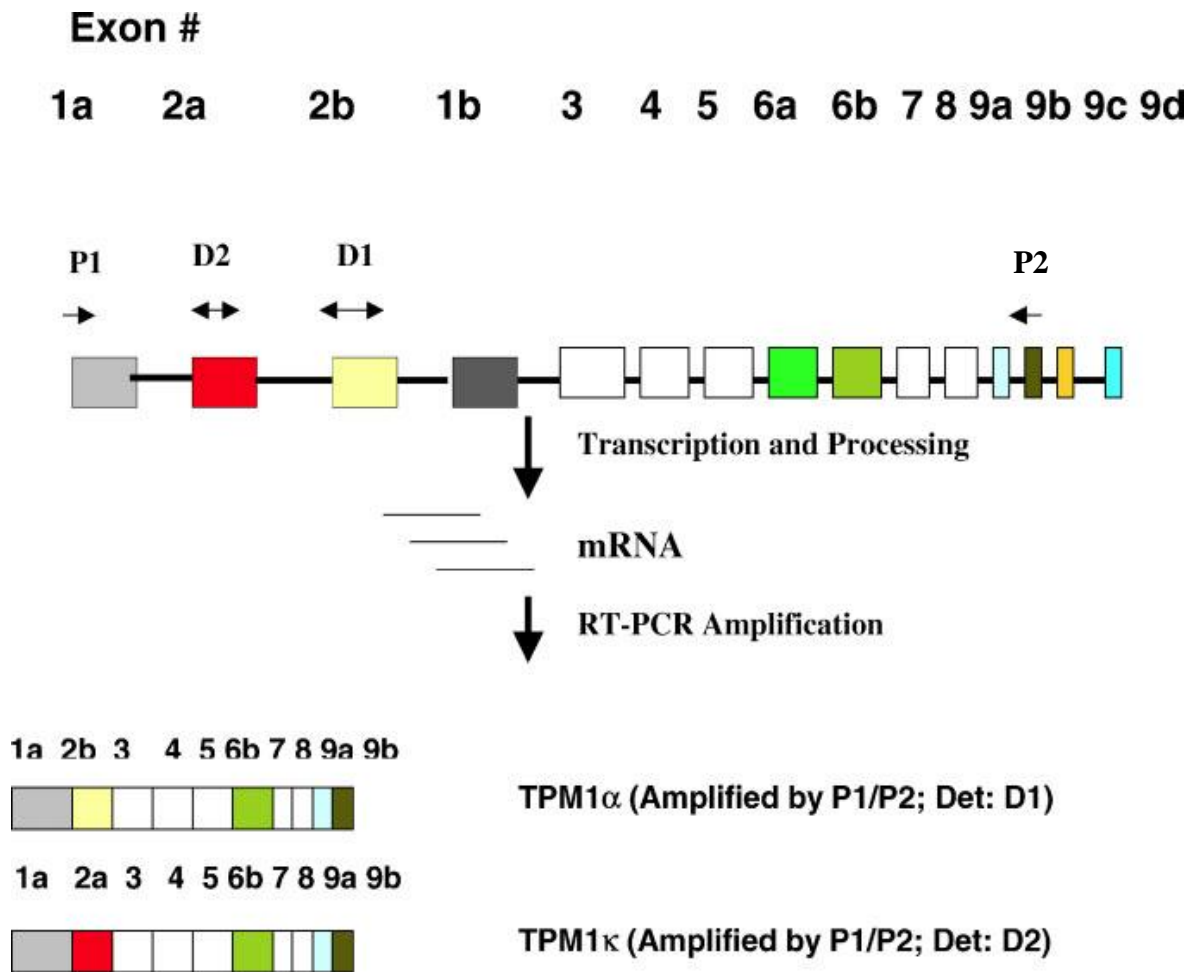
It is important to understand whether TPM1 $\alpha$  and TPM1 $\kappa$  play the same role in myofibril formation in cardiac tissues in a competitive manner. Or, do both isoforms take part in the

## ***I. The Role of Tropomyosin in Cardiac Myofibrillogenesis***

process of myofibrillogenesis in a very specific manner where each of them may play a critical role at different stages of myofibril formation? Again, such is the case with non-muscle myosin IIB, which is essential in pre-myofibril formation and then is replaced by the muscle specific myosin. At present, this team are planning to evaluate the progression of myofibrillogenesis in axolotl heart where one can control the process of cardiogenesis by regulating the environmental temperature. Differential epitope tagging of various TM isoforms will facilitate the identification and localization of the ectopically expressed TM protein molecules on sarcomeres using epitope specific antibodies and subsequent confocal microscopy and/or immunoelectron microscopy.

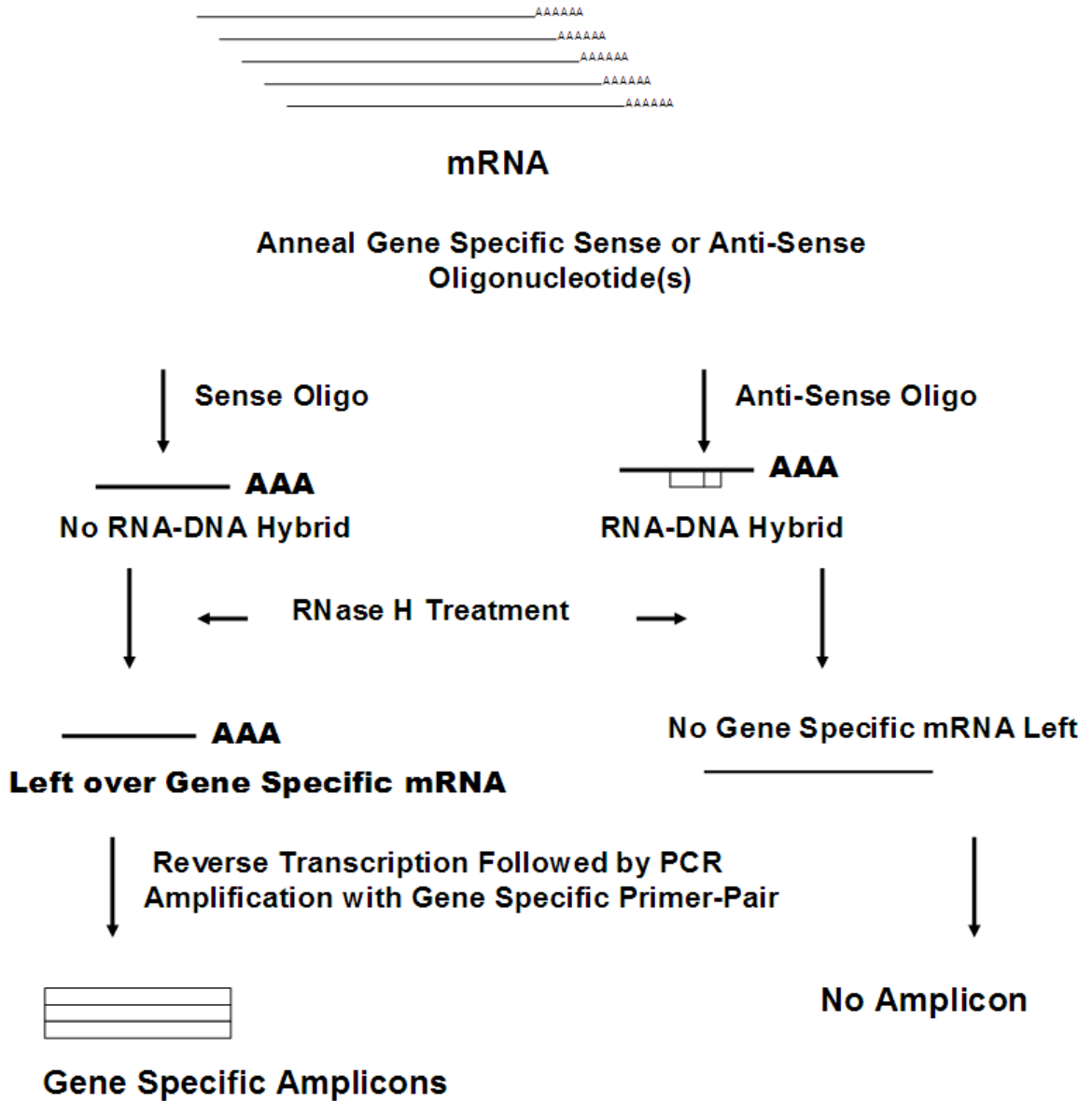
To summarise, *in vitro* analysis was used to confirm the critical specificity of the oligonucleotide compared to other TM isoforms. Reverse transcriptase polymerase chain reaction (RT-PCR) demonstrated decreased TPM1 $\kappa$  expression in embryonic hearts and confocal scanning microscopy showed disruption of myofibril organization and an associated decrease in contractility.

**Figure 4-1.** Strategy for amplification of TPM1 $\alpha$  and TPM1 $\kappa$  by RT-PCR using the same primer-pair and the location of isoform specific detector oligonucleotides for Southern hybridization.



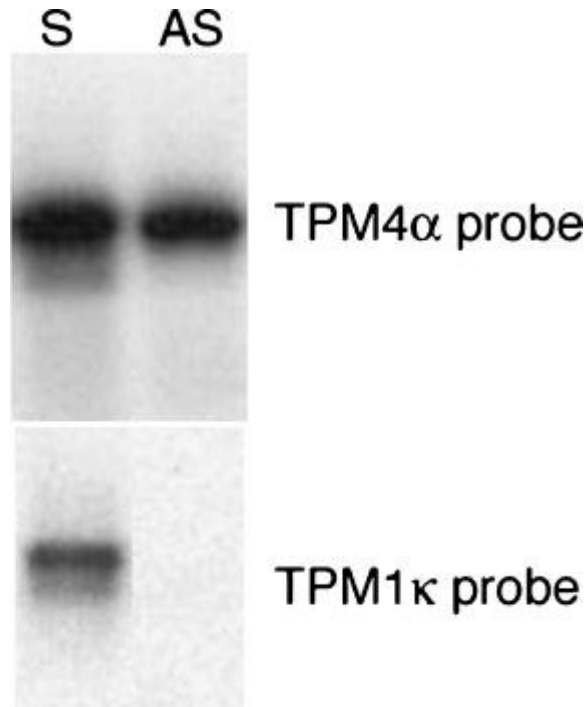
(# indicates number.)

Figure 4-2. Scheme for testing the *in vitro* specificity of sense and anti-sense oligonucleotides



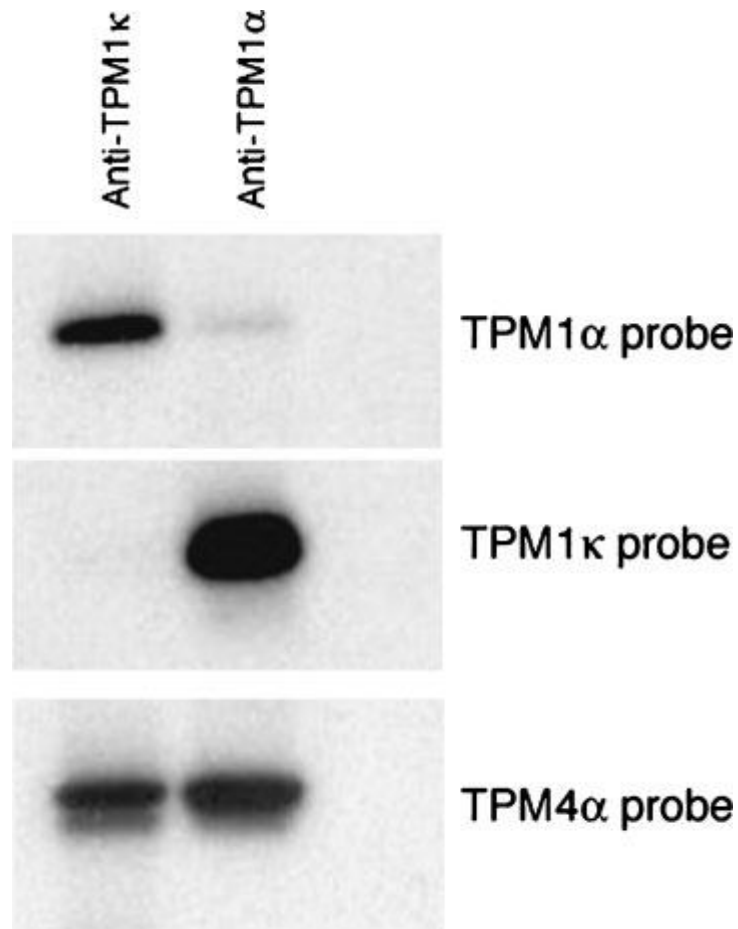
RNA-DNA hybrids are treated with Ribonuclease H (RNase H), a non-specific endonuclease, which degrades the RNA, but not the DNA nor unhybridised RNA.

**Figure 4-3.** RT-PCR showing specificity of TPM1 $\kappa$  anti-sense oligonucleotide in vitro.



TPM1 $\kappa$  sense (lane 1) and anti-sense (lane 2) treated axolotl heart RNA. Primer control lane was blank (not included). The Southern hybridization of PCR products amplified with either TPM4 $\alpha$  or TPM1 $\kappa$  specific primer pairs and probed with isoform specific oligonucleotides is shown. TPM4 $\alpha$  normally found in axolotl embryonic hearts was used as the control. The amount of TPM1 $\kappa$  transcripts was drastically reduced in the anti-sense treated RNA lane demonstrating the specificity of the TPM1 $\kappa$  anti-sense oligonucleotide compared to another predominant cardiac isoform, TPM4 $\alpha$ .

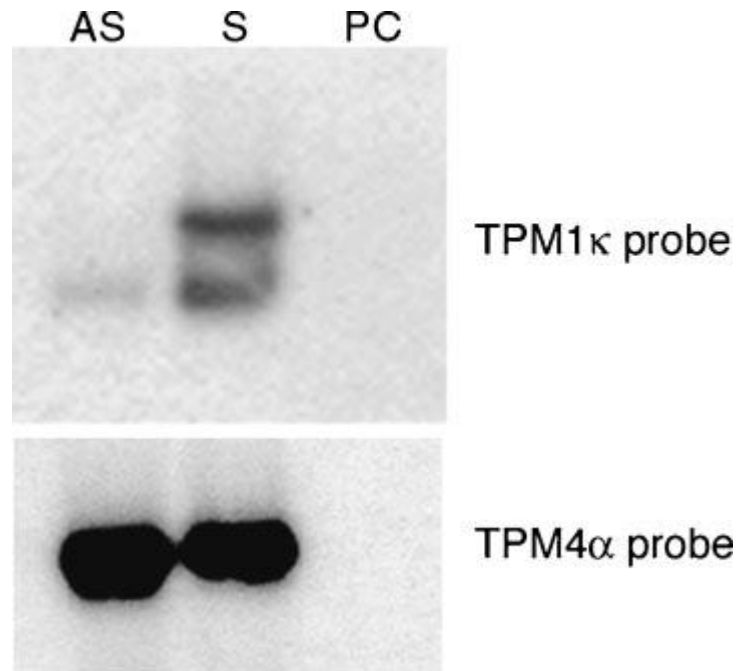
**Figure 4-4.** Anti-sense TPM1 $\kappa$  and anti-sense TPM1 $\alpha$  specificity in vitro.



Lane 1, Anti-sense TPM1 $\kappa$  treated RNA with TPM1 $\alpha$ , TPM1 $\kappa$ , and TPM4 $\alpha$  axolotl tropomyosin probes. Lane 2, Antisense TPM1 $\alpha$  treated RNA with TPM1 $\alpha$ , TPM1 $\kappa$ , and TPM4 $\alpha$  axolotl tropomyosin probes. Lane 3, Primer control. Shown is the Southern hybridization of PCR products amplified with either TPM1 $\alpha$ /TPM1 $\kappa$  or TPM4 $\alpha$  specific primers and probed with isoform specific oligonucleotides. TPM1 $\kappa$  expression was reduced with TPM1 $\kappa$  anti-sense treatment and TPM1 $\alpha$  expression was reduced with TPM1 $\alpha$  anti-sense treatment. TPM4 $\alpha$  was unaffected by either anti-sense oligonucleotide and was again used as a control. This demonstrates the specificity of the TPM1 $\kappa$  anti-sense oligonucleotide compared to another TM isoform (TPM1 $\alpha$ ) from the same gene.



**Figure 4-5.** Effect of TPM1 $\kappa$  sense and anti-sense oligonucleotides on transcript levels in vivo.

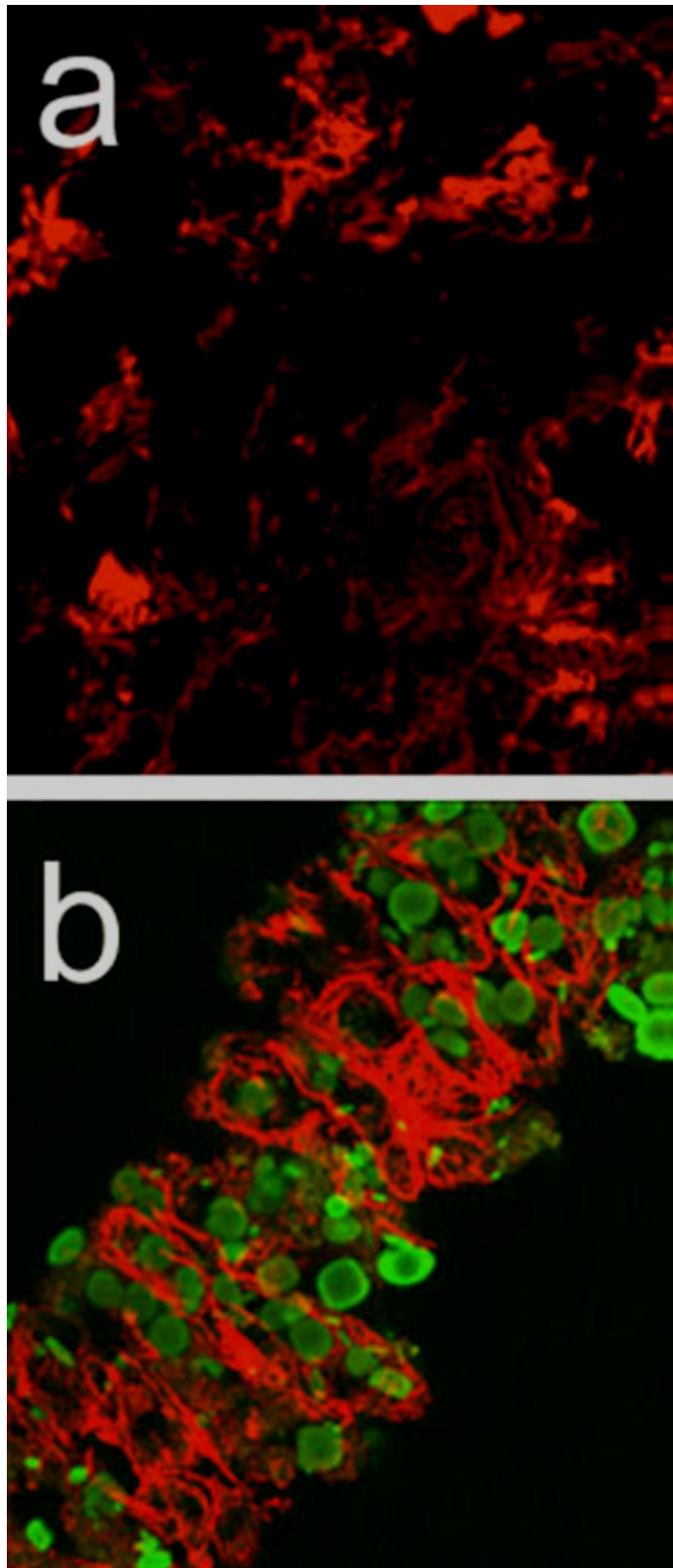


TPM1 $\kappa$  anti-sense (lane 1) and sense (lane 2) treated whole axolotl heart. TPM4 $\alpha$  probe was used as a control. Lane 3, Primer control. TPM1 $\kappa$  mRNA expression was reduced in whole normal hearts transfected with TPM1 $\kappa$  antisense oligonucleotide. The expression of TPM1 $\kappa$  was not affected when the hearts were transfected with the sense oligonucleotide. The expression of TPM4 $\alpha$  was again unaffected by transfection of either oligonucleotide.

**Figure 4-6 - Myofibril organization and entry of FITC-tagged oligonucleotide into cells of whole hearts.**

Scale bar = 50 $\mu$ m —

Confocal z-series images of stage 38 embryonic axolotl hearts transfected with either TPM1 $\kappa$  anti-sense or sense oligonucleotides. Immunodetection of sarcomeric tropomyosin using CH1 monoclonal antibody is shown in red. (a) TPM1 $\kappa$  anti-sense transfection disrupted the myofibril organization in normal axolotl heart compared to TPM1 $\kappa$  sense transfection. Very little organized structure is seen when examined by the tropomyosin staining. The secondary antibody is contained within amorphous areas in the cells. In (a) the cells are identifiable by black circular



are identifiable by black circular areas surrounded by staining. The amorphous staining can be seen at the periphery of the

## ***I. The Role of Tropomyosin in Cardiac Myofibrillogenesis***

black circular areas or at the cell membrane. Since this is a three dimensional projection, not all the cells and surrounding staining is the plane of focus. (b) Shows that the TPM1 $\kappa$  sense oligonucleotides did not affect the structure. Since no effect on myofibril structure with TPM1 $\kappa$  sense was observed, we tagged the oligonucleotide with FITC (green) to verify its presence and found it to be within the myocytes (panel b). Double staining of the nucleus (green) and the myofibrils at the periphery of the cells (red) can be seen. The green staining is ovoid in shape and primarily located at the centre of the cells (Zajdel *et al.*, 2000). Cells can be identified by the consistent myofibril linear and circular staining below the membrane, by the black non-staining area below the myofibril staining, and the green nuclear staining in the middle of the cells. This figure shows that TPM1 $\kappa$  plays a critical role in maintaining the myofibrillar structure in embryonic axolotl hearts. Note: panel (a) is at 60x to show the lack of myofibril structure at a higher resolution while panel (b) is at 20x to show the clear structure in conjunction with presence of the FITC tagged sense oligonucleotide

**Table 4-1. Nomenclature of various isoforms of TPM1 referred to in his study**

<b>TPM1 isoforms</b>	<b>Isoforms of tropomyosin currently known as</b>	<b>Exon composition</b>
<b>TPM1<math>\alpha</math></b>	<b>Striated muscle</b>	<b>1a, 2b, 3, 4, 5, 6b, 7,8, 9a/b</b>
<b>TPM1<math>\beta</math></b>	<b>Smooth muscle</b>	<b>1a, 2a, 3, 4, 5, 6b, 7,8,9d</b>
<b>TPM1<math>\gamma</math></b>	<b>TM-2 fibroblast</b>	<b>1a, 2b, 3, 4, 5, 6b, 7, 8,9d</b>
<b>TPM1<math>\delta</math></b>	<b>TM-3 fibroblast</b>	<b>1a, 2b, 3, 4, 5, 6a, 7, 8, 9d</b>
<b>TPM1<math>\epsilon</math></b>	<b>TM-5a fibroblast</b>	<b>1b, 3, 4, 5, 6b, 7, 8, 9d</b>
<b>TPM1<math>\kappa</math></b>	<b>Novel striated/cardiac muscle</b>	<b>1a, 2a, 3, 4, 5, 6b, 7, 8,9a/b</b>

**Table 4-2. Five day comparison of synchronous contractions in control, sense, and anti-sense treated whole hearts**

Day	Number of beating hearts (beats/min)		
	Control	Sense TPM1 $\kappa$	Anti-sense TPM1 $\kappa$
1	11/11 (17)	11/11 (15)	3/12 (13)
2	10/11 (30)	11/11 (38)	9/12 (25)
3	11/11 (36)	11/11 (38)	9/11 (28)
4	10/11 (36)	11/11 (38)	3/11 (12)
5	11/11 (37)	11/11 (32)	3/11 (11)

Published in 2005 in *Cardiovascular Toxicology* 5; 1-8.

## CHAPTER FIVE

# CARDIAC MYOFIBRIL FORMATION IS NOT AFFECTED BY MODIFICATION OF BOTH N- & C-TERMINI OF SARCOMERIC TROPOMYOSIN

### 5.0 ABSTRACT

Although the role of tropomyosin is well defined in striated muscle, the precise mechanism of how tropomyosin functions is still unclear. It has been shown that extension of either N- or C- terminus ends of sarcomeric tropomyosin do not affect cardiac myofibrillogenesis, but it is not known whether simultaneous extension of both ends affects the process. In order to study the structural/functional relationships of sarcomeric tropomyosin, we have chosen the cardiac mutant *Ambystoma mexicanum* because the heart is deficient in sarcomeric tropomyosin. In this study, we have made an expression construct, pEGFP.TPM4 $\alpha$ .E-L-FLAG that upon transfection into normal and mutant axolotl hearts in

organ culture, expresses GFP.TPM4 $\alpha$ .E- L-FLAG fusion protein in which both the N- and C- termini of TPM4 $\alpha$  are being extended. TPM4 $\alpha$  is one of the three tropomyosins expressed in normal axolotl hearts. Both confocal and electron microscopic analyses show that this modified sarcomeric tropomyosin can form organized myofibrils in axolotl hearts.

## **5.1 INTRODUCTION**

In vertebrate striated muscle, the thin filament, responsible for mediating Ca<sup>2+</sup> control of contraction and relaxation, consists largely of actin, tropomyosin (TM), and the troponin (Tn) complex (Tn-I, Tn-C and Tn-T). Tropomyosin is an alpha-helical, coiled-coil protein that binds end-to-end along the actin filament of seven actin monomers. It functions with the troponin complex to regulate actin-myosin interactions, which are dependent on Ca<sup>2+</sup> (Perry, 2001; Lees-Miller & Helfman, 1991; Zot *et al.*, 1986). The ends of tropomyosin are required for binding with actin and also for the cooperative regulation of actin filaments by other proteins like myosin, troponin-T (Palm *et al.*, 2003). Although the role of TM is well defined in striated muscles, the precise mechanism of how TM functions is still unclear. This is partly due to the complexity of the isoform diversity of different myofibrillar proteins including TM and also due to the incomplete knowledge of structural/functional relationships. There are four TM genes (*TPM1*, *TPM2*, *TPM3*, and *TPM4*), which exhibit a very high degree of conservation in species ranging from *Drosophila* to human (Lees-Miller & Helfman, 1991; Perry, 2001).

## ***I. The Role of Tropomyosin in Cardiac Myofibrillogenesis***

Amphibians have been widely used to study the process of induction, specification, and determination of embryonic tissue. This is especially true for urodeles, including the Mexican axolotl (*Ambystoma mexicanum*). *Ambystoma* is facultative neotenus and provides a valuable model to study development of the heart because it carries a lethal mutation (gene *c*) which affects only heart muscle. This cardiac mutation of the axolotl is a lethal recessive causing the embryo to die about a fortnight post hatching. The mutants have abnormal cardiomyogenesis. Morphological studies have shown that the myocardium lacks organized myofibrils, having instead large collections of amorphous material, but retains normal electrophysiological properties (Lemanski, 1973; 1979; Zhang *et al.*, 2004). As a result, the embryos die due to a lack of a functional circulation. The mutant axolotl heart provides a unique system for studying the intricate process of cardiac development and also examining the specific functional role of each TM isoform in this process. This is because the protein level of TM is profoundly diminished in *c/c* mutant hearts resulting in an absence of organized myofibrils and inability to beat (Lemanski, 1973; 1979). ). Most importantly, the mutant hearts can be rescued *in situ* by supplying exogenous TM protein or TM cDNA in an expression construct under the control of an appropriate promoter (Zajdel *et al.*, 1998; 2000; 2002). In addition, mutant hearts can be rescued by an RNA that is unrelated to tropomyosin. It is not known how this RNA modulates the expression of tropomyosin and its subsequent organization into *de novo* myofilaments in rescued mutant hearts (Lemanski *et al.*, 1996; Zhang *et al.*, 2003). Extensive molecular characterization of the various isoforms of TM expressed in the Mexican axolotl has been carried out, and so far three isoforms have been identified in cardiac tissues. These isoforms are designated as TPM1 $\alpha$ , TPM1 $\kappa$  and TPM4 $\alpha$ . (Luque *et al.*, 1997; Spinner *et al.*, 2002) (Table 1).



## ***I. The Role of Tropomyosin in Cardiac Myofibrillogenesis***

The aim of the present study was to understand the structural specificity of the end-to-end association of tropomyosin to form cardiac myofibrils *in situ*. For this purpose we have prepared an expression construct containing sarcomeric tropomyosin TPM4 $\alpha$  that has been modified at both N- and C- termini by fusing green fluorescent protein (GFP) at the N-terminal end and L-E-FLAG (a 10-mer peptide) (Metzger *et al.*, 2003) at the C-terminal end. The expression construct containing the double-tagged TPM4 $\alpha$  was transfected into mutant axolotl heart, which is practically devoid of sarcomeric tropomyosin protein. The ectopic expression of the GFP.TPM4 $\alpha$ .E-L-FLAG promotes myofibrillogenesis in mutant hearts as determined by confocal as well as scanning electron microscopic analyses.

### **5.2 MATERIALS AND METHODS**

#### **5.2a pEGFP.TPM4 $\alpha$ .E-L-FLAG expression construct**

TPM4 $\alpha$  cDNA was PCR amplified with

P1(+) (5'-GGA ATT CAT GGA GGC CAT CAA GAA-3') and

P2(-) (5'-GGG AGC TCT AAG GAA GTC ATA TCG TT-3') primer pair.

At the 5'-end of the P1 primer an EcoRI site was inserted followed by the TPM4 $\alpha$  sequences starting from ATG. At the 5'-end of the P2(-) primer, a SacI site was inserted followed by the TPM4 $\alpha$  sequences prior to the stop codon. In other words, we excluded the

## ***I. The Role of Tropomyosin in Cardiac Myofibrillogenesis***

stop codon so that any epitope such as FLAG can be added at the 3'-end contiguously. The PCR-amplified DNA was digested with *SacI* enzyme followed by the ligation with T4 ligase to the FLAG cassette that was made by annealing two oligonucleotides

L1 (5'-CGA TTA TAA AGA TGA TGA TGA TAA ATA AG-3')

L2 (5'-TCG ACT TAT TTA TCA TCA TCA TCT TTA TAA TCG AGC T-3').

The ligation mix was digested with *EcoRI* and *SalI* and was subsequently ligated to the pEGFP vector digested with the same enzymes (i.e., *EcoRI* and *SalI*). The ligation mix was then used for transforming *Escherichia coli* (Invitrogen) following the protocol supplied by the manufacturer. Positive clones containing TPM4 $\alpha$ .E-L-FLAG were picked up after filter hybridization with [<sup>32</sup>P]-labeled L2 oligonucleotide. DNA was isolated from the positive clones and the nucleotide sequence was determined for verification.

### **5.2b Embryo care and whole heart organ culture**

Normal and mutant axolotl embryos were obtained from matings between heterozygous (+/c x +/c) animals from the Indiana University axolotl colony and the axolotl colony at SUNY Upstate Medical University. Animals were maintained in aquaria in 50% Holtfreter's solution (29 mM NaCl, 0.45 mM CaCl<sub>2</sub>, 0.33 mM KCl, 0.1mM MgSO<sub>4</sub>, and 4.76 mM NaHCO<sub>3</sub>) and fed commercial salmon pellets. The embryos were staged according to the standard staging system (Bordzilovskaya *et al.*, 1989). Removal of normal and mutant hearts was performed on stages 35–39 embryos via dissection of anesthetized animals following our published protocol (Lemanski, 1973; 1979; Lemanski *et al.*, 1996;

## ***I. The Role of Tropomyosin in Cardiac Myofibrillogenesis***

Zajdel, *et al.*, 1998; 2000; 2002; Zhang *et al.*, 2003; 2004). Embryos at ‘heartbeat’ stage 34/35 (when beating starts) were removed from their jelly coats, washed several times and identified as normal or mutant based upon whether they had beating hearts. The culture medium was modified Steinberg’s solution, (58 mM NaCl, 0.67 mM KCl, 0.9 mM CaCl<sub>2</sub>, 0.2 mM MgSO<sub>4</sub>, 4.6 mM HEPES, pH 7.4) with 1% antibiotic/antimycotic (Gibco: 1000 units penicillin, 1 mg streptomycin, and 2.5 µg amphotericin B/liter) that was filter sterilized using 0.22 µm filter units before use. Using watchmaker forceps, non-beating mutant hearts and beating normal hearts were extirpated and placed individually in 10 µL drops of Steinberg’s solution in a sterile 60 mm Petri dish lined with parafilm. Culture dishes were placed in a humid chamber, oxygenated regularly and kept at 18 degrees C for the duration of the culture period. The heart explants were checked periodically under a dissecting microscope.

### **5.2c Transfection procedure**

Hearts were transfected via Lipofectin reagent (Invitrogen) using a standard procedure (Zajdel, *et al.*, 1998; 2000; 2002). Lipofectin reagent was mixed with Steinberg’s solution for 30–45 minutes room temperature at 0.28 mg/mL. Approximately 5 µg of pEGFP.TPM4 $\alpha$ .E-L-FLAG expression vector was added to the mix and allowed to incubate 15 minutes. The hearts were placed into 10 µL of transfection solution, incubated at 17°C, and monitored for beating daily. At 2 days post transfection, the hearts were transferred into fresh Steinberg’s solution and incubated for an additional 3 days. Hearts were then fixed with 2% paraformaldehyde for 1 hour for confocal analysis.

### **5.2d Confocal microscopy**

Whole mount immunostaining and confocal microscopy were performed. Monoclonal tropomyosin antibody (Lin *et al.*, 1985) was obtained from the Developmental Studies Hybridoma Bank. Anti-GFP mono/polyclonal antibodies (Clontech) and polyclonal anti-FLAG antibody (Sigma) were used to detect GFP and/or FLAG tagged tropomyosin proteins. Anti-rabbit rhodamine red secondary antibody and anti-mouse/anti-rabbit FITC (Jackson Immunohistochemicals) secondary antibodies at a dilution of 1:50 were used for detection of primary antibodies. Whole hearts were mounted onto slides in BioRad Fluorogard antifade reagent. Specimens were viewed on a BioRad MRC 1024ES confocal laser system mounted on a Nikon Eclipse E600 microscope. Control hearts and treated hearts were examined using identical confocal settings. A simultaneous or sequential (double staining) Z-series was made for each. Digital image processing was performed using LaserPics (BioRad).

### **5.2e Electron microscopy**

Normal and mutant transfected hearts were fixed for 1 hour at room temperature in glutaraldehyde-formaldehyde and picric acid, buffered to pH 7.4 with 0.1M phosphate buffer. Hearts were post-fixed with 1% osmium tetroxide in the same buffer for 40 minutes, dehydrated in a series of ethanol solutions, and embedded in Epon or Araldite. Sections of 50-90 nm were cut, stained with uranyl acetate and lead citrate, and viewed in a JEOL 100CX II electron microscope at an acceleration voltage of 80 kv (Lemanski *et al.*, 1996).

### **5.3 RESULTS**

The strategy for creating the TPM4 $\alpha$  fusion protein construct in pEGFP (Clontech) is presented in Figure 5-1. The expression construct was transfected into normal or mutant axolotl hearts using lipofectamine following the method of Zajdel *et al.* (1998; 2000; 2002). Five days post transfection, the hearts were stained with CH1 monoclonal antibody, which is specific for sarcomeric tropomyosin. Figure 5-2a represents a normal heart stained with CH1, which shows organized myofibrils. In contrast, the control mutant heart does not have organized myofibrils and also is deficient in tropomyosin protein (Figure 5-2b). However, upon transfection myofibril formation can be observed (Figure 5-2c).

The normal and mutant hearts were transfected with the same expression construct and after 5 days post transfection were stained with anti-GFP (monoclonal) and anti-FLAG (polyclonal) antibodies. Figure 5-3a depicts the normal heart stained with anti-GFP antibodies. The results suggest that GFP has been incorporated into organized myofibrils. Also, staining with anti-FLAG antibody shows incorporation of the FLAG epitope in organized myofibrils (Figure 5-3b). When these figures were superimposed onto one another, the GFP and FLAG signals were found to be co-localized in the normal heart (Figure 5-3c).

In mutant heart transfected with the pEGFP.TPM4 $\alpha$ .E-L-FLAG expression construct anti-FLAG and anti-GFP antibody staining showed evidence of tropomyosin TPM4 $\alpha$  fusion protein expression, followed by the formation of well-ordered myofibrils (Figures 5-4b and 5-4c respectively). This is confirmed by ultra-structure images of the normal, mutant and transfected mutant embryonic hearts in Figure 5-5.

## **5.4 DISCUSSION**

The fusion protein construct, pEGFP.TPM4 $\alpha$ .E-L-FLAG, showed the expression and subsequent incorporation of tropomyosin-4 $\alpha$  into well-organized myofibrils, in both the normal and mutant embryonic axolotl hearts (Figures 5-3 and 5-4). The superimposed image (Figure 5-3c) demonstrated the co-localization of GFP and FLAG, strongly suggesting that GFP.TPM4 $\alpha$ .E-L-FLAG is expressed in myocardium and is subsequently incorporated into organized myofibrils. The ectopically expressed TPM4 $\alpha$  appears to have had a rescuing effect upon the mutant heart by encouraging the development of myofibrils which are lacking in cardiac lethal mutants (Figures 5-4 and 5-5). This effect of TPM4 $\alpha$  (also known as ATmC-3) upon myofibrillar formation has been noted before (Spinner *et al.*, 2002). However, the current study is the first where this tropomyosin protein has been demonstrated to function ‘normally’ even though the N- and C-termini have been modified.

Tropomyosin, approximately 70 kDa, is a dimeric actin binding protein that can be homodimeric (TPM1/TPM1 or, TPM2/TPM2) or heterodimeric (TPM1/TPM2), with heterodimerization thermodynamically favoured (Gimona *et al.*, 1995). It is of interest to ask whether ectopically expressed GFP.TPM4 $\alpha$ .E-L-FLAG fusion protein itself can form dimers and then become incorporated into organized myofibrils? Alternatively, does this fusion protein form heterodimers with an endogenous sarcomeric tropomyosin in normal cardiomyocytes? Furthermore, is the heterodimer then incorporated into organized myofibrils? The results presented in Figure 5-2c suggest that the fusion protein, which is ectopically expressed in mutant heart lacking endogenous tropomyosin, can form homodimers. However, it could be argued that transfection of mutant hearts with the

## ***I. The Role of Tropomyosin in Cardiac Myofibrillogenesis***

expression construct could somehow induce the expression of another endogenous tropomyosin that is recognized by CH1 monoclonal antibody against tropomyosin, *or* that promotion of myofibril formation in mutant hearts takes place with tropomyosin that has been generated after the cleaving off of one or both fused epitopes from the fusion protein.

In order to show that the tropomyosin seen is the fusion protein itself, the post-transfected mutant hearts were stained with either anti-FLAG (Figure 5-4b) or anti-GFP antibodies (Figure 5-4c). The results presented in Figure 5-4 strongly suggest that indeed the GFP.TPM4 $\alpha$ .E-L.FLAG fusion protein is expressed and subsequently incorporated into organized myofibrils in mutant hearts, which are deficient in tropomyosin protein. Hence, it is tempting to conclude that GFP.TPM4 $\alpha$ .E-L.FLAG fusion protein is capable of forming homodimers in mutant heart tissue and the homodimer can thus be incorporated into organized myofibrils in mutant axolotl hearts. This is an important consideration from a biomedical point of view. Various missense mutations in tropomyosin and also in other myofibrillar proteins have been implicated in Familial Hypertrophic Cardiomyopathies in humans (FHC) (Bottinelli *et al.*, 1998; Muthuchamy *et al.*, 1999; Marston & Redwood, 2003).

FHC is a subset of Hypertrophic Cardiomyopathy (HCM), the most common cause of sudden death in young adults. It is a genetic disease with an autosomal dominant mode of inheritance with a few exceptions (Maron *et al.*, 1996). In FHC, one of the two alleles of the *TPM1* gene is mutated. So the question is whether the FHC phenotype is due to the incorporation of a homodimer of two mutant tropomyosin molecules or a heterodimer of a mutant and a wild-type of tropomyosin. This is particularly important for Asp175Asn or

## ***I. The Role of Tropomyosin in Cardiac Myofibrillogenesis***

Glu180Gly FHC mutations in tropomyosin since the 170-180 region in tropomyosin is the putative troponin binding region. Hence, it is still an open question whether the homodimers of Asp175Asn mutant tropomyosin can support the organization of myofibrils *in vivo*. Mutant axolotl hearts with tropomyosin deficiency present an ideal system for studying this question since only the ectopically expressed protein (tagged or untagged) is available for myofibril formation.

To substantiate the above confocal results at an ultra-structural level, transmission electron microscopy was carried out with normal, mutant, and transfected mutant hearts for confirmation of the formation of organized myofibrils in mutant hearts transfected with pEGFP.TPM4 $\alpha$ .E-L-FLAG expression construct. Consistent with published observations (Lees-Miller & Helfman, 1991; Lemanski, 1973), no organized myofibrils were seen in mutant hearts (Figure 5-5B) when compared to normal. On the contrary, organized myofibrils are evident in mutant hearts transfected with pEGFP.TPM4 $\alpha$ .E-L-FLAG (Figure 5-5C).

The N- and C- terminal ends of tropomyosin, required for high actin affinity, are encoded by alternatively expressed exons. The ends overlap to form continuous cables of tropomyosin along both sides of the actin filament, enabling co-operative interactions (McLachlan & Stewart 1975). Expression studies with a double fusion protein of sarcomeric tropomyosin in mutant axolotl suggest that the extension of both N- and C-terminal ends of the sarcomeric protein does not affect the formation of continuous cables along the actin filament. In addition, it also does not seem to affect the co-operative interaction of tropomyosin with other sarcomeric proteins, especially actin, as indicated by its incorporation into regular repeating myofibrils.



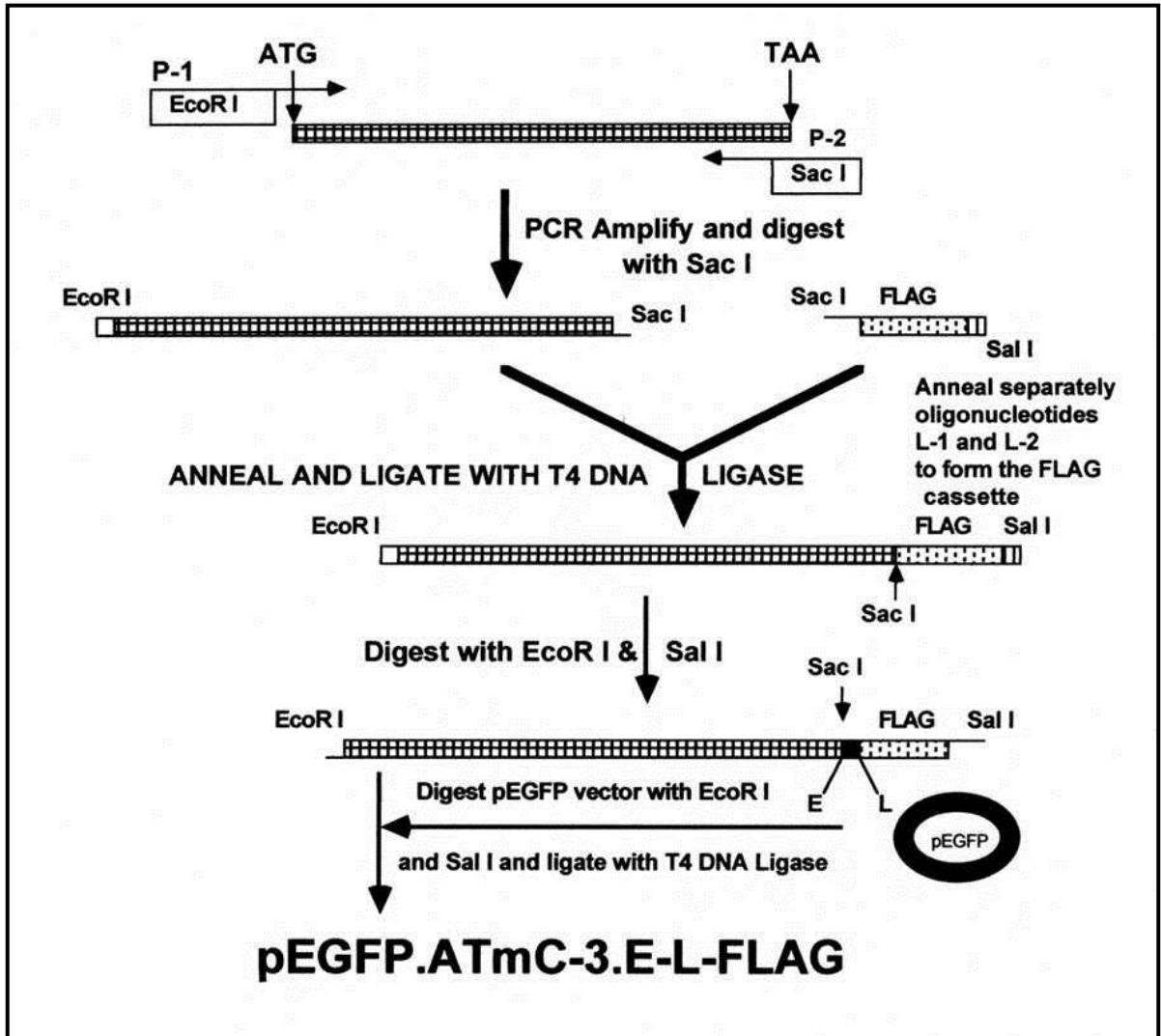
**Table 5-1. Nomenclature used for Tropomyosin isoforms in this chapter.**

<b>Nomenclature of various isoforms of tropomyosin referred to</b>	<b>The gene encoding the isoforms: new nomenclature (old nomenclature)</b>	<b>Isoforms of tropomyosin currently known as</b>	<b>Exon composition</b>	<b>Nomenclature used in previous publications on axolotl</b>
TPM1 $\alpha$	TPM1( $\alpha$ -TM)	Striated muscle	1a, 2b, 3, 4, 5, 6b, 7, 8, 9a/b	ATmC-1/ $\alpha$ -Tm-1
TPM1 $\beta$	TPM1( $\alpha$ -TM)	Smooth muscle	1a, 2a, 3, 4, 5, 6b, 7, 8, 9d	Sm $\alpha$ -Tm
TPM1 $\gamma$	TPM1( $\alpha$ -TM)	TM-2 fibroblast	1a, 2b, 3, 4, 5, 6b, 7, 8, 9d	
TPM1 $\delta$	TPM1( $\alpha$ -TM)	TM-3 fibroblast	1a, 2b, 3, 4, 5, 6a, 7, 8, 9d	
TPM1 $\epsilon$	TPM1( $\alpha$ -TM)	TM-5a fibroblast	1b, 3, 4, 5, 6b, 7, 8, 9d	
TPM1 $\kappa$	TPM1( $\alpha$ -TM)	Novel striated/cardiac	1a, 2a, 3, 4, 5, 6b, 7, 8, 9a/b	ATmC-2/ $\alpha$ -Tm-2
TPM2 $\alpha$	TPM2 ( $\beta$ -TM)	Striated/Skeletal muscle	1a, 2b, 3, 4, 5, 6b, 7, 8, 9a/b	
TPM3 $\alpha$	TPM3(hTMnm)	Skeletal Muscle	1a, 2b, 3, 4, 5, 6b, 7, 8, 9a/b	
TPM4 $\alpha$	TPM4 (TM4)	StrTM4	1a, 2b, 3, 4, 5, 6b, 7, 8, 9a/b	ATmC-3/Str.TM-4
TPM4 $\beta$	TPM4 (TM4)	Non-muscle TM4 in amphibians and avian species.	1b, 3, 4, 5, 6, 7, 8, 9?	

ATmC-1: Axolotl Tropomyosin Cardiac-1 (Zhang *et al.*, 2003); ATmC-2: Axolotl Tropomyosin Cardiac-2 (Zajdel *et al.*, 2002; Zhang *et al.*, 2003);

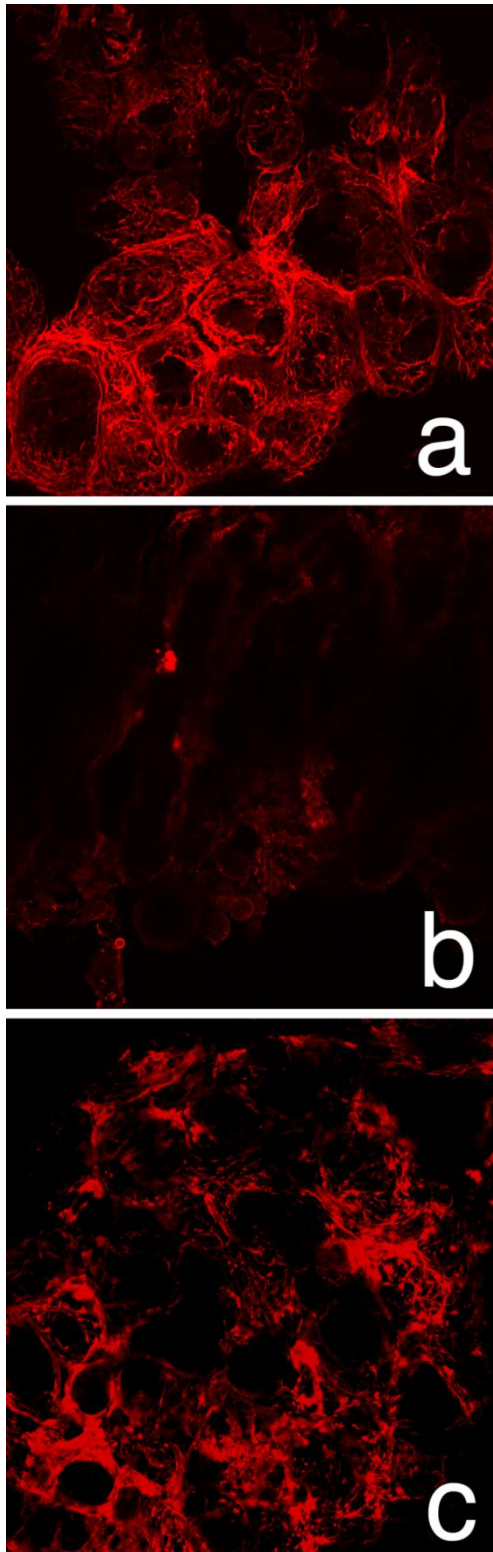
ATmC-3: Axolotl Tropomyosin Cardiac -3 (Luque *et al.*, 1997).

**Figure 5-1. The strategy for making pEGFP.TPM4 $\alpha$ .E-L-FLAG expression construct.**



The details of the strategy have been described under Materials and Methods. The expression of the fusion protein GFP.TPM4 $\alpha$ .FLAG is driven by cytomegalovirus promoter, which is an integral part of the pEGFP vector (Clontech).

Figure 5-2. Confocal micrographs of embryonic stage 39 hearts.



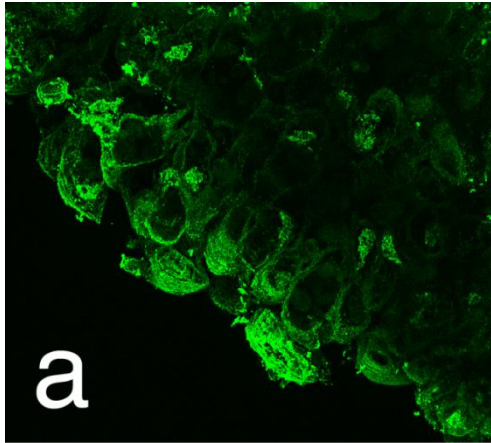
CH1 anti-tropomyosin staining shows well organized sarcomeric myofibrils in the normal heart (Figure 5-2a), which are absent in the mutant heart of the same stage (Figure 5-2b). However, mutant heart transfected with the expression construct pEGFP.TPM4 $\alpha$ .E-L-FLAG that expresses fusion protein shows abundant sarcomeric tropomyosin throughout the heart. The expressed fusion protein is well organized.

- (a) Normal heart stained with CH1.
- (b) Mutant heart stained with CH1.
- (c) Transfected mutant heart stained with CH1.

Our recent calcium spike experiments suggest that the wild-type and mutant hearts remain alive and have the normal electrophysiological properties after the entire lipofection process (Zhang *et al.*, 2004).

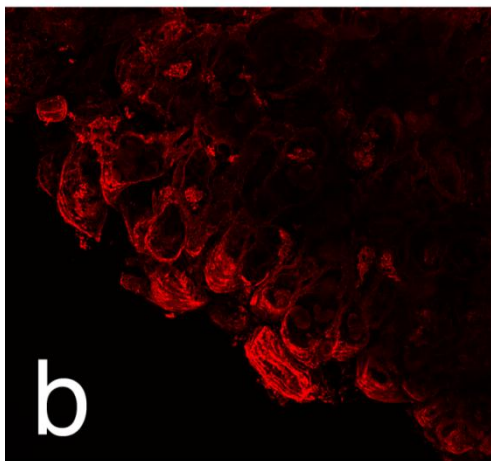
Scale bar = 50µm —

**Figure 5-3. Confocal micrograph of stage 39 normal transfected hearts stained with anti-GFP and anti-FLAG antibodies.**

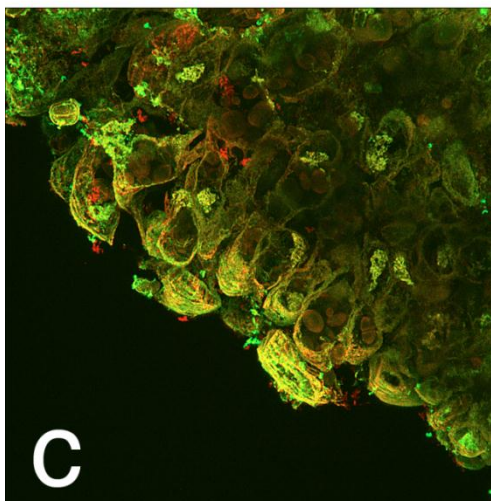


The results show that GFP.TPM4 $\alpha$ .FLAG fusion protein is expressed and subsequently incorporated into organized myofibrils in normal (and mutant hearts (see Figure 5-4)).


**(a)** Staining with anti-GFP.



**(b)** Staining with anti-FLAG.



**(c)** Co-localization of anti-GFP and anti-FLAG antibodies.

Scale bar = 100 $\mu$ m 

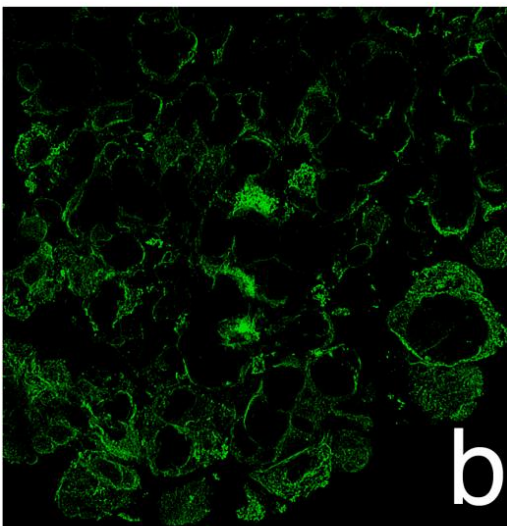
**Figure 5-4. Confocal micrograph of stage 39 mutant transfected hearts**

**with pEGFP.TPM4 $\alpha$ .E-L-FLAG constructs and stained with anti-GFP and anti-FLAG antibodies.**

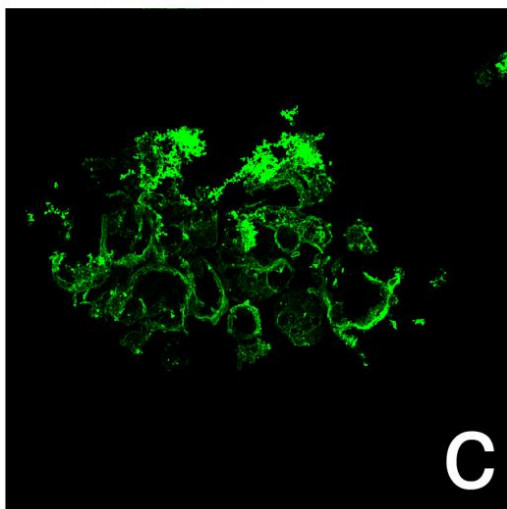
The results show that the fusion protein was expressed and subsequently organized in mutant axolotl hearts.




**(a)** Control mutant heart stained with anti-FLAG antibodies.



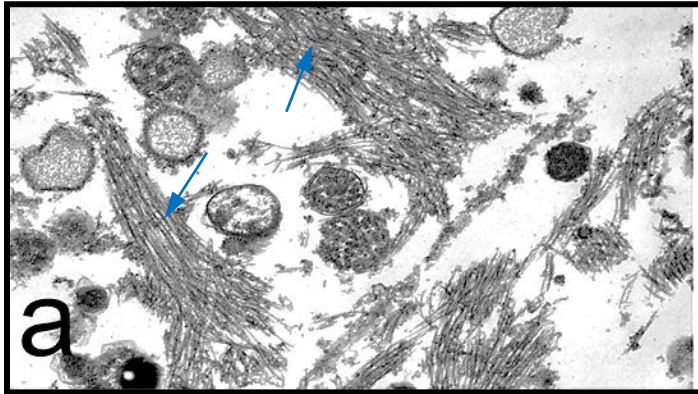
**(b)** Transfected mutant heart stained with anti-FLAG antibodies.



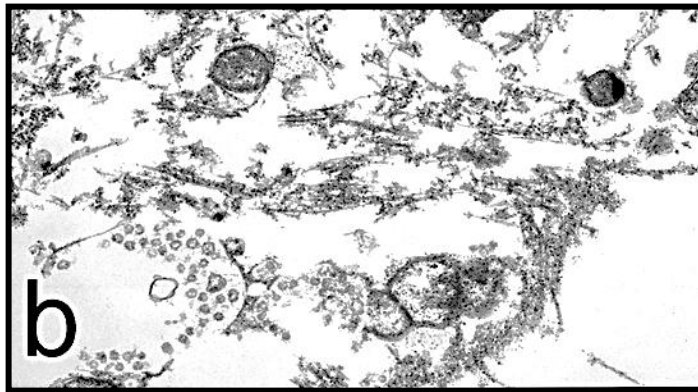
**(c)** Transfected mutant hearts stained with anti-GFP antibodies.

Scale bar = 50 $\mu$ m 

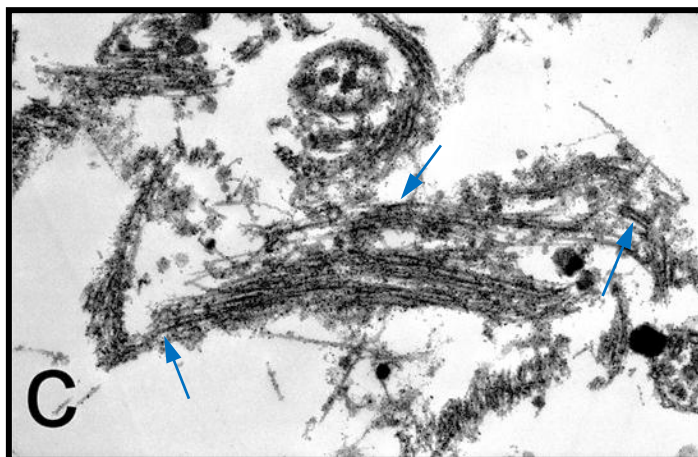
**Figure 5-5. Transmission electron micrograph of portions of normal, mutant, and pEGFP.TMP4 $\alpha$ .E-L-FLAG transfected mutant hearts of embryonic stage 39.**



**(a)** The normal heart shows well-differentiated myofibrils where Z-lines and I-bands can be identified (arrows).



**(b)** The mutant heart lacks myofibrils, but contains amorphous collections with dense bodies.

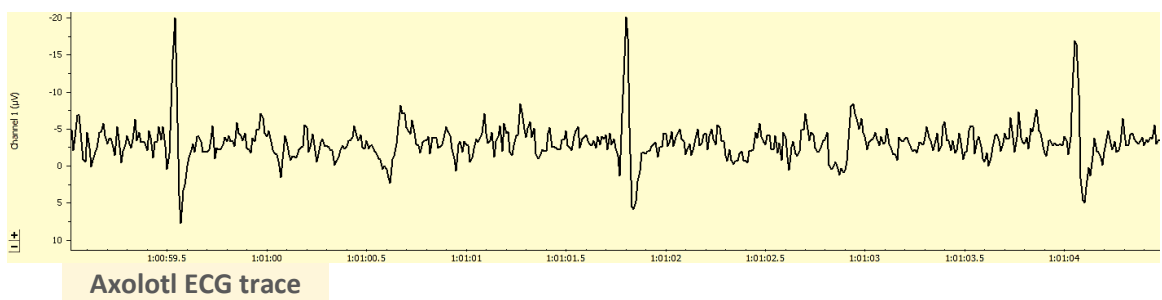


**(c)** Transfected mutant heart shows reduced amount of amorphous collections and organized myofibrils with identified Z-lines (arrows).

Scale bar = 25 $\mu$ m —

# Part II

## Neuroanatomy and Physiology of Cardiorespiratory Control



## **CHAPTER SIX**

### **INTRODUCTION AND GENERAL METHODOLOGY**

#### **6.0 ABSTRACT**

Part II of this thesis falls into two sections; (i) the distribution of the preganglionic vagal neurones in the medulla (Chapter 7), and (ii) the study of cardiorespiratory control in axolotls (Chapter 8). In Chapter 7, Fluoro-Gold, a retrograde neural-tracer was used to locate the vagal neurones in the neotenuous, metamorphosing and metamorphosed axolotls. Neotenuous axolotls only had one group of cells that were all located in the dorsal motor nucleus of the vagus (DMV). In the metamorphosing and metamorphosed there appeared to be a transition of cells from the DMV to a new ventrolateral position over the metamorphic course. It was hypothesised that this relocation could relate to the evolution of heart rate variability, and that this region may be equivalent to a primitive form of an area called the nucleus ambiguus found in higher organisms. Thus, in Chapter 8, the cardiac and ventilatory behaviour of neotenuous and metamorphosed axolotls was examined, along with pharmacological intervention. Atropine, a cholinergic muscarinic antagonist, raised the heart rate in both neotenuous and metamorphosed axolotls, indicating the presence of some vagal tone. The  $\beta$ -adrenergic antagonist propranolol caused a decrease in heart rate, indicating the presence of sympathetic control. Ventilation rates in the neotenuous generally followed that of the heart rate. However the metamorphosed form



showed a series of bradycardia-tachycardia oscillations immediately post ventilation, which may be indicative of respiratory sinus arrhythmia (RSA).

### **6.1 INTRODUCTION**

The axolotl, *Ambystoma mexicanum*, is an intriguing animal in which to study the changes associated with the transition from primarily aquatic to aerial modes of respiration. The neotenuous axolotl is perennibranchiate having external gill structures of three stalks (rami) on each side of the head, each consisting of fern-like filaments (fimbriae) plus internal gills located on paired branchial arches, plus poorly developed lungs, so respiratory gas exchange is predominantly carried out with the surrounding water (Duellman & Trueb, 1986). It is generally thought that the fimbriae, where the main role is to increase surface area for gas exchange, are longer (~8 mm) and more elaborately branched in healthy adult individuals that are found in stagnant waters, where oxygen levels may be relatively low. The opposite is true for axolotls that are in well aerated waters; they have much smaller gill filaments (Jones, P. *pers. comm.*; Malvin & Heisler, 1988). Some axolotls at University of Birmingham that were kept in well aerated water had filaments that were a mere 1 mm in length. Of course the genetic makeup of the animal would too determine the overall length of the gill filaments. The lungs in the neotenuous forms are rudimentary and are unlikely to play a major role in respiratory gas exchange, although these animals do come up to the surface periodically and buccal pump (gulp air from the surface). These periodic inflations may play a part in buoyancy control (Porter, 1972). The skin, as in all amphibians, is also

## ***II. Neuroanatomy and Physiology of Cardiorespiratory Control***

likely to be involved in some cutaneous respiration, with CO<sub>2</sub> excretion being more important than oxygen uptake (Feder & Burggren, 1985).

After metamorphosis the gills are resorbed and the lungs grow and are actively ventilated so that they now play the major role in respiratory gas exchange. The neotenus axolotl lungs are a pair of simple membranous sacs with simple alveoli. However, post metamorphosis, several anatomical alterations are observed within the lung to accommodate the new mode of ventilation. Coleman & Hessler (1997) found (1) lung volume increased to  $5.309 \times 10^{-2} \text{ cm}^3$ , more than three times that of neotenus form, (2) lung wall thickness (~50  $\mu\text{m}$ ) reduced by approximately one-third (as the surface area of the lumen increased), (3) there was approximately 12% increase in the length of the lung, and (4) many new small blood vessels vascularised the metamorphosed lung. All these changes are related with increasing the effectiveness of oxygen and carbon dioxide gas exchange associated with lung-dependent respiration. Associated with these morphological changes in the respiratory organs are marked changes in the associated cardiovascular (CV) system, with the branchial arches supplying the gills regressed and replaced by internal and external carotid arteries (Kolesová *et al.*, 2007). It can be anticipated that there will be changes in the control of physiological function associated with these morphological changes that would be reflected in changes in the central nervous system. Preliminary studies have indeed indicated evidence of some neuroanatomical changes associated with the switch to air breathing at metamorphosis (Ihmied, 1989; Taylor *et al.*, 2001).

## ***II. Neuroanatomy and Physiology of Cardiorespiratory Control***

Neuroanatomically, when looking at the vagal preganglionic neurones (VPN) in the medulla oblongata of a variety of species, there appeared to be a phylogenetic trend towards a progressive increase in the proportion of these neurones in a ventrolateral location outside of the dorsal vagal motonucleus (DVN) (Taylor, 1993). However, recent studies have revealed variation within groups, possibly related to the proportional relationship between central and peripheral control of cardiorespiratory interactions (CRI) (Taylor *et al.*, 2010). Elasmobranch fishes have around 10% of these neurones in a ventral lateral location and this seems to be associated with central interactions between respiratory and cardiac control centres. Other fish have less than 2% of VPN outside the DVN and; CRI seems to be determined predominantly by peripheral feedback loops. Some amphibians (e.g. *Xenopus*) have from 20-30% of VPN outside the DVN while others (e.g. *Rana*) have all of their VPN in the DVN. The functional correlations of these differences are the subject of present investigations (E. W. Taylor and others, unpublished observations). Reptiles have varying numbers of VPN outside of the DVN, though RSA was recorded from rattlesnakes, *Crotalus* (Campbell *et al.*, 2006). There is sparse information on birds but in the duck, *Anas* while only 2% of VPN are outside the DVN 30% of cardiac VPN (CVPN) are so placed, implying that 2 locations for CVPN may be of functional importance. In mammals generally more than 50% of VPN are outside the DVN and up to 80% of CVPN may be located in the nucleus ambiguus, an area ventro-lateral to the DVN (Bennett *et al.*, 1981; Taylor *et al.*, 1999).

Interestingly, it has been found that some neurones migrate from the medial position (DVN) to a more ventrolateral position during brain stem development in human embryos and foetuses (Brown, 1990; Windle (1933) in Bennett *et al.*, 1981). Generally, it seems that

## ***II. Neuroanatomy and Physiology of Cardiorespiratory Control***

as the number of PVN in the ventrolateral region increases so does the animal's reliance on lung ventilation. Therefore, this ventrolateral location may be involved in the ontogeny and evolution of lung breathing (and/or its control).

Before its innervation, the heart has myogenic rhythmicity, with the sinoatrial node being the pacemaker. Pacemaker cells spontaneously depolarise driving the rest of the myocardium to contract during systole, thereby determining heart rate. The depolarisation is thought to be caused by spontaneous  $\text{Ca}^{2+}$  release by the sinoatrial node cells. These cells have intracellular  $\text{Ca}^{2+}$  stores beneath the cell plasma membrane and  $\text{Ca}^{2+}$  is released in a cyclic way (Bogdanov *et al.*, 2001; Vinogradova *et al.*, 2002). Localised events cause cyclic  $\text{Ca}^{2+}$  release during diastolic depolarisation (Lakatta *et al.*, 2003). The cyclic  $\text{Ca}^{2+}$  variations appear to control the rate of action potentials, hence contributing to the final heart rate (Maltsev *et al.*, 2004). The diastolic depolarisation is driven by the activation of the hyperpolarisation-activated inward current, known as the funny or pacemaker current ( $I_f$ ) (Bucchi *et al.*, 2007; Verkerk *et al.*, 2009). Hyperpolarisation causes the f-channels to open and carry the inward current, thereby generating the diastolic depolarisation. This eventually leads to the threshold for  $\text{Ca}^{2+}$  channel activation and action potential firing. Studies suggest that spontaneous sarcoplasmic reticulum  $\text{Ca}^{2+}$  release may too be involved in sinus rhythm generation (Lakatta & DiFrancesco, 2009; Maltsev & Lakatta, 2009; Hata *et al.*, 1996).

The sympathetic limb of the autonomic centre increases heart rate and force of cardiac contraction via adrenaline binding on adrenoceptors of cardiac cells. This action is facilitated by the release of noradrenaline from the sympathetic fibres. When the  $\beta$ -

## ***II. Neuroanatomy and Physiology of Cardiorespiratory Control***

adrenergic receptors of the sinoatrial node cells are thus stimulated, there is an increase in the frequency and amplitude of spontaneous  $\text{Ca}^{2+}$  release in the subcellular space (Vinogradova *et al.*, 2002). It is thought that  $\beta$ -adrenoceptor stimulation increases cyclic adenosine monophosphate (cAMP) levels which activate ion channels that increase entry of  $\text{Ca}^{2+}$  into the myogenic cells from the extracellular fluid (Baruscotti *et al.*, 2005).

The cardiac vagal axons from the nucleus ambiguus (part of the parasympathetic limb) have a cardioinhibitory effect by release of the neurotransmitter acetylcholine which acts directly on cardiac  $\text{M}_2$ -muscarinic cholinergic receptors and slowing pacemaker cell activity in the SA-node of the heart. Parasympathetic signals activated through these receptors cause an outward current of potassium which contributes to the bradycardia. Vagal tone is the normal bradycardic effect on the heart rate by the vagus nerve (the tenth cranial nerve) which contains the parasympathetic fibres. Thus an increase in vagal discharge, and or a decrease in sympathetic signals would cause bradycardia, and tachycardia would result from an increase in sympathetic discharge and/or a decrease in parasympathetic discharge.

Since the respiratory and CV systems supply oxygen to the tissues and are responsible for removal of metabolically produced  $\text{CO}_2$ , it is important that these systems are functionally linked and work in harmony to deal with increasing and decreasing metabolic demands. Baroreceptors located in the carotid sinus and the aorta detect arterial pressure and cause modulation of the CV system appropriately; and chemoreceptors located in the carotid and aortic bodies detect circulatory changes in pH, partial pressure of  $\text{CO}_2$  and partial pressure of  $\text{O}_2$ , which act on the respiratory system to promote homeostasis (Daly & Jones, 1998).

## ***II. Neuroanatomy and Physiology of Cardiorespiratory Control***

Intriguingly, in many vertebrates the heart demonstrates beat-to-beat fluctuations, known as heart rate variability, which seems to be generated by fluctuations in the degree of vagal control (vagal tone) (McDonald (1980) in Taylor, 1994; Taylor *et al.*, 1999). Mechanoreceptors and chemoreceptors contribute to heart rate variability via the cardiorespiratory centre which then alters heart rate and blood pressure to maintain circulatory homeostasis. Humans show a slight increase in heart rate upon inspiration and a corresponding decrease during expiration, a phenomenon called RSA (Hyndman *et al.*, 1971).

RSA is the main contributor to HRV in human adults. The origin of RSA has been attributed to three main areas:– (i) *volume receptors* - increased diastolic filling during inspiration stimulates the right heart atrial volume receptors resulting in a reflex increase in heart rate, known as the Bainbridge reflex (Bainbridge, 1920); (ii) *lung expansion receptors* - inspirational lung expansion activates the pulmonary-cardiac reflex (Hering, 1895; Anrep *et al.*, 1936b); or is triggered by *central mechanisms* (Anrep *et al.*, 1936b). The general accepted consensus is that all three are involved in producing RSA with integration within the brain stem of the autonomic control of the heart (Yasuma & Hayano, 2004).

Lung expansion detectors, heart volume receptors and central mechanisms appear to contribute to this RSA *via* the vagus nerve which emanates from the cardiac vagal motoneurons in the brainstem and innervates the SA node (Anrep *et al.*, 1936a & b; Bainbridge, 1920; Jordan & Spyer In: Taylor, 1987). During the respiratory cycle, decrease in vagal nerve activity during inspiration and increase during expiration, causes the heart

## ***II. Neuroanatomy and Physiology of Cardiorespiratory Control***

rate to rise and fall respectively. In vagotomised animals or animals that have cholinergic antagonists, RSA is eradicated (Samaan, 1935; Anrep *et al.*, 1936b; Hamlin *et al.*, 1966; Coker *et al.*, 1984). Therefore it appears that there are mechanism(s) which interrupt vagal discharge during the breathing cycle, thereby producing HRV. An important contributor is the respiratory modulation of the baroreceptor reflex (Piepoli *et al.*, 1997). Normally when baroreceptors are stimulated during inspiration they would have an excitatory effect on vagal cardio-motorneurons which would cause a fall in heart rate. However, this is not observed as the afferent input from the baroreceptor is gated prior to the cardio-motorneurons during inspiration, thus causing an increase in HR (Melcher, 1980; Keyl *et al.*, 2000). Vagal inhibition is also mediated by a mechanism that involves lung stretch receptors which are stimulated lung inflation (Taha *et al.*, 1995). The lung stretch receptors also inhibit vagal discharge by acting on the brainstem and it is the afferent input from these receptors that cause the gating of the baroreceptor reflex (Jordan & Spyer, 1986). Changes in blood gas composition, detected by chemoreceptors, effect central respiratory drive, and increase RSA (Shykoff *et al.*, 1991). Therefore vagal discharge is inhibited directly and indirectly by inspiratory neurons (Spyer, 1989).

It can be seen that both peripheral and central mechanisms contribute to the generation of RSA, but crucially the generation is centrally integrated within the brainstem and the vagal innervation of the heart. Measurements of this respiratory related HR oscillation may provide an indication of autonomic function and integrity of the medulla oblongata, so it could be used to measure parasympathetic control, though this is contentious in humans (Katona & Felix, 1975; Hayano *et al.*, 1991; Grossman and Taylor, 2006).

## ***II. Neuroanatomy and Physiology of Cardiorespiratory Control***

In animal models heart and ventilation rates can be measured electrophysiologically to examine heart rate variability, hence parasympathetic control. The axolotl is an apt animal model to study the ontogeny of heart rate variability and related neural changes as it predominantly uses its gills when in the larval form, and upon metamorphosis, becomes a committed lung breather. The central nervous system is likely to undergo essential modifications in association with lung, and possibly heart, innervation and gill degeneration. Another advantage of using the axolotl is that it is neotenic (reaching sexual maturity whilst in its larval form) and, thus, large enough for valuable neuroanatomical and physiological examinations from larval to induced metamorphic life stages.

Thus the axolotl is an excellent animal model to use to determine if there is a direct correlation between the onset of heart rate variability and the ventrolateral migration of PVN. Measurement of heart rates and ventilation rates, along with collection of hind brain tissues of neotenic, metamorphosing and metamorphosed axolotls may yield a greater understanding of the functional roles of the migration pattern of VPN and their relationship with cardio-respiratory control.

### **6.2 AIMS AND OBJECTIVES**

The aim of the experimental studies in Part II of the present thesis sought to investigate the hypothesis that relocation of VPN relates to the onset of heart rate variability (HRV) in the committed lung breathing axolotl. It was thought that the relocation may cause physiological changes in heart rate which could be evidence for autonomic change.



## ***II. Neuroanatomy and Physiology of Cardiorespiratory Control***

Therefore the objectives of Part II were:

- To induce metamorphosis in axolotls (present Chapter). This would permit the observation of progressive developmental changes that occur from a larval, aquatic axolotl to the metamorphosed, lung breathing form.
- To examine the neuroanatomy of VPN in the medulla oblongata in the neotenus, metamorphosing and metamorphosed forms (Chapter 7). This was novel on metamorphosing axolotls, and, although one study already looked at VPN's in the neotenus and metamorphosed forms (Ihmied, 1989), it was interesting to compare findings, especially since this study used the newer technique of fluorescent retrograde tracing by intraperitoneal injection.
- To record heart and ventilation rates in the neotenus and metamorphosed axolotls and then, with drug intervention, to determine if there is evidence of HRV, especially in the latter forms. Drug intervention would determine the level of cholinergic and adrenergic effect upon the heart and ventilation rates (Chapter 8).

### **6.3 MATERIALS AND METHODS**

#### **6.3a Axolotls**

The experimental animals were bred from the resident colony at University of Birmingham, maintained in a holding room with water and air temperature at  $15 \pm 2.0$  °C

## ***II. Neuroanatomy and Physiology of Cardiorespiratory Control***

and  $20.0 \pm 2.0^{\circ}\text{C}$  respectively, with an alternating 12:12-h light cycle. Neotenuous axolotls (*A. mexicanum*) were kept in shallow plastic tanks (60 x 35 x 20 cm (*lwh*)) containing 50% Holtfreter's solution (100% solution per litre: NaCl, 3.5 g; KCl, 0.05 g; CaCl<sub>2</sub>, 0.1 g; NaHCO<sub>3</sub>, 0.2 g; MgSO<sub>4</sub>·7H<sub>2</sub>O, 0.2 g) diluted in dechlorinated tap water (Asashima *et al.*, 1989). This solution acts to prevent infection ([www.ambystoma.org/AGSC/](http://www.ambystoma.org/AGSC/)) and increase hardness of water, which axolotls prefer ([www.axolotl.org/requirements.htm#hardness](http://www.axolotl.org/requirements.htm#hardness)). They were fed with beef or lamb heart three times per week. Axolotls used were of either gender, aged 17 months, with a mean ( $\pm$ SE) weight of  $72.2 \pm 2.8$  g.

### **6.3b Induction of metamorphosis**

Axolotls remain neotenuous as they do not release thyronine hormone from the thyroid gland. This results in a block in the thyroxin pathway and thus failure to metamorphose naturally (Norris & Platt, 1973; Taurog, 1974). However, metamorphosis can be experimentally induced using triiodo-L-thyronine (T<sub>3</sub>) or thyroxine (T<sub>4</sub>) (Norris & Platt, 1973; Taurog, 1974). Axolotls may be immersed in a T<sub>3</sub> or T<sub>4</sub> solution (Volk *et al.*, 1998; Maake *et al.*, 1999; Brown, 1997; Rosenkilde & Ussing, 1996). Rosenkilde recommends using a dosage between 20-40 nM of T<sub>3</sub>, initially dissolved in 0.6% sodium carbonate (*pers. comm.*), but Brown (1997) routinely used 30 nM of T<sub>4</sub> as it was found to be remarkably non-toxic. Metamorphosis may also be induced by intramuscular or intraperitoneal injection of T<sub>3</sub> or T<sub>4</sub> (Prahlad & DeLanney 1965; Gahlenbeck & Bartels, 1970; Crawford & Vincenti, 1998; De Groeff *et al.*, 2000; Gaur *et al.*, 2001).

The above methods were initially tried and resulted in a very poor success rate. After seeking advice from the David Mortimer, the resident vet of Biomedical Science Unit,

## ***II. Neuroanatomy and Physiology of Cardiorespiratory Control***

University of Birmingham, and the Home Office, I was permitted to try variations of the published methods, so that the University could have a working protocol for the induction of metamorphosis in axolotls as specific, useful information in this area was lacking. This was thought to be especially pertinent as it would prevent the repetitions of metamorphic failures by future researchers and hence reduce mortality rates. Therefore the preferred procedure used in this study was a modification from those that are already published.

Axolotls were injected intramuscularly with  $T_3$  at a concentration of 1.9  $\mu\text{g}$  per gram body weight. Around 7 days post induction the holding tanks were gently tilted up at one end so as to provide a 'beaching' area and some large drain pipes were cut in half and placed into the tanks to provide shelter/cover as the axolotls preferred to be under cover (Figure 6-1). Gravel ( $\leq 1.5\text{cm}$  diameter) was taken out as a couple of axolotls were found to have ingested them following a post mortem examination to establish the cause of death. At this time they refused to take food. For optimum hygiene the water was changed daily to prevent contamination of shedding skin (Figure 6-2) by microbes. Most axolotls started to come out of the water on days 9-11 post induction, although some took much longer (see Figure 6-3). Around 14 days post induction some axolotls showed signs of 'rebound' effect - where the moulting appeared to be incomplete, thus leaving layers of dead cells on the skin surface (see Figure 6-4). The rebound effect is thought to be due to insufficient or lack of thyroid hormone after induction of metamorphosis. To remedy this, the axolotl was immersed in a weak solution of  $T_3$  (20 nM) as advised by Rosenkilde & Dube (*pers. comm.*). However, the axolotl was always provided with an 'island' by placement of appropriately sized rocks or slabs. The immersion solution strength was gradually reduced from 20 nM to 5 nM over a 6 week period. Rosenkilde suggested that incompletely

## ***II. Neuroanatomy and Physiology of Cardiorespiratory Control***

metamorphosed individuals, having unsloughed skin, can be kept in a 6 nM solution of the hormone, which was sufficient to ensure moulting of the skin and the onset of feeding (*pers. comm.*). From  $30 \pm 5$  days the axolotls were fully metamorphosed and were feeding (see Figures 6-5(C) & (D)). The reducing weight of all the axolotls was recorded throughout the metamorphic process.

### **6.3c Experimental stages**

The developmental stages used in the neuroanatomical and studies were neotenuous, metamorphosing (mid-metamorphic) and metamorphosed. For electrophysiological recordings only neotenuous and metamorphosed were used. Neotenuous axolotls were the normal larval, sexually mature forms; mid-metamorphic stage was determined by those having just gill stubs left and a preference for being out of the water (Figures 6-5(A) & (B)); and metamorphosed stage was determined as those individuals that had fully metamorphosed and were readily taking food (Figures 6-5(C) & (D)).

### **6.3d Outcome**

Due to the problems initially encountered with induction of metamorphosis there was a shortage of time and lack of sufficient number of animal availability. Each axolotl can take over a month to fully metamorphose. As a consequence, only one animal of each stage was used as an example to show the changes that are involved in the VPN neuroanatomy. Nevertheless, selection pressure for anatomical structures that are important in survival would be very similar within species and so with the axolotls, each developmental stage is bound to be highly representative.

## *II. Neuroanatomy and Physiology of Cardiorespiratory Control*

**Figure 6-1. Axolotl habitat setup during metamorphic induction.** The tank was lifted so that the water would be available only at one end. The slope was gradual so that the axolotl could walk out with ease. Cut drain pipes provided cover and the sponge, moss and rocks provided different substrates for the axolotl to sit on.



**Figure 6-2. Shedding sheets of skin in the tank during metamorphosis.** White strip is 4 cm long.



**Figure 6-3. Transition from aquatic to aerial habit.** Axolotl coming out of the water for the first time on day 9 (A), day 10 (B). On day 13 this axolotl (C) only had some gill atrophy and came out of the water for the first time on day 21 (D) post induction. Strip of paper is 4 cm long.



## II. Neuroanatomy and Physiology of Cardiorespiratory Control

**Figure 6-4. Rebound effect.** (A) Axolotl 26 days post induction showing some signs of ‘rebound’ effect of insufficient hormone. There is a layer of dead cells in the skin (arrowheads). (B) Five days after immersion in 20nM hormone solution the skin is shiny and smooth, the normal appearance of amphibian skin. Strip of white paper is 4cm long.



**Figure 6-5. Aerial metamorphic changes.** (A) Two axolotls that are at mid-metamorphosing stage as indicated by the presence of gill stubs and the preference of being out of the water throughout the day. Photograph was taken 14 days post induction of metamorphosis. The white strip is 4 cm long. (B) Another mid-metamorphic stage (see gills), although induction took place 29 days ago. (C) Photograph of an almost fully metamorphosed axolotl taking food (beef heart) on day 32 post induction. (D) A fully metamorphosed axolotl. Photograph taken on day 40 post induction.





**ACKNOWLEDGMENTS**

Surgical procedures in Part II of this thesis were initially carried out by Prof E. W. Taylor for demonstration purposes. After which they were carried by me under supervision.

The procedures were carried out under project licence number PIL 40/6730

I would like to thank Hamish Campbell and Stuart Egginton for their help and advice in the preliminary power spectral analysis work, and for the use of the PowerLab system to record ECG in Chapter 8.

**CHAPTER SEVEN**

**NEUROANATOMY OF VAGAL PREGANGLIONIC NEURONES IN THE  
NEOTENOUS, METAMORPHOSING AND METAMORPHOSED  
AXOLOTL, *AMBYSTOMA MEXICANUM*.**

**A RETROGRADE STUDY USING FLUORESCENT  
FLUOROGOLD TRACER**

## **7.0 INTRODUCTION**

This chapter was the study of the neuroanatomical changes that may be associated with the transition from gill breathing (neotenuous) to obligate lung breathing (metamorphosed) in the Mexican axolotls, *Ambystoma mexicanum*. The dorsal nucleus of the vagus nerve (DVN) is located in the medulla oblongata (Chapter 1). The medulla oblongata is known to contain centres that deal with autonomic, involuntary functions. For instance, the respiratory centre regulates breathing depth and rate by chemosensors, and the cardiac centre regulates heart rate through sympathetic and parasympathetic inputs. The nA is in the medulla located in a ventral lateral position in mammals and is thought to interact with the DVN in regulating cardiorespiratory functions. Indeed it is thought to be involved in the onset of RSA in humans ((Hou *et al.*, 2009; Taylor, 1994). Activity in these ventrolateral vagal motoneurons varies with mode of respiration in fish and mammals. Generally, as detailed in Chapters 1 and 6, there appears to be a phylogenetic trend towards an increase in the proportion of VPN in the ventrolateral location outside of the DVN (Taylor *et al.*, 1999) that appears to be associated with increase in reliance of lung breathing. However, some variation is seen in the actual proportion found in this ventrolateral area (Taylor *et al.*, 2010). Therefore this ventrolateral group may be involved in the transition to lung breathing, and it may be a primitive equivalent of the mammalian nA.

VPN in the brain stem of axolotls were labelled with a fluorescent neural tracer. The fluorochrome, Fluoro-Gold (FG) (Fluorochrome, Inc., Sigma-Aldrich), whose active agent is hydroxystilbamidine methanesulfonate, (Wessendorf, 1991) is a monosynaptic

## ***II. Neuroanatomy and Physiology of Cardiorespiratory Control***

retrograde axonal tracer (Schmued & Fallon, 1986). It has been found to label VPN when introduced into an animal by intraperitoneal injection (Leong & Ling, 1990; Cheng *et al.*, 1997; Cheng & Powley 1999; 2000; Akhavan *et al.*, 2006), since it specifically labels preganglionic autonomic and motor neurons in the brain stem. FG does not cross the blood-brain barrier and so it only labels the central neurons with peripheral axons. This means that no interneurons are labelled in the brain nor spinal cord (Persson & Havton, 2009). FG appears to be taken up by the peripheral termini during post-synaptic reuptake of neurotransmitter (Ambalavanar & Morris, 1989), and is localised within the cell bodies and proximal dendrites of labelled neurones (Schmued *et al.*, 1989). More specifically, fluorogold is found to accumulate within intracellular lysosomes (Wessendorf, 1991; Persson & Havton, 2009) and it also binds to the A-T-rich regions of DNA (Festy & Daune, 1973; Festy *et al.*, 1975). When a fluorochrome molecule absorbs light radiation it becomes electronically excited and then returns to its original state by emitting radiation at almost always a longer wavelength than the excitation wavelength. Using optical filter systems the emitted wavelength can be selected by blocking out all other wavelengths. The fluorochrome is then seen as bright objects against a black background. FG is excited by UV light at <330 nm and <390 nm and has peak emission at <450 nm and <600 nm. The effectiveness of the use of FG to label vagal neurons has been demonstrated by Powley *et al.* (1987) and so it was decided to use this retrograde label in the present study owing to its simple administration.

## **7.1 AIMS AND OBJECTIVES**

The aim of this chapter was to re-examine the findings of the appearance of a ventral lateral group of VPN in metamorphosed axolotls (Ihmied, 1989). Unlike the previous study, this was done with using a minimally invasive technique of using an intraperitoneal injection of a retrograde fluorescent tracer, Fluoro-Gold (FG) that is known to trace vagal motoneurons. In the previous study the researcher used HRP which involves finding, exposing and then crushing the nerves which is likely to introduce more errors than this, more refined, method. In addition, the previous study did not study the VPN in mid-metamorphosing axolotls, so this was novel.

This chapter links with the hypothesis that the ventrolateral relocation of VPN relates to the onset of HRV in the obligate lung breather. Therefore, the first aim of Part II of the thesis was to establish that there are neuroanatomical changes in the DVN and surrounding areas pre-, during, and post-metamorphosis.

Therefore the objectives this Chapter were:

- To examine the neuroanatomy of VPN in the medulla oblongata in the neotenus, metamorphosing and metamorphosed forms. This was achieved by collecting the medulla oblongata's at the appropriate stages and processing them for frozen sectioning. The sections were viewed using a fluorescence microscope to make cell counts rostral and caudal of obex, where the DVN is known to be located.

## **7.2 METHODS**

For retrograde labelling of VPN fluorogold was dissolved in distilled water to give 3 mg/ml concentration according to established protocols (Cheng *et al.*, 1997; 1999; 2000) and kept at 4°C until use and re-use after mixing. The axolotls (*A. mexicanum*) were held in position and a volume of 3.3 µl per gram axolotl weight of the concentrate was administered (since Cheng *et al.* (1999) used 1 ml per 300g rat) intraperitoneally. The angle of the needle was perpendicular to the skin surface and the needle was held in position for a few seconds after administration of the fluorogold. When the needle was drawn out gentle pressure was applied to the injection site to prevent leaking. The axolotls were then returned to their developmental stage specific habitat and treated normally for 10-12 days before collection of neotenuous, metamorphosing and metamorphosed stages. The animals behaved completely normally after the FG injection.

### **7.2a Perfusion system**

After the required survival time the axolotls were deeply anaesthetised with 0.2% solution of buffered (NaHCO<sub>3</sub>) tricaine methane sulphonate (MS222) and transferred to an operating dish. Note that the metamorphosing and metamorphosed axolotls were placed in a small plastic chamber (volume 500 ml) with their head raised out of the anaesthetic solution to prevent possible drowning (Figure 7-0(A)). The axolotls remained in some MS222 solution whilst perfusion took place. An incision was made in the chest area to reveal the sacral plates which were carefully pinned back to expose the chest cavity. The

## ***II. Neuroanatomy and Physiology of Cardiorespiratory Control***

pericardial membrane was cut open to expose the beating heart. A polyethylene tubing (PE10 Intramedic) cannula was gently placed into the truncus arteriosus by puncturing obliquely as shown in Figure 7-0(B). The animals were then perfused with frog saline (firstly each chemical was made to a [1M] and then the following volumes were used to make up to 1L with distilled water; NaCl, 115 ml; KCl, 3.2 ml; NaHCO<sub>3</sub>, 2.4 ml; CaCl<sub>2</sub>, 2.7 ml) containing 0.3% heparin for approximately 30 minutes to flush out the red blood cells and then, once the perfusate was running clear, the fixative was perfused through the animal (10% neutral buffered formaldehyde, Surgipath, Europe) for 1 hour (see Figure 7-0(C)).

The brain and some of the spinal cord was dissected out carefully (Figure 7-0.1(A)) and post fixed for up to 8 hours at 4°C in 20-30 ml of the same fixative used for perfusion, with a change of solution half way. The sample was washed with buffer and placed in 10% sucrose phosphate buffer (to cryoprotect) at 4°C overnight with one change during this time. The following day the portion of interest (Figure 7-0.1(B)) was transferred to embedding media (OCT), with orientation noted on the foil box container, and then gently lowered into liquid nitrogen. The sample was stored at -70°C until ready for sectioning.

### **7.2b Sectioning and mounting**

Sections were cut at a thickness of 20 µm using a -20°C cryostat with a fixed, regularly sharpened blade, mounted onto *Superfrost* glass slides (Surgipath) and were left at room temperature to air dry overnight. The following day the slides were placed in phosphate

## ***II. Neuroanatomy and Physiology of Cardiorespiratory Control***

buffered saline for 10-15 mins to wash out the embedding media and then dehydrated through a graduated series of alcohols (ethanol) (30%, 50%, 70%, 95%, 2 x 100%) for 2 mins each and finally cleared in xylene twice for 5 mins each. The slides were dried in air briefly, then mounted with Fluoromount (BDH) and coverslipped. These were left overnight at room temp in the dark.

The sections were viewed using a photomicroscope with ultraviolet epi-illumination at a wavelength of 365 nm that caused labelled cells to fluoresce, emitting light at a wavelength of 420 nm. Digital images of the fluorescing cells were captured using an image analysing system (Quips Pathvision package, Apple Mac). Once the obex was located, cell body counts were made using sections that were 60  $\mu\text{m}$  apart, both in a caudal and rostral direction from the obex.



**Figure 7-0 (A) Mid-metamorphic stage axolotl being anaesthetised in MS222.** A pile of absorbent towels act as a head rest to ensure airways are out of the solution and so prevent possible drowning. There is sufficient anaesthetic traversing the relatively permeable amphibian skin to induce sleep, although this took longer in metamorphosing and metamorphosed axolotls than in the neotenus. **(B) Cannulation of the truncus arteriosus.** The end of the cannula was cut obliquely and 4-5 mm was eased into the vessel in a rostral direction and then held in place by suturing. A small incision was made in the auricle to allow the blood and perfusate to flow out. Note that the ventricle is deplete of red blood cells due to perfusion and the thickness of the ventricular tissue is relatively thin, hence the ‘white’ appearance.

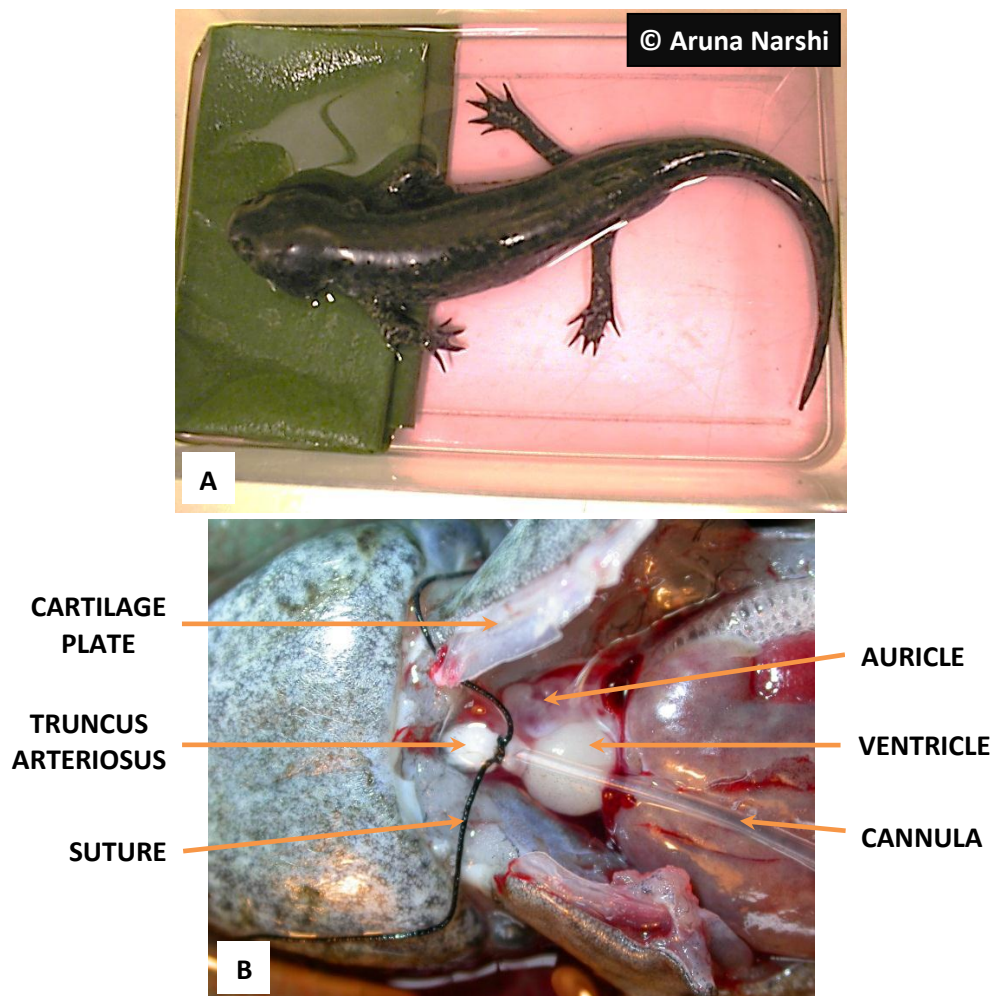


Figure 7-0 (C) Arrangement of the perfusion system.

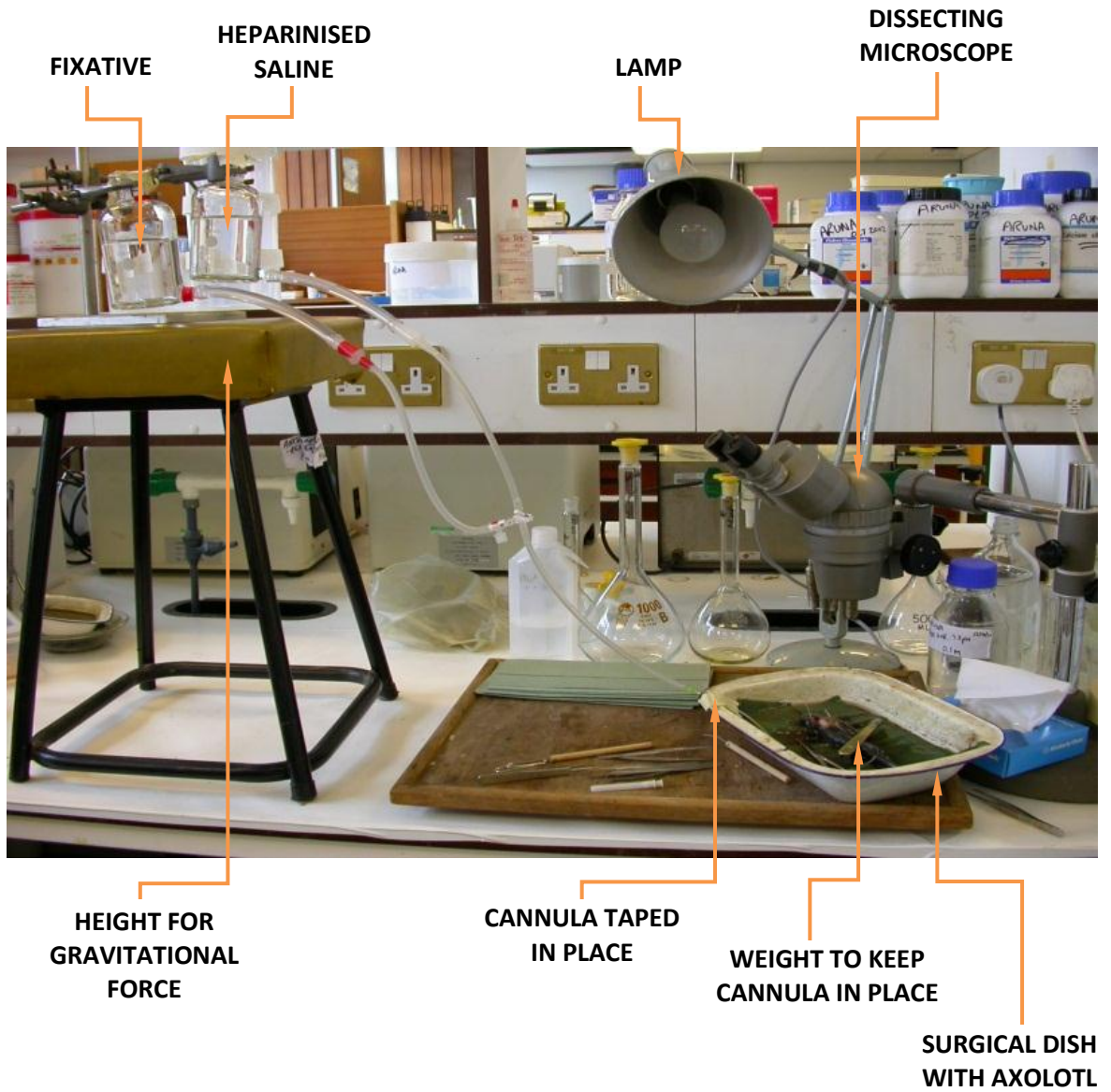


Figure 7-0.1 (A) Dorsal surface of the axolotl (*A. mexicanum*) brain. The choroid plexus of the fourth ventricle has been removed

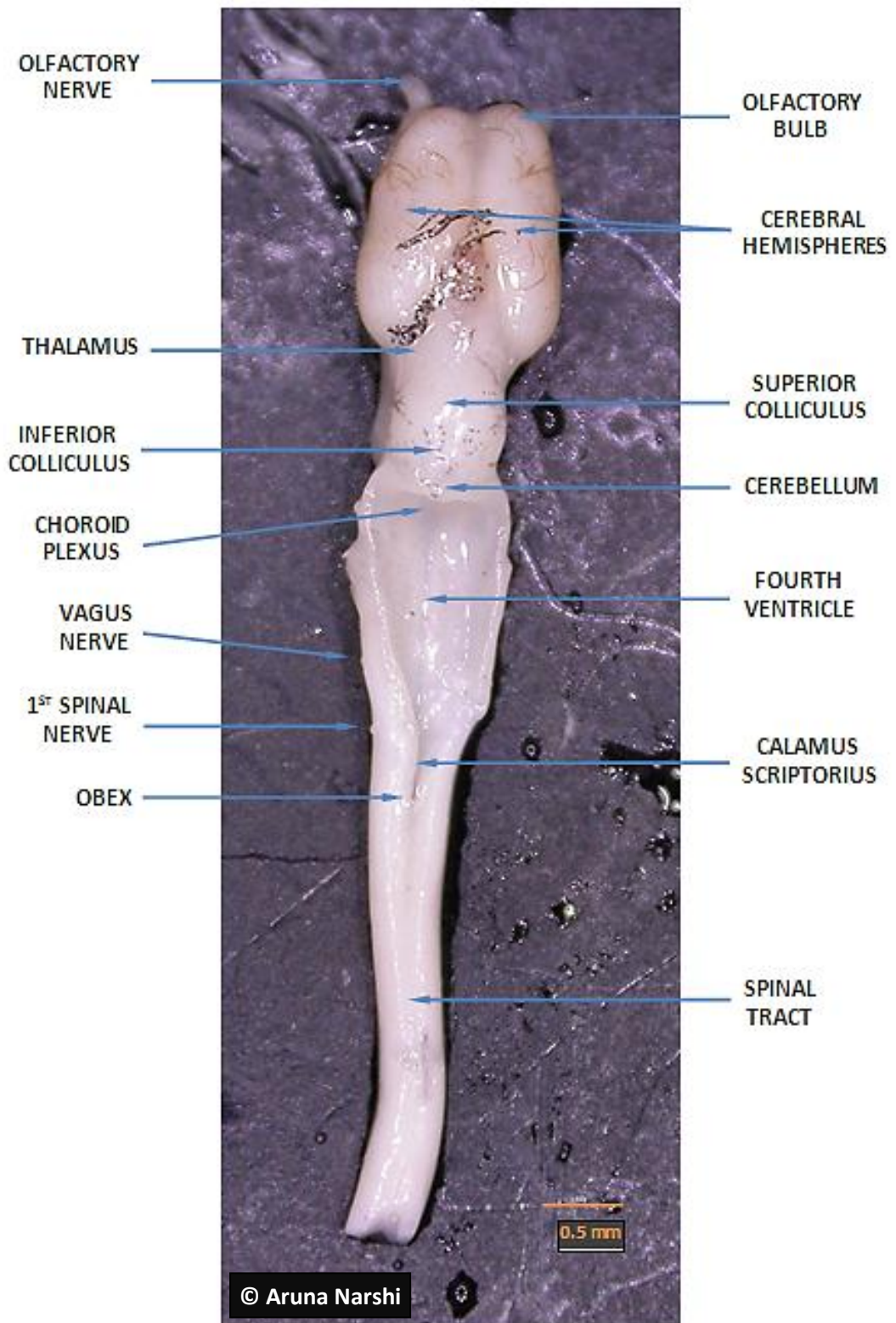
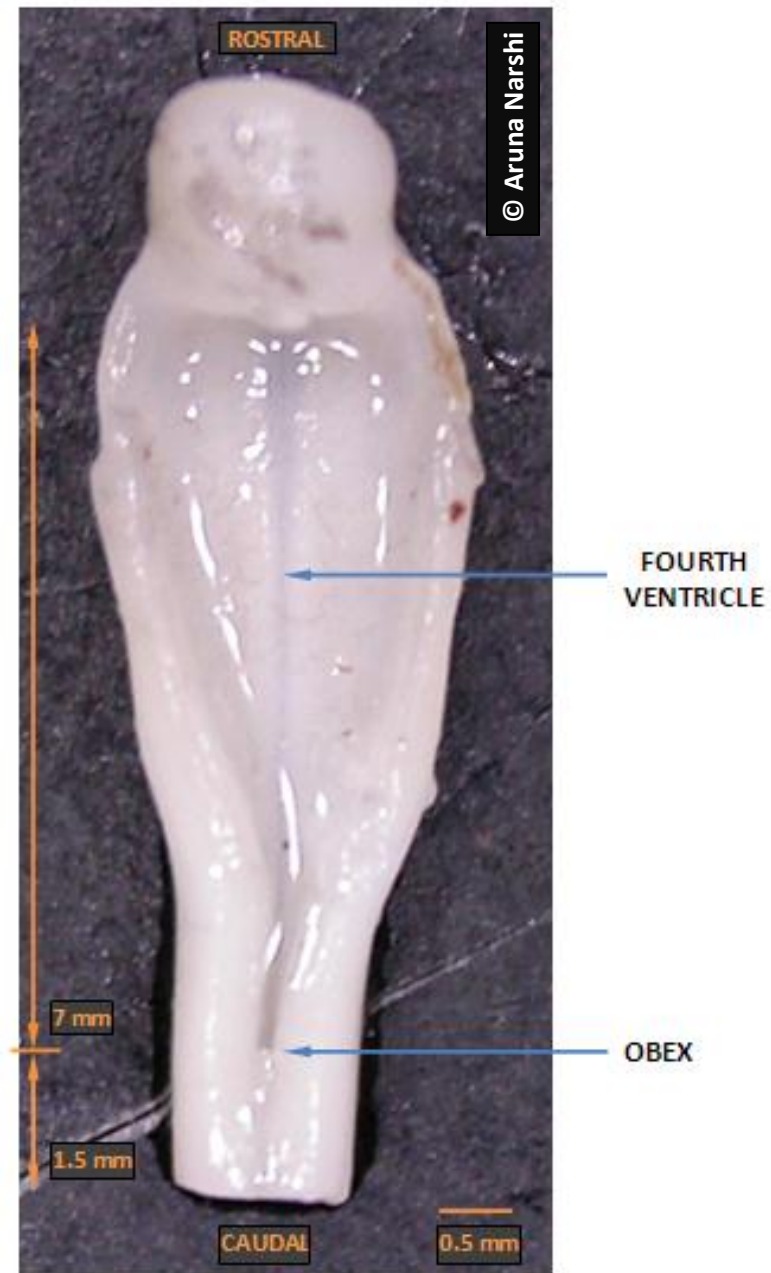


Figure 7-0.1 (B) Section of brain embedded for neuroanatomical studies.



### **7.3 RESULTS**

The medulla oblongata of neotenuous, metamorphosing and metamorphosed axolotls was processed, sectioned and viewed as described in the methods. When view the obex was located first and then the sections used for cell counts were 60  $\mu\text{m}$  apart (every third section as they were 20  $\mu\text{m}$  thick). Counts were made in both a rostral and caudal direction relative to the obex. VPN cell bodies that were labelled with the FG retrograde tracer were counted using and fluorescence microscope. The total number of VPN's found in the dorsal medial area (where the DVN would be) were:

Neotenuous ( <i>n=1</i> )	647
Metamorphosing ( <i>n=1</i> )	633
Metamorphosed ( <i>n=1</i> )	488

In the neotenuous axolotl the vagal preganglionic neurones (VPN) spanned an area from 1.5 mm caudal to obex, to just over 4mm rostrally. That's a span of 5.5 mm. The majority of the VPN were distributed around obex to 3 mm rostral, but the largest group was found at around 4 mm rostral from obex (Figure 7-1(A)). The metamorphosing axolotl had slightly less VPN in the medial region, but still showed a concentrated area at 4mm rostral of obex. There were more cells in 1-2 mm rostral to obex range in comparison to the neotenuous (Figure 7-1(B)). The metamorphosed axolotl had the least number of VPN in this region, but the distribution was essentially very similar to that of the metamorphosing (Figure 7-1(C)). The number of VPN in the ventrolateral area for each type of axolotl was:

Neotenuous	0
Metamorphosing	97
Metamorphosed	109

## II. Neuroanatomy and Physiology of Cardiorespiratory Control

In the ventrolateral zone there were no VPN in the neotenus axolotl, and around a hundred in both metamorphosing and metamorphosed. The VPN in these axolotls were generally distributed around 2.0 – 3.5 mm rostrally from obex (Figure 7-1(D) and (E)). In addition to these fluorogold stained cells the mid-metamorphic axolotl had 40 VPN in an area that was intermediate between the medial and lateral regions of the hind brain (Figure 7-1(F)).

Total number of VPN in the medulla were:

### Medial:-

#### *Rostral of Obex*

Neotenus: 583	Metamorphosing: 563	Metamorphosed: 415
---------------	---------------------	--------------------

#### *Caudal of Obex*

Neotenus: 64	Metamorphosing: 54	Metamorphosed: 74
--------------	--------------------	-------------------

### Total medial

<b>Neotenus: 647</b>	<b>Metamorphosing: 617</b>	<b>Metamorphosed: 489</b>
----------------------	----------------------------	---------------------------

### Lateral:-

#### *Rostral of Obex*

Neotenus: 0	Metamorphosing: 83	Metamorphosed: 89
-------------	--------------------	-------------------

#### *Caudal of Obex*

Neotenus: 0	Metamorphosing: 14	Metamorphosed: 20
-------------	--------------------	-------------------

### Total lateral

<b>Neotenus: 0</b>	<b>Metamorphosing: 97</b>	<b>Metamorphosed: 109</b>
--------------------	---------------------------	---------------------------

## ***II. Neuroanatomy and Physiology of Cardiorespiratory Control***

The topographical organisation of the VPN in the hind brains of neotenuous, metamorphosing and metamorphosed axolotl was graphed in Figure 7-2.

Digital microscopic images of the VPN in the specific regions graphed in Figure 7-2 were taken. Figures 7-3.0 to 7-3.6 show some of the fluorescing cells in the neotenuous axolotl. Discrete fluorescing groups were observed in the dorsal medial region. There were mainly undifferentiated neurones in the central grey area that appeared as spherical bodies. More mature cells, as recognised by having dendrites, were closer to the periventricular area, (the area adjacent to the white matter) than the fourth ventricle (see Figure 7-3.1 for example). The VPN images of the metamorphosing axolotl are shown in Figures 7-4.0 to 7-4.7. The hind brain sections appear to show a lateral group forming and some migrating cells (Figures 7-4.1, 7-4.2 and 7-4.4). Some were found in an area between the medial and lateral groups (Figures 7-4.4, 7-4.5 and 7-4.7). Figures 7-5.0 to 7-5.8 show the VPN of the metamorphosed hind brain. The cell bodies in this axolotl were relatively large in comparison to the neotenuous sections (for example, Figure 7-5.2). VPN had migrated into the white matter creating at a new ventrolateral location in the metamorphosed axolotls (Figures 7-5.3 – 7-5.5, and 7-5.8).

## **7.4 DISCUSSION**

The preganglionic vagal neurones (VPN) in the neotenus medulla oblongata were round, quite small at 15 – 20  $\mu\text{m}$  diameter and apparently undifferentiated (Figures 7-3.0 – 7-3.6). As fluorogold causes the cell bodies of VPN and particularly their nuclei (Festy & Daune, 1973; Festy *et al.*, 1975) to fluoresce brightly, but does not label other features of the neurons, such as *distant* axons and dendrites (Schmued *et al.*, 1989), this may reflect limitations on the labelling of cell structures by the neural tracer. However, it could also indicate that the neurons are relatively undifferentiated in the neotenus brain. This is not that surprising as they are neotenic, hence, large, although sexually mature, tadpoles.

The metamorphosed brain had more differentiated cells (Figures 7-5.0 – 7-5.8) and, as can be seen, they tended to be much larger, at around 40  $\mu\text{m}$  diameter, than those in the neotenus. The VPN in the metamorphosed medulla also appeared to be differentiated, having definable proximal dendrites and axons and the classic stellate shape (Figures 7-5.5 and 7-5.8, for example).

The neotenus axolotls had distinct clusters of VPN as seen in the digital micrographs. The metamorphosing and metamorphosed sections showed VPN clustered in the dorsal vagal motonucleus (DVN) region, in a ventrolateral position and some in the area between the two. Intriguingly, the metamorphosed and the metamorphosing axolotls had some migrating cells which were described as such owing to their torpedo-like morphology (Figure 7-5.1). These migrating cells were orientated in a ventro-lateral position, suggesting that they were relocating to that position. The cells in the intermediate location



## ***II. Neuroanatomy and Physiology of Cardiorespiratory Control***

may suggest migration. Although in the mammalian brain stem there are VPN in the reticular formation, between the DVN and nA (Ranson *et al.*, 1993). However, if they were transitioning from the grey matter area (near the fourth ventricle or the periventricular area) then their presence in the intermediate zone would be logical. Indeed, others have found evidence of VPN migrating from DVN to a ventrolateral position during brain development in humans (Brown, 1990) and cats (Windle (1933) in Bennett *et al.*, 1981). Curiously the metamorphosing axolotl in Figure 7-4.3 had cells that appeared to be dividing. Fluorogold is known to stain intracellular lysosome in intact cells (Wessendorf, 1991; Persson & Havton, 2009) and also bind to DNA (Festy & Daune, 1973; Festy *et al.*, 1975). The staining in the micrograph is strongest at opposite poles of the enlarged VPN, suggesting imminent cytokinesis. However, the use of a mitotic marker would be required to definitively know if the neuronal blast cells seen in the central grey just migrate to the periventricular (and eventually the white matter) or if they migrate and then also divide.

The number of cells in the medial region of neotenus, metamorphosing and metamorphosed axolotl hind brains gradually decreased in number, whereas those in the lateral region progressively increased in number. This, along with the digital images, strongly suggests cells are migrating from a dorsal-medial region to a ventrolateral area. The total number of cells found in the metamorphosed axolotl was 597, of which 109 were located in the ventrolateral area (the rest in the DVN). Consequently, 18% of all VPN were in the new ventrolateral position. This figure is slightly higher than one already published of 14% for axolotls (Ihmied, 1989). However, this author used the horseradish peroxidase (HRP), a retrograde intra-axonal neural tracer, which requires manual nerve damage for the tracer to be taken up. Damaged axons could theoretically take less HRP up as they could

## ***II. Neuroanatomy and Physiology of Cardiorespiratory Control***

be crushed too much, or the HRP may not be taken up due to insufficient number of damaged axons. Hence, this would potentially result in some variability. There would be more reliability with using the fluorescent retrograde tracer Fluorogold as it labels all VPN without the need for any damage to the nerves nor invasive surgery on the animal. Thus fluorogold labelling, *via* injection after which the animals can be left to behave normally for at least a week, is a much better option for tracing VPN.

In the periventricular area of both the metamorphosing and the metamorphosed axolotl there was clear evidence of differentiating cells that were totally absent in the neotenus. Therefore, during the transition from gill to lung breathing, the brain does appear to undergo changes in the DVN and surrounding regions. It is known that the DVN and surrounding area, in particular the ventrolateral area, is involved in cardiorespiratory control and that in mammals the ventrolateral VPN cluster, designated the nucleus ambiguus (nA), contains predominantly cardiac VPN (Bennett *et al.*, 1981; Taylor *et al.*, 1999). Hence the relocation of the DVN cells to a more ventrolateral area could suggest that the metamorphosed axolotls possess a primitive nA. The nA in humans generates rhythmic sinus arrhythmia, that is an increase in heart rate upon inspiration (Hyndman *et al.*, 1971). This is caused by a temporary reduction in vagal tone which slows the heart (McDonald (1980) in Taylor, 1994; Taylor *et al.*, 1999). It would be most interesting to find out if the metamorphosed axolotl displays heart rate variability too which could suggest that the migration of VPN to a ventrolateral position has a functional role in a committed lung breather. Therefore, the ventrolateral VPN cluster may be involved in cardiorespiratory control. This was investigated in Chapter 8.

Figure 7-1. The distribution of cell bodies of vagal preganglionic neurones in the hind brain of the axolotl. Neurones were stained with Fluorogold.

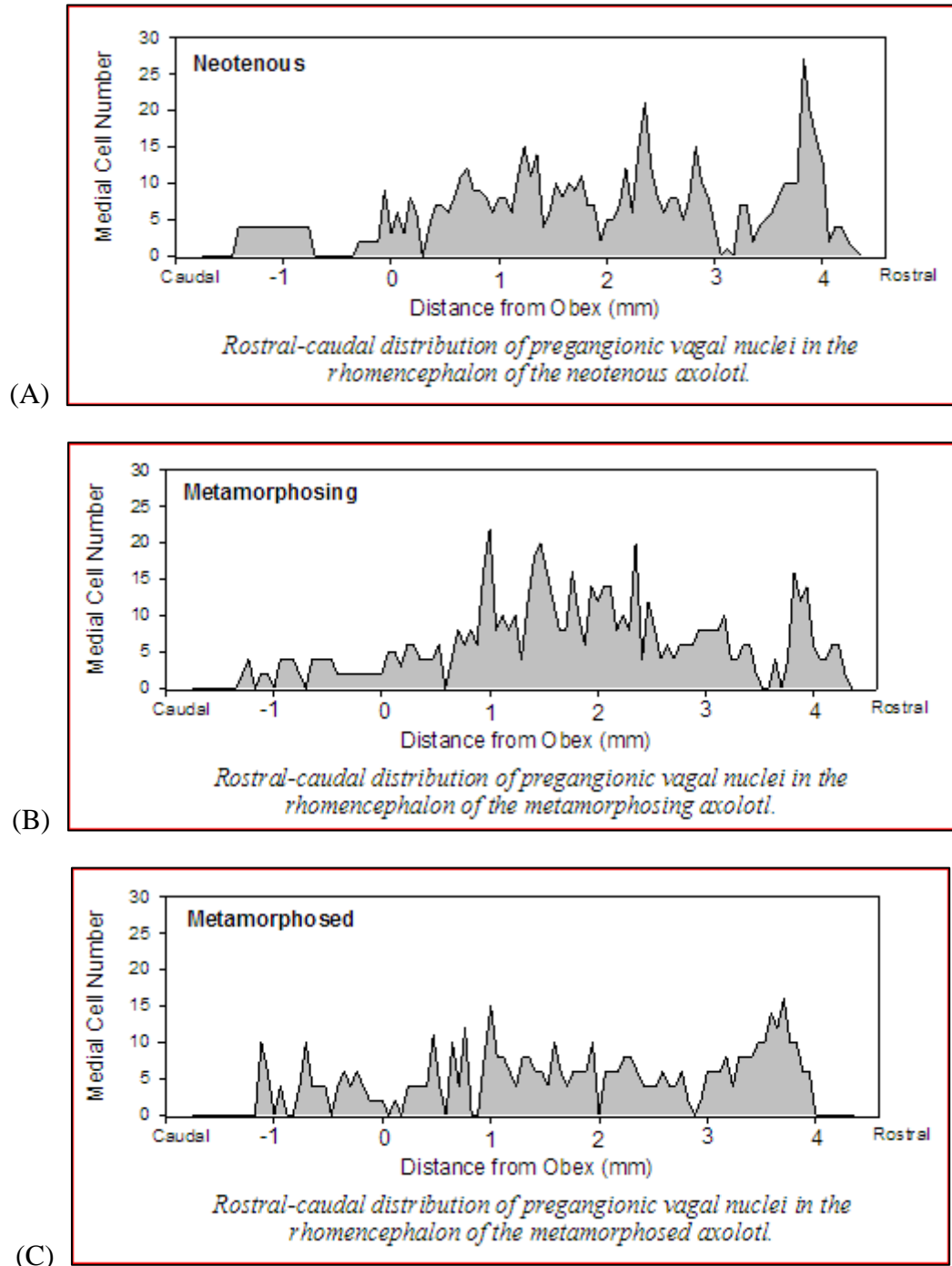
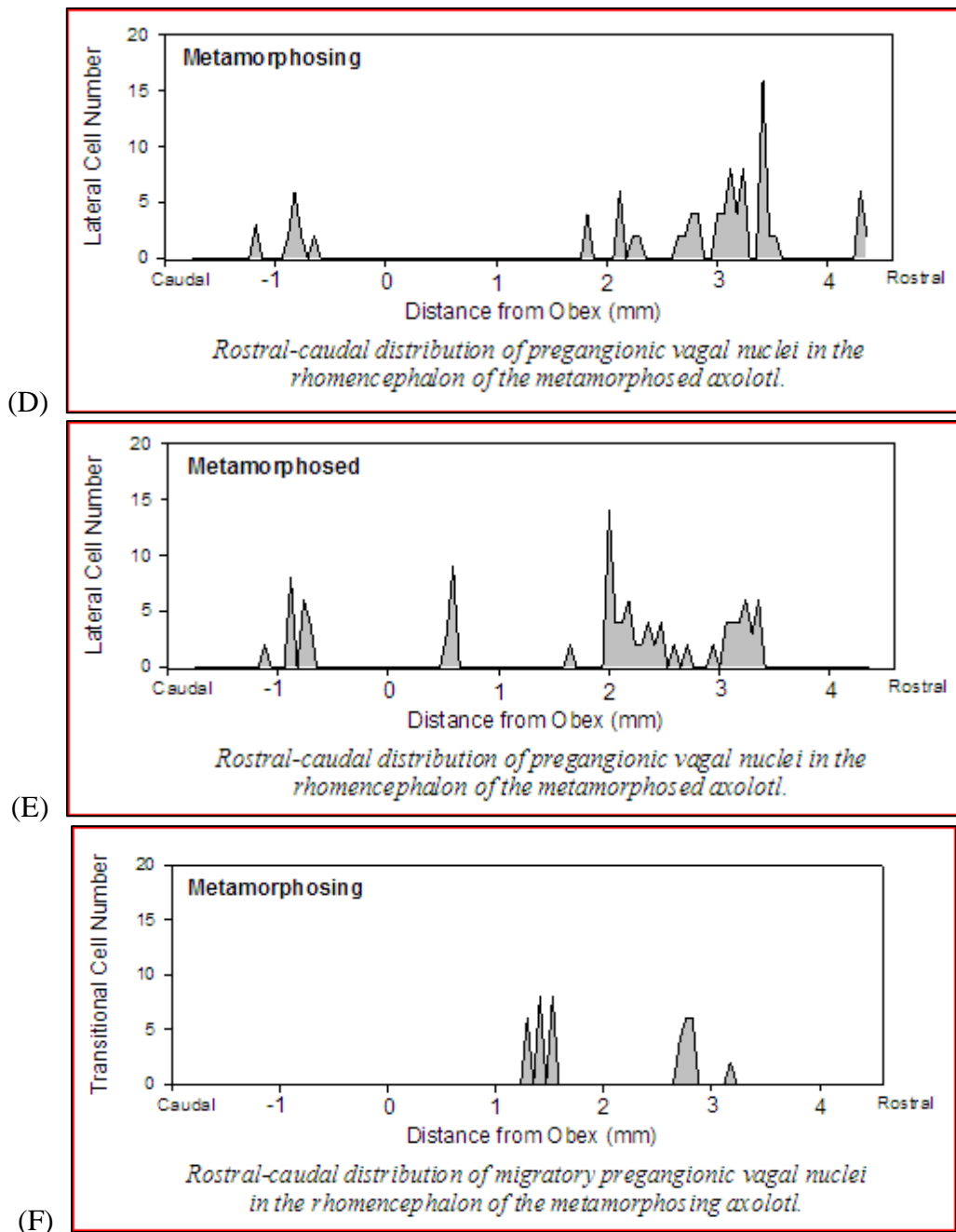
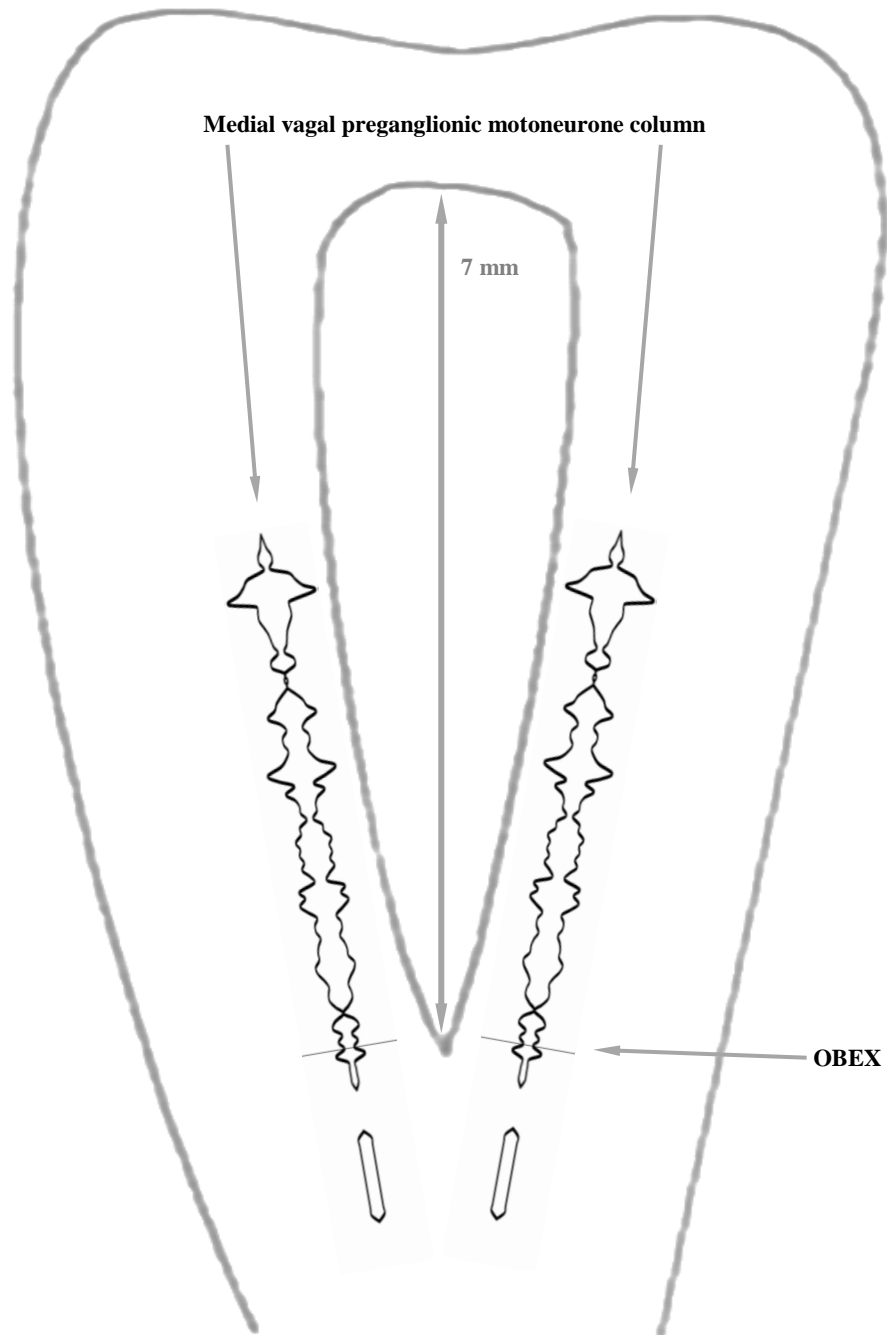


Figure 7-1. The distribution of cell bodies of vagal preganglionic neurones in the hind brain of the axolotl (continued). Neurones were stained with Fluorogold.



**Figure 7-2. (A) Diagram of the neotenus axolotl medulla oblongata.** The topographical reconstruction of the whole vagus motor column as indicated by Fluorogold labelled cell body counts. Positions were determined by relative distance from the obex.



**Figure 7-2. (B) Diagram of the metamorphosing axolotl medulla oblongata.** The topographical reconstruction of the whole vagus motor column as indicated by Fluorogold labelled cell body counts. Positions were determined by relative distance from the obex.

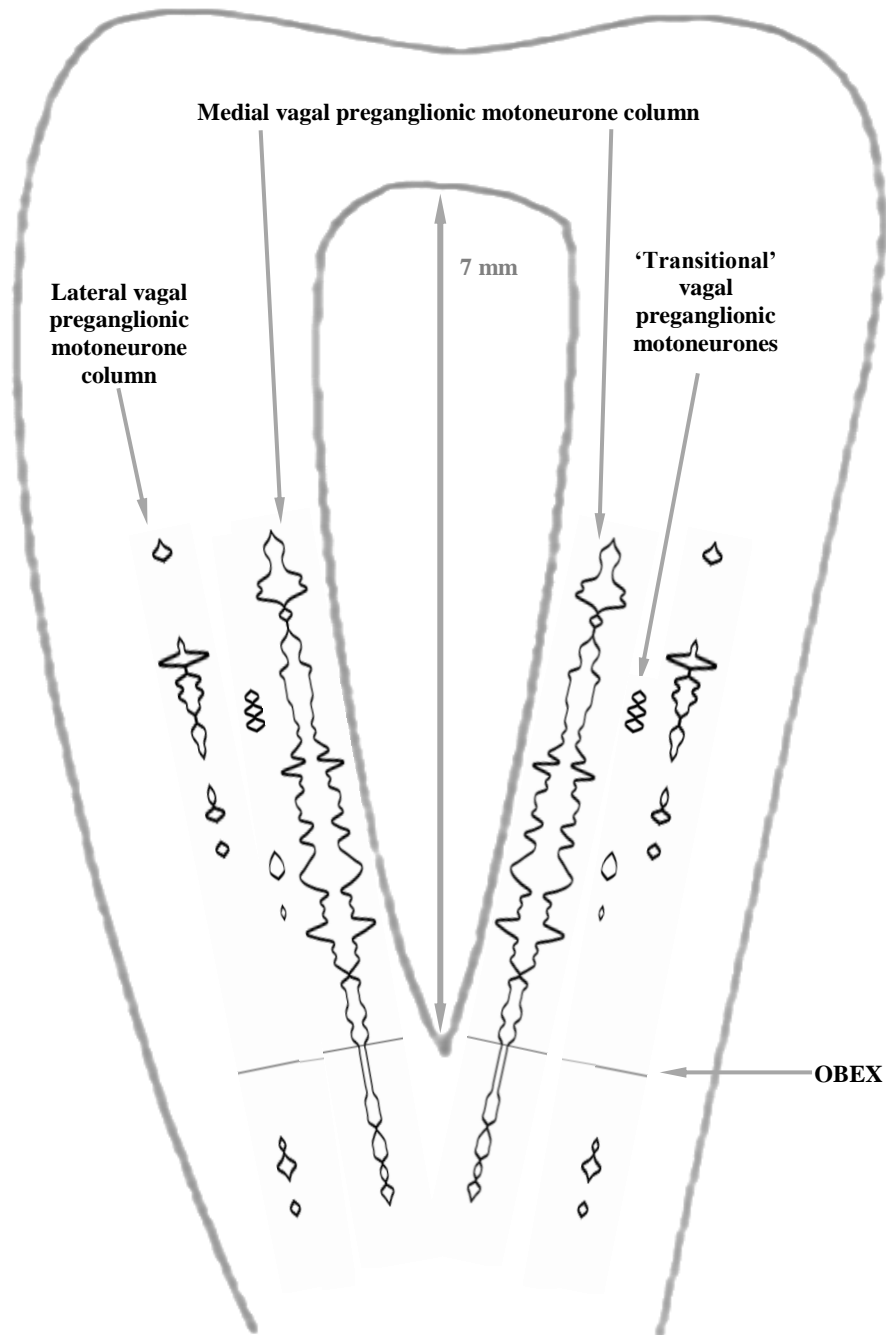


**Figure 7-2. (C) Diagram of the metamorphosed axolotl medulla oblongata.** The topographical reconstruction of the whole vagus motor column as indicated by Fluorogold labelled cell body counts. Positions were determined by relative distance from the obex.

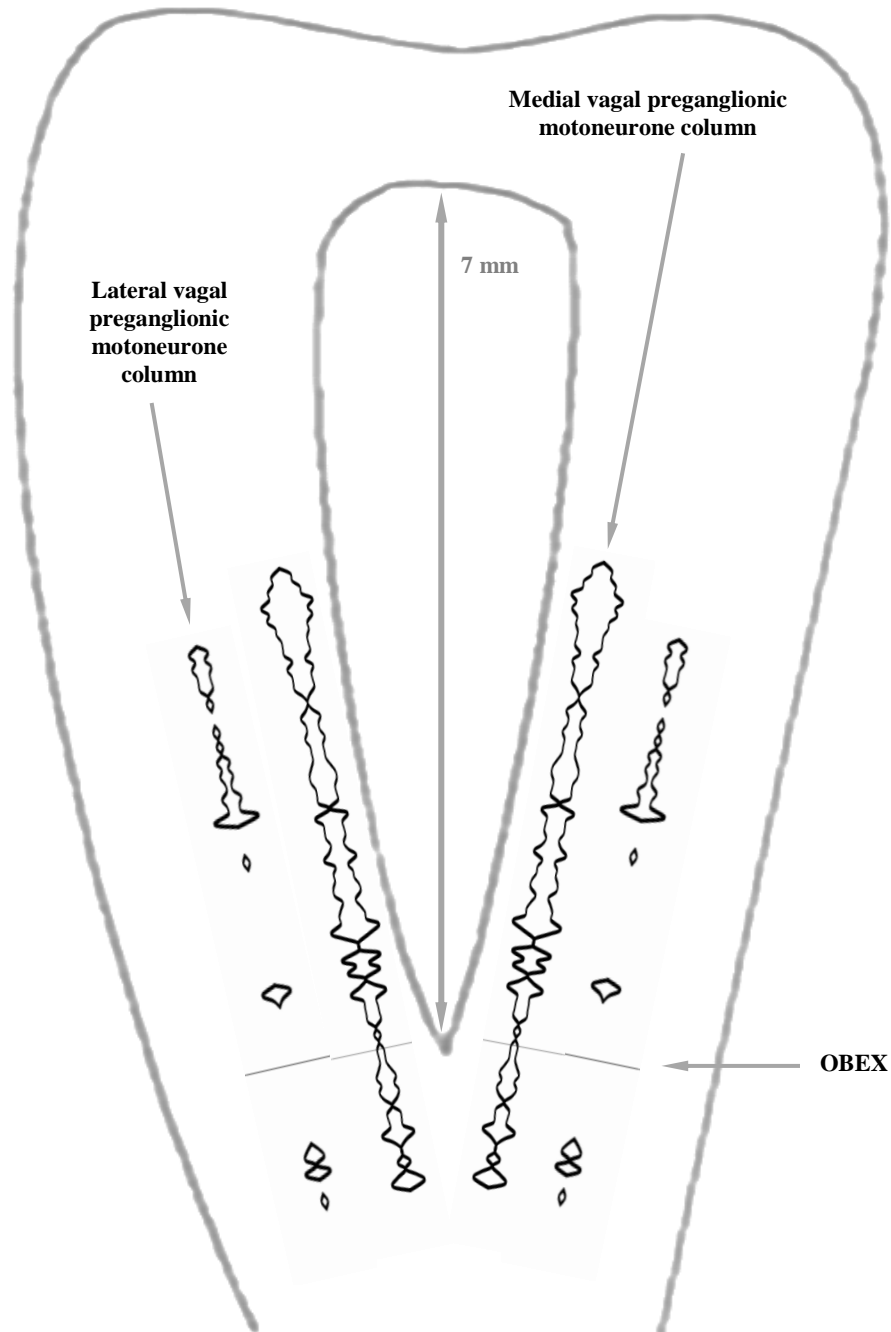


**Figure 7-3.0 Neotenus axolotl medulla oblongata.** Blue arrows correspond to the location of the Fluorogold images on the following pages.

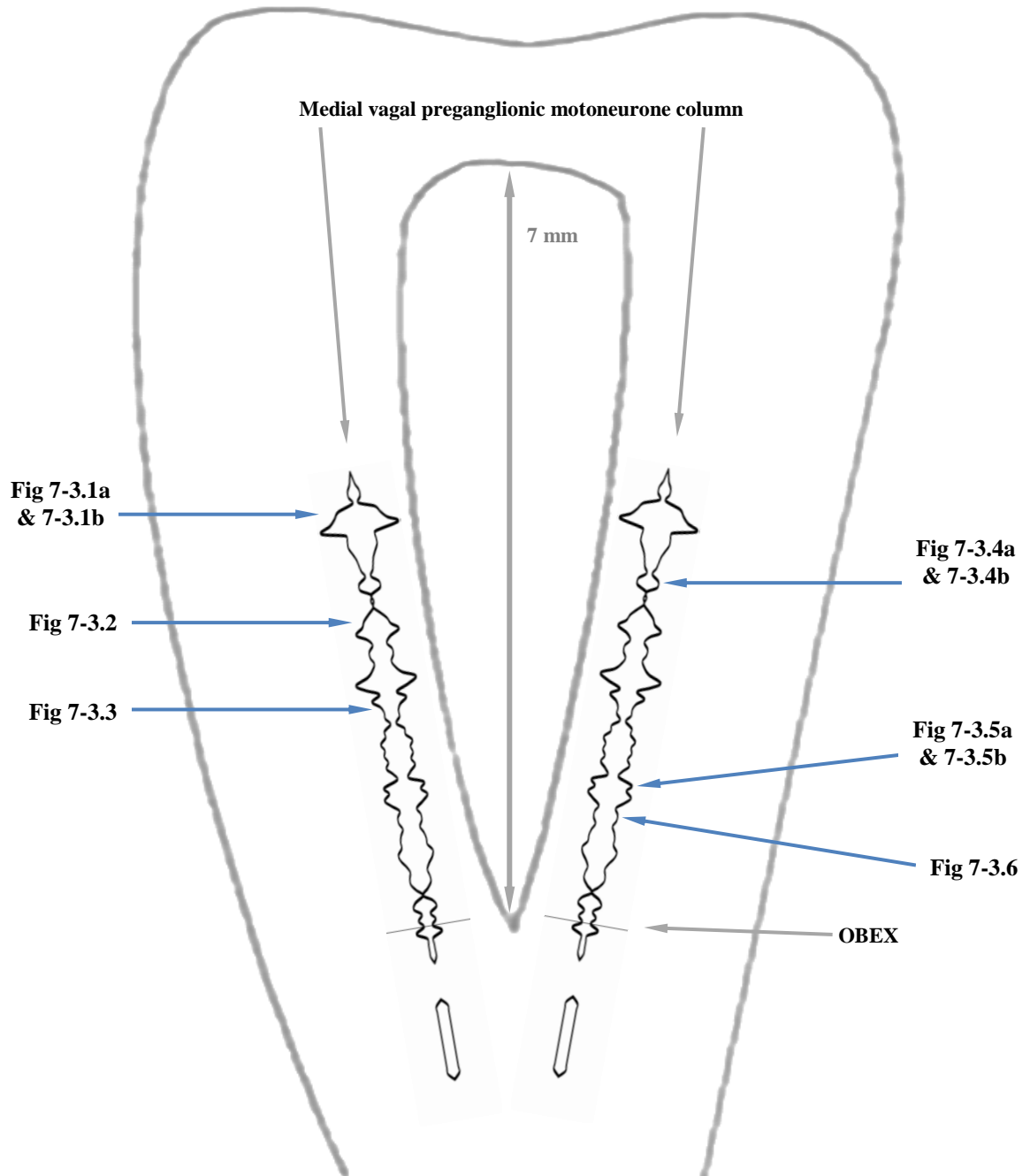
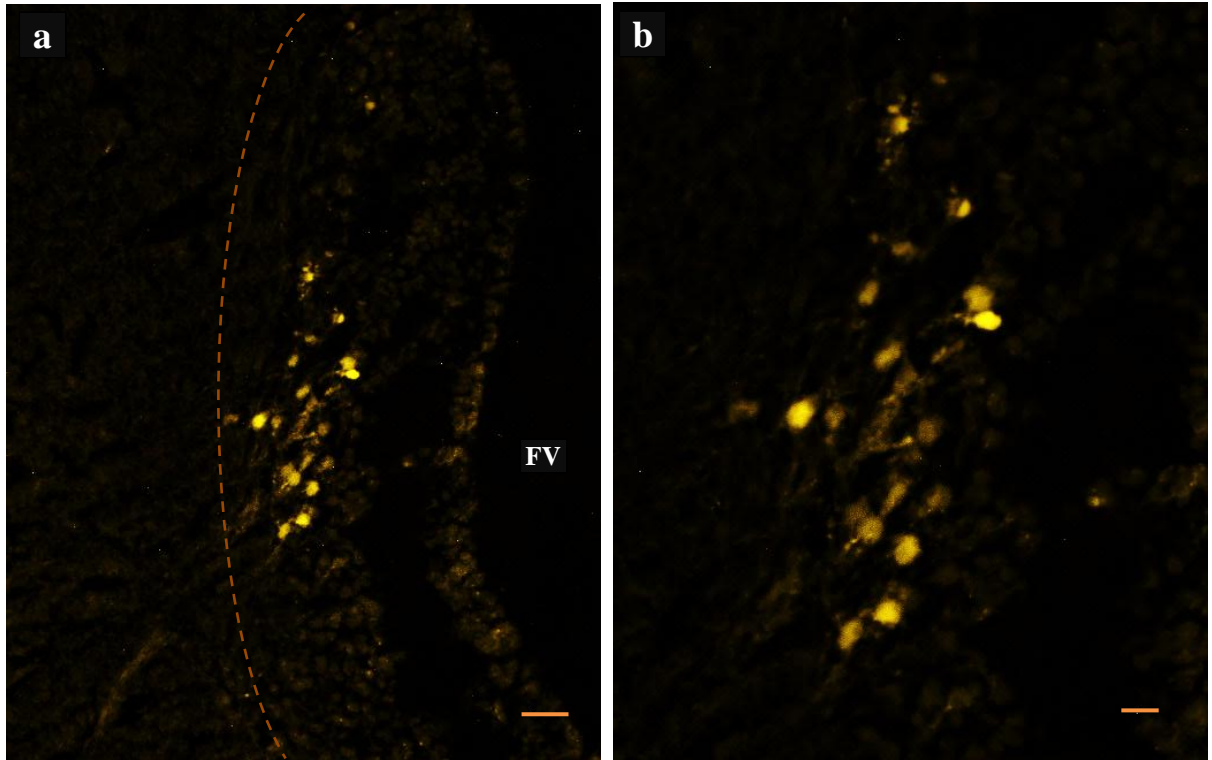




**Figure 7-3.1** Micrographs of transverse 20  $\mu\text{m}$  sections of neotenus axolotl medulla oblongata showing a medial group of vagal preganglionic neurons labelled with fluorescent tracer Fluorogold.



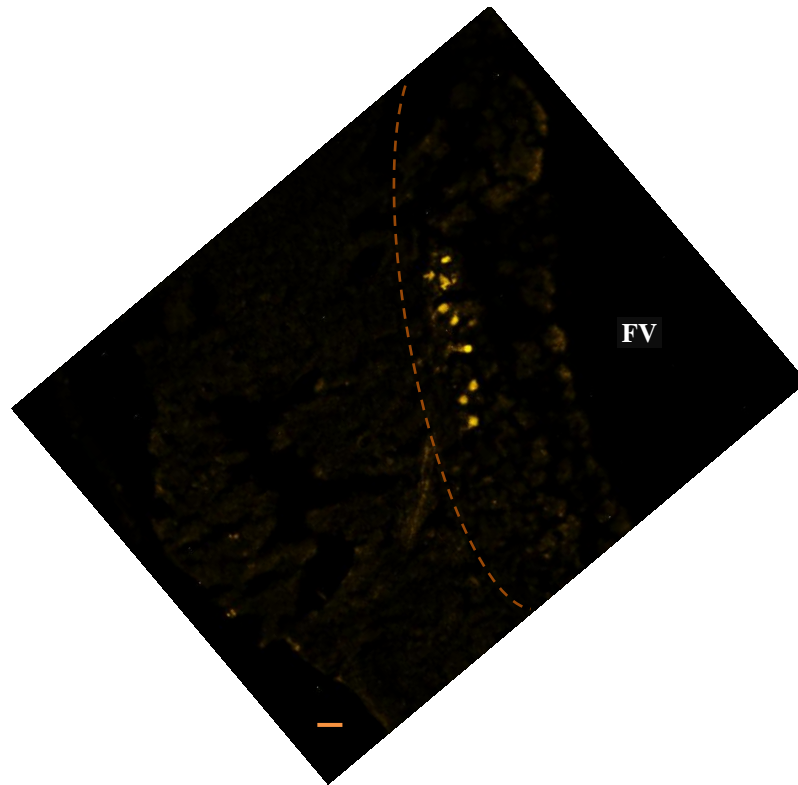
**(a)** – Grey matter to right of orange line; white matter to the left.

Bar = 30  $\mu\text{m}$ . FV = fourth ventricle.

**(b)** – Image (a) at a higher magnification.

Bar = 20  $\mu\text{m}$

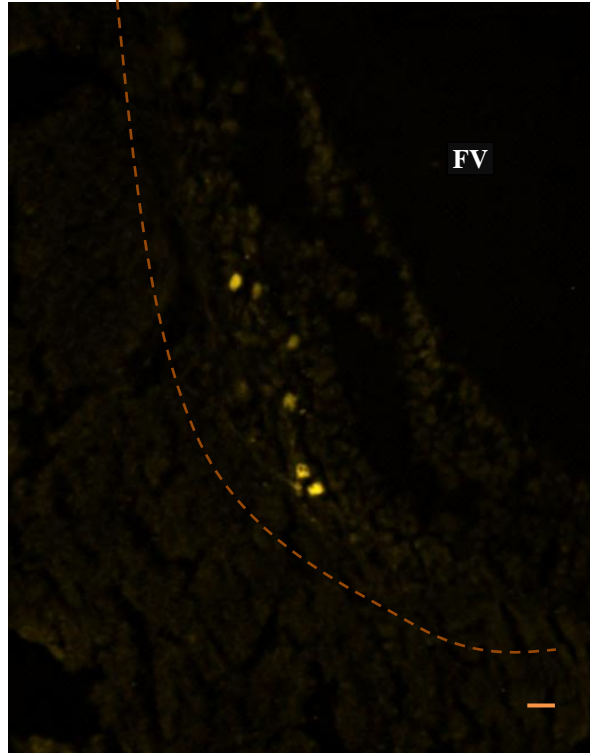
**Figure 7-3.2** Photomicrograph of transverse 20  $\mu\text{m}$  sections of neotenus axolotl medulla oblongata showing a medial group of preganglionic motoneurons labelled with Fluorogold.



Grey matter to right of orange line; white matter to the left.

Bar = 30  $\mu\text{m}$ . FV = fourth ventricle.

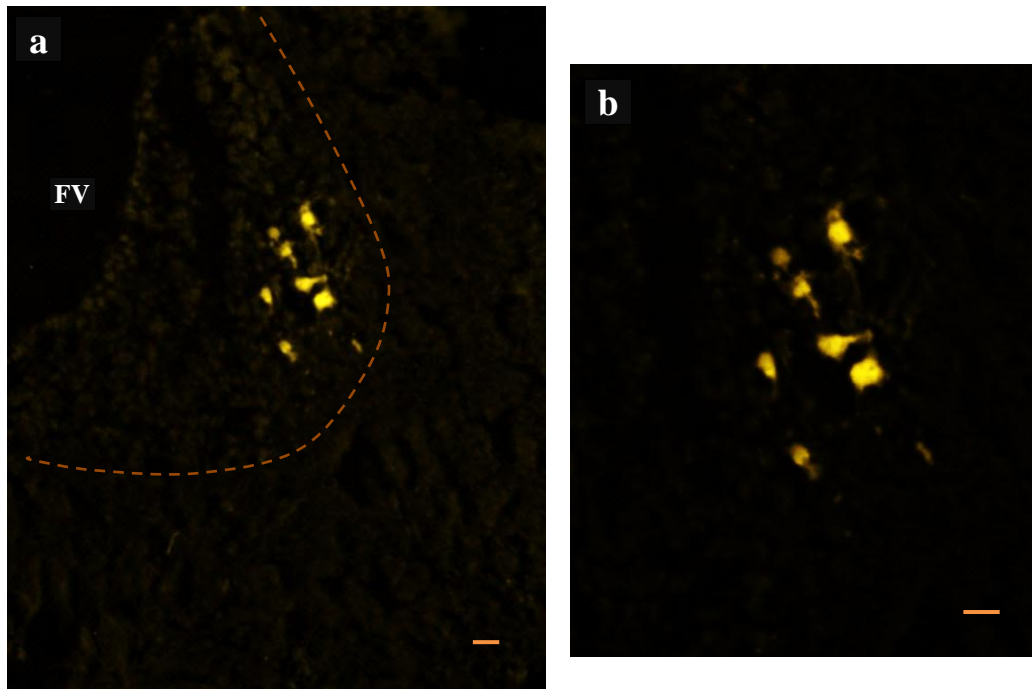
**Figure 7-3.3** Micrograph of transverse 20  $\mu\text{m}$  sections of neonous axolotl hind brain showing a medial group of preganglionic neurons with fluorescent tracer Fluorogold.



Grey matter to right of orange line; white matter to the left.

Bar = 30  $\mu\text{m}$ . FV = fourth ventricle.

**Figure 7-3.4** Micrographs of transverse 20  $\mu\text{m}$  sections of neonous axolotl medulla showing a medial group of vagal preganglionic neurons with fluorescent tracer Fluorogold.



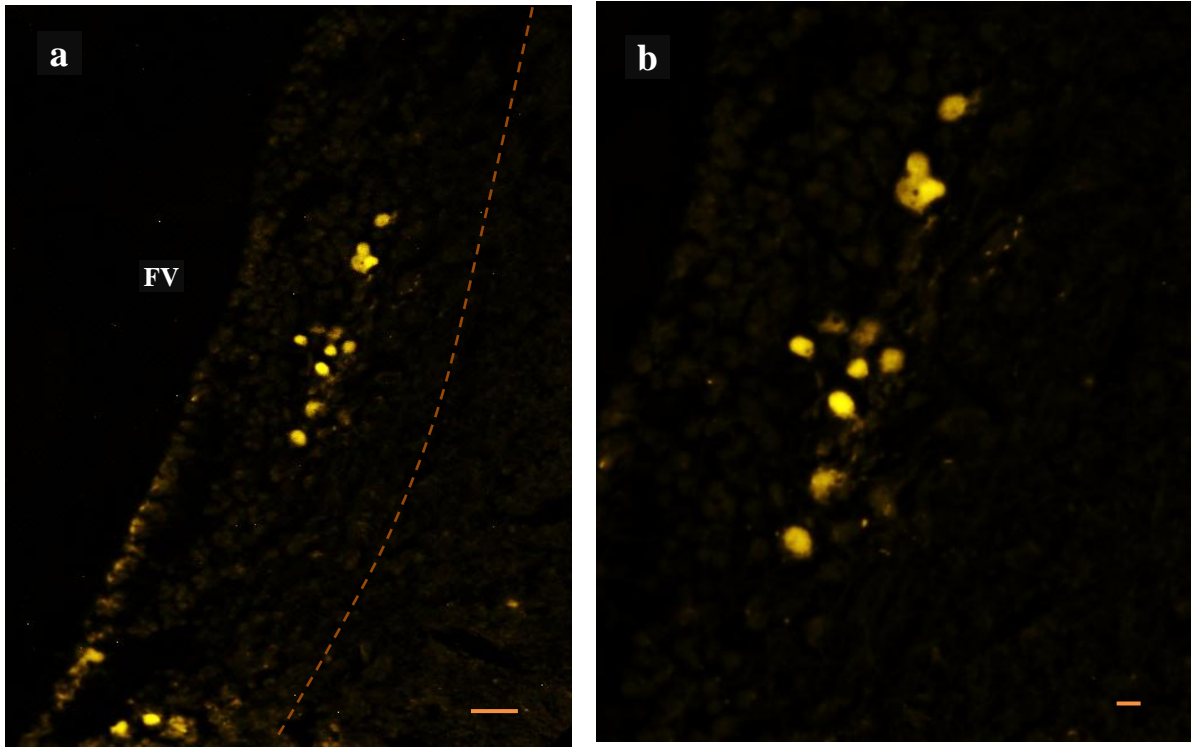
**(a)** – Grey matter to left of orange line; white matter to the right.

Bar = 20  $\mu\text{m}$ . FV = fourth ventricle.

**(b)** – Image (a) at a higher magnification.

Bar = 20  $\mu\text{m}$

**Figure 7-3.5** Micrographs of transverse 20  $\mu\text{m}$  sections of unmetamorphosed axolotl medulla showing vagal preganglionic motoneurons labelled with retrograde fluorescent tracer Fluorogold.



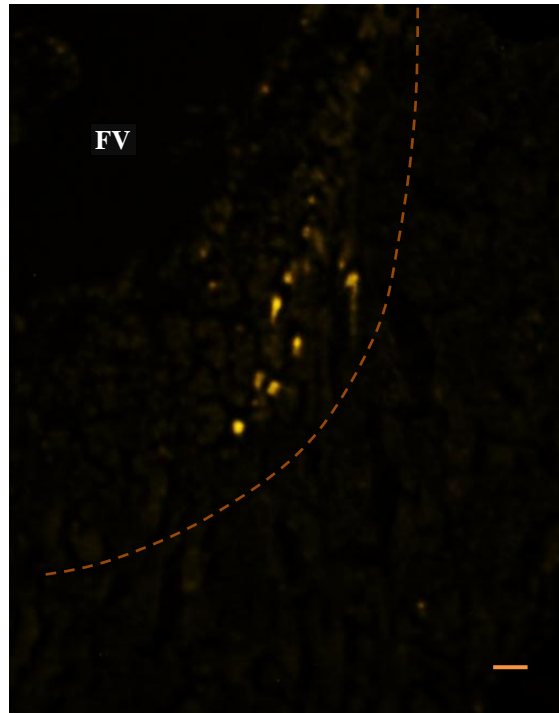
**(a)** – Grey matter to left of orange line; white matter to the right.

Bar = 30  $\mu\text{m}$ . FV = fourth ventricle.

**(b)** – Image (a) at a higher magnification.

Bar = 10  $\mu\text{m}$

**Figure 7-3.6** Micrograph of transverse 20  $\mu\text{m}$  sections of neotenus axolotl medulla oblongata showing a medial group of preganglionic neurons labelled with fluorescent tracer Fluorogold.



Grey matter to right of orange line; white matter to the left.

Bar = 30  $\mu\text{m}$ . FV = fourth ventricle.

**Figure 7-4.0** Mid-metamorphosed axolotl medulla oblongata. Blue arrows correspond to the location of the Fluorogold images on the following pages.

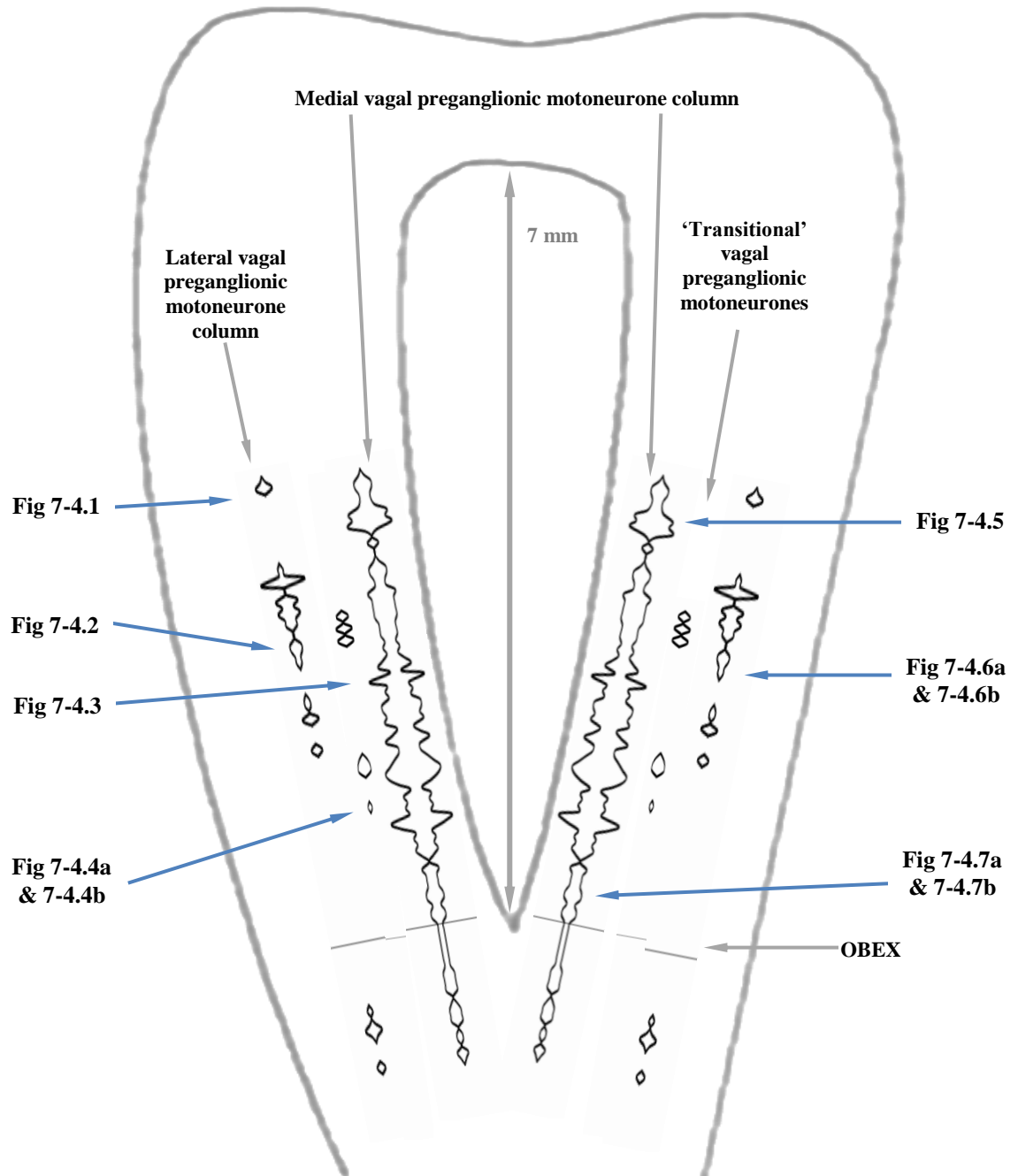
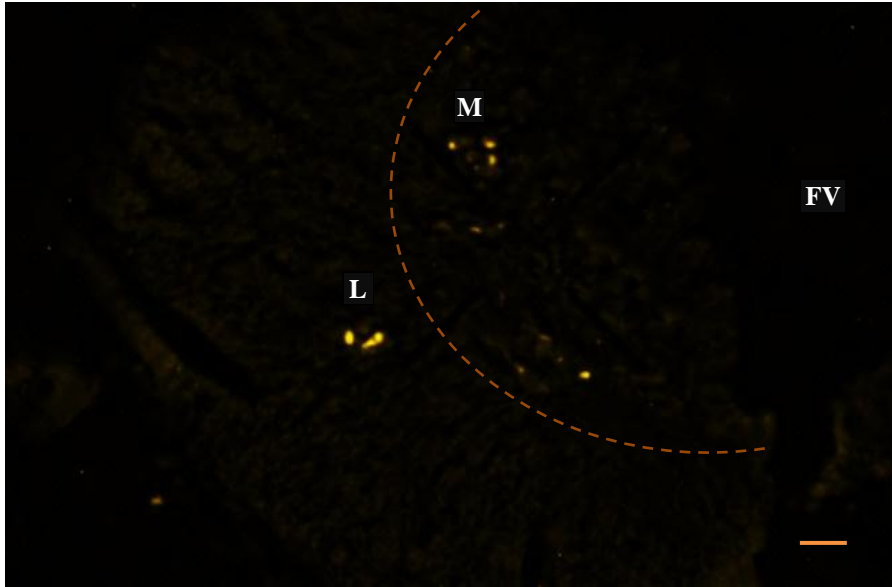


**Figure 7-4.1** Photomicrograph of transverse 20  $\mu\text{m}$  sections of mid-metamorphosed axolotl medulla oblongata showing vagal preganglionic motoneurons labelled with fluorescent tracer Fluorogold.

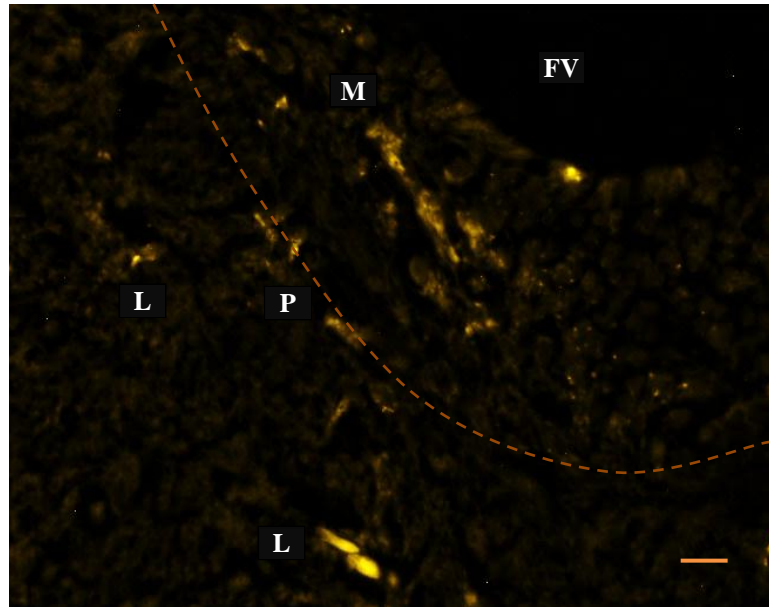


Section shows the shape of cell bodies that appear to be migrating to a ventrolateral location (L). The migrating cells are larger than those in the medial area. Grey matter is to the right of the orange line and white matter towards the left.

Bar = 60  $\mu\text{m}$ . L = lateral group. M = medial group. FV = fourth ventricle.



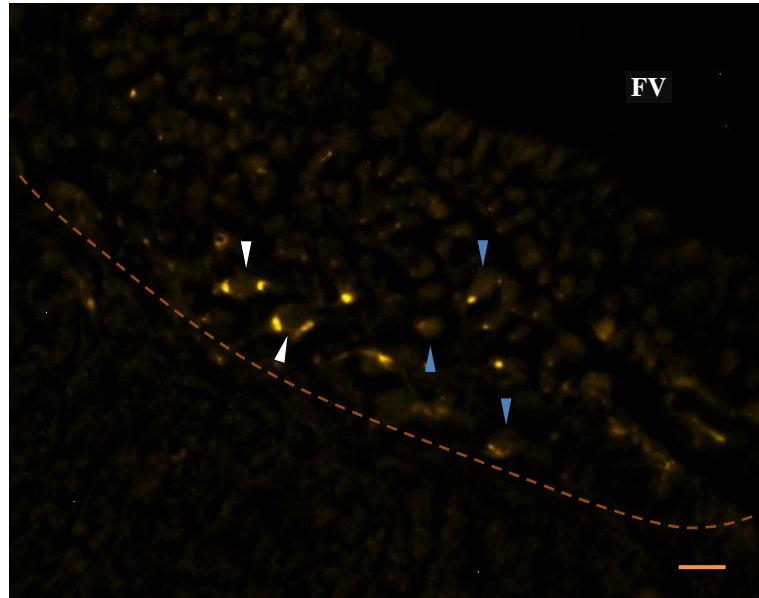
**Figure 7-4.2** Micrograph of transverse 20  $\mu\text{m}$  sections of mid-metamorphosed axolotl medulla showing preganglionic motoneurons labelled with retrograde fluorescent tracer Fluorogold.



Section shows the shape of cell bodies that appear to be migrating to a ventrolateral location (L). The migrating cells and some in the medial area are larger than those found in the neotenuous axolotl. Grey matter to the top of the orange line; white matter towards the bottom.

Bar = 40  $\mu\text{m}$ . L = lateral group. P = periventricular group. M= medial group. FV = fourth ventricle.

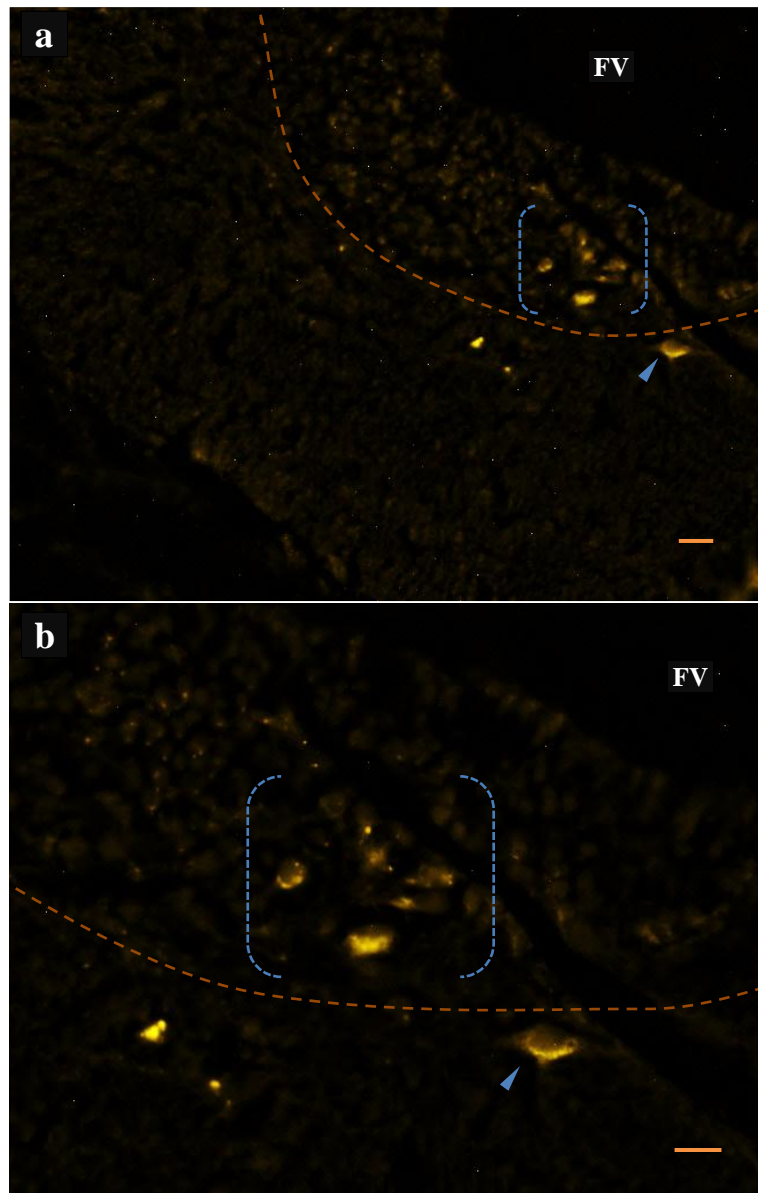
**Figure 7-4.3** Micrograph of transverse 20  $\mu\text{m}$  sections of mid-metamorphosed axolotl medulla oblongata showing vagal preganglionic motoneurons labelled with fluorescent tracer Fluorogold.



A medial group of neurones showing some cells that are larger than those found in the grey matter of the neotenuous axolotl (blue arrowheads). Some cells may be dividing as suggested by Fluorogold DNA staining which shows intensity at polar ends of the enlarged cells (white arrowheads). Grey matter to the top of the orange line; white matter towards the bottom.

Bar = 30  $\mu\text{m}$ . FV = fourth ventricle.

**Figure 7-4.4** Micrograph of transverse 20  $\mu\text{m}$  sections of mid-metamorphosed axolotl medulla showing preganglionic motoneurons labelled with fluorescent tracer Fluorogold.



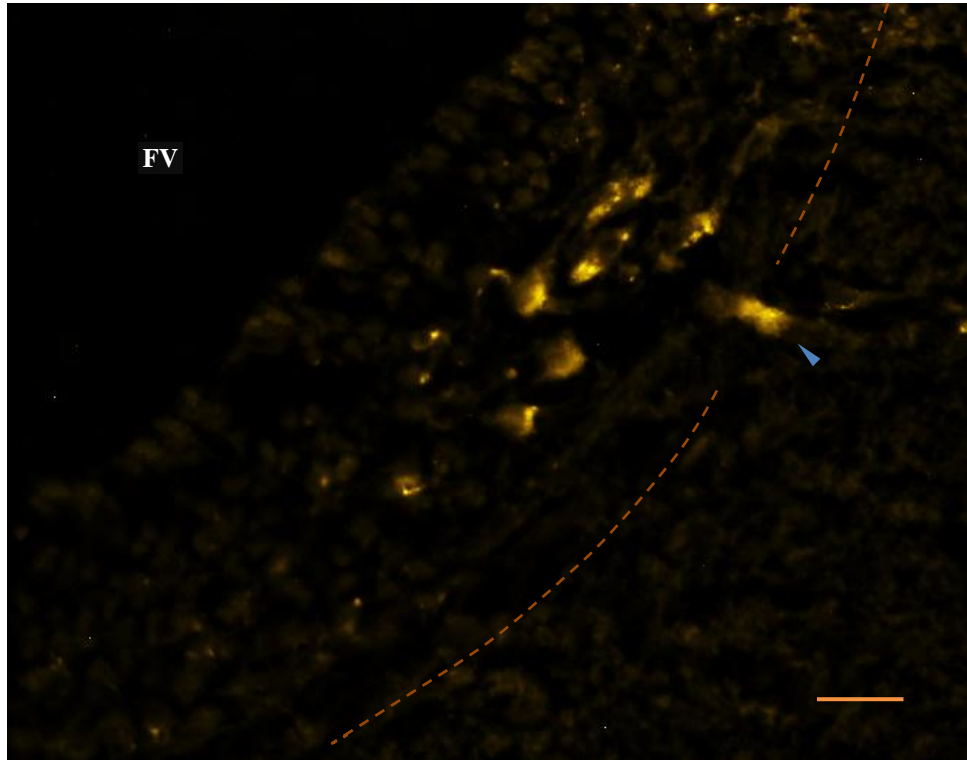
**(a)** – Large migrating neuron in the periventricular white matter area (blue arrowhead).

There is a clump of cells which are larger than the rest in the medial area (parenthesis).

Bar = 40  $\mu\text{m}$ . FV = fourth ventricle.

**(b)** – Image (a) at a higher magnification. Bar = 20  $\mu\text{m}$

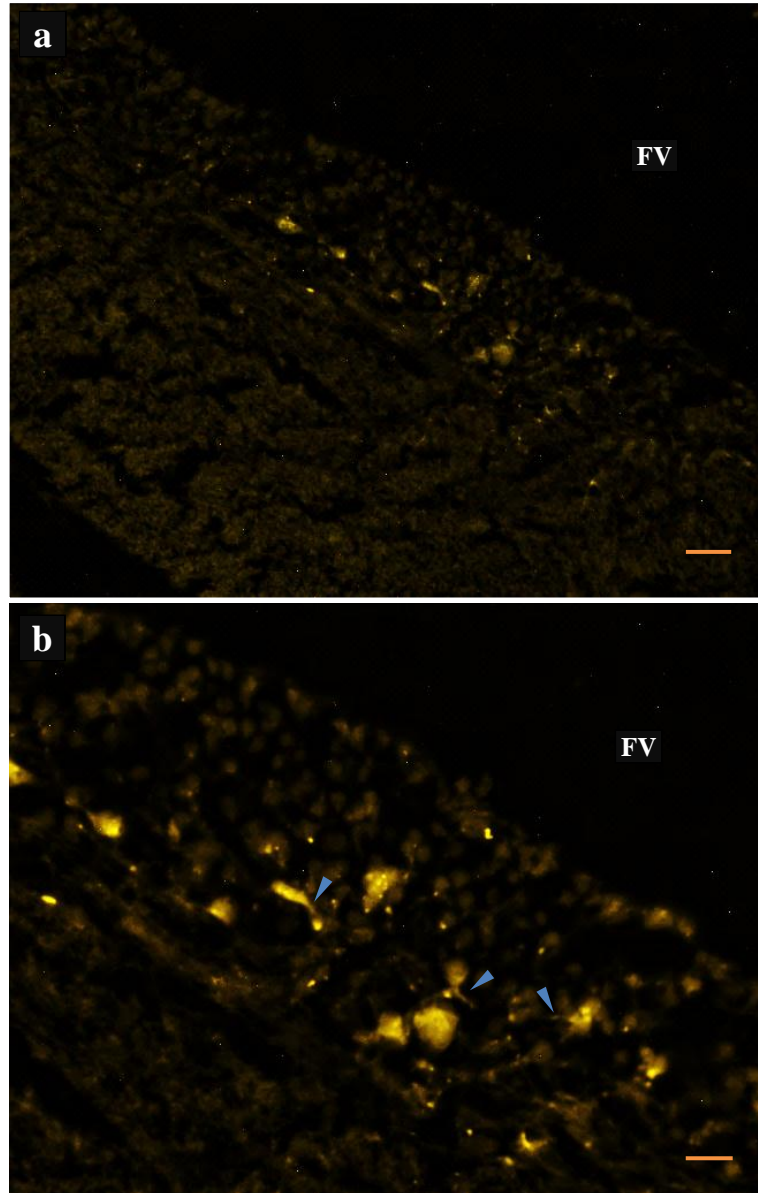
**Figure 7-4.5** Micrograph of transverse 20  $\mu\text{m}$  sections of mid-metamorphosed axolotl medulla oblongata showing vagal preganglionic motoneurons labelled with fluorescent tracer Fluorogold.



A medial group of motoneurons that are larger than those found in the neotenuous axolotl medial zone. One cell is just on the outside of the periventricular area which appears to be migrating towards the white matter (blue arrowhead). Grey matter above the orange line.

Bar = 40  $\mu\text{m}$ . FV = fourth ventricle.

**Figure 7-4.6** Micrograph of transverse 20  $\mu\text{m}$  sections of mid-metamorphosed axolotl medulla showing preganglionic motoneurons labelled with fluorescent tracer Fluorogold.

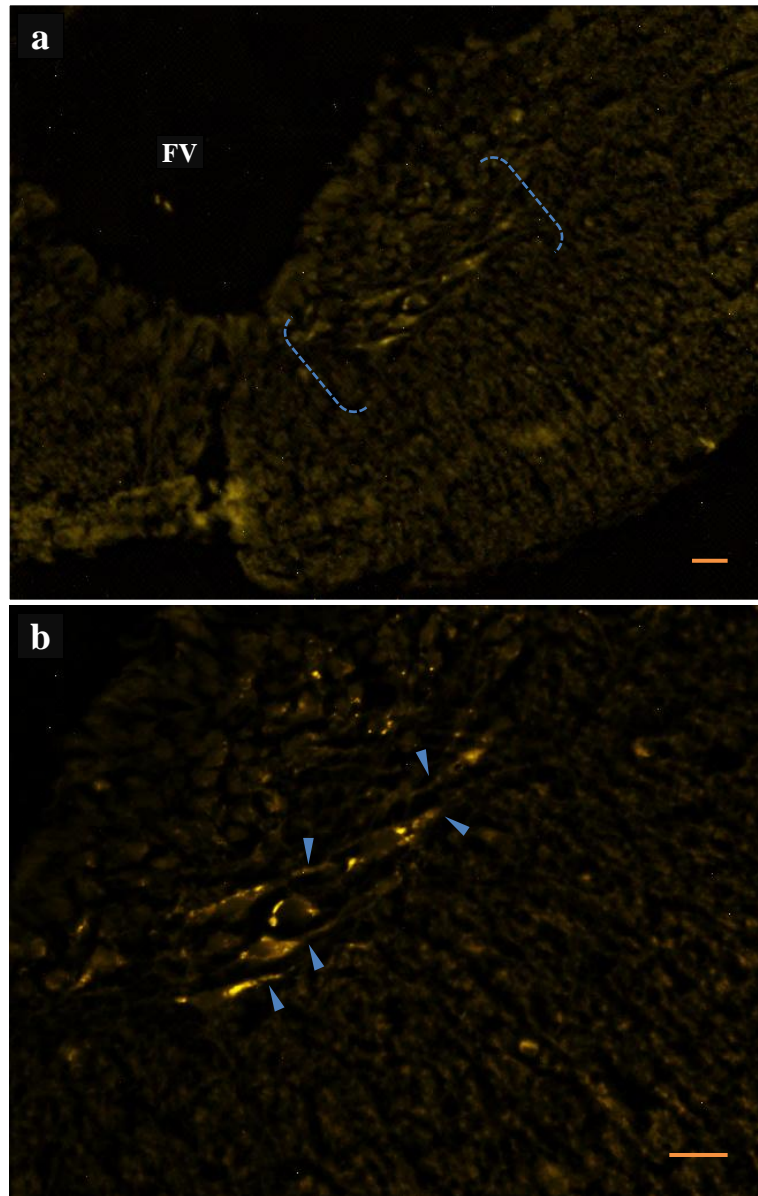


**(a)** – A medial group of vagal preganglionic motoneurons. Some are large, unlike those found in the neotenuous axolotl medulla.

Bar = 70  $\mu\text{m}$ . FV = fourth ventricle.

**(b)** – Image (a) at a higher magnification. Primary dendrites are labelled with the tracer (blue arrowheads). Bar = 35  $\mu\text{m}$

**Figure 7-4.7** Micrograph of transverse 20  $\mu\text{m}$  sections of mid-metamorphosed axolotl medulla showing preganglionic motoneurons labelled with fluorescent tracer Fluorogold.



**(a)** – On the border of the grey matter and periventricular white matter there is a medial group of neurones which appear to be differentiating owing to their large size and dendrites (parenthesis).

Bar = 40  $\mu\text{m}$ . FV = fourth ventricle.

**(b)** – Image (a) at a higher magnification. Primary dendrites are labelled with the tracer (blue arrowheads) and the cell bodies are large (white arrowheads). Bar = 40  $\mu\text{m}$

**Figure 7-5.0 Metamorphosed axolotl medulla oblongata.** Blue arrows correspond to the location of the Fluorogold images on the following pages.

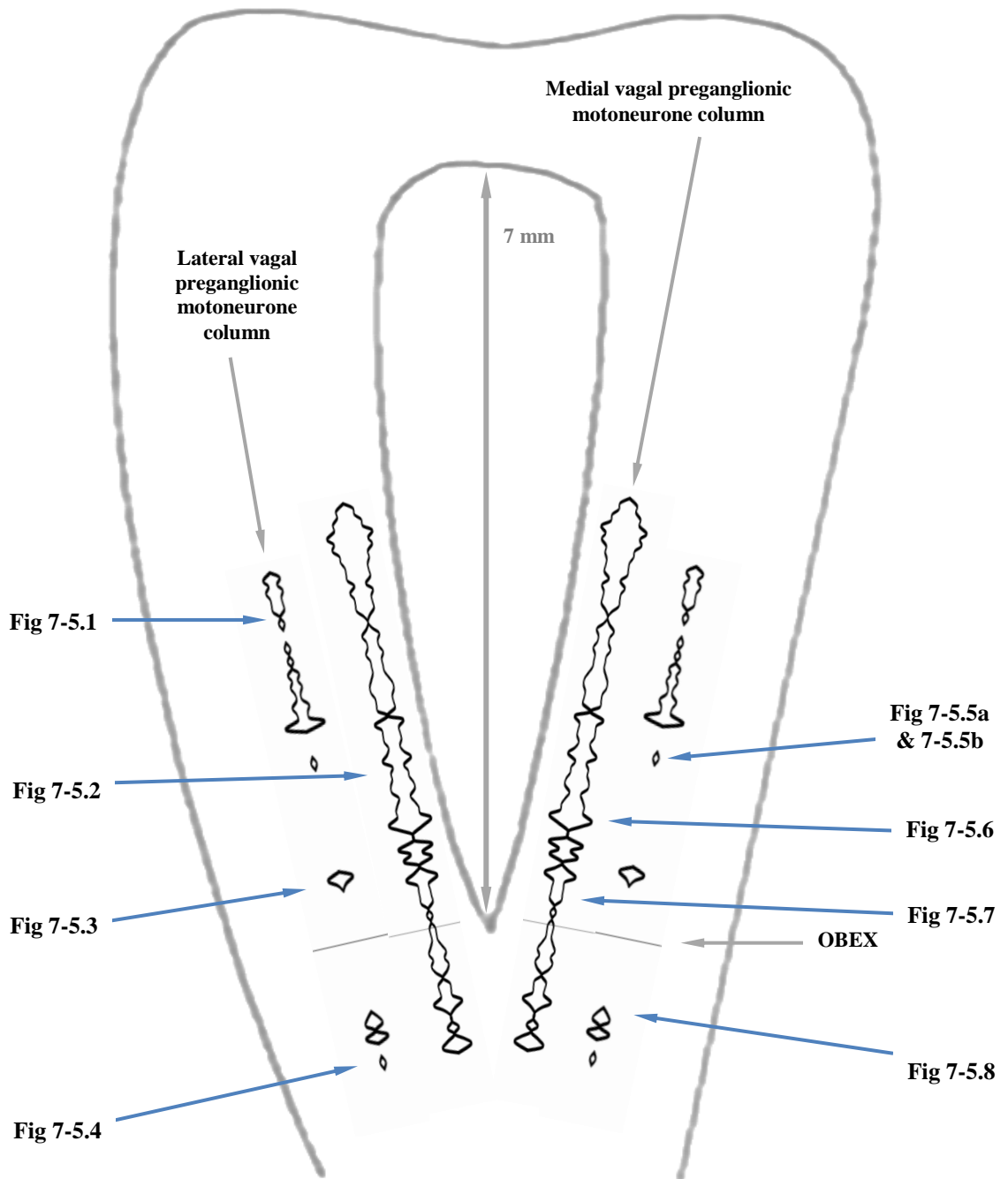
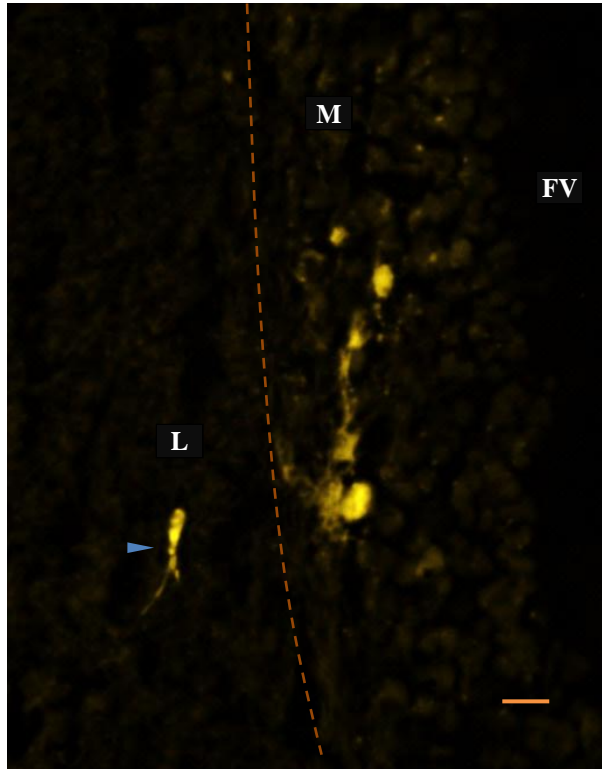


**Figure 7-5.1** Micrograph of transverse 20  $\mu\text{m}$  section of metamorphosed axolotl medulla oblongata showing vagal preganglionic motoneurons labelled with the fluorescent tracer, Fluorogold.

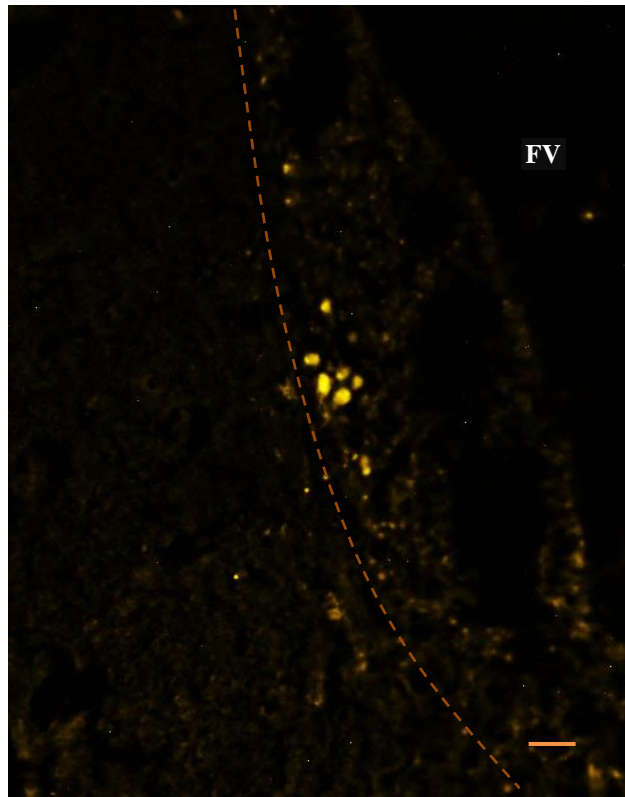


Section showing a group of relatively enlarged cells in the medial area (M) and a migrating neuron with long dendrites (blue arrowhead) projecting ventrolaterally (L). Grey matter on the right of the orange line.

Bar = 40  $\mu\text{m}$ . FV = fourth ventricle.



**Figure 7-5.2** Micrograph of transverse 20  $\mu\text{m}$  section of metamorphosed axolotl medulla showing preganglionic neurones labelled with Fluorogold.



A group of enlarged neurones within the medial area. Grey matter on the right of the orange line.

Bar = 60  $\mu\text{m}$ . FV = fourth ventricle.

**Figure 7-5.3** Micrograph of transverse 20  $\mu\text{m}$  section of metamorphosed axolotl hind brain showing preganglionic neurones labelled with Fluorogold.

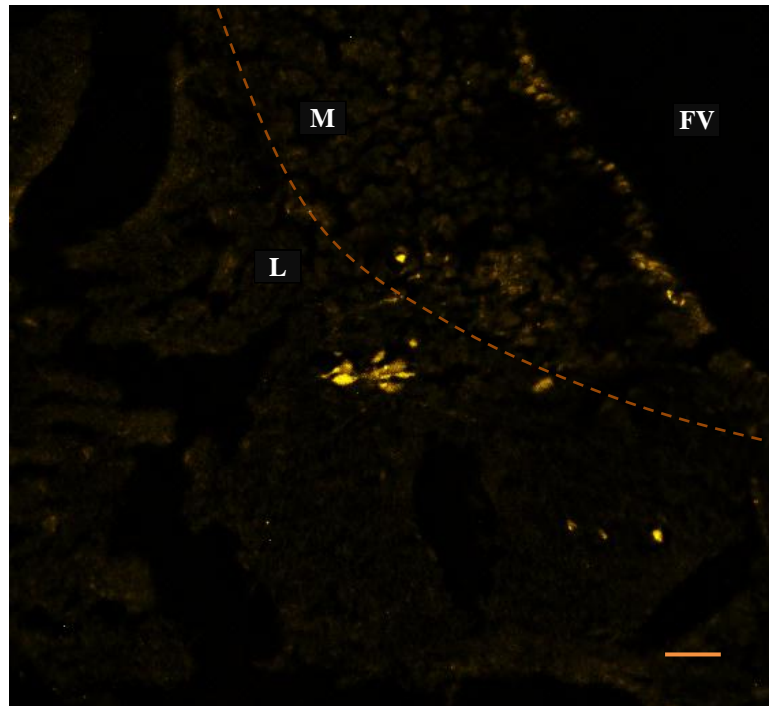


Image shows a group of enlarged migrating vagal preganglionic motoneurons within the lateral area (L). Grey matter on the top right of the orange line.

Bar = 70  $\mu\text{m}$ . M = medial. FV = fourth ventricle.

**Figure 7-5.4** Micrograph of transverse 20  $\mu\text{m}$  section of metamorphosed axolotl hind brain showing preganglionic neurones labelled with Fluorogold.

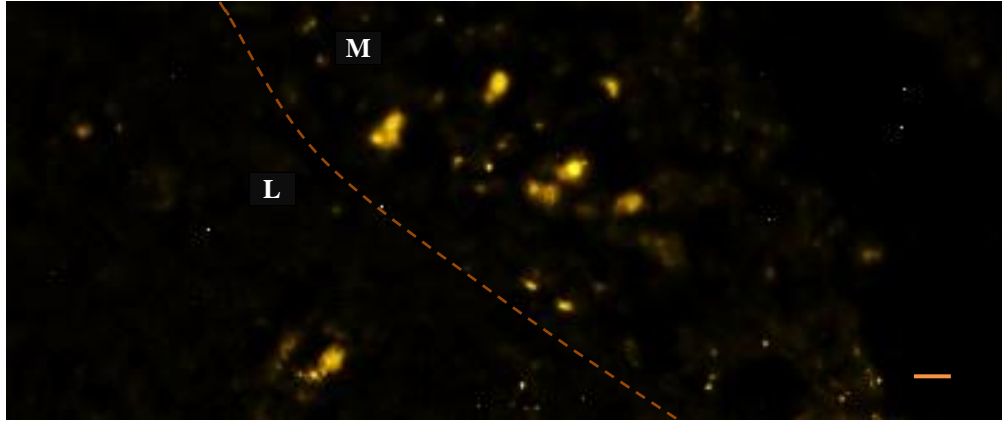
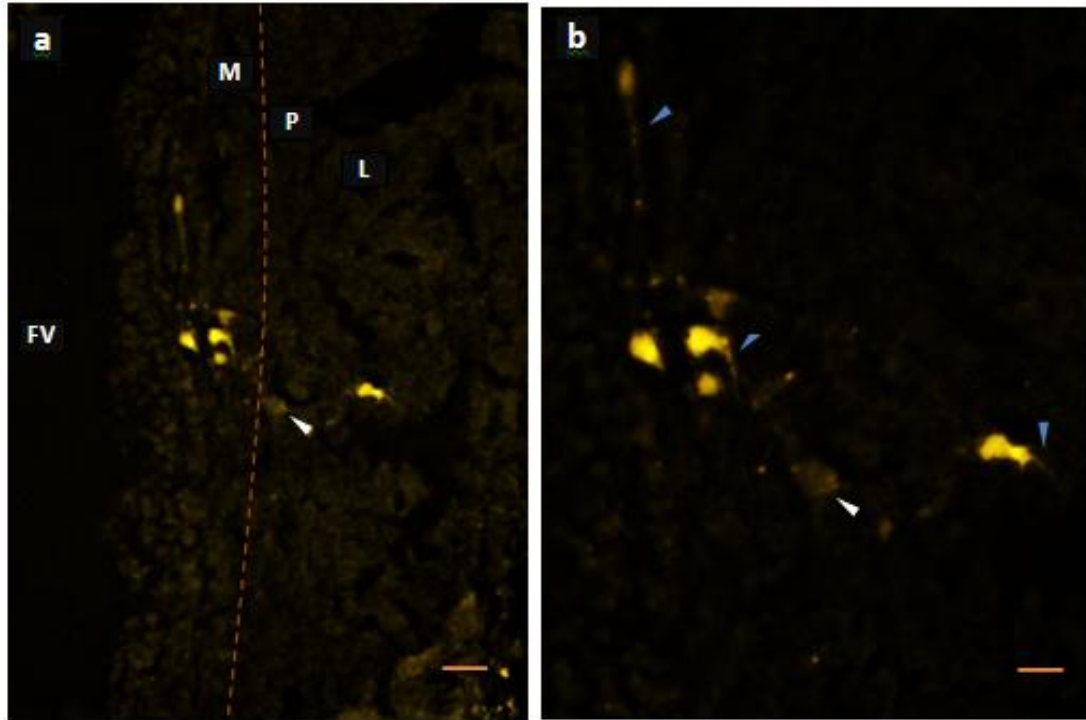


Image shows a group of vagal preganglionic motoneurons in two distinct groups: the lateral group on the left of the orange line (L) and the medial group on the right of the orange line (M), part of the grey matter

Bar = 30  $\mu\text{m}$ .

**Figure 7-5.5** Micrograph of transverse 20  $\mu\text{m}$  section of metamorphosed axolotl medulla showing preganglionic neurones labelled with Fluorogold.



**(a)** – Section showing a group of neurones in the medial area (M), a motoneurone that is relatively large (white arrowhead) in the periventricular area, and a vagal preganglionic neurone in the lateral area (L). Grey matter to left of orange line; white matter to the right.

Bar = 60  $\mu\text{m}$ . FV = fourth ventricle.

**(b)** – Image (a) at a higher magnification, showing the migrating neurone (white arrowhead) and dendrites on other cells that are relatively large and appear to be migrating and / or projecting ventrolaterally.

Bar = 30  $\mu\text{m}$

**Figure 7-5.6** Micrograph of transverse 20  $\mu\text{m}$  section of metamorphosed axolotl medulla showing preganglionic neurones labelled with Fluorogold.

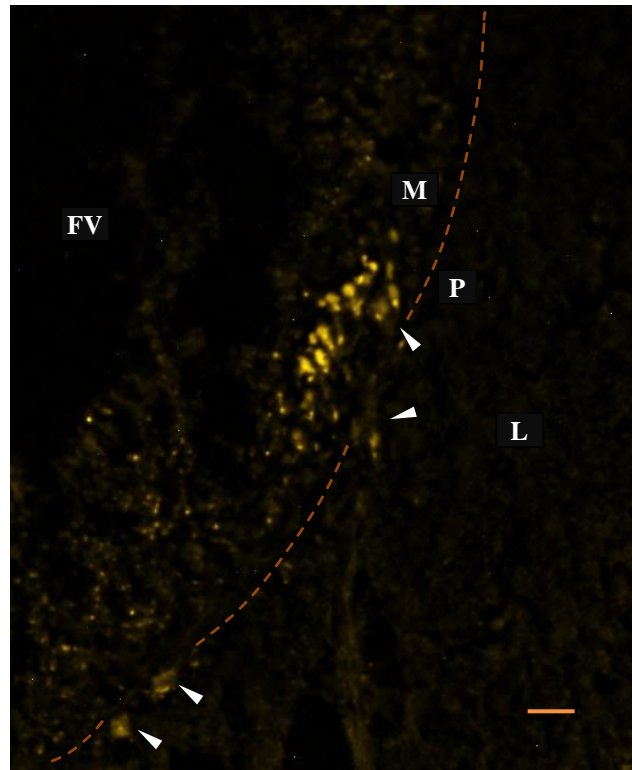
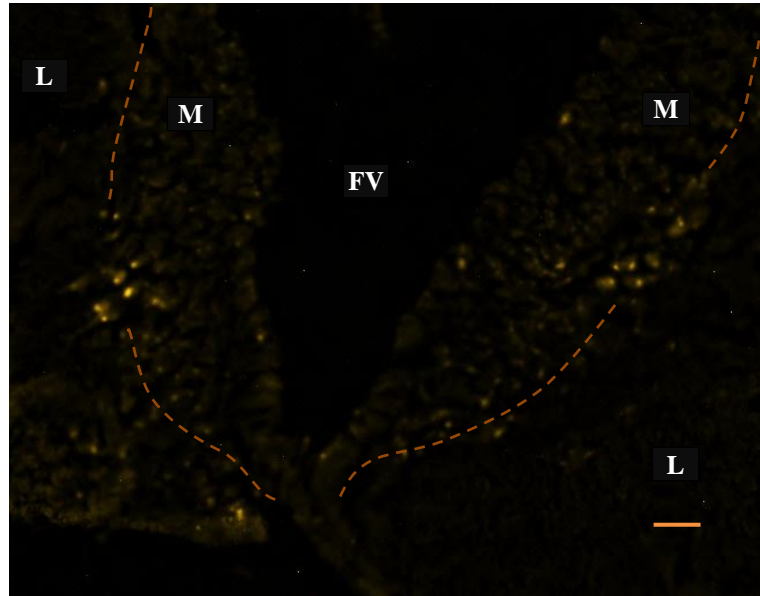


Image shows a group of medial motoneurons. In the vicinity of the periventricular area (P) there are a few neurones that are enlarged and appear to be migrating (white arrowheads). The grey matter is on the left hand side of the orange dotted line.

Bar = 45  $\mu\text{m}$ . FV = fourth ventricle. M = medial. L = lateral.

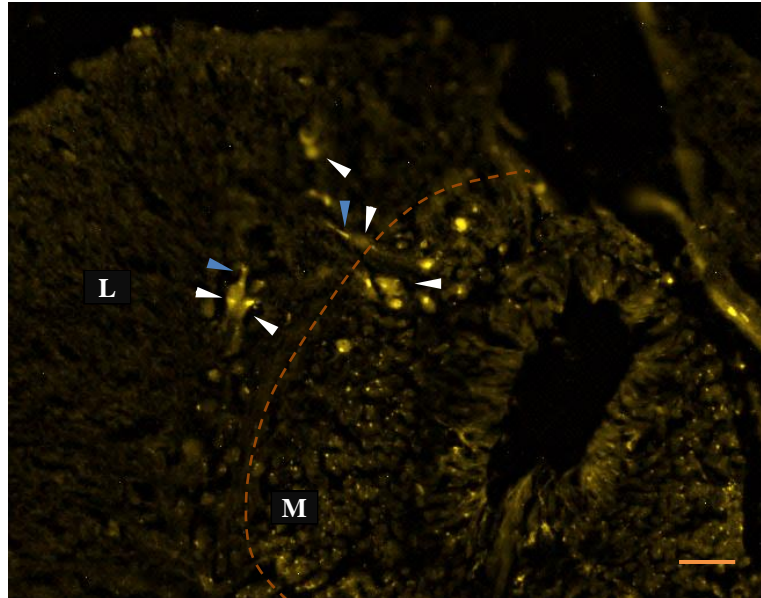
**Figure 7-5.7** Micrograph of transverse 20  $\mu\text{m}$  section of metamorphosed axolotl medulla showing preganglionic neurones labelled with Fluorogold.



Section shows the medial group of neurons on both sides of the fourth ventricle. These cells are in the vicinity of the periventricular white matter.

Bar = 60  $\mu\text{m}$ . FV = fourth ventricle. M = medial. L = lateral.

**Figure 7-5.8** Micrograph of transverse 20  $\mu\text{m}$  section of metamorphosed axolotl medulla oblongata/upper spinal cord junction showing vagal preganglionic motoneurons labelled with the retrograde tracer, Fluorogold.



Section shows neurons in the medial area that appear to be migrating laterally (white arrowheads). These migrating cells have clear primary dendrites (blue arrowheads). The relatively large, migrating cells are in the vicinity of the periventricular white matter. The contrast and brightness of the image has been set to allow visualisation of tissue morphology to aid orientation.

Bar = 60  $\mu\text{m}$ . M = medial. L = lateral.

**CHAPTER EIGHT**

**CARDIORESPIRATORY PHYSIOLOGY OF THE  
NEOTENOUS AND METAMORPHOSED AXOLOTL,  
*AMBYSTOMA MEXICANUM***



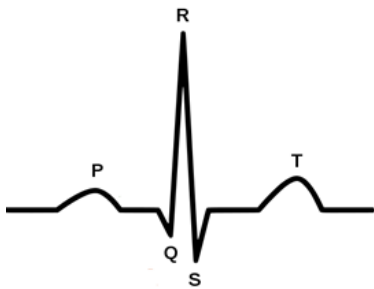
## **8.0 INTRODUCTION**

This chapter was the study of the changes that may be associated with metamorphosis. The neotenus axolotl is a gill breather, but when it is induced to metamorphose by introduction thyroid hormone (Chapter 6), it becomes a committed lung breather. It is thought that after the axolotl has metamorphosed, the relocation of VPN to a more ventrolateral location of the DVN (Chapter 7) may be linked with the onset of HRV. Activity in subpopulations of cardiac vagal motoneurons vary with mode of respiration in fish and mammals. Therefore this new ventrolateral location may be a primitive equivalent of the nA region in the mammalian brain which is known to be involved in the onset of RSA in humans (Hou *et al.*, 2009; Taylor, 1994). In humans, heart rate increases with inspiration and decreases when exhalation occurs. This is caused by inhibitory signals to the nA which prevents the vagal nerve from being stimulated. Normally the vagal nerve exerts an inhibitory effect on the heart rate by increasing parasympathetic input to heart, which decreases the rate of SA node firing. When expiration occurs the cells in the nA are activated which cause the heart rate to fall.

The use of drugs to block either parasympathetic or sympathetic control can give an indication of the influence of these autonomic branches upon the heart. For instance, atropine, a competitive antagonist for the muscarinic acetylcholine receptor, will block parasympathetic vagal influence, whose normal effect is to slow heart rate. Propranolol is a non-selective beta blocker and so blocks the effects of the sympathetic system, whose actions are normally to increase heart rate. Thus the effect of drug intervention will provide clues to the extent of cholinergic and adrenergic control of the heart rate.

## II. Neuroanatomy and Physiology of Cardiorespiratory Control

HRV can be seen on an ECG trace as the RR-intervals, of the PQRST wave (see diagram below), will be of different lengths and they would be related to the ventilation cycle if there is cardio-respiratory coupling. Therefore, the relocation of VPN to a ventrolateral position may cause physiological changes in heart rate which could be evidence for autonomic change.



P wave represents the wave of depolarisation that spreads from the SA node throughout the atria. This is followed by a brief isoelectric period which represents the time in which the impulse is travelling within the AV node and the bundle of His. The QRS complex represents ventricular depolarisation. The isoelectric period following the QRS is the time at which the entire ventricle is depolarised. The T wave represents ventricular repolarisation.

### 8.1 AIMS AND OBJECTIVES

The aim of this chapter was describe the cardiac and ventilatory changes associated with the transition from neotenus to metamorphosed axolotl (*A. mexicanum*). This was achieved by inserting electrodes to record ECGs, and recording ventilation rates and patterns of the neotenus and metamorphosed axolotls. Parasympathetic and sympathetic blockade was used to show the relative influence of these on heart and ventilation rates.

Therefore the objectives of Chapter 8 were:

- To record heart and ventilation rates / patterns in the neotenus and metamorphosed axolotls and then to determine if there is evidence of HRV in the latter forms (Chapter 8).
- To investigate the relative control of the heart rate in the neotenus and the metamorphosed axolotls by the sympathetic and parasympathetic branches of the autonomic system by injecting propranolol and atropine, respectively.

## **8.2 METHODS**

The heart and ventilation rates were recorded for neotenuous and metamorphosed axolotls. Firstly they were anaesthetised in 0.1% solution of buffered (NaHCO<sub>3</sub>) tricaine methane sulphonate (MS222) before being transferred to an operating table. To anaesthetise, metamorphosed axolotls were placed in a 500 ml plastic chamber with their heads raised above the anaesthetic solution as described in Chapter 7. The neotenuous forms were left submerged in the solution. Throughout the surgical procedure the neotenuous axolotls remained in contact with MS222 solution by way of gill irrigation, whereas the metamorphosed axolotls were laid in a shallow depth of the solution to facilitate dermal diffusion. In both cases this ensured the animals were under anaesthetic throughout the operation.

### **8.2a Surgery**

Once the axolotls were fully anaesthetised, determined by loss of righting reflex, 2 electrodes were inserted to read heart rate. These copper wire electrodes (0.5 mm) were made in advance: One end was soldered onto 1.5 mm<sup>2</sup> silver plated crimp contacts (RS Components Ltd) and insulation at the tip of the other end was stripped away over approximately 2 mm to make a good contact surface to pick up the electrocardiogram (ECG) signal. The exposed end was inserted into the tip of a hypodermic needle (23G x 1.25") for 3-4 mm (stripped portion inclusive) then carefully folded back ensuring that the point of the needle was clear. Each hypodermic needle was then gently inserted subdermally into the chest area on the ventral side of the animal close to the axis of the forelimb. The electrode was twisted to make a loop around itself to prevent tugging and then sutured onto the skin securely. The needle was carefully pulled away, thus leaving the

## ***II. Neuroanatomy and Physiology of Cardiorespiratory Control***

implanted electrode in place. This was done for both the right and left sides of the chest (Figure 8-0(A)). The ECG electrodes were then wrapped over and either sutured into place on the dorsal side of the neotenus axolotl (Figure 8-0(B)) or taped in place in the case of the metamorphosed form (Figure 8-0(C)). Following surgery the neotenus axolotls were placed in small plastic chamber (volume 500ml) with a flow of dechlorinated aerated tap water and the metamorphosed in a shallow dish of water, ensuring airways were above the water line by placement of paper towels, until awake. All axolotls recovered within 2 hours of anaesthetisation and began normal swimming/walking and breathing movements. They were then transferred back to their appropriate habitat and allowed to recover from the anaesthetic for an hour before baseline ECG recordings were taken (mainly to check electrode conduction efficacy). Recovery was checked by eliciting an overt response to the animal to stretching its toes. Complete recovery over at least 24 hours was allowed before pharmacological intervention.

### **8.2b Experimental protocol**

The following day the ECG leads were connected to record heart rates. The system employed was the Neurolog System 1401 (Digitimer) which had the AC NL105 amplifier and filters. The voltage fluctuations were pre-amplified by an Isleworth A101 Preamplifier. The Neurolog system was connected to a Viglen Genie PCI 4DX266 computer, and heart rate data was captured and displayed using either the processing Spike2 software (*via* CED1401 Intelligent Interface (Cambridge Electronics Design) hardware) or ChartLab software (ADInstruments), when using AD Instruments PowerLab system. Typically, raw data was sampled continuously at 100 Hertz for as long as possible when the animals were still to achieve clear ECG traces. The raw data was displayed continually in real time and

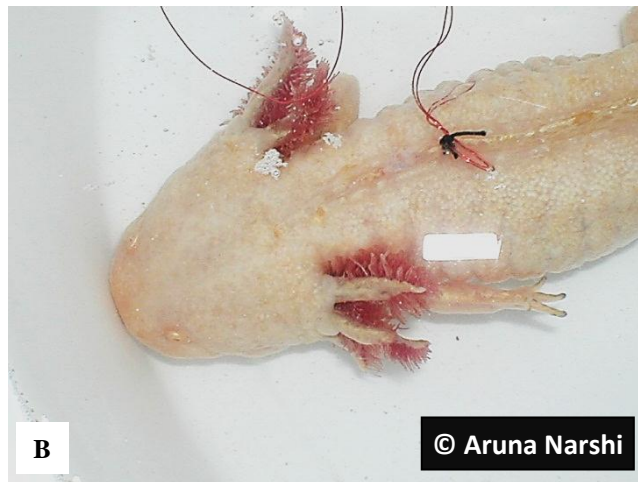
## ***II. Neuroanatomy and Physiology of Cardiorespiratory Control***

simultaneously stored to hard disk. Ventilation rates were visually observed over 20 minute window frames during the ECG sampling period and were digitally marked onto the ECG trace by manually pressing a key on the keyboard.

The heart rate is controlled by vagal cholinergic inhibitory signals and sympathetic adrenergic excitatory nerves. Inhibitory signals cause bradycardia, and excitatory signals cause tachycardia. Acetylcholine is the primary neurotransmitter of the vagus nerve, and atropine opposes the effect of acetylcholine by blocking the muscarinic cholinceptors on the heart. Thus atropine was introduced via intraperitoneal injection ( $1 \text{ mg kg}^{-1}$ ) to detect changes in heart rate. An hour later the axolotls were injected with propranolol (at  $0.1 \text{ mg kg}^{-1}$ ), a catecholamine receptor antagonist. It acts by blocking the  $\beta$ -adrenergic receptors of the CV system, thereby abolishing the excitatory effect of the catecholamine noradrenaline. Heart and ventilation rate were measured before, at and after the injection of drugs, in both neotenus and metamorphosed axolotls.

## II. Neuroanatomy and Physiology of Cardiorespiratory Control

**Figure 8-0 Electrode placement.** (A) ECG electrodes looped and sutured in place. The electrodes were secured by suturing on the dorsal ridge (B) or with insulation tape (C) depending on axolotl form.



## **8.3 RESULTS**

### **8.3a Neotenuous axolotl**

The neotenuous axolotls display rhythmic ventilation and surfacing behaviour. Ventilation was noted by gill twitching under the water surface and taking breaths at the surface before submerging again. Figure 8-1 shows the ECG picking up the buccopharyngeal movements of a neotenuous axolotl at rest. The interval between surface breaths was  $20.0 \pm 2.5$  min, thus there were 3 to 4 surface breaths taken per hour. The gill twitch frequency was, on average,  $17 \pm 7$  beats per minute (bpm). In general it was observed that the rate and intensity of gill twitching gradually increased to culminate in a surface breath. This was followed by an immediate bout of slower gill twitches in the water followed by a period of slight gill twitch movements or complete stillness before a gradual increase in the rate and intensity of gill twitches, to commence the cycle again (for example, see Figure 8-4(C)). The heart and ventilation rates appear to be synchronous, and the heart rate did not show variability around a gill twitch (Figure 8-2), nor after a surface breath as the R-R intervals of the 'PQRST' ECG wave remained the same (Figure 8-3).

There was a marked increase in both heart and gill twitch rate post atropine injection. For example, the heart rate more than doubled, from 16 bpm (Figure 8-3(B)), to 54 bpm (Figure 8-4). The gill ventilation went up by 7 bpm to 18, as also shown in Figure 8-4. In all neotenuous cases the effect of the atropine took place within 2 minutes of the injection as indicated by a rise in resting heart rate, reaching the maximum number of bpm in  $18.75 \pm 2.39$  mins (mean  $\pm$ SE). An hour later the mean heart rate did not return to resting level of 16 bpm, and was at  $39 \pm 2.93$  beats  $\text{min}^{-1}$ .

After one hour of being injected with atropine the axolotls were injected with propranolol. This resulted in an apparent decrease in heart rate and gill ventilation rate, when compared to atropine (Figure 8-5). After 1.5 to 2 hours heart rate returned to that of resting rate, but gill ventilation and air breaths varied from some demonstrating an increase in air breaths, some just an increase in gill ventilation and some showed no change in gill ventilation. However, the rhythm of a gradual beat frequency increase before an air breath, followed by a gradual decrease before increase, remained. Axolotls injected with saline did not display any changes in heart and ventilation rates.

### **8.3b Metamorphosed axolotl**

The metamorphosed axolotl ventilation rate was recognised as a deeper breath intake by lowering of the buccal cavity lower and for a slightly longer period of time than when making regular buccal movements. These generally occurred at around 2 minute intervals (Figure 8-6). They displayed irregular heartbeats when compared with the neotenus forms. There were cyclic rhythms of bradycardia followed by tachycardia as indicated by the R-R interval (Figure 8-7).

Atropine increased the heart rate and eliminated bradycardia. The maximum mean heart rate was achieved in 3.2 minutes  $\pm$  0.58 (SE) after which it took 16.67  $\pm$  2.58 minutes (mean  $\pm$  SE) for heart rate to reach normal resting rate. Figure 8-8 shows the effects of atropine on the heart rate of a metamorphosed axolotl.



## ***II. Neuroanatomy and Physiology of Cardiorespiratory Control***

Propranolol reduced the heart rate over time. The first reduction occurred within  $6.5 \pm 0.5$  minutes post injection. The mean time ( $\pm$ SE) to reach heart rates lower than those recorded for resting rate was  $28.4 \pm 13.12$  minutes and they remained at this level for at least an hour. Figure 8-9 show the effects of propranolol on the ECG trace of a metamorphosed axolotl.

The effect of these drugs on ventilation was conflicting. Some axolotls displayed an increase in ventilation, whereas others displayed a reduction. Therefore there was not clear pattern with either of the drugs. The metamorphosed axolotl used in Figures 8-8 and 8-9 demonstrated an initial reduction in ventilation rate from 30 to 18 and then an increase to 48 ventilations per hour following atropine injection. Propranolol elicited an increase in ventilation rate, but this was not an immediate response. Metamorphosed axolotls displayed no changes in heart and ventilation rate when injected with saline.

The same axolotl continued to display heart rate variability 8 days post-surgical implantation of electrodes. Ventilation resulted in immediate bradycardia, followed by tachycardia in an oscillatory fashion (Figure 8-10).

### **8.3c Comparisons of neotenus and metamorphosed axolotls**

The heart rate for the neotenus was lower than that of the metamorphosed. The mean neotenus heart rate was 27.20 and metamorphosed was 34.47 bpm (Figure 8-11). The neotenus heart beats show an oscillatory pattern which was not as pronounced in the metamorphosed (Figure 8-12).

The neotenuous and metamorphosed axolotls demonstrated the same response to atropine and propranolol but there were differences in the magnitude of the effects. After atropine injection the heart rate of the neotenuous axolotl almost doubled, but for the metamorphosed there was only a third rise in heart rate. After propranolol both forms of axolotls reached a mean heart rate of 24.4 bpm (Figure 8-11). In both neotenuous and metamorphosed groups the animals displayed no changes in heart and ventilation rates after being injected with saline.

### **8.4 DISCUSSION**

Electrocardiograms (ECG) and ventilation rates were measured in the present study to test the hypothesis that the relocation (or migration (Windle, 1933)) of vagal preganglionic neurones (VPN) to a ventrolateral position may relate to the generation of heart rate variability in the metamorphosed axolotl, *Ambystoma mexicanum*. In Chapter 7 there was evidence of cells migrating to the ventrolateral location by the presence of torpedo / spindle shaped cells that have been associated with cell migration. These cells appeared to move from the dorsal vagal motor nucleus (DVN) (see Figures 7-4.2, 7-4.4, 7-4.5, 7-5.1, 7-5.3, 7-5.5, 7-5.6 and 7-5.8 in Chapter 7). The ventrolateral location may be a primitive nucleus ambiguus (nA) counterpart seen in mammals, which is known to contain cardiac vagal-preganglionic neurons (CVPN). The CVPN in the nA appear to be involved in respiratory and cardiac rhythms, whereas those found in the DVN are not involved in the respiratory cycle (Taylor *et al.*, 2010).

## ***II. Neuroanatomy and Physiology of Cardiorespiratory Control***

The neotenuous axolotl demonstrated a ventilatory rhythm. After an air breath, the gills, once underwater again, would twitch very slightly (gill ventilation). After a while the intensity of gill ventilation gradually increased. This sometimes resulted in the axolotl, which is usually quite still in the water, to want to move around. After a few movements the neotenuous axolotl would suddenly come up and take a gulp of air before quickly submerging again, thus starting the cycle over again (see Figure 8-4(C) for an example of the cycle, but note that this cycle is much faster than that normally occurring at rest and when there is no drug intervention). This would suggest the possibility of the presence of mechano- and or chemo-receptors on the gills. Unlike fish that actively vent their gills by swimming, and therefore, oxygenating them efficiently, the axolotl generally stays very still in the water. This may lead to a systemic increase of CO<sub>2</sub> through metabolic activity, which could be detected by chemoreceptors and cause the gills to ventilate more forcefully via mechanoreceptors stimuli.

Gill ventilation generally appeared to be synchronous with heart rate when gill twitching was observed, but the overall mean frequency of gill ventilation did not match heart rate due to a reduction in gill twitches post an air breath. Figure 8-2 shows evidence of cardio-respiratory coupling. Note that when the period between two gill twitches increases so does the interval between the R-R spikes on the ECG. Therefore there appears to be some modulation of heart rate with ventilation, but there is clearly no evidence of heart rate variability with ventilation, where one would expect to see a regular pattern of tachycardia upon inspiration events (as seen in humans and known as respiratory sinus arrhythmia). The absence of heart rate variability with respiration is supported by preliminary power spectral analysis of beat-to-beat changes in resting heart rate (Figure 8-13) and the

## ***II. Neuroanatomy and Physiology of Cardiorespiratory Control***

tachogram (Figure 8-12(A)) of a neotenuous axolotl. Both figures resemble those seen in traces from fish (Campbell, *pers. comm.*). The ventilation rate for this neotenuous axolotl was around 14.2 seconds and the heart rate was around 19.5 beats  $\text{min}^{-1}$ . This can produce aliasing and cause the power spectrum to show as a series of peaks as the spectrum folds in on itself (Campbell *et al.*, 2004; Taylor *et al.*, 2006)

The ECG trace of a resting metamorphosed axolotl showed a significant increase in the heart rate compared to that of the neotenuous (Figure 11). This was reflected in the shorter period between R-R intervals and there was generally more variation in the R-R intervals when compared with the neotenuous forms. The tachogram of the metamorphosed axolotl in Figures 8-12(B)–(D) show a very different pattern to that of the neotenuous which showed a regular oscillatory fish-like pattern. The metamorphosed heartbeats appear to drift in comparison, indicative of some long and short term cardiorespiratory control. Preliminary examination of the possibility of cardiorespiratory interaction was sought using power spectral analysis. This showed a peaked at a frequency of 0.0079 Hz, a time domain of 126.6 seconds. This matched the frequency of the ventilations of that animal, and indeed, this ventilation pattern of around 2 minutes was also observed in other metamorphic individuals (Figures 8-6(A) and (C)). Hence the metamorphosed axolotl does appear to show heart rate variability around ventilation, but not around buccal movements. Unfortunately, due lack of animal availability and shortage of time meant that only one metamorphosed axolotl was used for the spectral analysis. More metamorphosed axolotls would need to be used in the future to make a more convincing, and statistically significant argument.

## ***II. Neuroanatomy and Physiology of Cardiorespiratory Control***

Upon close inspection there was clear tachycardia and bradycardia with the metamorphosed axolotl ECG traces (Figures 8-7(A)-(D)). In Figures 8-7(B), 8-8(A) and 8-10(A) and (B), the ECG trace showed that a ventilation event was followed by bradycardia, and *then* a tachycardia. So there was a lag before the tachycardia. This is also seen on the metamorphosed tachogram where the RR-intervals get further apart post ventilation and before tachycardia (Figure 8-12). In humans tachycardia results from inspiration causing stimulation of lung stretch receptors which results in a reduction in vagal tone, so perhaps this is the case with metamorphosed axolotls too. If it is, then perhaps the air that is taken in during a gulp remains in the buccopharyngeal cavity for a short while, causing the initial bradycardia (and lag in tachycardia), and then the *some* of the air is inspired (into the lungs), activating stretch receptors and reducing vagal tone as indicated by the first tachycardia after a ventilation event. To explain the less pronounced bradycardia and tachycardia that appear to occur in-between the 2 minute ventilation cycle (Figure 8-12), it can be suggested that, perhaps the air that is taken in during ventilation does not enter the circulatory system in one go. Maybe the metamorphosed axolotls are able to retain some of the ventilated air within the buccal cavity and release it into the respiratory system in a rhythmic fashion, thereby causing a rhythmic bradycardia and tachycardia as seen on the ECG.

Interestingly, this rhythmic pattern may be remnant of gill twitches (i.e., anatomically derived from the same structures that produced gill twitches in the neotenus form) that cause *modulated inspiration* by, somehow controlled buccal movements in the metamorphosed axolotl. Regular buccal movements have been noted to play an olfactory role (see Wang *et al.*, 1999), but it might be possible that the buccal cavity is also used to

## ***II. Neuroanatomy and Physiology of Cardiorespiratory Control***

not only hold the inspired air, but also to gradually allow it to enter the lungs in a rhythmic fashion, like the rhythmic cycle of gill twitching. (During metamorphosis, the gill twitches seen in the neotenus could be replaced with oscillatory buccal movements that produce the tachycardia and bradycardia (not the usual buccal movements that are normally seen – which occur at a much faster, regular rate); and the surface breaths that are displayed by the neotenus could be modified to the 2 minute ventilation rate seen in the metamorphosed. This could explain the cyclic bradycardia and tachycardia between the more obvious ventilations if it is assumed that the tachycardia is resulting from lung stretch receptors inhibitory effect on vagal tone. Of course there are likely to other stimuli that could cause inhalation per se, such as peripheral chemoreceptors in central vasculature and chemoreceptors in the brain. It is apparent that more research needs to take place in order to understand the cause of the less pronounced oscillatory cycles of bradycardia and tachycardia between the 2 minute ventilation events.

Surface breath frequency in the resting neotenus axolotl is around  $3.5 \text{ h}^{-1}$ . The ventilation rate in the metamorphosed axolotl is higher at around  $30 \text{ h}^{-1}$ . A higher rate of ventilation would be expected in the metamorphosed as they do not possess gills and so cannot ventilate ‘passively’ (when compared with surface breathing), by gill twitching nor moving around more in the water to ‘ram’ ventilate, and their skin becomes more keratinised and so there is less diffusion of oxygen through the skin post metamorphosis. Furthermore, they have more musculature on their terrestrially adapted limbs and the heart muscle too appears to show an increase in trabeculation (Figure 8-14) as indicated by Farmer (1999). These changes would increase the metabolic demands placed upon the metamorphic axolotl and thus an increase in ventilation rate would seem appropriate.

## ***II. Neuroanatomy and Physiology of Cardiorespiratory Control***

The neotenuous and metamorphosed axolotls responded by an increase in heart rate following muscarinic receptor blockade using atropine. This demonstrates that they both possessed inhibitory vagal signals on the heart. However the actual response between the two groups was quite different. Although both forms responded by showing an increase in heart rate within 2-3 minutes (Figure 8-4(A) and 8-8(B)), the neotenuous axolotls heart rate continued to rise to twice the resting rate over a 20 minute period, but the metamorphosed heart rate only rose by around 30% of the resting heart rate and within the first 3-4 minutes, much sooner than that seen in the neotenuous form. Furthermore, the metamorphosed axolotls returned to their resting heart rates after 18 minutes whereas the neotenuous form reached their maximum heart rate in around that time and they did not return to the normal resting rate even after an hour. This could suggest that vagal tone is not as effectively modulated in the neotenuous axolotl as it is in the metamorphosed. Parasympathetic control appears to be quite diffuse, but dominant in the neotenuous as it had a doubling of heart rate, whereas vagal tone in the metamorphosed appears to be more finely controlled owing to the return to homeostatic heart rate levels much quicker than that seen in the neotenuous. It is tentative to suggest that perhaps this extra control comes from the ventrolateral cells, but, of course, the exact mechanisms would have to be examined further.

In the case with propranolol, both axolotl forms showed a reduction in heart rate within 4-6 minutes of being injected (Figures 8-5(A) and 8-9(A)). However, it took the metamorphosed axolotls only 30 minutes (mean value) to reach their lowest heart rate (the metamorphosed in Figure 8-9(B) took 9 minutes), whereas the neotenuous forms took over

## ***II. Neuroanatomy and Physiology of Cardiorespiratory Control***

1.5 hours (Figure 8-5(B)). Furthermore, with this set of data, there wasn't a significant difference between normal and propranolised heart rates with the neotenus. This may indicate that their heart rate is predominantly modulated by cholinergic influence, and that adrenergic input is minor. The recovery of the neotenus and metamorphosed was comparable as they both had low heart rates for a long time post propranolol administration (almost 2 hours in the neotenus (Figure 8-5(B)) and at least 70 minutes in the case of the metamorphosed (Figure 8-9(F)). It is interesting to also note that when sympathetic control was blocked in both, the neotenus and metamorphosed axolotls, the heart rate was, on average, 24 bpm (Figure 8-11). This is likely to be the pacemaker rate of the heart since the atropine (injected an hour before) would block all vagal control and sympathetic control would have been blocked by propranolol; so only the intrinsic cardiac pacemaker rate would be acting on heart rate at this point.

The gill ventilation rate in the neotenus increased with atropine but not at the same magnitude as heart rate; heart rate increased by almost 200%, but gill ventilation only increased by around 44% (Figures 8-2, 8-3(B) and 8-4(B)). This constraint in magnitude is likely due to the biomechanics of physically not being able to move the gills at a faster rate, and is also likely to be compensated by the axolotl demonstrating more air breaths to meet the demands of an increasing heart rate. However, the number of air breaths taken did not increase significantly, but interestingly, the axolotls did want to move around more, probably in an attempt to increase ventilation at the gill surface. When under hypoxic conditions the neotenus forms do show an increase in air breaths (McKenzie & Taylor, 1996), but if there is sufficient oxygen in the water then they may be stimulated to want to move around more in order to 'ram' ventilate when metabolic demands increase. Gill



## ***II. Neuroanatomy and Physiology of Cardiorespiratory Control***

ventilation reached maximum twitch rate at the same time as the maximum heart rate (20 minutes) (Figure 8-4(B)) and with propranolol administration the gill twitch rate decreased with heart rate (Figure 8-5(B)). This is a clear demonstration of cardiorespiratory coupling. Moreover, since there is a bigger change in heart and ventilation rates post atropine than with propranolol, the neotenus axolotl's basic resting heart rate must be significantly dampened by acetylcholine from the tenth cranial nerve. They show a relatively high degree of vagal tone, and some excitatory sympathetic control by noradrenaline.

The ventilation rate in the metamorphosed axolotl, as defined by a more forceful buccal depression (Wang *et al.*, 1999) was at 2 minute intervals when resting. However the ECG did not always pick up the buccal movements (Figure 8-8(B)). This could be due to the axolotl taking particularly shallow ventilations or limitations in measuring device and so future studies should consider a more sensitive way of measuring ventilation. After 13 minutes post atropine injection the heart rate and ventilation rate returned to normal (Figure 8-8(C)). However, after a further 9 minutes the ventilation rate went down to  $18 \text{ h}^{-1}$ , even though the heart rate was normal (Figure 8-8(D)). This followed by an increase in ventilation to  $48 \text{ h}^{-1}$  (but not in heart rate) after a further 8 minutes (Figure 8-8(E)). The increase in ventilation rate could be to compensate for the earlier reduction in ventilation. Interestingly, the axolotl appeared to yawn during the higher rate ventilation period. Yawning is known to be a reflex mechanism that is triggered by a drop in circulatory oxygen levels. At this time the return of bradycardia and tachycardia is observed, although it takes a further 9 minutes (40 minutes post atropine administration) for the ECG wave to return to normal, with longer bradycardia post a ventilation event (Figure 8-8(F)). Atropine abolished heart rate variability indicating that the variability is caused by the decrease in

## ***II. Neuroanatomy and Physiology of Cardiorespiratory Control***

vagal discharge (Figure 8-8(B)). The effect of atropine on ventilation was no longer observed after 50 minutes.

Propranolol too had varied effects on ventilation in the metamorphosed axolotl. With heart rate there was an almost immediate decrease, falling to 22bpm after 9 minutes of injection (Figure 8-9(B) and remaining there for at least 68 minutes after (Figure 8-9(F)). However, ventilation did not follow this trend. Nine minutes after the injection there was the lowest fall in ventilation at 12 per hour. It can be seen that this coincides with the lowest heart rate recorded. So when sympathetic control is removed and thus heart rate falls, the first response is a drop in ventilation rate. But then, like that seen with atropine, there appears to be a compensatory mechanism that comes into play, causing an increase in ventilation, culminating in the maximum level of 30 per hour (the normal rate, when heart rate is normal with no drug intervention), by 45 mins post propranolol injection (even though there is no change in heart rate) (Figures 8-9(C) and (D)). The  $\beta$ -adrenergic receptors obviously slow down the heart, but there must be peripheral or central chemoreceptors that possibly detect an increase in CO<sub>2</sub> levels, due to slowing of the heart rate, that trigger the hyperventilation observed. Around 10 minutes later the ventilation drops again, to less than the normal rate (this might be due to the low heart rate) and continues to fall to 18 ventilations per hour after over an hour post propranolol injection (Figures 8-9(E) and (F)). Therefore, taking into account the observations made with atropine and propranolol on the metamorphosed cardiorespiratory system, it can be seen that the ventilation and heart rates are not coupled like that seen in the neotenus axolotl.

## ***II. Neuroanatomy and Physiology of Cardiorespiratory Control***

In summary, the metamorphosed axolotls show evidence of heart rate variability and ventilation patterns that did not always couple with heart rate. This indicates that there must be more than one area of the central nervous system that controls in the internal homeostasis of gas exchange. It could be possible that the relocation of VPN to the ventrolateral position from the DVN (Chapter 7) help to co-ordinate respiration and heart rate more tightly. Modified cardiorespiratory control post metamorphosis is likely to include innervation changes in the lungs and heart too. In contrast, the cardiorespiratory system of the neotenus axolotl functions very much like that of a fish and show coupled cardiorespiratory interactions.

**Figure 8-1.** An example of the underwater buccal movements of a neotenus axolotl as picked up by ECG electrodes. A few were marked manually at the time of recording (dotted lines) to aid identification on the ECG trace. Labels ‘B’ denote the **buccal movements**. (24h post-surgery.)

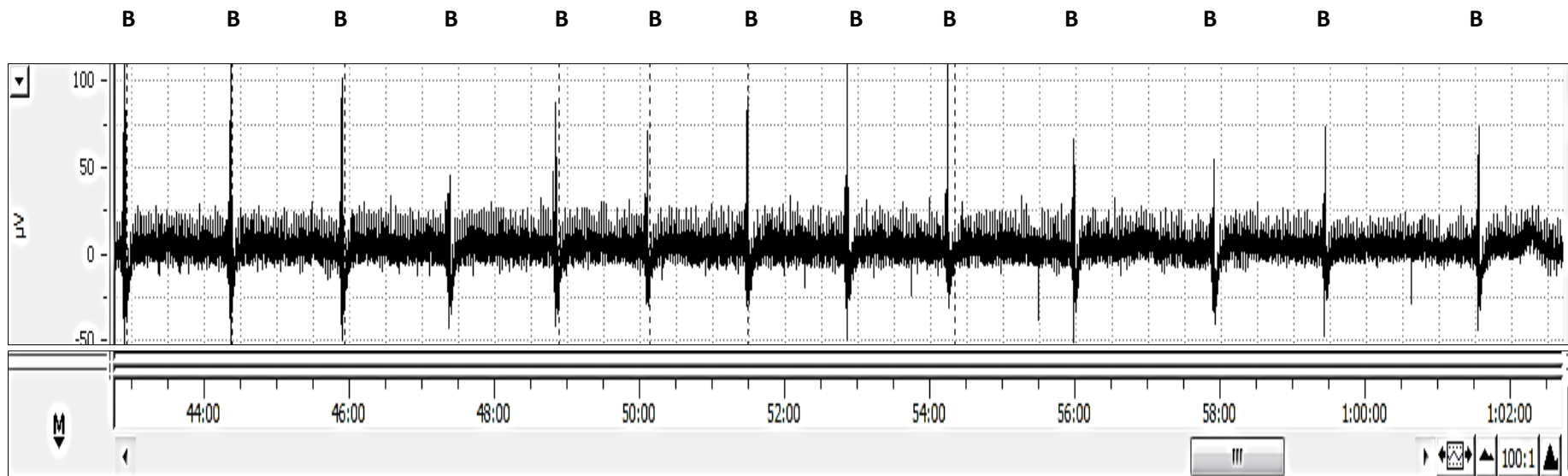


**Figure 8-2.** The heart rate appears to be occurring around ventilation bouts. The tall spikes on the trace are the R spikes of the QPRST wave and the downward spikes are the ventilation gill twitches (V). There was no evidence of any variability in heart rate around the gill twitches. The average heart rate for this neotenuous axolotl was 22 bpm, and the gill ventilation rate on this ECG trace was 14 bpm (28 in the 2 mins). (24h post-surgery.)

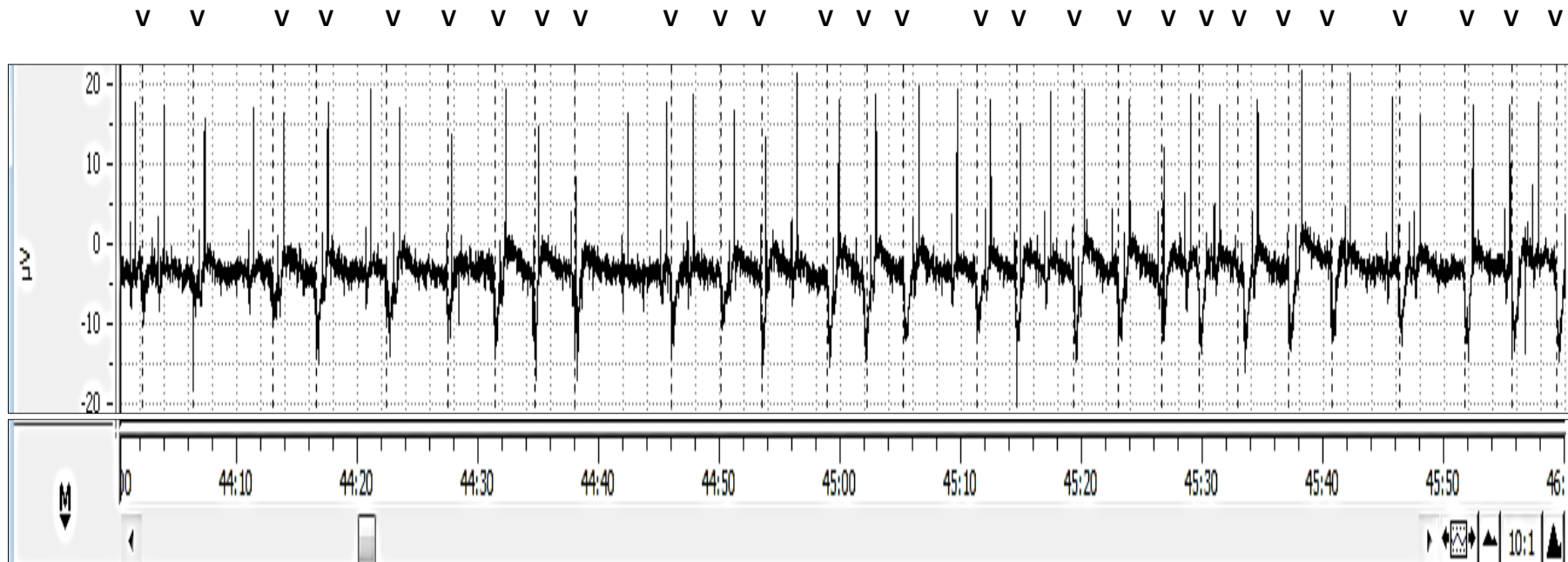


**Figure 8-3. Heart rate around an air gulp did not change, indicating there was no heart rate variability present in the neotenus axolotls. Figures (A) and (B) are two different neotenus axolotls.**

(A) Heart rate is 20 bpm before and after the surface breath (SB). (4 days post-surgery.)

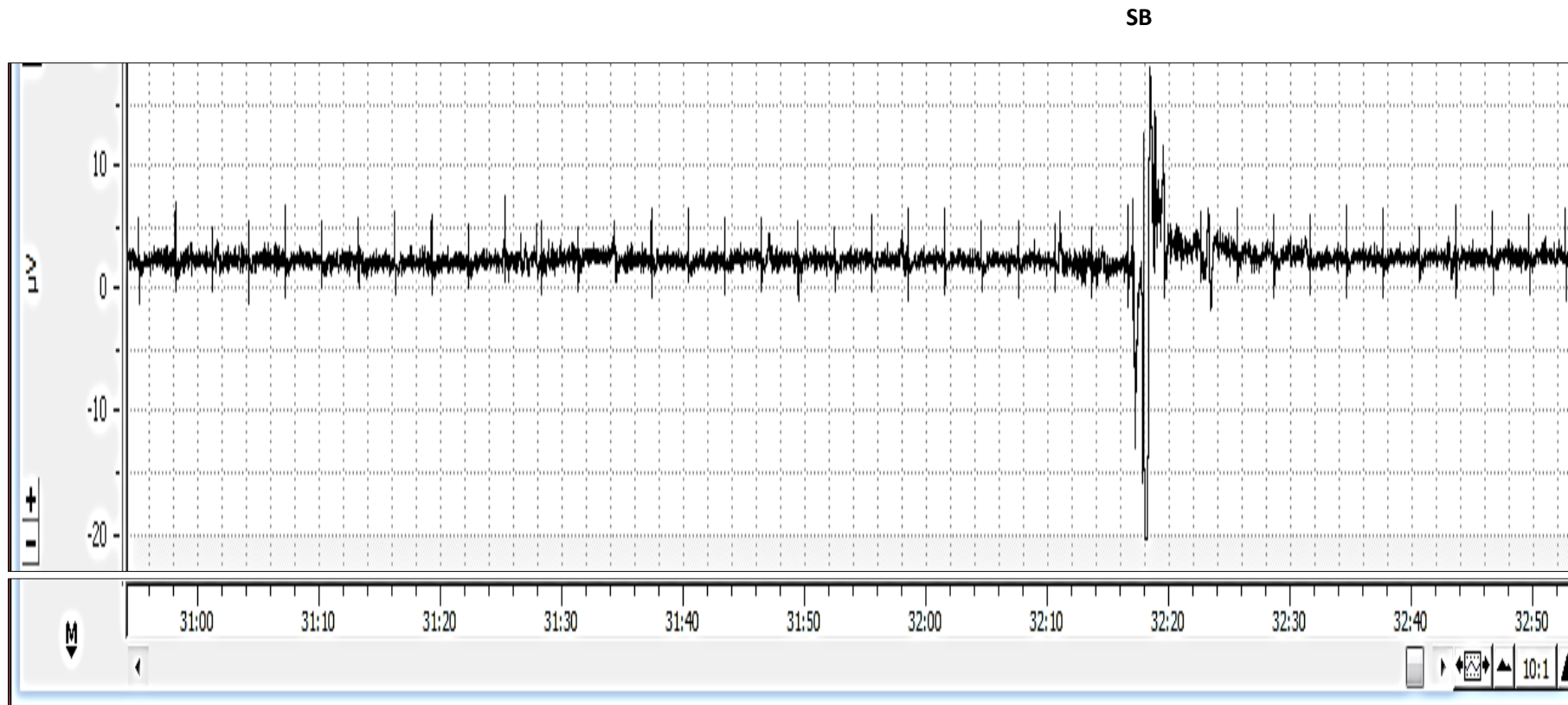


**Figure 8-3. Heart rate around a surface breath did not change, indicating there was no heart rate variability present in the neotenuous axolotls. Figures (A) and (B) are two different neotenuous axolotls.**

(B) Heart rate was 16 bpm and gill twitch (V) rate was 11/min. (SB – surface breath.) (24h post-surgery.)

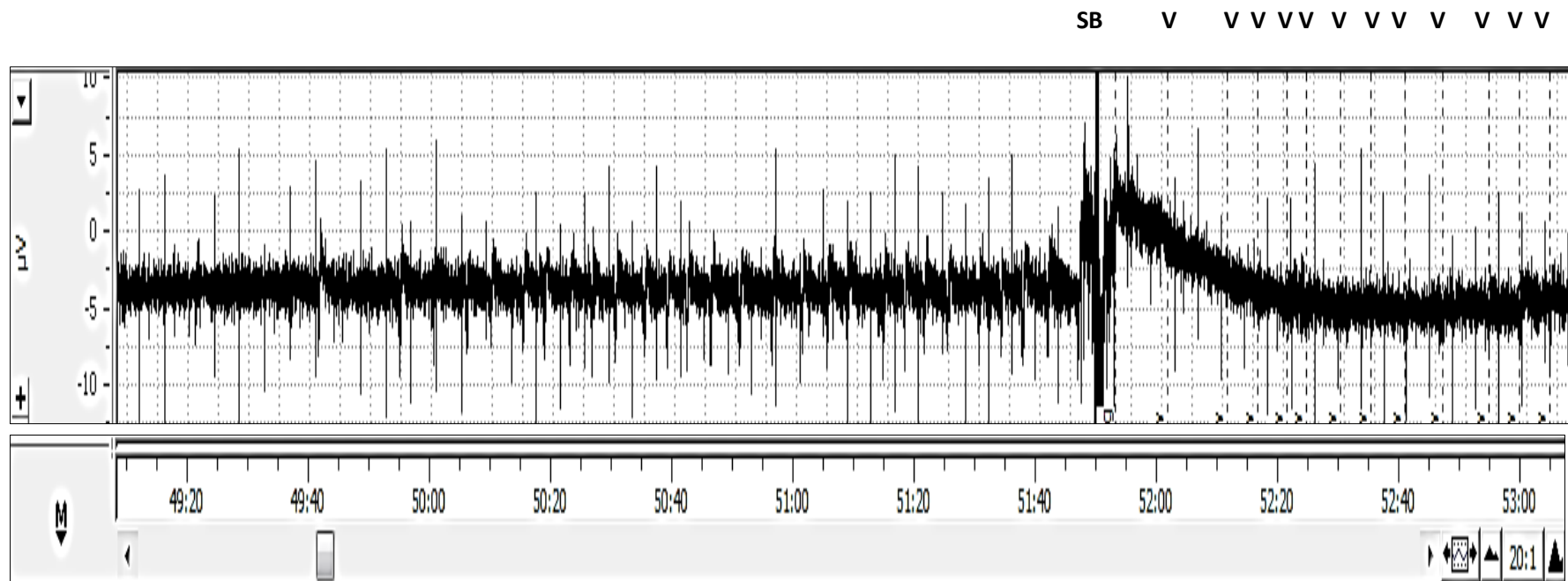


**Figure 8-4. Changes in heart rate and gill ventilation rate post atropine injection in the neotenus axolotl. (24h post-surgery.)**

(A) This is the same axolotl as in Figure 3(B) where the heart rate was 16 bpm and gill ventilation (V) rate was 11/min. The heart rate is now 54 bpm and the gill ventilation rate is 18 per minute. Measurement was taken 15 minutes after atropine injection.

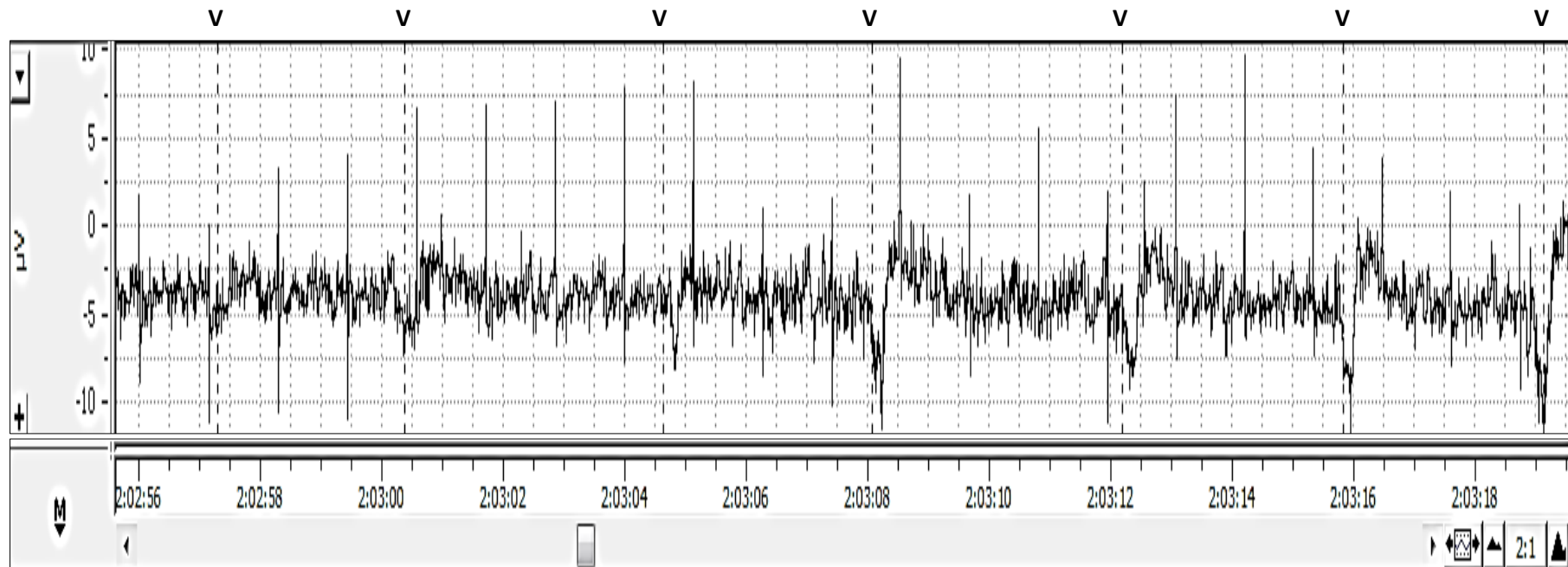
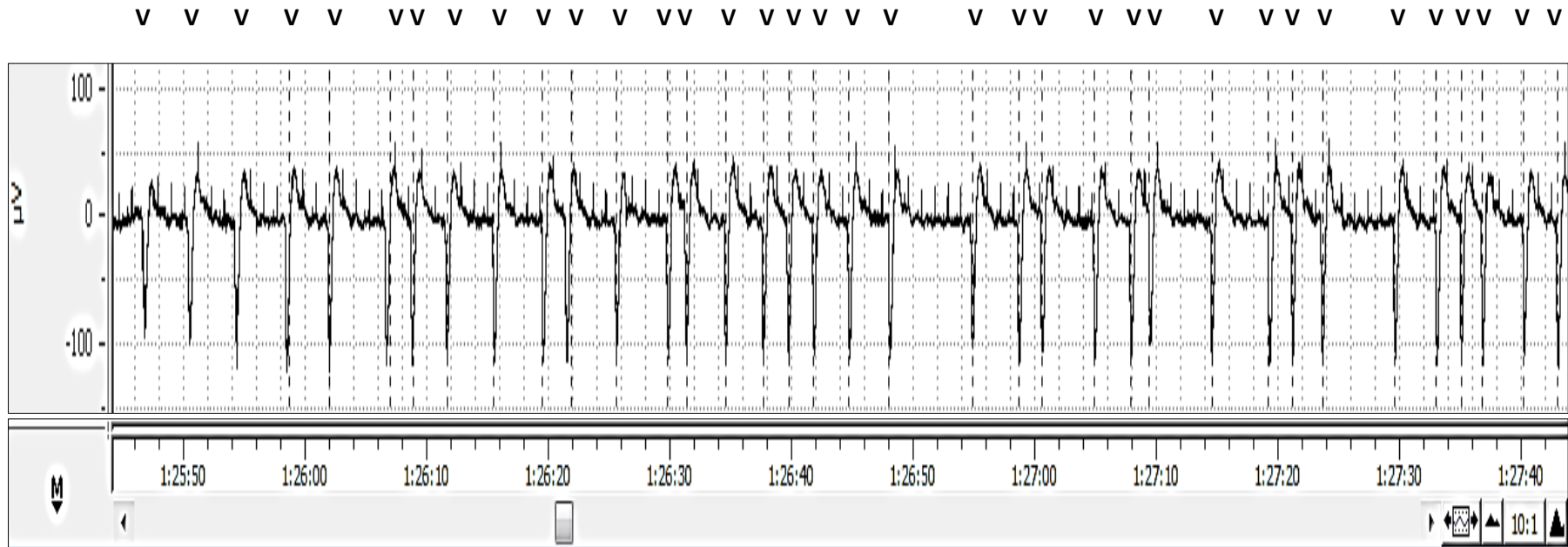




Figure 8-4. Changes in heart rate and gill ventilation rate post atropine injection in the neotenus axolotl. (24h post-surgery.)

(B) This is the same axolotl as in Figure 2, 20 minutes after being injected with atropine. The heart rate has risen from 22 bpm to 58 bpm; ventilation (V) rate has increased by 6 to 18 per minute.





**Figure 8-5. Effect of propranolol upon heart rate and gill ventilation rate.** This neotenus axolotl is the same one as in Figure 3(B) and Figure 4(A). (24h post-surgery.)

(A) ECG trace 10 minutes after propranolol injection. Heart rate has reduced from 46 bpm just before propranolol injection (given one hour after atropine) to 30 bpm. The gill ventilation (V) rate is now 12 bpm.

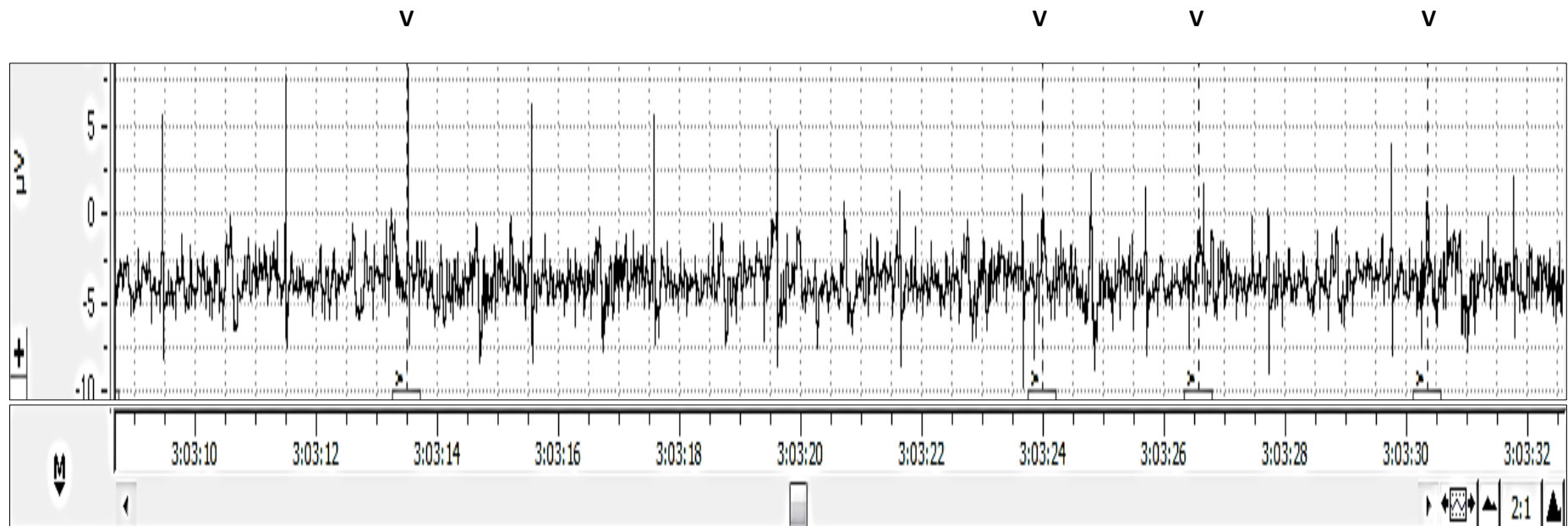


**Figure 8-5. Effect of propranolol upon heart rate and gill ventilation rate.** This neotenus axolotl is the same one as in Figure 3(B) and Figure 4(A). (24h post-surgery.)

(B) Heart rate returns to that at resting after almost 2 hours post propranolol injection. Heart rate is at 15 bpm; but the gill ventilation (dashed vertical lines) is still relatively high at 12 bpm. (SB – surface breath.)

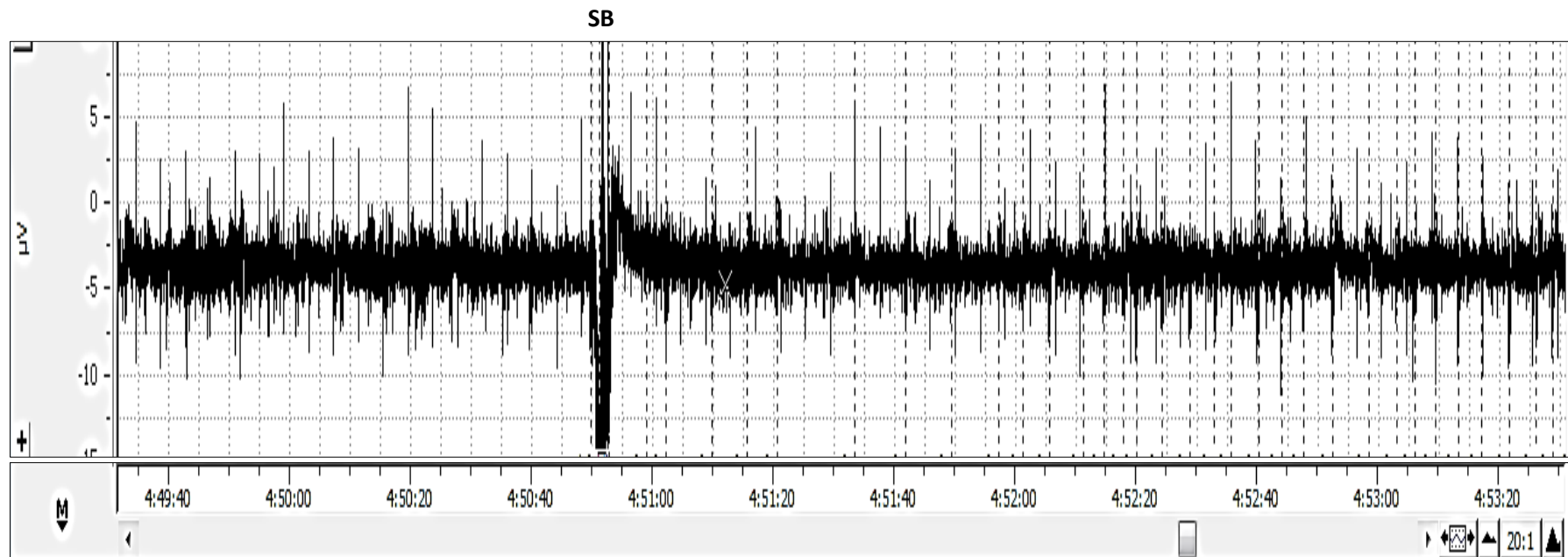


**Figure 8-6. Ventilation rate in the metamorphosed axolotls was around 2 minute intervals.**

(A) The chart below shows there are 9 ventilations (V) in this 16 minute period. Note that there appears to be some evidence of variation in heart rate between the ventilations. This is indicated by a group of RR-intervals separated by a gap, suggestive of a longer RR-interval (highlighted in the oval). (1h post-surgery.)

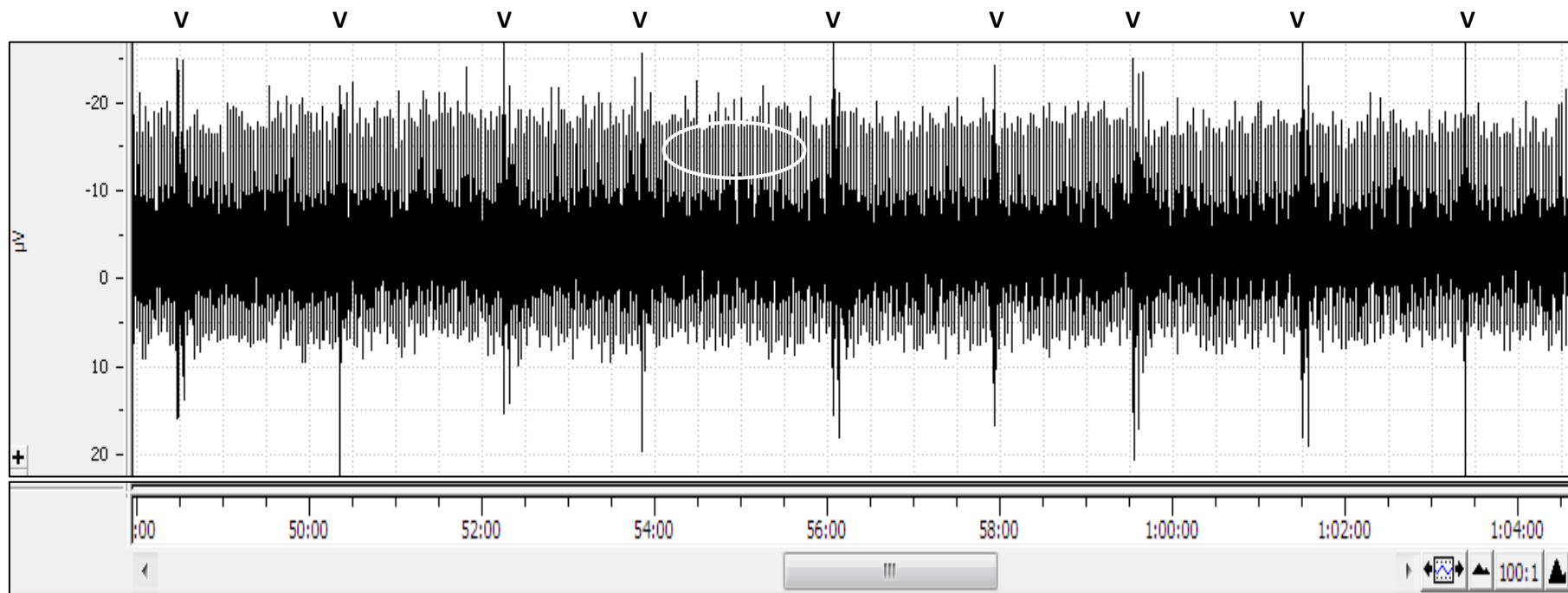


Figure 8-6. Ventilation rate in the metamorphosed axolotls was around 2 minute intervals.

(B) A larger scale of the same animal ECG. There are 5 ventilations (V) in the 9 minute interval. (24h post-surgery.)

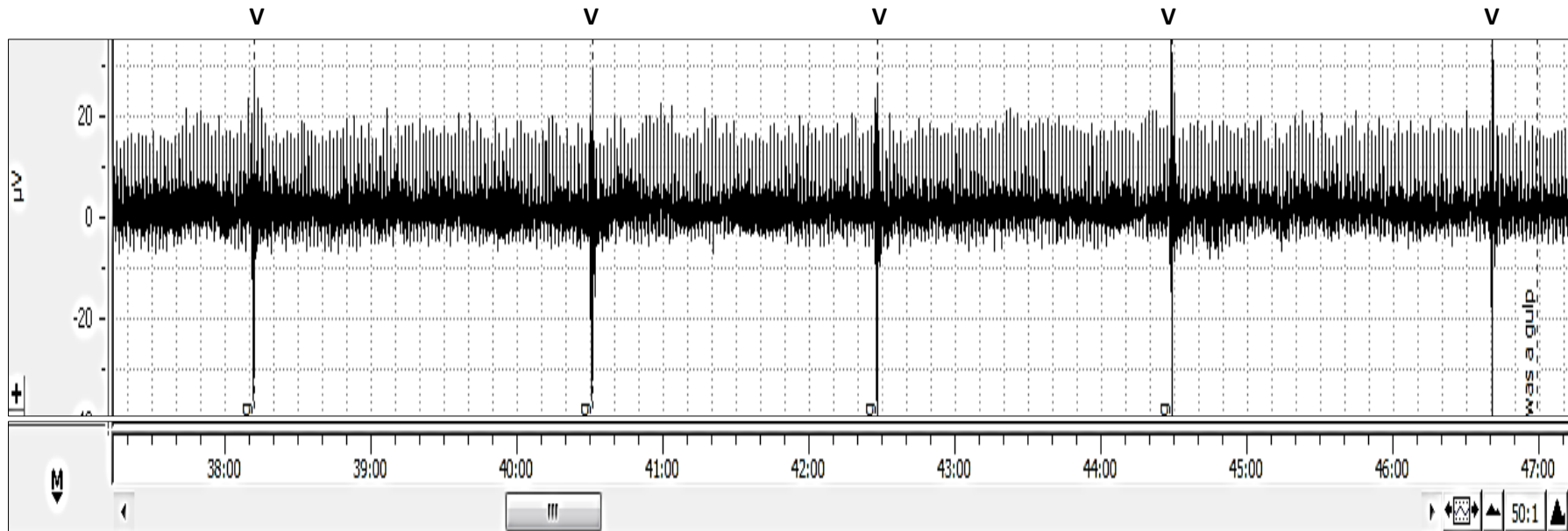
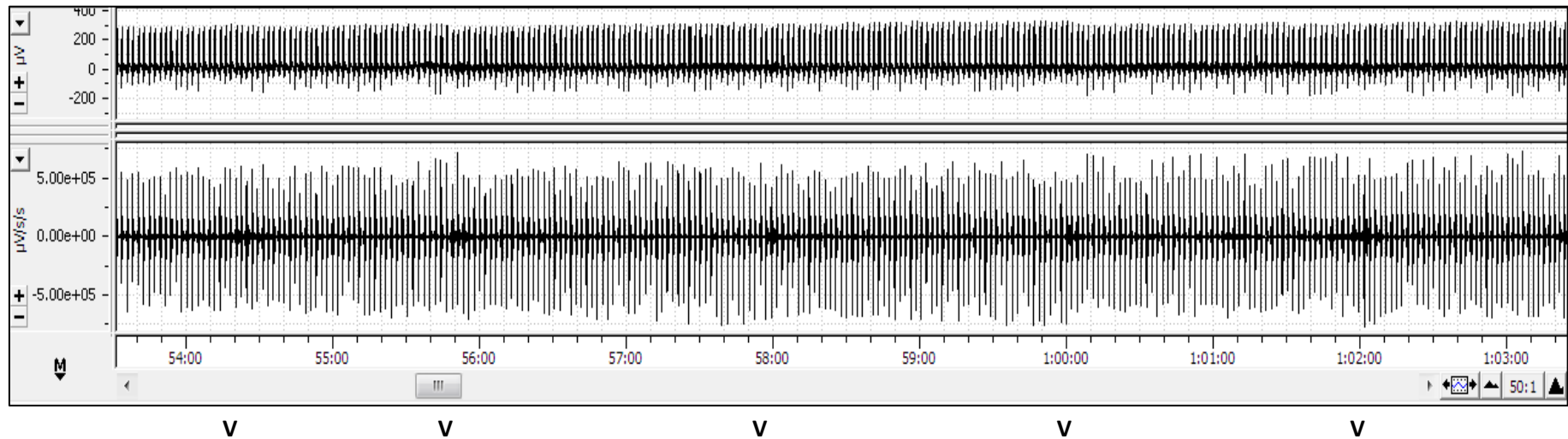


Figure 8-6. Ventilation rate in the metamorphosed axolotls was around 2 minute intervals.

(C) Ventilation rate in another metamorphosed axolotl. There are 5 ventilations in the 9 minute period (~30/h). The ventilations are marked with 'V' underneath the chart, from 54 minutes, 25 seconds onwards. The second trace was achieved by using the digital filter (band-pass) solely to aid clearer visualisations of the ventilations. (24h post-surgery.)



**Figure 8-7. Bradycardia and tachycardia in the metamorphosed axolotl.**

(A) This is the same animal as in Figure 6(A) & (B). Heart rate variability can be seen in the gross traces as white gaps amongst the black R-R spikes. The inverted colour section was magnified and the R-R intervals were digitally measured using ChartLab as shown. The time period between R-R intervals are recorded below the expanded trace (seconds).

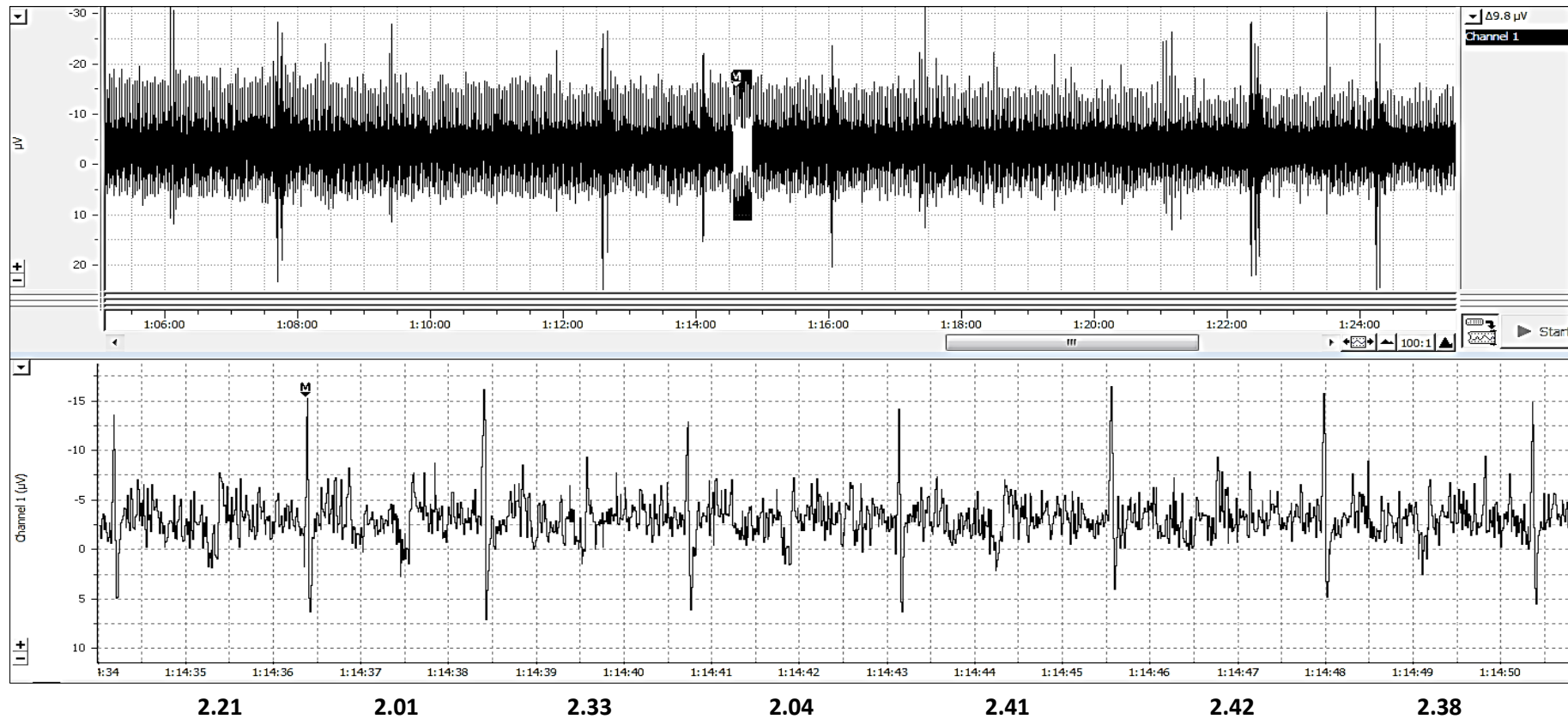
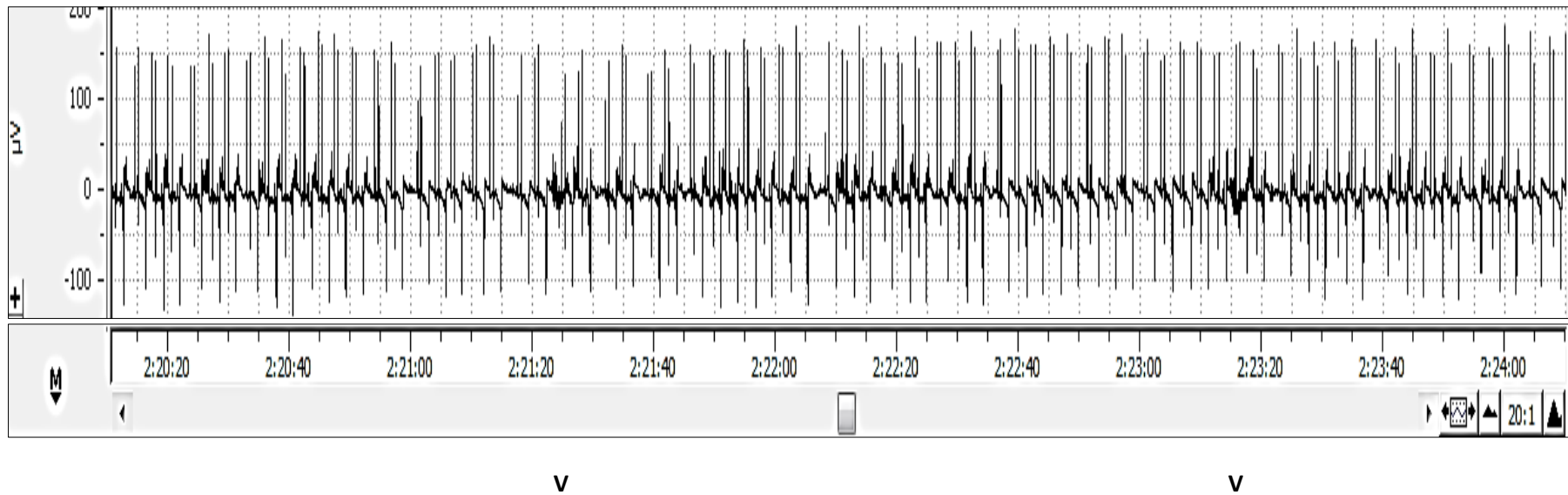




Figure 8-7. Bradycardia and tachycardia in the metamorphosed axolotl.

(B) An example of heart rate variability in another metamorphosed axolotl. There is clear variation between the two ventilations, marked underneath by 'V'. (9 days post-surgery.)



**Figure 8-7. Bradycardia and tachycardia in the metamorphosed axolotl.**

(C) This is the same animal as in Figure 7(B), but 26 days post-surgery. The inverted colour section in the middle trace was magnified (bottom trace) to digitally measure the R-R intervals using ChartLab. The time period between R-R values are written underneath the bottom trace (seconds), starting with the furthest left of the two spikes. The upper trace is the raw ECG; the middle trace was digitally filtered (band-pass) for smoothing. (Discrepancies in exact electrode placement can produce double spikes as seen in this trace.)

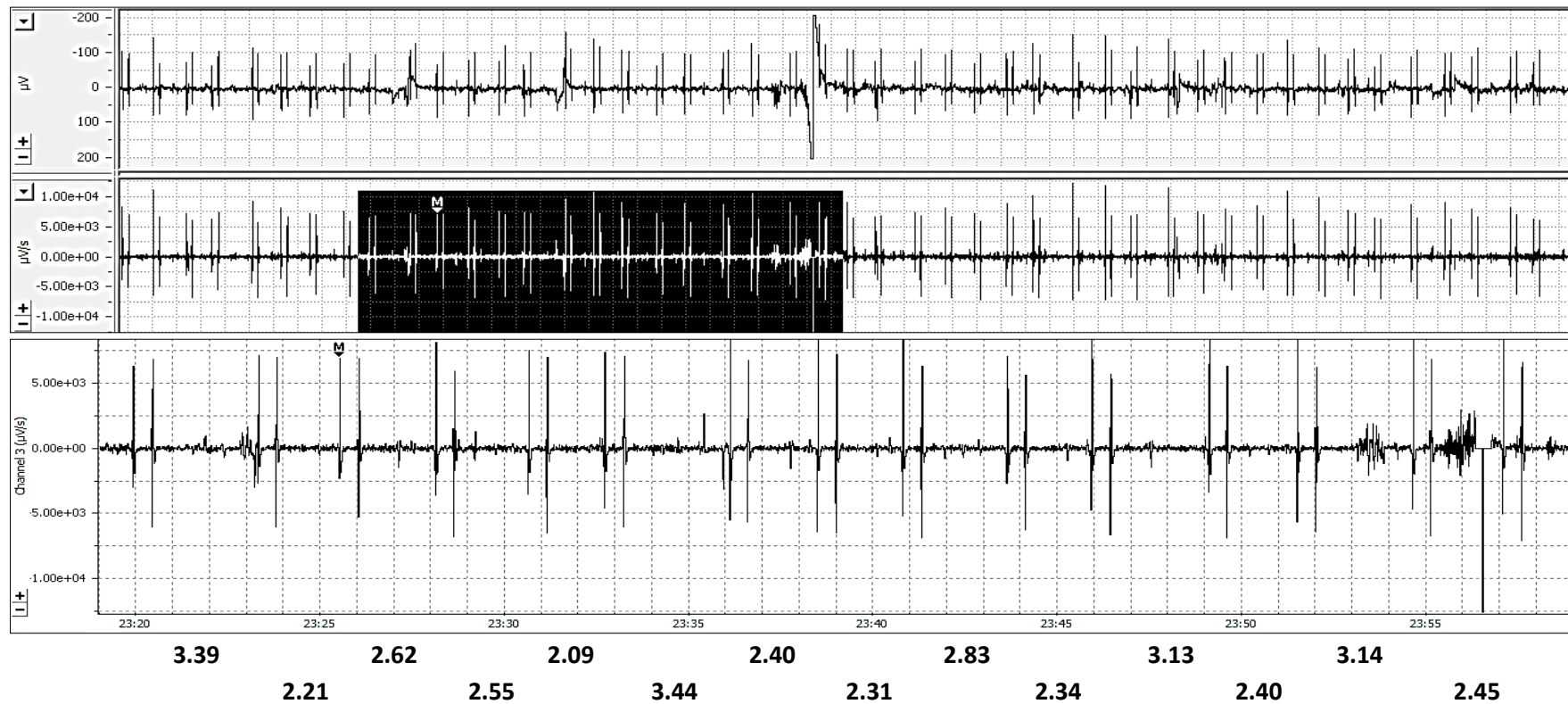
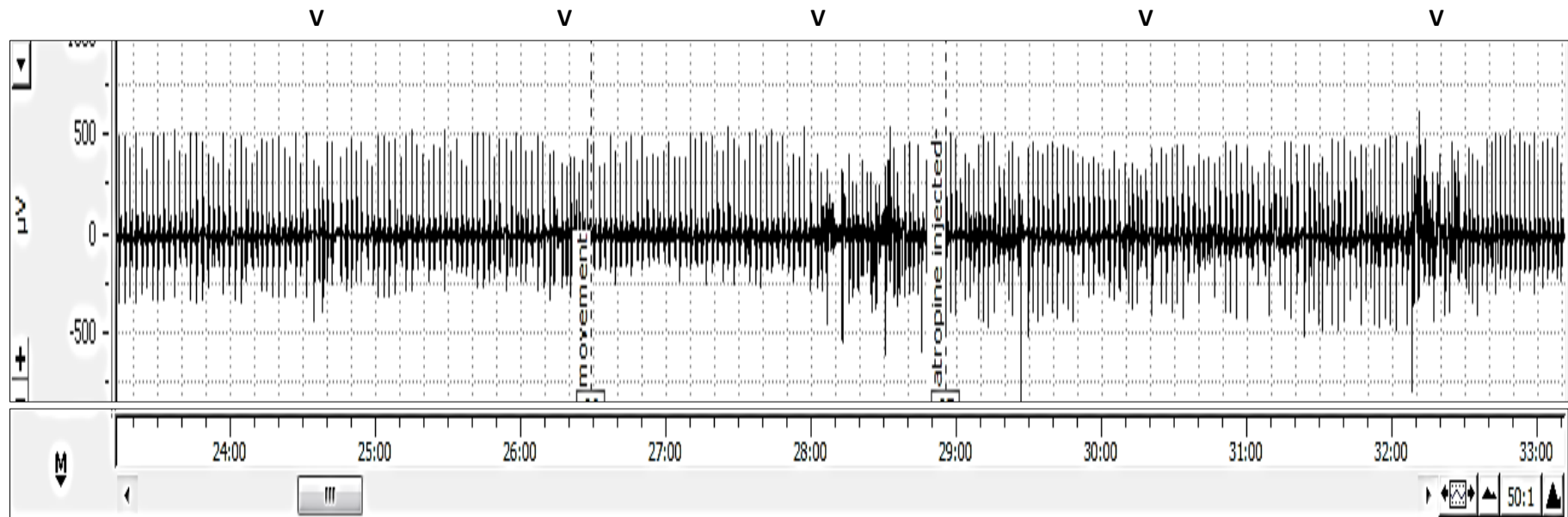


Figure 8-8. The effect of atropine on the heart rate and ventilation rate of a metamorphosed axolotl. (24h post-surgery.)

(A) Just prior to atropine administration. Bradycardia is followed by tachycardia. The axolotl ventilated (V) at approximately 2 minute intervals ( $30 \text{ hour}^{-1}$ ). The heart rate before atropine was 27 bpm. Atropine was injected at 28 minutes, 50 seconds on this ECG trace.



**Figure 8-8. The effect of atropine on the heart rate and ventilation rate of a metamorphosed axolotl. (24h post-surgery.)**

(B) Chart starts at 4 minutes post atropine injection and at this time the heart rate rose to 33 bpm. Heart rate variability (HRV) is apparent before 37 minutes on the chart scale, but is not afterwards. Ventilation could not be observed until 40.4 minutes, although the ECG trace may have picked one up at 34 minutes. The heart rate at 39 minutes was 30 bpm.

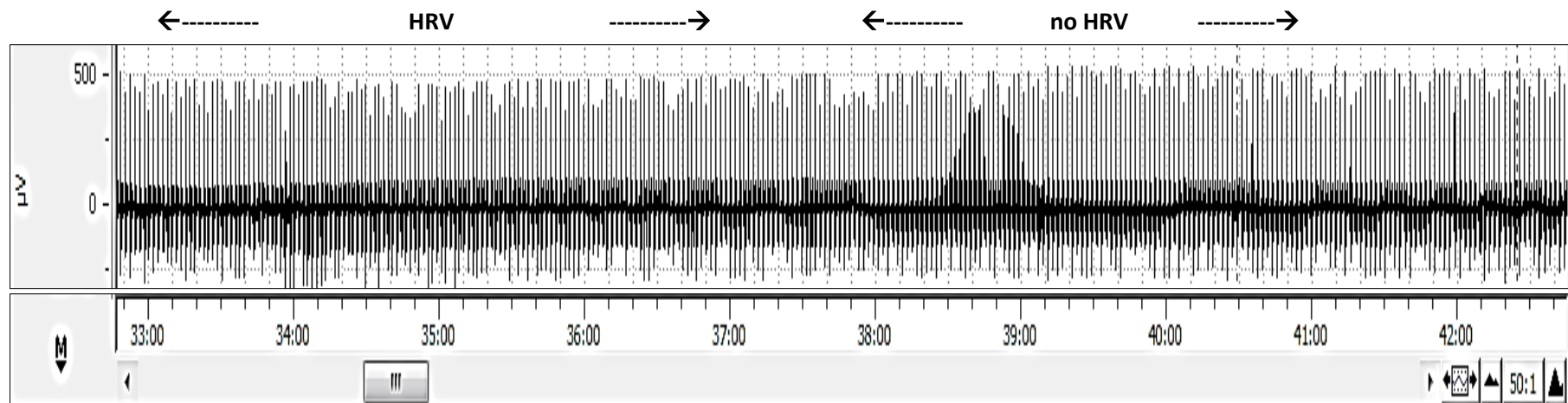


**Figure 8-8. The effect of atropine on the heart rate and ventilation rate of a metamorphosed axolotl. (24h post-surgery.)**

(C) Chart starts at 13 minutes post atropine injection. The heart rate at 49 minutes (on chart scale) was 27 bpm. The ventilation rate (V) is still 30 per hour. There was some bradycardia and tachycardia, although it was not as pronounced as that seen before atropine (Figure 8(A)).

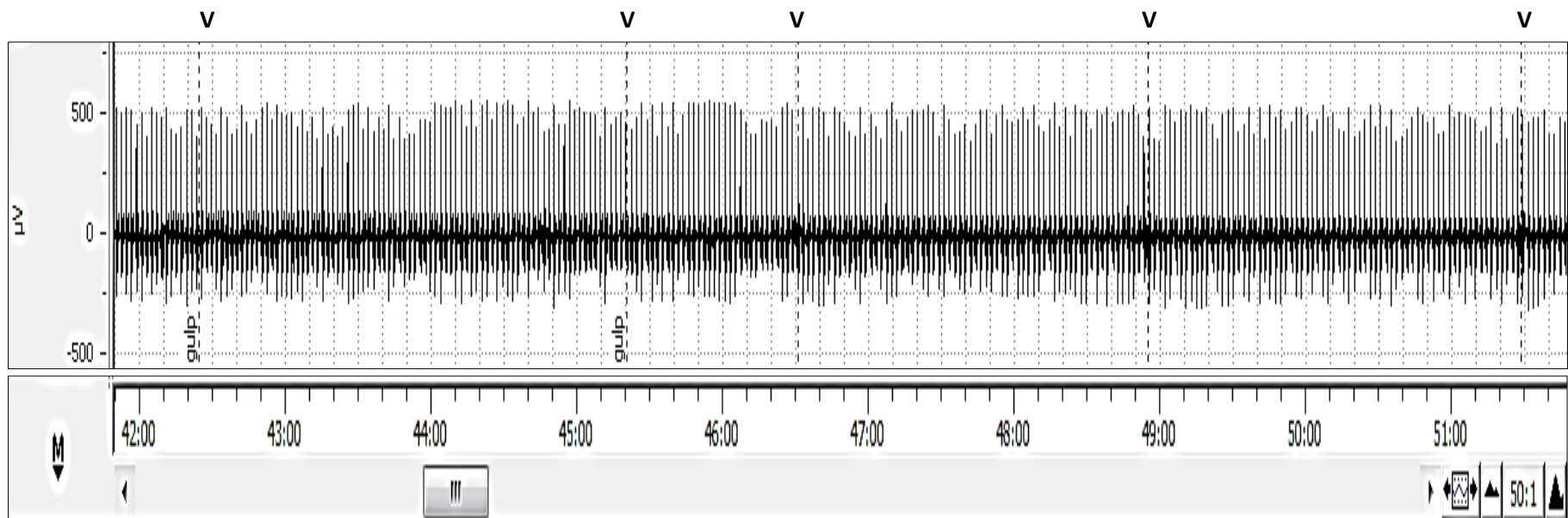


**Figure 8-8. The effect of atropine on the heart rate and ventilation rate of a metamorphosed axolotl. (24h post-surgery.)**

D) Chart starts at 22 minutes post atropine injection. At the 1 hour mark of the chart, the heart rate was 28 bpm and the ventilation rate (V) in this trace is 18 per hour.

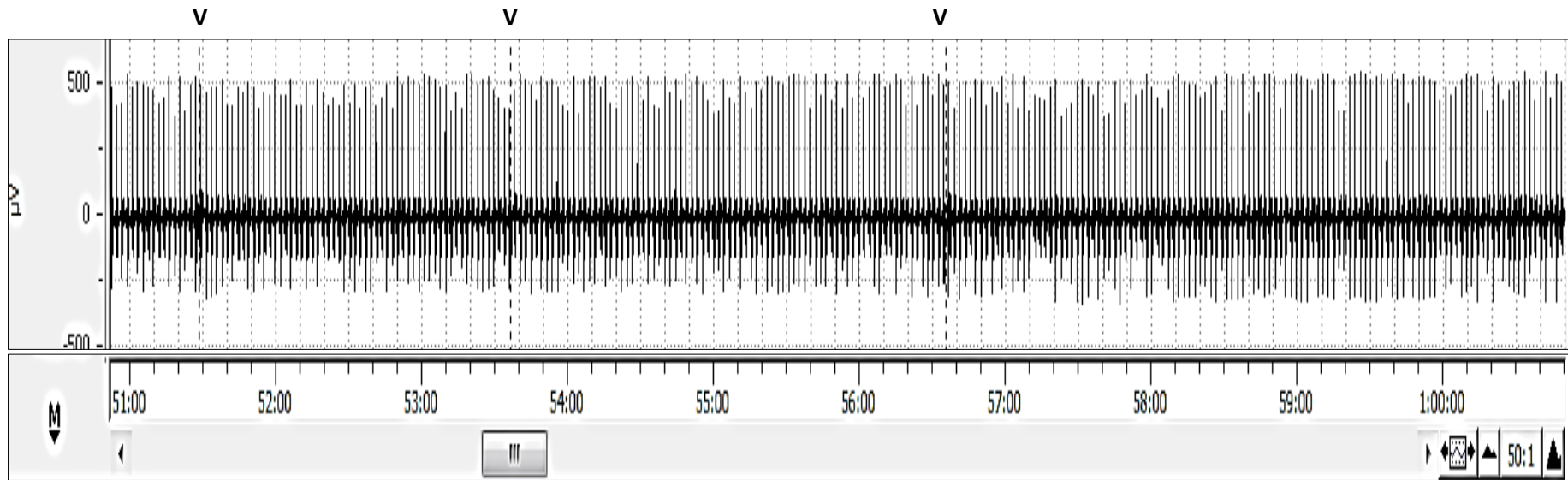
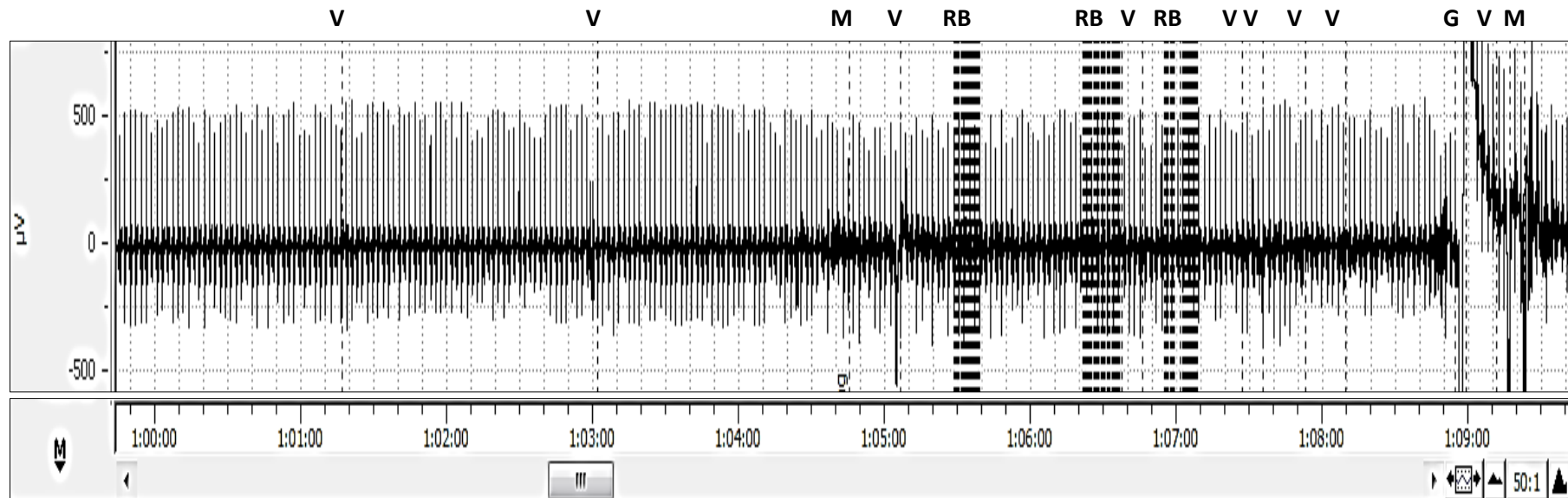


Figure 8-8. The effect of atropine on the heart rate and ventilation rate of a metamorphosed axolotl. (24h post-surgery.)

(E) Chart starts at 31 minutes post atropine injection. The heart rate was 28 bpm in this trace. The ventilation rate increased to 48 per hour, which includes one episode of gaping (G) that looked like yawning near 1h 9min on the scale. There were some very rapid buccal movements (RB) and are separate from ventilation (V). The chart shows there was some brady- and tachy-cardia. (M – movement.)



**Figure 8-8. The effect of atropine on the heart rate and ventilation rate of a metamorphosed axolotl. (24h post-surgery.)**

(F) Chart starts at 40 minutes post atropine injection. The heart rate was 26 bpm in this trace. The ventilation rate (V) decreased to  $42 \text{ h}^{-1}$ , and the axolotl moved around a lot. The brady- / tachy-cardia resemble that seen before atropine injection (Figure 8(A)) with relatively long bradycardic episodes. The ventilation rate is still higher than with no drug intervention. The RB denotes rapid buccal movements; M – movement.

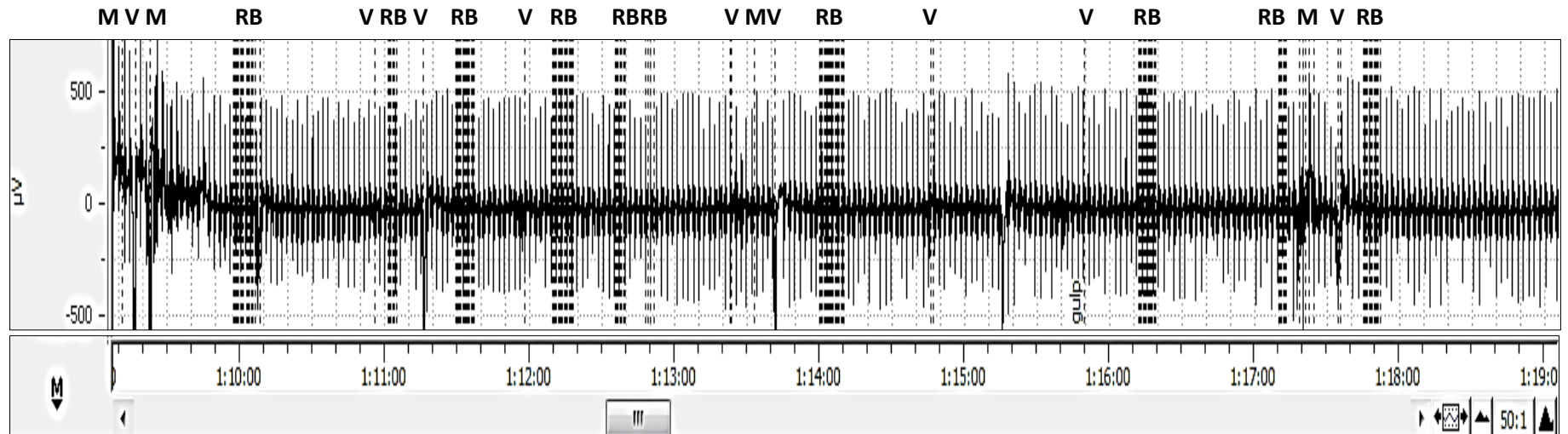




**Figure 8-9. The effect of propranolol on the heart and ventilation rate of a metamorphosed axolotl.** Atropine was administered 75 mins before propranolol. (25h post-surgery.)

(A) Propranolol administration. The heart rate just before the injection was 28 bpm. Within 3 minutes of propranolol injection the heart rate reduced to 26 beats  $\text{min}^{-1}$ . The ventilation rate (V) was 18 per hour. The interval between the ventilation was therefore longer at just over 3 minutes.

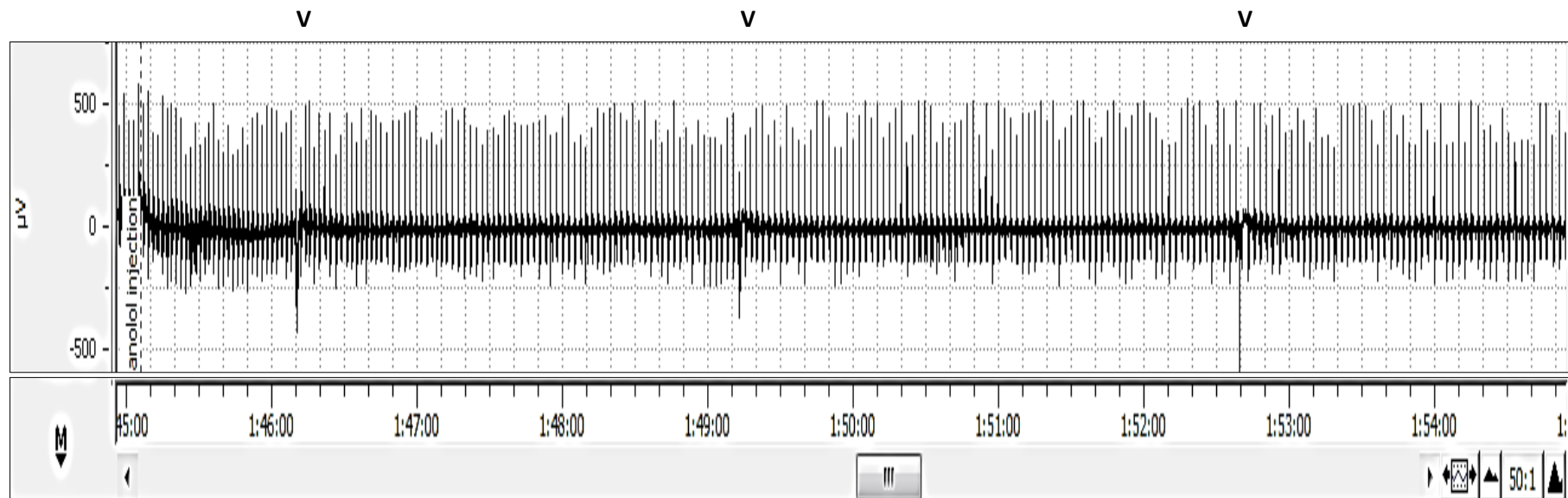


**Figure 8-9. The effect of propranolol on the heart and ventilation rate of a metamorphosed axolotl.** Atropine was administered 75 mins before propranolol. (25h post-surgery.)

(B) The chart starts at 9 minutes post propranolol injection. The heart rate was at 22 bpm, and the ventilation rate in this axolotl reduced to 12 per hour (marked V).

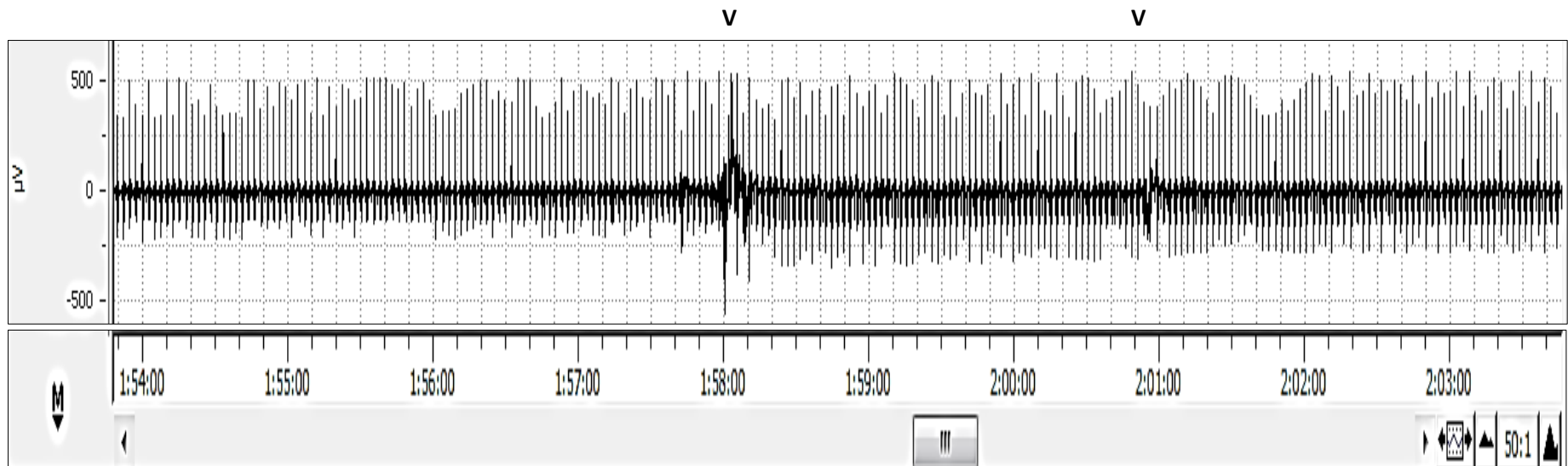


**Figure 8-9. The effect of propranolol on the heart and ventilation rate of a metamorphosed axolotl.** Atropine was administered 75 mins before propranolol. (25h post-surgery.)

(C) The heart rate remained at 22 bpm after 18mins post propranolol administration. There were no obvious bradycardia and tachycardia, except for the bradycardia at 2h 9m 40s that followed the deep ventilation. There were a few ventilation bouts (V) and the rate for this period was 24 per hour.

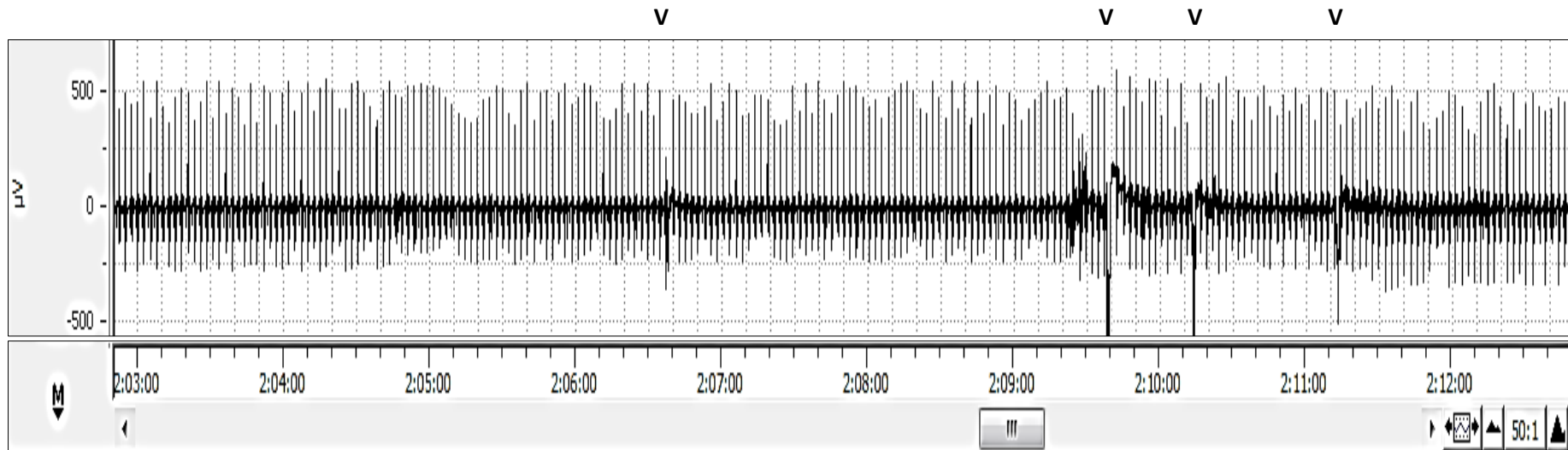


**Figure 8-9. The effect of propranolol on the heart and ventilation rate of a metamorphosed axolotl.** Atropine was administered 75 mins before propranolol. (25h post-surgery.)

(D) The heart rate remained at 22 bpm after 45 minutes post injection. There was a bradycardia (b) at 2h 39m (chart scale) following a deep ventilation (V), and there were 5 ventilations in total ( $30 \text{ hour}^{-1}$ ) on this trace.

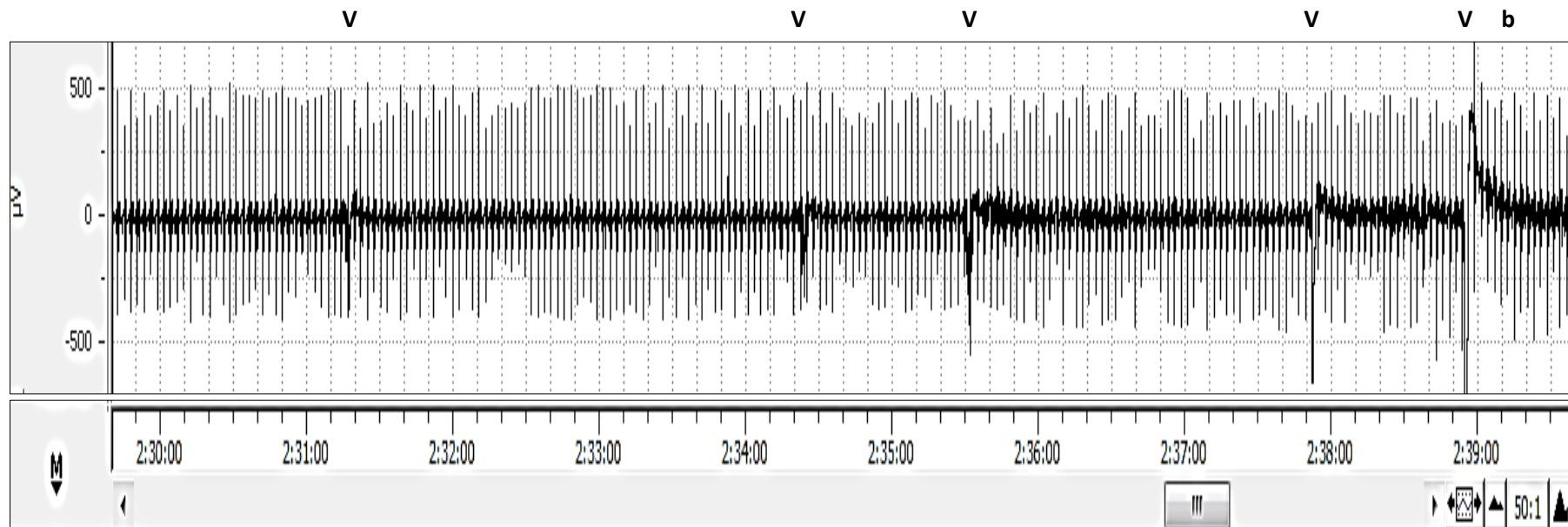


**Figure 8-9. The effect of propranolol on the heart and ventilation rate of a metamorphosed axolotl.** Atropine was administered 75 mins before propranolol. (25h post-surgery.)

(E) ECG trace at 54–64 minutes post propranolol injection. There was no change in the heart rate (22bpm). There are clear bradycardia (b) episodes following deep ventilation (V) and then tachycardia (t). The ventilation rate in this trace is  $24 \text{ hour}^{-1}$ , but was 18 breaths per hour after 75 mins post injection (Figure 9(F) inclusive). (Some of the bradycardia and tachycardia are labelled to highlight their appearance on this trace.)

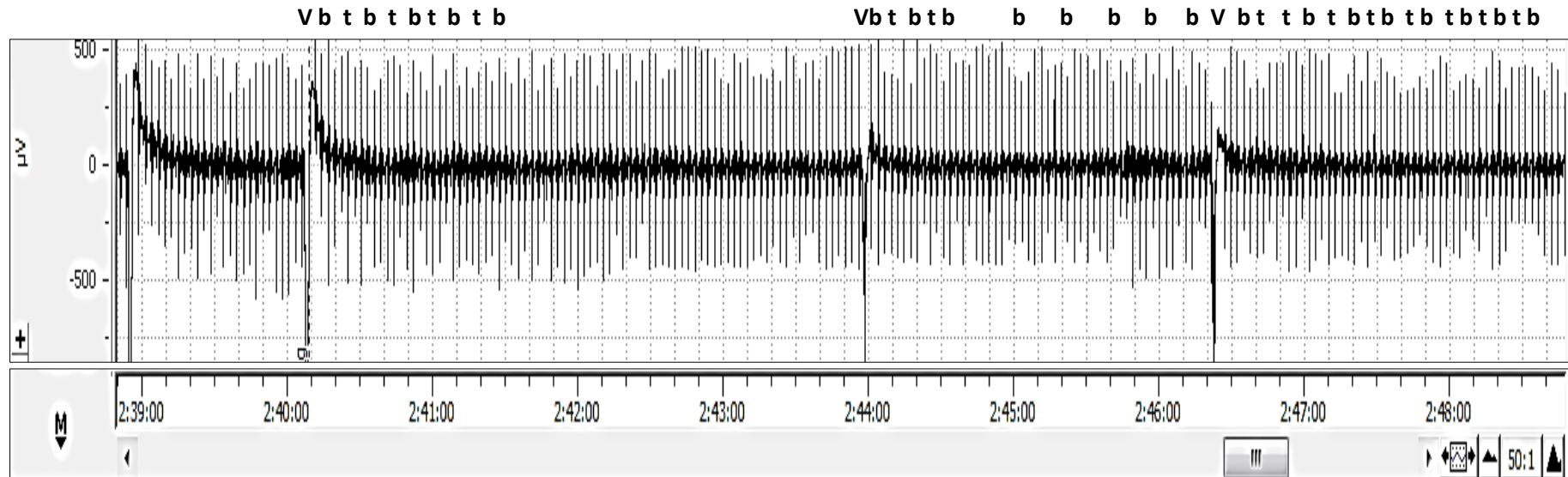


**Figure 8-9. The effect of propranolol on the heart and ventilation rate of a metamorphosed axolotl.** Atropine was administered 75 mins before propranolol. (25h post-surgery.)

(F) Chart begins at 1hr 8 mins post propranolol injection. The heart rate has been unchanged since the first decrease 9 mins after the injection (Figure 9(B)) and remained at  $22 \text{ beats min}^{-1}$ . Ventilation rate was 18 breaths per hour, thus unchanged since 75 mins post propranolol introduction. The upper chart is the raw ECG trace; the lower chart is derived (derivative function on ChartLab software) from the raw data and is presented as it shows the tachycardia/bradycardia (t, b) episodes more clearly when the RR spikes are almost the same height. (V – ventilation.)

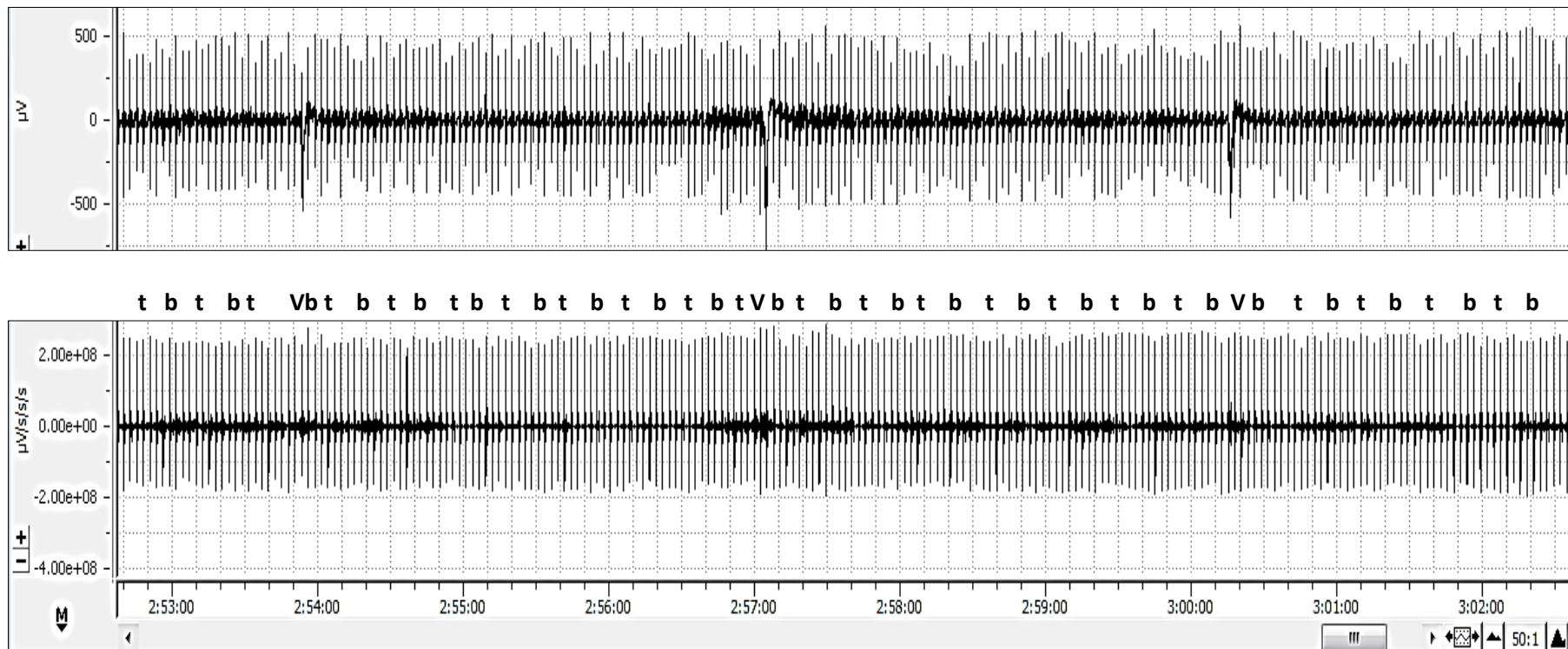


**Figure 8-10. Heart rate variability in the metamorphosed axolotl.** This is the same animal as used in Figures 8 and 9. (8 days post-surgery.) ECG trace showing a relatively long RR interval (bradycardia (b)) after ventilation (V). There was a short delay after the ventilation before bradycardia that was immediately followed by tachycardia (t). The vertical dashed lines in the upper chart are regular buccal movements (RB). These were marked to check they did not conflict with the ECG or ventilation traces. The top chart is digitally filtered (high-pass) and the lower chart is the derivative of the upper chart which is presented solely for ease of visualisation of oscillations.

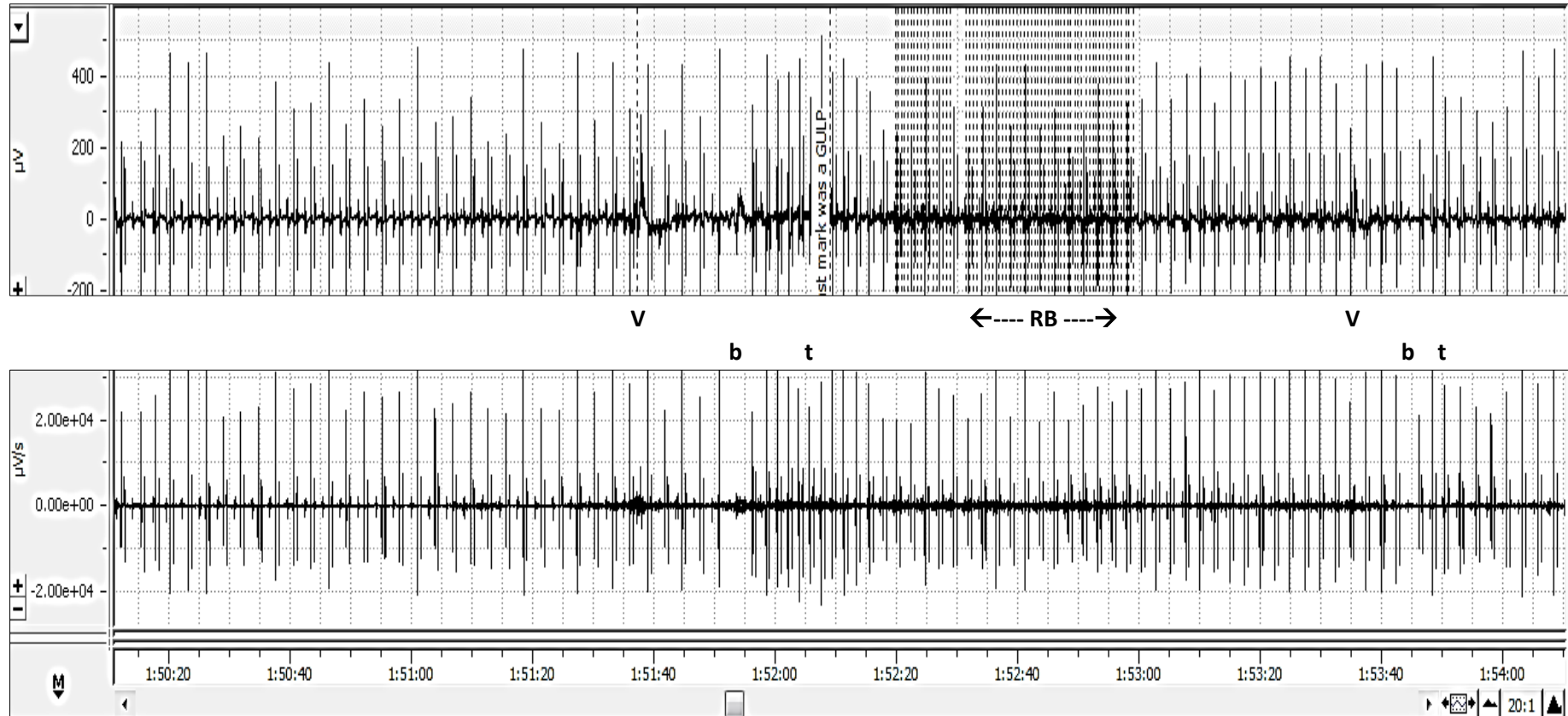
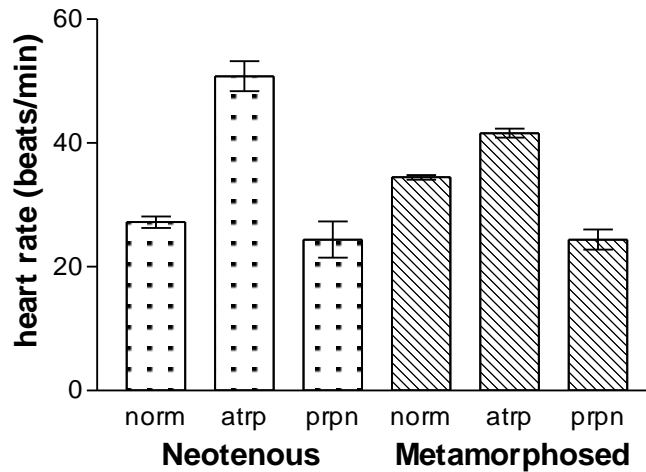


**Figure 8-11. The effect of atropine and propranolol on the heart rate of the neotenus and the metamorphosed axolotl ( $n = 5$  each). Heart rate rose in both after atropine and decreased to lower than resting level following propranolol.**



Means ( $\pm$ SE) are:

***Neotenus***

Normal heart rate  $27.20 \pm 0.92$ ; atropinised  $50.8 \pm 2.4$ ; propranolised  $24.4 \pm 2.9$

Paired t-test showed there was significant difference between normal and atropinised heart rate ( $p < 0.05$ ), but not between normal and propranolised ( $p = 0.12$ )

***Metamorphosed***

Normal heart rate  $34.47 \pm 0.38$ ; atropinised  $41.6 \pm 0.7$ ; propranolised  $24.4 \pm 1.6$

Paired t-test showed there was significant difference between normal and atropinised heart rate ( $p < 0.05$ ) and between normal and propranolised ( $p < 0.05$ )

Unpaired t-test showed there was a significant difference in the resting neotenus and metamorphosed heart rates ( $p < 0.05$ ).



**Figure 8-12. Tachograms of the neotenus and metamorphosed axolotl.**

(A) The neotenus HR shows an oscillatory pattern that with a relatively high amplitude in the short term range (beat to beat) but in the long term range it is fairly stable at around  $3000 \pm 1000$  milliseconds, with the exception of beat 151, which may be an artefact caused by axolotl movement. Note that 161 beats would represent about 8 minutes of recording in the neotenus.

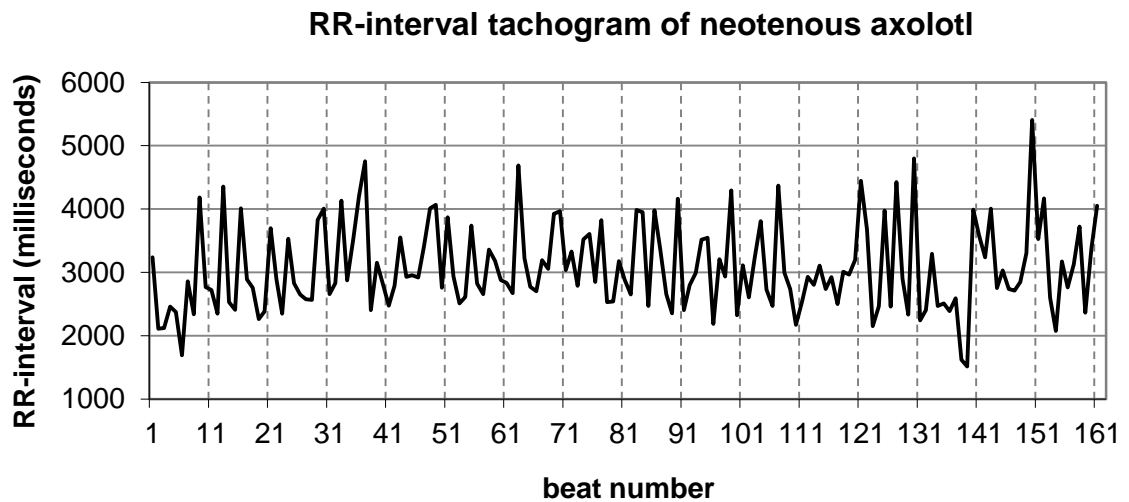
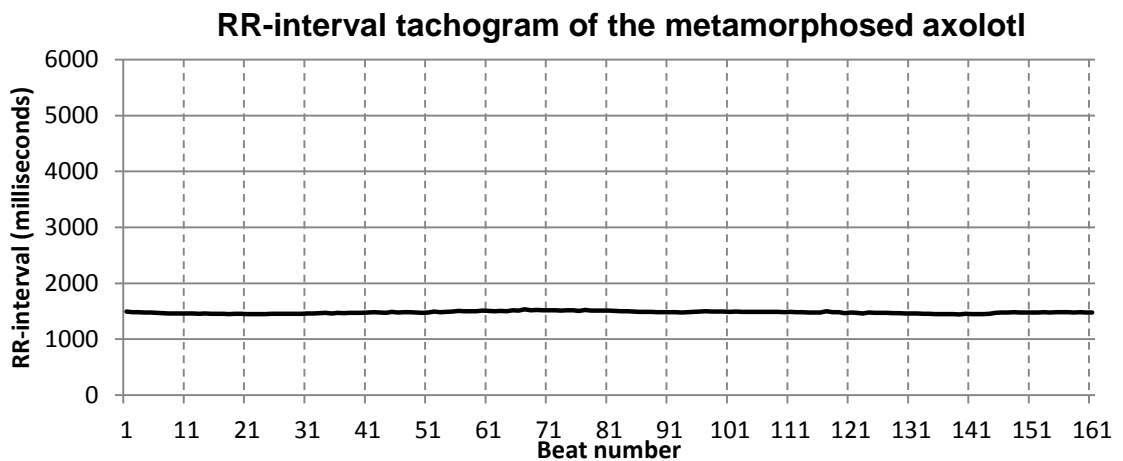


Figure 8-12. Tachograms of the neotenus and metamorphosed axolotl.

(B) The RR-intervals for the metamorphosed axolotl are less fluctuating over the same number of beats. The HR appears to be under more regulation in comparison to the neotenus. Note that 161 beats would represent about 4 minutes of recording in the metamorphosed.



(C) When the y-axis is expanded a 'drifting' RR-interval is evident, indicative of some regulatory mechanism that attempts to maintain homeostasis. Note that 161 beats would represent about 4 minutes of recording in the metamorphosed.

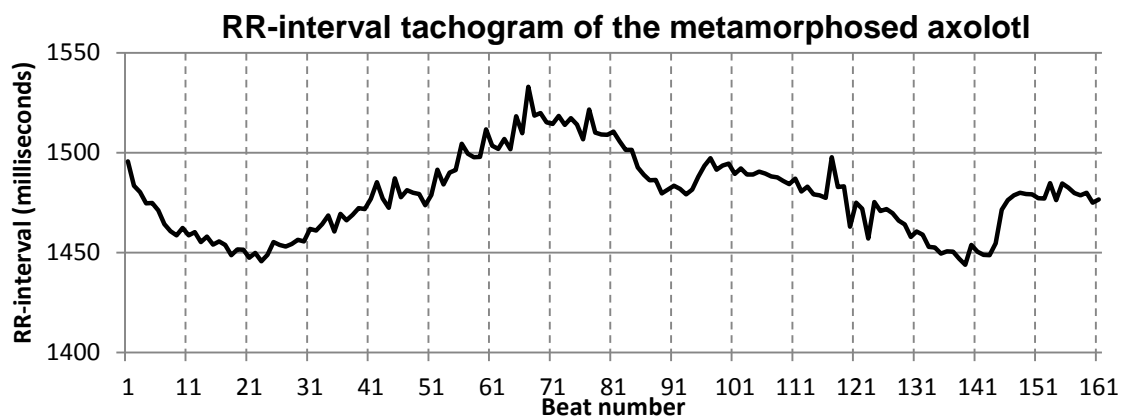


Figure 8-12. Tachograms of metamorphosed and neotenuous axolotl.

(D) The arrows indicate where the animal ventilated. Over the short term, between ventilation bouts, there is a brief increase in the RR-interval, indicative of bradycardia. This follows tachycardia/bradycardia oscillations. The ventilation bouts occur approximately every 88 beats, which is around every 2 minutes. This long term trace (571 beats, ~ 14 minutes) shows variation in RR-intervals of  $1550 \pm 1000$  ms, similar to the neotenuous, but the variation is of a 'drifting' nature.

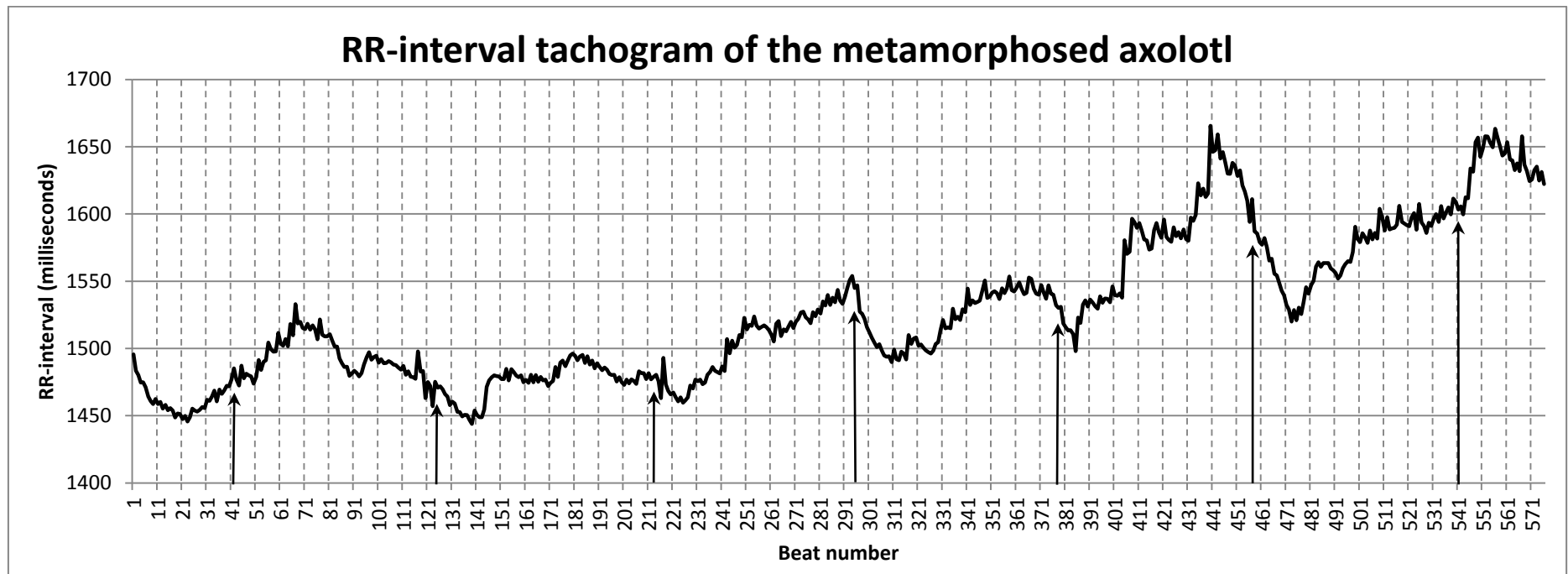
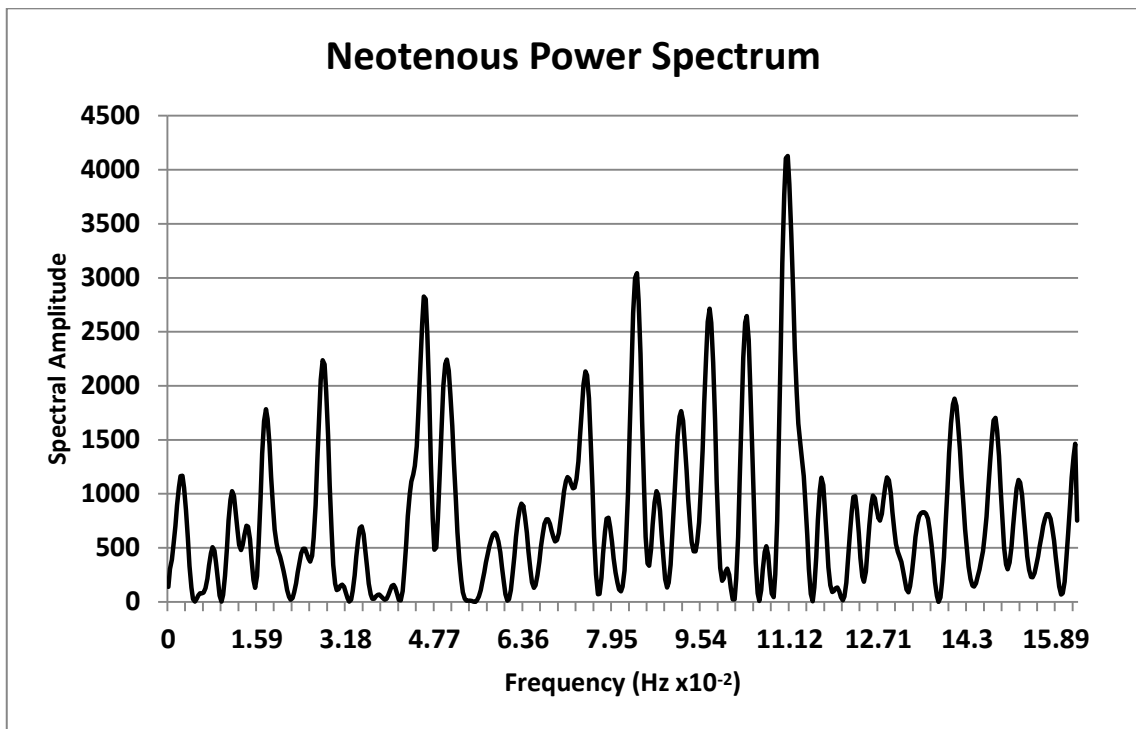
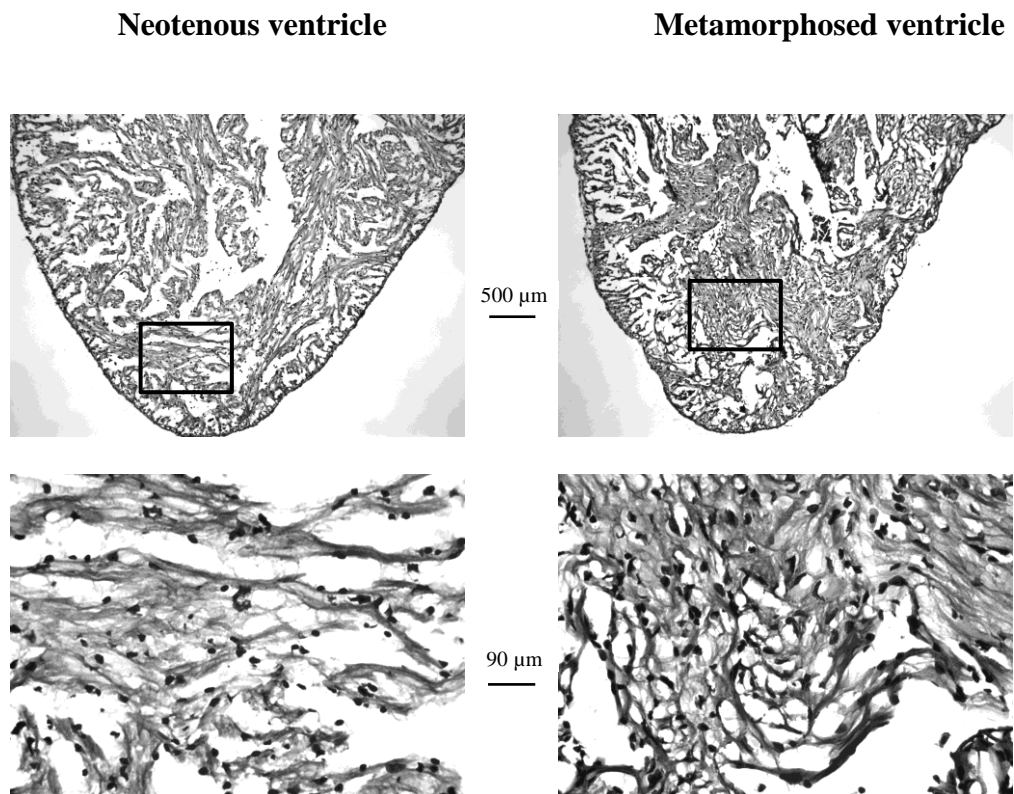


Figure 8-13. Power spectrum analysis of a neotenus axolotl. The data was taken from tachogram (Figure 8-12(A)).



**Figure 8-14. Haematoxylin and eosin staining of neotenuous and metamorphosed axolotl hearts.** The neotenuous heart has a ‘spongy’ ventricle with generally disorganised myofibrils. Since the neotenuous axolotls have gills and can respire cutaneously too, it is not so important that the heart be as functionally effective as a metamorphosed axolotl. The metamorphosed axolotl becomes a committed lung breather and so would need a more robust pump to circulate oxygenated blood. Consequently, the metamorphosed heart shows more organised myofibrils and an increase in trabeculation in comparison with the neotenuous. (See Appendix for staining details.)



Boxed areas in the upper images are the enlarged sections in the lower images.

## CHAPTER NINE

### CONCLUDING REMARKS AND FUTURE DIRECTIONS

In Part I of the thesis the embryonic axolotl (*Ambystoma mexicanum*) heart was found to be a very useful model in which to study the role of tropomyosin in myofibrillogenesis. The hearts of *cardiac* mutant axolotls are an ideal system for studying myofibrillogenesis in vitro because they are deficient in the sarcomeric tropomyosin protein, which results in the disarray of myofibrils. Furthermore, the mutant embryos survive for a short period of time without establishing normal circulation. Tropomyosin is a ~70 kDa coiled dimer that acts in close association with actin and troponin units. Together, these proteins are involved with contraction and relaxation of myofibrils. Three isoforms of axolotl tropomyosin have been identified and were used (ATmC-1, ATmC-2, ATmC-3).

A delivery system, using cationic liposome transfection was found to be an effective tool for the introduction of nucleic acids into the embryonic cardiac cells. The use of anti-sense oligonucleotide mediated inhibition of mRNA expression has proven useful in determining what role a particular protein may play in cellular functions. Thus, this method was used to either promote, when using mutant hearts, or block, in wild-type hearts, the expression of the tropomyosin isoforms. Thus it was found that tropomyosin has a significant role in the promotion of myofibrillogenesis. Axolotl tropomyosin isoforms were found to be heart

region specific. The ATmC-1 isoform affected the outflow tract area and ATmC-3 is important in ventricular myofibrils and functional beating of the heart.

The structure-function role of tropomyosin was also examined, i.e., did alterations in tropomyosin structure affect myofibrillogenesis? Previous studies focused on modification of just one end of the tropomyosin protein. In this study, both, the 5' and 3' ends, were modified and it was found that it did not affect myofibrillogenesis.

With the finding of the novel human tropomyosin isoform TPM1 $\kappa$  (*TPM1* gene), and now knowing that it can effect myofibrillogenesis in the axolotls, means that the *cardiac* mutant model can be used for the study of heritable cardiomyopathies in man that are caused by mutated tropomyosin. For instance, a mutation in one of the alleles of the *TPM1* gene is known to cause familial hypertrophic cardiomyopathies, and, moreover, a subset of these causes sudden death in young adults.

Part II of the thesis looked at the cardiorespiratory interactions associated with metamorphosis. The neuroanatomy work showed that there is a new group of vagal preganglionic neurones in the ventral lateral location post metamorphosis. It is not definitive to know from this study if these cells are *de novo* (by mitosis, perhaps?) or indeed they are the immature, blast-like cells that have migrated from the central grey and differentiated. A more specific marker for both migration and mitosis would be useful to use in the future in order to find out.

The heart rate work showed that the metamorphosed axolotls (now obligate lung breathers) do indeed show heart rate variability which is caused by fluctuations in vagal tone. However the pattern was not the same as that seen in humans where upon inspiration the heart rate rises. In the metamorphosed axolotl there appeared to be a bradycardia before the tachycardia.

For both Part I and Part II there is plenty of scope for more work for greater understanding. The embryonic heart work could be clinically significant in the future, but also on an academic level to understand how exactly the tropomyosin promotes myofibrillogenesis. The heart rate variability of the metamorphosed axolotls is most intriguing and has not been studied in close detail before. Further work could look at the causes of the oscillatory bradycardia and tachycardia seen between the ventilation bouts. It is likely that, as of yet unknown, mechanoreceptors and chemoreceptors that would contribute to the fine tuning of cardiorespiratory control required for an obligate lung breather.



## APPENDIX

### **Haematoxylin and Eosin Staining Method**

The five to six inch long salamanders, *Ambystoma mexicanum*, were obtained from the Indiana Axolotl Colony. To induce metamorphosis the axolotls were intraperitoneally injected with thyroxin (Sigma) at a concentration of 2µg per gram body weight. The control neotenus axolotls were not injected. Complete metamorphosis was determined by the total loss of gills and the axolotls spending most, if not all, its time on land. This change took 30 days and resulted in a 30% loss in weight. During the same period the neotenus axolotls gained a 30% body weight. The mid-metamorphic stage was determined visually by observation of the length of gill stub which reduced to 0.5cm. This stage took 18 days and resulted in a 10% weight loss.

### **Tissue preparation**

Hearts were dissected and immediately fixed in 4% paraformaldehyde and left o/n. The following day they were transferred into 10% sucrose made in phosphate buffer (pH 7.2) and left o/n. The hearts were placed in embedding media (OCT) and cooled gently over dry ice and then transferred to -20°C o/n. They were then stored in -70°C until ready for use. Sections were cut at 14 µm using a 2800 Frigocut N cryostat.

### **H & E staining**

Heart sections were stained using a standard H&E staining protocol with Gills No.1 Haematoxylin (6 mins) and Chromotrope 2R (3 mins). The sections were mounted using Permount<sup>®</sup>.

## REFERENCES AND BIBLIOGRAPHY

- Akhavan, M., Hoang, T.X. & Havton, L.A. (2006) Improved detection of fluorogold-labeled neurons in long-term studies. *J Neurosci Methods*. **152**:156-162.
- Ambalavanar R & Morris, R. (1989) Fluoro-Gold injected either subcutaneously or intravascularly results in extensive retrograde labelling of CNS neurones having axons terminating outside the blood-brain barrier. *Brain Research*. **505**; 171-175.
- Anrep, G.V., Pascual, W. & Rossler, R. (1936) Respiratory variations of the heart rate. The central mechanism of sinus arrhythmia and the interrelationships between central and reflex mechanisms. *Proc. Roy. Soc. London Series* **B119**: 218-230.
- Armstrong, J. B. (1989) A Turing model to explain heart development. *Axolotl. Newslett.* **18**, 23-25.
- Armstrong, J. B. & Malacinski, G. M. (1989) *Developmental Biology of the Axolotl*. Oxford University Press.
- Asashima, M., Malacinski, G.M. & Smith, S.C. (1989) Surgical manipulation of embryos. In J.B. Armstrong and G.M. Malacinski (eds.), *Developmental Biology of the Axolotl*. Oxford University Press, New York. pp. 255-263.
- Augustinsson, A., Fange, R., Johnels, A. & Ostlund, E. (1956) Histological physiological and biochemical studies on the heart of two cyclostomes, hagfish (*Myxine*) and lamprey (*Lampetra*). *J. Physiol.* **131**, 257-276.
- Bainbridge, F.A. (1915) The influence of venous filling upon the rate of the heart. *J. Physiol.* **50**, 65-84.
- Baruscotti M, Bucchi A, DiFrancesco D. (2005) Physiology and pharmacology of the cardiac pacemaker ("funny") current. *Pharmacol Ther.* **107**:59-79.
- Bell, P., Rundquist, I., Svensson, I., and Collins, V.P. (1987) Use of cytofluorometry to evaluate binding of antibodies to the cytoskeleton of cultured cells. *J. Histochem. Cytochem.* **35**: 1381-1388.
- Bennett, J.A., Kidd, C., Latif, A.b. & McWilliam, P.N. (1981) A horseradish peroxidase study of vagal motoneurons with axons in cardiac and pulmonary branches of the cat and dog. *Q. J. Exp. Physiol.* **66**: 145-154

- Bennett, T. (1974) Peripheral and autonomic nervous systems. In: *Avian Biology*, vol. IV. (eds. D. S. Farner, J. S. King and K. C. Parkes) pp 1-77. Academic Press, London, New York,
- Berger, P. J. & Burnstock, G. (1979) Autonomic nervous system In: *Biology of the Reptilia*, Vol. X. (ed. C. Gans), pp. 1-57. Academic Press, London, New York.
- Bathula, R., Hughes, A.D., Panerai, R., Potter, J., Thom, S.A., Francis, D.P., Shore, A.C., Kooner, J. & Chaturvedi, N. (2010) Indian Asians have poorer cardiovascular autonomic function than Europeans: this is due to greater hyperglycaemia and may contribute to their greater risk of heart disease. *Diabetologia*. **53**:2120-8.
- Bhatia, R., Dube, D.K., & Lemanski, L.F. (1996) Nucleotide sequence and expression of ribosomal protein S3 mRNA during embryogenesis in the Mexican axolotl (*Ambystoma mexicanum*). *Biochem. & Mol. Biol. Int.* **38**, 1079-1085.
- Bhatia, R., Gaur, A., Lemanski, L. F. and Dube, D. K. (1998) Cloning and sequencing of the cDNA for an RNA-binding protein from the Mexican axolotl: binding affinity of the in vitro synthesized protein. *Biochem. Biophys. Acta.* **1398**, 265-274.
- Bidder, F. (1868) Die Endigungweise der Herzzweige des N. vagus beim Frosch. *Arch. Anat. Physiol. Wiss. Med.* 1-50.
- Bogdanov, K.Y., Vinogradova, T.M. & Lakatta, E.G. (2001) Sinoatrial nodal cell ryanodine receptor and Na-Ca exchanger: molecular partners in pacemaker regulation. *Circ. Res.* **88**:1254–1258.
- Bolton, T. B. (1971) The structure of the nervous system. In: *Physiology and Biochemistry of the Domestic Fowl*. (eds. D. J. Bell and B. M. Freeman), pp 641-673. Academic Press, London, New York.
- Bolton, T. B. & Raper, C. (1966) Innervation of the domestic fowl and the guinea pig ventricles. *J. Pharm. Pharmacol.* **18**, 192-193.
- Bordzilovskaya, N., Detlaff, T. A., Duhon, S. and Malacinski, G. M. (1989) Developmental-stage series of axolotl embryos. In: *Developmental Biology of the Axolotl*. (ed. J. B. Armstrong and G. M. Malacinski), pp. 201-221. Oxford University Press, New York.

- Bordzilovskaya, N.P., Detlaff, T.A., Duhon, S.T. and Malacinski, G.M. (1989). Developmental stage series of axolotl embryos. In: Armstrong J. B., Malacinski G.M., editors. *Developmental biology of the axolotl*. Oxford: Oxford Press. pp 201–219.
- Bottinelli, R., Coviello, D.A., Redwood, C.S., Pellegrino, M.A., Maron, B.J., Spirito, P., Watkins, H. and Reggiani, C.R. (1997) A mutant tropomyosin that causes hypertrophic cardiomyopathy is expressed in vivo and associated with an increased calcium sensitivity, *Circ. Res.* **82**:106–115.
- Brainerd, E.L. & Owerkowicz, T. (2006) Functional morphology and evolution of aspiration breathing in tetrapods. *Respir. Physiol. Neurobiol.* **154**: 73–88.
- Bray, D & Hollenbeck, P. J. (1989) Growth cone motility and guidance. *Annu. Rev. Cell Biol.* **4**, 43-61.
- Brown, D.D. (1997) The role of thyroid hormone in zebrafish and axolotl development. *Proc Natl Acad Sci U S A.* **94**:13011-6.
- Brown, J.W. (1990) Prenatal development of the human nucleus ambiguus during the embryonic and early fetal periods. *Am J Anat.* **189**:267-83.
- Butler, P. J. & Jones, D. R. (1982) The comparative physiology of diving in vertebrates. *Adv. Comp. Physiol. Biochem.* **8**, 179-364.
- Bucchi A, Barbuti A, Baruscotti M, DiFrancesco D. (2007) Heart rate reduction via selective 'funny' channel blockers. *Curr Opin Pharmacol.* **7**:208–213.
- Campbell, G. (1970) Autonomic nervous systems. In: *Fish Physiology, vol. IV*. Eds. W. S. Hoar & D. J. Randall. Academic Press, London, New York. pp 109-132.
- Campbell, G., Gibbins, I. L., Morris, J. L., Furness, J. B., Costa, M., Oliver, A. M., Beardsley, A. M. & Murphy, R. (1982) Somatostatin is contained in and released from cholinergic nerves in the heart of the toad *Bufo marinus*. *Neuroscience* **7**, 2013-2023.
- Campbell, H.A., Taylor, E.W. & Egginton, S. (2004) The use of power spectral analysis to determine cardiorespiratory control in the short-horned sculpin *Myoxocephalus scorpius*. *J Exp Biol.* **207**:1969-76.

- Campbell, H. A. Leite, C. A.C., Wang, T., Skals, M., Abe, A. S., Egginton, S., Rantin, F. T., Bishop, C. M. and Taylor, E. W. (2006). Evidence for a respiratory component, similar to mammalian respiratory sinus arrhythmia, in the heart rate variability signal from the rattlesnake, *Crotalus durissus terrificus*. *J.exp. Biol.* **209**, 2628-2636.
- Campbell, N.A., Reece, J.B. & Mitchell, L.G. (1999) *Biology*. 5<sup>th</sup> Ed. Addison Wesley.
- Carlson, A. J. (1904) Contributions to the physiology of the heart of the California hagfish (*Bolellstoma dombeyi*). *A. Allg. Physiol.* **4**, 259-288.
- Chen, Y., Li, M., Liu, H. & Wang, J. (2007) The airway-related parasympathetic motoneurons in the ventrolateral medulla of newborn rats were dissociated anatomically and in functional control. *Exp Physiol.* **92**:99-108.
- Cheng, Z. & Powley, T.L. (2000) Nucleus ambiguus projections to cardiac ganglia of rat atria: an anterograde tracing study. *J Comp Neurol.* **424**:588-606.
- Cheng, Z., Powley, T.L., Schwaber, J.S. & Doyle, F.J. 3rd. (1997) Vagal afferent innervation of the atria of the rat heart reconstructed with confocal microscopy. *J Comp Neurol.* **381**:1-17.
- Cheng, Z., Powley, T.L., Schwaber, J.S. & Doyle, F.J. 3rd. (1999) Projections of the dorsal motor nucleus of the vagus to cardiac ganglia of rat atria: an anterograde tracing study. *J Comp Neurol.* **410**:320-341.
- Clayton, L. and Johnson, M.H. (1998) Tropomyosin in pre-implantation mouse development: identification, expression, and organization during cell division and polarization. *Exp. Cell Res.* **238**:450-464.
- Coker, R. Koziell, A. Oliver, C. & Smith, S.E. (1984) Does the sympathetic nervous system influence sinus arrhythmia in man? Evidence from combined autonomic blockade. *J. Physiol.* **356**, 459-464.
- Coleman, C.M. & Hessler, A.C. (1997) Thyroxine induced metamorphosis in a neotenic axolotl (*Ambystoma mexicanum*): gills, lungs, and capillaries. *Axolotl Newsletters* **26**: 4-9.
- Cooley, B.C. and Bergstrom, G. (2001) Multiple combinations of alternatively spliced exons in rat tropomyosin-a gene mRNA: Evidence for new isoforms in adult tissues and cultured cell. *Arch. Biochem. Biophys.* **390**:71-77.

- Crawford, K. & Vincenti, D.M. (1998) Retinoic acid and thyroid hormone may function through similar and competitive pathways in regenerating axolotls. *J Exp Zool.* **282**:724-38.
- Crossley, D. 2<sup>nd</sup>. & Altimiras, J. (2000) Ontogeny of cholinergic and adrenergic cardiovascular regulation in the domestic chicken (*Gallus gallus*). *Am J Physiol Regul Integr Comp Physiol.* **279**: R1091-8.
- Dabiri, G.A., Turnacioglu, K.K., Sanger, J.M. & Sanger, J.W. (1997) Myofibrillogenesis visualized in living embryonic cardiomyocytes. *Proc Natl Acad Sci U S A.* **94**:9493-8.
- Daly, M.D. & Jones, J.F. (1998) Respiratory modulation of carotid and aortic body reflex left ventricular inotropic responses in the cat. *J Physiol.* **509**:895-907.
- De Groeff, B., Darrass, V.M., Arckens, L., Gerets, H.H.J., Kuhn, E.R. & Geris, K.L. (2000) Changes of thyrotropin-releasing hormone (TRH) levels in brain regions and pituitary during induced metamorphosis of *Ambystoma mexicanum*. *Netherlands J Zool.* **50**: 343-354.
- Dergacheva, O., Griffioen, K.J., Neff, R.A. & Mendelowitz, D. (2010) Respiratory modulation of premotor cardiac vagal neurons in the brainstem. *Respir Physiol Neurobiol.* **174**:102-10.
- Denz, C. R., Narshi, A., Zajdel, R. W. and Dube, D. K. (2004) Expression of a novel cardiac-specific tropomyosin isoform in humans. *Biochem. Biophys. Res. Comm.* **320**: 1291-1297.
- Divon, M.Y., Kanter, Y. & Barzilai D. (1983) A simple test for autonomic neuropathy in diabetes. *J. Med. Sci.* **19**, 208-213.
- Drysdale, T.A., Tonissen, K.F., Patterson, K.D., Crawford, M.J. & Krieg, P.A. (1994) Cardiac troponin-I is a heart-specific marker in the *Xenopus* embryo - Expression during abnormal heart morphogenesis. *Dev. Biol.* **165**, 432-441.
- Duellman, W. E. and L. Trueb. (1986) *Biology of Amphibians*. McGraw-Hill, New York.
- Easton, H.S., Armstrong, J.B., & Smith, S.C. (1994) Heart specification in the Mexican axolotl (*Ambystoma mexicanum*). *Dev. Dyn.* **200**, 313-320.
- Ebashi, S. (1980) Regulation of Muscle Contraction. *Proc. Roy. Soc. Ser. B.* **207**: 259-286.
- Elliott, T. R. (1905) The action of adrenaline. *J. Physiol. (Lond.)* **32**, 401-467.

- Etkin, W. (1964) Metamorphosis. In: *Physiology of the Amphibia*. (ed. J. A. Moore), pp. 427-469. Academic Press, New York.
- Falck, B., Mecklenburg, C., Myhrberg, H. & Persson, H. (1966) Studies in adrenergic and cholinergic receptors in the isolated hearts of *Lampetra fluviatilis* (Cyclostomata) and *Pleuronectes platessa* (Teleostei). *Acta. Physiol. Scand.* **68**, 64-71.
- Farmer, C.G. (1999) Evolution of the vertebrate cardio-pulmonary system. *Annu. Rev. Physiol.* **61**:573-92.
- Feder, M.E. & Burggren, W.W. (1985) Cutaneous gas exchange in vertebrates: design, patterns, control and implications. *Biol. Rev.* **60**: 1-45.
- Feldman, J.L. & Del Negro, C.A. (2006) Looking for inspiration: new perspectives on respiratory rhythm. *Nat. Rev. Neurosci.* **7**:232-242.
- Feldman, J.L., Mitchell, G.S. & Nattie, E.E. (2003) Breathing: rhythmicity, plasticity, chemosensitivity. *Annu. Rev. Neurosci.* **26**:239-266.
- Felgner, P.L., Gadek, T.R., Holm, M., Roman, R., Chan, H.W., Wenz, M., Northrop, J.P., Ringold, G.M., and Danielson, M. (1987) Lipofection: a highly efficient, lipid-mediated DNA-transfection procedure. *Proc. Natl. Acad. Sci. USA.* **84**:7413-7417.
- Felgner, P. L., Tsai, Y. L., and Sukhu, L, (1995). Improved cationic lipid formulations for *in vivo* gene therapy. *Ann NY Acad Sci* **772**:126-139.
- Festy, B. & Daune, M. (1973) Hydroxystilbamidine, a non-intercalating drug as a probe of nucleic acid conformation. *Biochemistry.* **12**:4827-4834.
- Festy, B., Sturm, J. & Daune, M. (1975) Interaction between hydroxystilbamidine and DNA. *Biochim Biophys Acta* **407**:24-42.
- Fransen, M.E., & Lemanski, L.F. (1988) Myocardial cell relationships during morphogenesis in normal and cardiac lethal mutant axolotls, *Ambystoma mexicanum*. *Am. J. Anat.* **183**, 245-57.
- Friedland, D.R., Eden, A.R. & Laitman, J.T. (1995) Naturally occurring motoneuron cell death in rat upper respiratory tract motor nuclei: a histological, fast DiI and immunocytochemical study of the nucleus ambiguus. *J Neurobiol.* **26**:563-78.
- Fritsche, R. (1997) Ontogeny of Cardiovascular Control in Amphibians. *Amer. Zool.* **37**, 23-30.

- Fuldner, R. A., Lim, S. S., Greaser, M. L. and Lemanski, L. F. (1984) Accumulation and localisation of troponin-T in developing hearts of *Ambystoma mexicanum*. *J. Embryol. Exp. Morph.* **84**, 1-17.
- Gahlenbeck H, Bartels H. (1970) Blood gas transport properties in gill and lung forms of the axolotl (*Ambystoma mexicanum*). *Respir Physiol.* **9**:175-82
- Gaskell, W. H. (1884) On the augmentor (accelerator) nerves of the heart of cold-blooded animals. *J. Physiol. (Lond.)* **5**, 46-48.
- Gao, X. and Huang, L. (1995) Cationic liposome-mediated gene transfer. *Gene Ther.* **2**: 710–22.
- Gaur, A., Bhatia, R., Spring-Mills, E., Lemanski, L., & Dube, D. (1998) The heart of metamorphosing Mexican axolotl but not that of the cardiac mutant is associated with the upregulation of Hox A5. *Biochem. Biophys. Res. Commun.* **245**, 746-751.
- Gaur, A., Lemanski, L., & Dube, D. (1998) Cloning, sequencing and expression of a novel homeobox gene *AxNox-1* from the Mexican axolotl. *Gene* **216**, 179-188.
- Gaur, A., Lemanski, L., & Dube, D. (1995) Identification and expression of a homologue of the murine *HoxA5* gene in the Mexican axolotl (*Ambystoma mexicanum*). *Gene* **162**, 249-253.
- Gaur, A., Zajdel, R.W., Bhatia, R., Isitmangil, G., Denz, C.R., Robertson, D.R., Lemanski, L.F. & Dube, D.K. (2001) Expression of HoxA5 in the heart is upregulated during thyroxin-induced metamorphosis of the Mexican axolotl (*Ambystoma mexicanum*). *Cardiovasc Toxicol.* **1**:225-35.
- Gilbert, S.F. (1994) *Developmental Biology*, 4th Ed. Sinauer Associates, Inc.
- Gimona, M., Watakabe, A. and Helfman, D. M. (1995). Specificity of dimer formation in tropomyosins: Influence of alternatively spliced exons on homodimer and heterodimer assembly. *Proc. Natl. Sci. Acad. USA.* **92**:9776-9780.
- Glick, G. & Braunwald, E. (1965) Relative roles of the sympathetic and parasympathetic nervous systems in the reflex control of heart rate. *Circ. Res.* **16**, 363-375.
- Golitsina, N. L., An Y., Greenfield N. J., Thierfelder L., Iizuka K., Seidman J. G., Seidman C. E., Lehrer S. S. and Hitchcock-DeGregori, S. E. (1997) Effects of two familial hypertrophic cardiomyopathy-causing mutations on  $\alpha$ -tropomyosin structure and function. *Biochemistry.* **36**:4637–4642. (See also corrections to this article in *Biochemistry.* 1999. **38**:3850.)



- Greene, C. W. (1902) Contribution to the physiology of the California hagfish, *Polistotrema stoutii*. II. The absence of regulative nerves for the systemic heart. *Am. J. Physiol.* **6**, 318-324.
- Grossman, P. and Taylor, E. W. (2007) Toward a proper understanding of respiratory sinus arrhythmia: Relations to cardiac vagal tone, evolution and biobehavioral functions. *Biol. Psychol.* **74**, 263-285.
- Hamlin, R. L. Smith, C. R. & Smetzer, D. L. (1966) Sinus arrhythmia in the dog. *Am. J. Physiol.* **210**, 321-328.
- Hardy, S., Thézé, N., Lepetit, D., Allo, M. R., and Thiebaud, P. (1995) The *Xenopus laevis* TM-4 gene encodes non-muscle and cardiac tropomyosin isoforms through alternative splicing. *Gene.* **156**: 265-70.
- Harris, C.L. (1996) *Concepts in Zoology*, 2<sup>nd</sup> Ed. Harper Collins College Publishing.
- Hata, T., Noda, T., Nishimura, M. & Watanabe, Y. (1996) The role of Ca<sup>2+</sup> release from sarcoplasmic reticulum in the regulation of sinoatrial node automaticity. *Heart Vessels.* **11**:234–241.
- Hayano, J., Sakakibara, Y., Yamada, M., Mukai, S., Fujinami, T., Yokoyama, K., Watanabe, Y. & Takata, K. (1991) Accuracy of assessment of cardiac vagal tone by heart rate variability in normal subjects. *Am. J. Cardiol.* **67**, 199-204.
- Heathcote, R.D. & Sargent P.B. (1984) The Genesis and Differentiation of Neurons in a Frog Parasympathetic Ganglion. *Dev. Biol.* **105**, 102-114.
- Hedberg, A., Minneman, K. P. and Molinoff, P. B. (1980) Differential distribution of  $\beta$ -1 and  $\beta$ -2 adrenergic receptor in cat and guinea pig heart. *J. Pharmacol. Exp. Ther.* **212**, 503-508.
- Heimann, K., Percival, J.M., Weinberger, R., Gunning, P. and Stow, J.L. (1999) Specific isoforms of actin-binding proteins on distinct populations of Golgi-derived vesicles. *J. Biol. Chem.* **274**:10743–10750.
- Hickman, C.P., Roberts, L.S. & Larson, A. (2001) *Integrated Principles of Zoology*. 11<sup>th</sup> Ed. McGraw-Hill.
- Hill, C.S., & Lemanski, L.F. (1979) Morphological studies on cardiac lethal mutant salamander heart in organ culture. *J. Exp. Zool.* **209**, 1-20.
- Hirsch, E.F., Jellinek, M. & Cooper, T. (1964) Innervation of the systemic heart of the California hagfish. *Circ. Res.* **14**; 212-217.

- Hirsch, M.R., Tiverton, M.C., Guillemot, F., Brunet, J.-F., & Giordis, C. (1998) Control of noradrenergic differentiation and Phox2a expression by MASH1 in the central and peripheral nervous system. *Development* **125**, 599-608.
- Hook, J., Lemckert, F., Qin, H., Schevzov, G. and Gunning, P. (2004) Gamma tropomyosin gene products are required for embryonic development. *Mol. Cell. Biol.* **24**: 2318–2323.
- Hou, L., Tang, H., Chen, Y., Wang, L., Zhou, X., Rong, W. & Wang, J. (2009) Presynaptic modulation of tonic and respiratory inputs to cardiovagal motoneurons by substance P. *Brain Res.* **1284**:31-40.
- Humphrey, R. R. (1972) Genetic and experimental studies on the mutant gene (c) determining absence of heart action in embryos of the Mexican axolotl (*Ambystoma mexicanum*). *Dev. Biol.* **27**, 365-375.
- Hyndman, B. W., Kitney, R. I., Sayers, B. McA. (1971) Spontaneous rhythms on physiological control systems. *Nature* **233**, 339-341.
- Ihmied, Y.M., & Taylor, E.W. (1992) Relocation of preganglionic vagal motoneurons in the brainstem of the axolotl at metamorphosis. *J. Physiol.* **446**, 165.
- Ihmied, Y.M. (1989) Respiratory and cardiovascular control in the African clawed toad, *Xenopus laevis*, and the axolotl, *Ambystoma mexicanum*: A neuroanatomical and physiological study. **Ph.D. Thesis**. University of Birmingham.
- Ingram, A. J. (1970) *Tumour induction in the axolotl, Ambystoma mexicanum*. PhD thesis, University of Southampton.
- Iriuchijima, J. (1959) Sympathetic and vagal discharges in the cardiac nerve of the toad. *Tohoku J. Exp. Med.* **71**, 109-119.
- Jensen, D. (1965). The aneural heart of the hagfish. *Ann. N.Y. Acad. Sci.* **127**: 443–458.
- Johansen, K. & Reite, O. B. (1964) Cardiovascular responses to vagal stimulation and cardioacceleration blockade in birds, duck (*Anas boscas*) and seagull (*Larus argentatus*). *Comp. Biochem. Physiol.* **12**, 479-488.
- Jones, D.R. & Milsom, W.K. (1982) Peripheral receptors affecting breathing and cardiovascular function in non-mammalian vertebrates. *J. Exp. Biol.* **100**; 59-91.)
- Katona, P. G. & Felix, J. I. H. (1975) Respiratory sinus arrhythmia: non-invasive measure of parasympathetic cardiac control. *J. Appl. Physiol.* **39**, 801-805.

- Keyl, C., Dambacher, M., Schneider, A., Passino, C., Wegenhorst, U. & Bernardi, L. (2000) Cardiocirculatory coupling during sinusoidal baroreceptor stimulation and fixed-frequency breathing. *Clin Sci (Lond)*. **99**:113-24.
- Kirby, M. L., McKenzie J. W. and Weidman, T. A. (1980) Developing innervation of the chick heart: A histofluorescence and light microscopic study of sympathetic innervation. *The Anatomic Record*. **196**, 333-340.
- Kirby, M.L. & Stewart, D.E. (1983) Neural crest origin of cardiac ganglion cells in the chick embryo: Identification and extirpation. *Dev. Biol.* **97**, 433-443.
- Kirby, M.L. (1988) Nodose placode contributes autonomic neurons to the heart in the absence of cardiac neural crest. *J. Neurosci.* **8**, 1089-1095.
- Kirby, M.L. & Waldo K.L. (1995) Neural crest and cardiovascular patterning. *Circ. Res.* **77**, 211-215.
- Kirby, S. and Burnstock, G. (1969) Pharmacological studies of the cardiovascular system in the anaesthetised sleepy lizard (*Tiliqua rugosa*) and toad (*Bufo marinus*). *Comp. Biochem. Physiol.* **28**, 321-332.
- Klein, W. & Owerkowicz, T. (2006) Function of intracoelomic septa in lung ventilation of amniotes: lessons from lizards. *Physiol. Biochem. Zool.* **79**: 1019–1032.
- Kohn, A.Z., Hoxha, Z., Balan, K.V., Martin, R.J., Haxhiu, M.A., Wilson, C.G., Mayer, C.A, & Kc, P. (2009) Developmental changes in brainstem neurons regulating lower airway caliber. *Pediatr Res.* **65**:509-13.
- Kolesová, H., Lametschwandtner, A. & Roček, A. (2007) The evolution of amphibian metamorphosis: insights based on the transformation of the aortic arches of *Pelobates fuscus* (Anura). *J. Anat.* **210**: 379–393.
- Kunikullaya, K.U., Kirthi, S.K., Venkatesh, D. & Goturu, J. (2010) Heart rate variability changes in business process outsourcing employees working in shifts. *Indian Pacing Electrophysiol J.* **10**:439-46.
- LaFrance, S. M., and Lemanski, L. F. (1995) Immunofluorescent confocal analysis of tropomyosin in developing hearts of normal and cardiac mutant axolotls. *Int. J. Dev. Biol.* **38**: 695-700.

- Laing, N.G., Wilton, S.D., Akkari, P.A., Dorosz, S., Boundy, K., Kneebone, C., Blumbergs, P., White, S., Watkins, H. and Love, D.R. (1995) A mutation in the alpha tropomyosin gene TPM3 associated with autosomal dominant nemaline myopathy. *Nat Genet* **9**(1):75–79.
- Lakatta, E.G., DiFrancesco, D. (2009) What keeps us ticking: a funny current, a calcium clock, or both? *J Mol Cell Cardiol.* **47**:157–170.
- Lakatta, E.G., Maltsev, V.A., Bogdanov, K.Y., Stern, M.D. & Vinogradova, T.M., (2003) Cyclic variation of intracellular calcium: a critical factor for cardiac pacemaker cell dominance. *Circ. Res.* **92**:e45–e50.
- Larsen, W.J. (1997) *Human Embryology*, 2nd Ed. Churchill Livingstone.
- Lee, J.T. and Jaenisch, R. (1996) A method for high efficiency YAC lipofection into murine embryonic stem cells. *Nucleic Acids Res.* **24**, 5054–5.
- Lees-Miller, J. P., and Helfman, D. M. (1991) The molecular basis for tropomyosin isoform diversity. *Bioessays.* **13**, 429-437.
- Lemanski, L.F. (1973a) Morphology of Developing Heart in Cardiac Lethal Mutant Mexican Axolotls, *Ambystoma mexicanum*. *Dev. Biol.* **33**, 312-333.
- Lemanski, L.F. (1973b) Heart development in the Mexican salamander, *Ambystoma mexicanum*. I. Gross anatomy, histology, & histochemistry. *J. Morph.* **139**, 301-328.
- Lemanski, L.F. (1973c) Heart development in the Mexican salamander, *Ambystoma mexicanum*. II. Ultrastructure. *Am. J. Anat.* **136**, 487-526.
- Lemanski, L.F. (1976) Morphological and biochemical abnormalities in hearts of cardiac mutant salamanders (*Ambystoma mexicanum*). *J. Supramolec. Struc.* **5**, 221-238.
- Lemanski, L.F. (1979) Role of tropomyosin in actin filament formation in embryonic salamander heart cells. *J. Cell. Biol.* **82**:227–238.
- Lemanski, L.F., Paulson, D.J. & Hill, C.S. (1979) Normal anterior endoderm corrects the heart defect in cardiac mutant salamander. *Science* **204**, 860-862.
- Lemanski, L.F., Fuldner, R. A. Paulson, D. J. (1980) Immunofluorescence studies for myosin, alpha-actinin and tropomyosin in developing hearts of normal and cardiac lethal mutant Mexican axolotls, *Ambystoma mexicanum*. *J. Embryol. Exp. Morph.* **55**, 1-15.

- Lemanski, L.F., Nakatsugawa, M., Lemanski, S., Zajdel, R., Salsbury, K., McLean, M., & Dube, D.K. (1998) Chimeric axolotls produce embryos with 100% cardiac mutant phenotype. *Am. Soc. Cell Biol. Ann. Meeting. 9*, Abstract No. 861.
- Lemanski, L.F., Nakatsugawa, M., Bhatia, R., Erginel-Unaltuna, N., Spinner, B. and Dube, D.K. (1996) Characterization of an RNA which promotes myofibrillogenesis in embryonic cardiac mutant axolotl hearts. *Biochem. Biophys. Res. Comm.* **229**:974–981.
- Leong, S.K. & Ling, E.A. (1990) Labelling neurons with fluorescent dyes administered via intravenous, subcutaneous or intraperitoneal route. *J Neurosci Methods.***32**:15-23.
- Lin, J. J., Chou, C. S. & Lin, J. L. (1985) Monoclonal antibodies against chicken tropomyosin isoforms: production, characterisation, and application. *Hybridoma.* **4**, 223-242.
- Lin, M.-F., DaVolio, J., and Garcia, R. (1993) Cationic liposome-mediated incorporation of prostatic acid phosphatase protein into human prostate carcinoma cells. *Biochem. Biophys. Res. Commun.* **192**: 413-419.
- Lin, J. J-C., Helfman, D.M., Hughes, S.H. and Chou, C-S. (1985). Tropomyosin isoforms in chicken embryo fibroblasts. Purification, characterization, and changes in Rous sarcoma virus-transformed cells. *J. Cell. Biol.* **100**:692-703.
- Loewi, O. (1921) Über humorale Übertragbarkeit der Herznervenwirkung. I. Mitteilung. *Pflüger's Arch. Gesamte Physiol. Menschen. Tiere.* **189**, 239-242.
- Lukomskaya, N. J. and Michelson, M. J. (1972) Pharmacology of the isolated heart of the lamprey, Lamprey, *Lampetra fluviatilis*. *Comp. Gen. Pharmacol.* **3**, 213-225.
- Luque, E.A., Lemanski, L.F., & Dube, D.K. (1994) Molecular cloning, sequencing and expression of an isoform of cardiac alpha-tropomyosin from the Mexican axolotl (*Ambystoma mexicanum*). *Biochem. & Mol. Biol. Int.* **203**, 319-325.
- Luque, E.A., Spinner, B.J., Dube, S., Dube, D.K., & Lemanski, L.F. (1997) Differential expression of a novel isoform of alpha-tropomyosin in cardiac and skeletal muscle of the Mexican axolotl (*Ambystoma mexicanum*). *Gene* **185**, 175-180.
- Luque, E., Spinner, B.J., Dube, S., Dube, D.K., and Lemanski, L.F. (1997) Differential
- Lutz, B. R. (1930) Reflex cardiac and respiratory inhibition in the elasmobranch *Scyllium canicula*. *Biol. Bull.* **59**, 170-178.

- Lynn, G. D. and Wachowski, H. E. (1951) The thyroid gland and its functions in cold-blooded vertebrates. *Quart. Rev. Biol.* **26**, 123-168.
- Lyons, G.E. (1996) Vertebrate heart development. *Curr. Opin. Genet. Dev.* **6**:454–460.
- Mak, A.S. and Smillie, L.B. (1981) Structural interpretation of the two-site binding of troponin on the muscle thin filament. *J. Mol. Biol.* **149**:541–550.
- Maake, C., Kloas, W., Szendefi, M. & Reinecke, M. (1999) Neurohormonal peptides, serotonin, and nitric oxide synthase in the enteric nervous system and endocrine cells of the gastrointestinal tract of neonatal and thyroid hormone-treated axolotls (*Ambystoma mexicanum*). *Cell Tissue Res.* **297**:91-101.
- Macchi, V., Snenghi, R., De Caro, R. & Parenti, A. (2002) Monolateral hypoplasia of the motor vagal nuclei in a case of sudden infant death syndrome. *J Anat.* **200**:195-8.
- Malone, R.W., Felgner, P.L., and Verma, I.M. (1989) Cationic liposome-mediated RNA transfection. *Proc. Natl. Acad. Sci. USA* **86**: 6077-6081.
- Maltsev, V.A. & Lakatta, E.G. (2009) Synergism of coupled subsarcolemmal Ca<sup>2+</sup> clocks and sarcolemmal voltage clocks confers robust and flexible pacemaker function in a novel pacemaker cell model. *Am J Physiol Heart Circ Physiol.* **296**: H594–H615.
- Maltsev, V.A., Vinogradova, T.M., Bogdanov, K.Y., Lakatta, E.G. & Stern, M.D. (2004) Diastolic calcium release controls the beating rate of rabbit sinoatrial node cells: Numerical modelling of the coupling process. *Biophysical J.* **86**; 2596-2605.
- Malvin, G.M. & Heisler, N. (1988) Blood flow patterns in the salamander, *Ambystoma tigrinum*, before, during and after metamorphosis. *J Exp Biol.* **137**: 53-74.
- Markwald, R., Trusk, L.F., Gittenberger, A. C., and Poelman, R.E. (1996) Cardiac morphogenesis: formation and septation of the primary heart tube. In: *Handbook of Experimental Pharmacology vol. 124/I: Drug Toxicity in Embryonic Development.* (ed. R.J. Kavlock and G. Daston), pp. 11–40. Springer-Verlag, New York.
- Maron, B.J., Shirani, J., Poliac, L.C., Mathenge, R., Roberts, W.C. and Mueller, F.O. (1996). Sudden death in young competitive athletes. Clinical, demographic, and pathological profiles. *JAMA.* **276**:199-204.
- Martson, S.B. and Redwood, C.S. (2003) Modulation of thin filament activation by breakdown or isoform switching of thin filament proteins: physiological and pathological implications, *Circ. Res.* **93**:1170–1178.

- May, O. & Arildsen, H. (2011) Long-term predictive power of heart rate variability on all-cause mortality in the diabetic population. *Acta Diabetol.* **48**: 55-9.
- McKenzie, D.J. & Taylor, E.W. (1996) Cardioventilatory responses to hypoxia and NaCN in the neotenus axolotl. *Resp. Physiol.* **106**: 255-262.
- McLachlan, A. D. and Stewart, M. (1975). Tropomyosin coiled-coil interactions: Evidence for an unstaggered structure. *J. Mol. Biol.* **98**:293-304.
- Meiri, K. F., Bickerstaff, L. E. & Schwob, J. E. (1991) Monoclonal antibodies show that kinase C phosphorylation of GAP-43 during axogenesis is both spatially and temporally restricted *in vivo*. *J. Cell Biol.* **112** (5), 991-1005.
- Melcher, A. (1980) Carotid baroreflex heart rate control during the active and the assisted breathing cycle in man. *Acta Physiol Scand.* **108**:165-71.
- Melinek, R., & Mirolli, M. (1988) The organisation of the cardiac ganglion of the axolotl (*Ambystoma mexicanum*). *J. Auton. Nerv. Syst.* **24**, 29-39.
- Metzger, J. M., Michele, D.E., Rust, E.M., Borton, A.R. and Westfall, M.V. (2003). Sarcomeric thin filament regulatory isoforms. *J. Biol. Chem.* **278**:13118-13123.
- Milsom, W.K., Chatburn, J. & Zimmer, M.B. (2004) Pontine influences on respiratory control in ectothermic and heterothermic vertebrates. *Respir. Physiol. Neurobiol.* **143**: 263–280.
- Mittal, R.K. & Balaban, D.H. (1997) The esophagogastric junction. *N Engl J Med.* **336**:924-932.
- Moalli, R., Meyers, R. S., Jackson, D. C. & Millard, R. W. (1980). Skin circulation of the frog, *Rana catesbeiana*, distribution and dynamics. *Resp. Physiol.* **40**: 137 -148.
- Mohun, T.J., Ming Leong, L., Weninger, W.J. & Sparrow, D.B. (2000) The Morphology of Heart Development in *Xenopus laevis*. *Developmental Biology* **218**: 74–88.
- Moore, M.W., Klein, R.D., Farinas, I., Sauer, H., Armainini, M., Philips, H., Reichardt, L.F., Ryan, A.M., CarverMoore, K., & Rosenthal, A. (1996) Renal and neuronal abnormalities in mice lacking GDNF. *Nature* **382**, 76-79.
- Moore, P. B., and Lemanski, L. F. (1982) Quantification of tropomyosin by radioimmunoassay in developing hearts of cardiac mutant axolotls, *Ambystoma mexicanum*. *J. Musc. Res. Cell Mot.* **3**, 161-167.

- Muthuchamy, M., Pieples, K., Rethinasamy, P., Hoit, B., Grupp, I.L., Boivin, G.P., Wolska, B., Evans, C., Solaro, R.J. and Wieczorek, D.F. (1999) Mouse model of a familial hypertrophic cardiomyopathy mutation in  $\alpha$ -tropomyosin manifests cardiac dysfunction. *Circ. Res.* **85**:47–56.
- Nadal-Ginard, B. (1990) Muscle cell differentiation and alternative splicing, *Curr. Opin. Cell Biol.* **6**:96–104.
- Nadal-Ginard, B. (1990) Muscle cell differentiation and alternative splicing. *Curr. Opin. Cell Biol.* **2**:1058–1064.
- Navaratnam, V. (1965) The ontogenesis of cholinesterase activity within the heart and cardiac ganglia in man, rat, rabbit and guinea-pig. *J. Anat.* **99**, 459-467.
- Navaratnam, V. (1987) *Heart Muscle: Ultrastructural Studies*. Cambridge University Press.
- Naylor, W. G. and Howells, J. E. (1965) Phosphorylase a/b ratio in the lamprey heart. *Nature.* **207**, 81.
- Nielsen, K. C. and Owman, Ch. (1968) Difference in cardiac adrenergic innervation between hibernators and non-hibernating mammals. *Acta. Physiol. Scand.* **74**, Suppl. **316**, 1-30.
- Nielsen, K. C., Owman, Ch. And Santini, M. (1969) Anastomosing adrenergic nerves from the sympathetic trunk to the vagus at the cervical level in the cat. *Br. Res.* **12**, 1-9.
- Nilsson, S. (1983) *Autonomic nerve function in the vertebrates*. Springer-Verlag. Berlin.
- Nishibatake, M., Kirby, M.L., & Van Mierop, L.H. (1987) Pathogenesis of persistent truncus arteriosus and dextroposed aorta in the chick embryo after neural crest ablation. *Circulation* **75**, 255-264.
- Norris, D.O. & Platt, J.E. (1973) Effects of pituitary hormones, melatonin and thyroidal inhibitors on radioiodide uptake by the thyroid glands of larval and adult tiger salamander, *Ambystoma tigrinum* (Amphibia, Caudata). *Gen. Comp. Endocrinol.* **21**; 368-376.
- Olson, E.N., & Srivastava, D. (1996) Molecular pathways controlling heart development. *Science* **272**, 671-676.
- Palm, T., Greenfield, N.J. and Hitchcock-DeGregori, S.E. (2003). Tropomyosin ends determine the stability and functionality of overlap and troponin T complex. *Biophys. J.* **84**:3181-3189.



- Pappano, A.J. (1977) Ontogenetic development of autonomic neuroeffector transmission and transmitter reactivity in embryonic and fetal hearts. *Pharmacol. Rev.* **29**, 3-33.
- Parakkal, P.F. & Matoltsy, A.G. (1964) A study of the fine structure of the epidermis of *Rana pipiens*. *J Cell Biol.* **20**:85-94.
- Pattyn, A., Morin, X., Cremer, H., Goridis, C., & Brunet, J.-F. (1999) The homeobox gene *Phox2b* is essential for the development of autonomic neural crest derivatives. *Nature* **399**, 366-370.
- Percival, J.M., Thomas, G. Cock, T.A., Gardiner, E.M., Jeffrey, P.L., Lin, J.J., Weinberger, R.P. and Gunning, P. (2000) Sorting of tropomyosin isoforms in synchronised NIH 3T3 fibroblasts: evidence for distinct microfilament populations. *Cell Motil. Cytoskelet.* **47**:189–208.
- Perry, S.V. (2001) Vertebrate tropomyosin: distribution, properties and function, *J. Muscle Res. Cell Motil.* **22**:5–49.
- Persson, S. & Havton, L.A. (2009) Retrogradely transported fluorogold accumulates in lysosomes of neurons and is detectable ultrastructurally using post-embedding immuno-gold methods. *J Neurosci Methods.* **184**:42-47.
- Petterson, K. and Nilsson, S. (1979) Nervous control of the branchial vascular resistance of the Atlantic cod, *Gadus morhua*. *J. Comp. Physiol.* **129**, 179-183.
- Piepoli, M., Sleight, P., Leuzzi, S., Valle, F., Spadacini, G., Passino, C., Johnston, J. & Bernardi, L. (1997) Origin of Respiratory Sinus Arrhythmia in Conscious Humans. An Important Role for Arterial Carotid Baroreceptors. *Circulation* **95**:1813-1821.
- Pittenger, M.F., Kazzaz, J.A. and Helfman, D.M. (1994) Functional properties of non-muscle tropomyosin isoforms. *Curr. Opin. Cell Biol.* **1**:96–104.
- Porter, K. R., 1972, Herpetology: London, W.B. Saunders.
- Prabhakar, R., Boivin, G. P., Grupp, I. L., Hoit, B., Arteaga, G., Solaro, J. R. and Wieczorek, D. F. (2001) A Familial Hypertrophic Cardiomyopathy  $\alpha$ -Tropomyosin Mutation Causes Severe Cardiac Hypertrophy and Death in Mice *J. Molecular and Cellular Cardiology* **33** (10): 1815-1828.
- Prahlad, K.V. & DeLanney, L.E. (1965) A study of induced metamorphosis in the axolotl. *J Exp Zool.* **160**:137-45.
- Priede, I. G. (1974) The effect of swimming activity and section of the vagus nerves in heart rate in rainbow trout. *J. Exp. Biol.* **60**, 305-319.

- Priola, DE. V., O'Brien, W. J., Dail, W. G. and Simpson, W. W. (1981) Cardiac catecholamine stores after cardiac sympathectomy, 6-OH-DA, and cardiac denervation. *Am. J. Physiol.* **240**, H889-H895.
- Ramsey, J.P., Reinert, L.K., Harper, L.K., Woodhams, D.C. & Rollins-Smith, L.A. (2010) Immune defenses against *Batrachochytrium dendrobatidis*, a fungus linked to global amphibian declines, in the South African clawed frog, *Xenopus laevis*. *Infect Immun.* **78**: 3981-92.
- Randall, D. J. and Stevens, E. Don. (1967) The role of adrenergic receptors in cardiovascular changes associated with exercise in salmon. *Comp. Biochem. Physiol.* **21**, 415-424.
- Randall, W. C. and Armour, J. A. (1977) Gross and microscopic anatomy of the cardiac innervation. In: *Neural regulation of the heart*. Ed. W. C. Randall. Oxford University Press.
- Ransom, W. B. and Thompson, D'Arcy W. (1886) On the spinal and visceral nerves of cyclostomata. *Zool. Anz.* 9, 421-426.
- Ranson, R.N., Butler, P.J., & Taylor, E.W. (1993) The central localization of the vagus nerve in the ferret (*Mustela putorius furo*) and the mink (*Mustela vison*). *J Auton Nerv Syst.* **43**:123-37.
- Rekling, J.C. & Feldman, J.L. (1998) PreBotzinger complex and pacemaker neurons: Hypothesized site and kernel for respiratory rhythm generation. *Annu. Rev. Physiol.* **60**: 385–405.
- Rethinasamy, R., Muthuchamy, M., Hewett, T., Bovin, G., Wolska, B.M., Evans, C., Solaro, R.J. and Wiczorek, D.F. (1998) Molecular and physiological effects of alpha-tropomyosin ablation in the mouse. *Cir. Res.* **82**:116–123.
- Rhee, D., Sanger, J.M. and Sanger, J.W. (1994) The premyofibril: Evidence for its role in myofibrillogenesis. *Cell Motil. Cytoskel.* **28**:1–24.
- Rosenkilde, P. & Ussing, A.P. (1996) What mechanisms control neoteny and regulate induced metamorphosis in urodeles? *Int J Dev Biol.* **40**:665-73.
- Rybak, B. and Cortot, H. (1956) La valvule sino-auriculaire, isolée du coeur de *Scyllium canicula*, preparation de choise pour l'étude de l'automatisme myocardique. *C. R. Socl. Biol. Paris.* **150**, 2216-2218.

- Saetersdal, T. S., Sorensen, E., Myklebust, R. and Helle, K. B. (1975) Granule containing cells and fibres in the sinus venosus of elasmobranches. *Cell Tissue Res.* **163**, 471-490.
- Samaan, A. (1935) The antagonistic cardiac nerves and heart rate. *J. Physiol.* **83**, 332-340.
- Satchell, G. H. (1971) *Circulation in Fishes*. Cambridge University Press.
- Schmued, L.C. & Fallon, J.H. (1986) Fluoro-Gold: a new fluorescent retrograde axonal tracer with numerous unique properties. *Brain Res.* **377**:147-54.
- Schmued, L.C., Kyriakidis, K., Fallon, J.H. & Ribak, C.E. (1989) Neurons containing retrogradely transported Fluoro-Gold exhibit a variety of lysosomal profiles: a combined brightfield, fluorescence, and electron microscopic study. *J Neurocytol.* **18**:333-43.
- Schwaber, J. S. and Cohen, D. H. (1978) Electrophysiological and electron microscopic analysis of the vagus nerve of the pigeon, with particular reference to the cardiac innervation. *Br. Res.* **147**, 65-78.
- Sessa, G. and Weissmann, G. (1968) Phospholipid spherules (liposomes) as a model for biological membranes. *J. Lipid Res.* **9**, 310-8.
- Shah, A.J., Su, S., Veledar, E., Bremner, J.D., Goldstein, F.C., Lampert, R., Goldberg, J. & Vaccarino, V. (2011) Is Heart Rate Variability Related to Memory Performance in Middle-Aged Men? *Psychosom Med.* **73**: 475-482.
- Shykoff, B.E., Naqvi, S.S., Menon, A.S. & Slutsky, A.S. (1991) Respiratory sinus arrhythmia in dogs. Effects of phasic afferents and chemostimulation. *J Clin Invest.* **87**:1621-7.
- Skene, J. H. P. & Willard, M. (1981) Axonally transported proteins associated with growth in rabbit central and peripheral nervous system. *J. Cell Biol.* **89**, 96-103
- Smith, D.G., Berger, P.J. & Evans, B.K. (1981) Baroreceptor control of heart rate in the conscious toad, *Bufo marinus*. *Am. J. Physiol.* **241**; R307-311.
- Smith, J.C., Ellenberger, H.H., Ballanyi, K., Richter, D.W. & Feldman, J.L. (1991) Pre-Bötzinger complex: a brainstem region that may generate respiratory rhythm in mammals. *Science* **254**; 726-729.
- Smith, S.C., & Armstrong, J.B. (1993) Reaction-diffusion control of heart development: Evidence for activation and inhibition in precardiac mesoderm. *Dev. Biol.* **160**, 535-542.

- Smith, S.C., & Armstrong, J.B. (1991) Heart development in normal and cardiac-lethal mutant axolotls: a model for the control of vertebrate cardiogenesis. *Differentiation* **47**, 129-134.
- Spinner, B. J., Dube, D. K. and Lemanski, L. F. (1997a) Expression studies of a cardiac TM-4 type tropomyosin. *Molec. Biol. Cell.* **8**, 373a
- Spinner, B. J., Dube, D. K. and Lemanski, L. F. (1997b) Tissue specific expression of a novel alpha-tropomyosin isoform. *Molec. Biol. Cell.* **8**, 347a
- Spinner, B.J., Zajdel, R. W., McLean, M. D., Denz, C. R., Dube, S., Mehta, S., Choudhury, A., Nakatsugawa, M., Dobbins, N., Lemanski, L. F. and Dube, D. K. (2002) Characterization of a TM-4 Type Tropomyosin That Is Essential for Myofibrillogenesis and Contractile Activity in Embryonic Hearts of the Mexican Axolotl. *J. of Cell. Biochem.* **85**: 747-761.
- Spyer, K. M. (1982) Central nervous integration of cardiovascular control. *J. Exp. Biol.* **100**, 109-128.
- Spyer, K.M. (1989) Neural mechanisms involved in cardiovascular control during affective behaviour. *Trends Neurosci.* **12**:506-13.
- Srivastava, D. and Olson, E. (1997) Knowing in your hearts what's right. *Trends Cell Biol.* **7**:447-453.
- Starr, C., Diaz, J.G., and Lemanski, L.F. (1989) Analysis of actin and tropomyosin in hearts of cardiac mutant axolotls by two-dimensional gel electrophoresis, western blots and immunofluorescent microscopy. *J. Morphol.* **201**: 1-10.
- Taha, B.H., Simon, P.M., Dempsey, J.A., Skatrud, J.B. & Iber, C. (1995) Respiratory sinus arrhythmia in humans: an obligatory role for vagal feedback from the lungs. *J Appl Physiol.* **78**:638-45.
- Tak, L.M., Janssens, K.A., Dietrich, A., Slaets, J.P. & Rosmalen, JG. (2010) Age-specific associations between cardiac vagal activity and functional somatic symptoms: a population-based study. *Psychother Psychosom.* **79**: 179-87.
- Taurog, A. (1974) Effects of TSH and long acting thyroid stimulator on thyroid (131)-I metabolism and metamorphosis of the Mexican axolotl (*Ambystoma mexicanum*). *Gen. Comp. Endocrinol.* **24**; 257-266.
- Taylor, E.W. (ed.) (1987). '*Neurobiology of the Cardiorespiratory System*'. Manchester University Press. (424 pages).

- Taylor, E.W. (1993) The neuroanatomy of central cardiorespiratory control in vertebrates. *Funktionsanalyse Biologischer System* **23**, 149-159.
- Taylor, E.W. (1994) The evolution of efferent control of the heart in vertebrates. *Cardioscience* **5**, 173-181.
- Taylor, E.W., Jordan, D. & Coote, J.H. (1999) Central control of the cardiovascular and respiratory systems and their interactions in vertebrates. *Physiol. Rev.* **79**: 855-916.
- Taylor, E.W., Jordan, D. & Coote, J.H. (1999) Central control of the cardiovascular and respiratory systems and their interactions in vertebrates. *Physiol. Rev.* **79**: 855-916.
- Taylor, E. W., Al-Ghamdi, M. S., Ihmied, I. H., Wang., T. & Abe, A. S. (2001) The neuroanatomical basis of central control of cardiorespiratory interactions in vertebrates. *Exp Physiol.* **86**: 771-6
- Taylor, E.W., Campbell, H.A., Levings, J.J., Young, M.J., Butler, P.J. & Egginton, S. (2006) Coupling of the respiratory rhythm in fish with activity in hypobranchial nerves and with heartbeat. *Physiol Biochem Zool.***79**:1000-9.
- Taylor, E.W., Leite, C.A.C. and Skovgaard, N. (2010) Autonomic control of cardiorespiratory interactions in fish, amphibians and reptiles. *Braz. J. Med. Biol. Res.* **43**, 600-610.
- Taylor, G.M., Nol, E. & Boire, D. (1995) Brain regions and encephalization in anurans: adaptation or stability? *Brain Behav Evol.* **45**:96-109.
- Thierfelder, L., Watkins H., MacRae C., Lamas R., McKenna W., Vosberg H. P., Seidman J. G., and Seidman C. E. (1994) Alpha-tropomyosin and cardiac troponin T mutations cause familial hypertrophic cardiomyopathy: a disease of the sarcomere. *Cell.* **77**:701–712.
- Torday, J.S., Rehan, V.K., Hicks, J.W., Wang, T., Maina, J., Weibel, E.R., Hsia, C.C., Sommer, R.J. & Perry, S.F. (2007) Deconvoluting lung evolution: from phenotypes to gene regulatory networks. *Integr Comp Biol.* **47**:601-9.
- Verberne, M.E., Gittenberger-De Groot, A.C., Van Iperen, L. & Poelmann R.E. (1999) Contribution of the Cervical Sympathetic Ganglia to the Innervation of the Pharyngeal Arch Arteries and Heart in the Chick Embryo. *The Anatomical Record.* **255**, 407-419.

- Verkerk, A.O., van Ginneken, A.C.G. & Wilders, R. (2009) Pacemaker activity of the human sinoatrial node: Role of the hyperpolarization-activated current,  $I_f$ . *Int. J. Cardiol.* **132**; 318–336.
- Vinogradova, T.M., Bogdanov, K.Y., & Lakatta, E.G. (2002)  $\beta$ -adrenergic stimulation modulates ryanodine receptor  $Ca^{2+}$  release during diastolic depolarization to accelerate pacemaker activity in rabbit sinoatrial nodal cells. *Circ. Res.* **90**:73–79.
- Völk, H., Charlemagne, J., Tournefier, A., Ferrone, S., Jost, R., Parisot, R. & Kaufman, J. (1998) Wide tissue distribution of axolotl class II molecules occurs independently of thyroxin. *Immunogenetics.* **47**:339-49.
- Vrhovski, B., Schevzov, G., Dingle, S., Lessard, J.L., Gunning, P. and Weinberger, R.P. (2003) Tropomyosin isoforms from the gamma gene differing at the C-terminus are spatially and developmentally regulated in the brain. *J. Neurosci. Res.* **72**:373–383.
- Waldo, K.L., Lo, C.W., Kirby, M.L. (1999) Connexin 43 expression reflects neural crest patterns during cardiovascular development. *Dev. Biol.* **208**, 307-323.
- Wang, X. & Halvorsen, S. W. (1998) Reciprocal Regulation of Ciliary Neurotrophic Factor Receptors and Acetylcholine Receptors during Synaptogenesis in Embryonic Chick Atria. *J. Neurosci.* **18** (18) 7372-7380.
- Wang, T., Hedrick, M.S., Ihmied, Y.M. and Taylor, E.W. (1999) Control and interaction of the cardiovascular and respiratory systems in anuran amphibians. *Comp Biochem Physiol* **124**: 393-406
- Ward, S.M., Lemanski, L.F., Erginel-Unaltuna, N., & Dube, D.K. (1995) Cloning , sequencing and expression of an isoform of cardiac C-protein from the Mexican axolotl (*Ambystoma mexicanum*). *Biochem. & Mol. Biol. Int.* **213**, 225-231.
- Ward, S.M., Spinner, B.J., Dube, A., Gaur, A., Erginel-Unaltuna, N., Lemanski, L.F., & Dube, D.K. (1996) Expression of myosin heavy chain transcripts in normal and cardiac mutant Mexican axolotls. *Biochem. & Mol. Biol. Int.* **38**, 113-121.
- Wessendorf, M.W. (1991) Fluoro-Gold: composition, and mechanism of uptake. *Brain Res.* **553**:135-48.
- West, J.B., Watson, R.R. & Fu, Z. (2007) The human lung: did evolution get it wrong? *Eur Respir J.* **29**:11-7.
- Wheeler, T. & Watkins, P. J. (1973) Cardiac denervation in diabetes. *Br. Med. J.* **4**, 584-586.

- Whiteley, M., & Armstrong, J.B. (1991) Ectopic expression of a genomic fragment containing a homeobox causes neural defects in the axolotl. *Biochem. & Cell Biol.* **69**, 366-374.
- Wieczorek, D.F. Smith, C.W.J. and Nadal-Ginard, B. (1988) The rat alpha-tropomyosin gene generates a minimum of six different mRNAs coding for striated, smooth, and nonmuscle isoforms by alternative splicing. *Mol. Cell. Biol.* **8**:679–694.
- Windle, W.F. (1933). Neurofibrillar development in the central nervous system of cat embryos between 8 and 12 mm long. *J Comp Neurol* **58**: 643-723.
- Wood, W. G., Britton, B. J. and Irving, M. H. (1979) Effects of adrenergic blockade on plasma catecholamine levels during adrenaline infusion. *Horm. Metab. Res.* **11**, 52-57.
- Xu, H., Miller, J., and Liang, B.T. (1992) High-efficiency gene transfer into cardiac myocytes. *Nucleic Acid Res.* **20**: 6425-6426.
- Yamauchi, A. (1969) Innervation of the vertebrates heart as studied with the electron microscope. *Arch Histol. Jpn.* **31**, 83-117.
- Yasuma, F. & Hayano, J. (2004) Respiratory sinus arrhythmia: Why does the heartbeat synchronize with respiratory rhythm? *Chest* **125**: 683-690.
- Yopak, K.E., Lisney, T.J., Darlington, R.B., Collin, S.P., Montgomery, J.C. & Finlay, B.L. (2010) A conserved pattern of brain scaling from sharks to primates. *Proc Natl Acad Sci U S A.* **107**:12946-51.
- Young, J. Z. (1933) The autonomic nervous system of Selachians. *Quart. J. Micr. Sci.* **15**, 571-624.
- Zajdel, R., Zhu, Y.Z., Fransen, M.E., & Lemanski, L.F. (1995) Primary cell culture and morphological characterisation of mutant cardiomyocytes from embryonic Mexican axolotl. *Am. Soc. Cell Biol. Ann. Meeting.* **6**, Abstract No. 879.
- Zajdel, R.W., McLean, M.D., Lemanski, S.L., Muthuchamy, M., Wieczorek, D.F., Lemanski, L.F. and Dube, D.K. (1998) Ectopic expression of tropomyosin, *Dev. Dyn.* **213**:412–420.
- Zajdel, R.W., Dube, D.K., and Lemanski, L.F. (1999) The cardiac mutant Mexican axolotl is a unique animal model for evaluation of cardiac myofibrillogenesis. *Exp. Cell Res.* **248**: 557-66.

- Zajdel, R.W., McLean, M.D., Lemanski, L.F. and Dube, D.K. (2000) Alteration of cardiac myofibrillogenesis by Lipofectin mediated delivery of exogenous proteins and nucleic acids into whole embryonic hearts. *Anat. Embryol.* **210**: 217–222.
- Zajdel, R.W., Choudhury, A., Dube, S., Mehta, S. and Dube, D.K. (2000). Transfection of anti-sense oligonucleotide into whole hearts using cationic liposomes. *Focus (Gibco BRL)*. **22**:28-30.
- Zajdel, R.W., McLean, M.D., Isitmangil, G., Wiczorek, D.F., Lemanski, L.F., and Dube, D.K. (2000) Alteration of cardiac myofibrillogenesis by liposome-mediated delivery of exogenous proteins and nucleic acids into whole embryonic hearts. *Anat. Embryol. (Berl)* **201**: 217-28.
- Zajdel, R.W., Sanger, J.M., Denz, C.R., Lee, S., Dube, S., Poiesz, B.J., Sanger, J.W. and Dube, D.K. (2002) A novel striated tropomyosin incorporated into organized myofibrils of cardiomyocytes in cell and organ culture, *FEBS Lett.* **520**:35–39.
- Zajdel, R.W., Denz, C.R., Lee, Dube, S., Ehler, S., Perriard, E. E., Perriard, J.- C. and Dube, D.K. (2003) Identification, characterization, and expression of a novel a-tropomyosin isoform in cardiac tissues in developing chicken, *J. Cell. Biochem.* **89**:427–439.
- Zelphati, O. and Szoka, F.C., Jr. (1996) Mechanism of oligonucleotide release from cationic liposomes. *Proc. Natl. Acad. Sci. USA* **93**: 11493-11498.
- Zhang, C., Dube, D.K., Huang, X., Zajdel, R.W., Bhatia, R., Foster, D., Lemanski, S.L. and Lemanski, L. F. (2003). A point mutation in bioactive RNA results in the failure of mutant heart correction in Mexican axolotls. *Anat. Embryol.* **206**:495-506.
- Zhang, C., Meng, F., Huang, X.P., Zajdel, R., Lemanski, S.L., Foster, D., Erginel-Unaltuna, N., Dube, D.K. and Lemanski, L.F. (2004). Downregulation of N1 gene expression inhibits the initial heart beating and heart development in axolotls. *Tissue & Cell.* **36**:71-81.
- Zot, H.G. Guth, K. and Potter, J. D. (1986). Fast skeletal muscle skinned fibers and myofibrils reconstituted with N-terminal fluorescent analogues of troponin C. *J. Biol. Chem.* **261**:15883-15890.



